Time-Dependent Solutions of Gravity

A dissertation presented
by

Gregory Chapman Jones

to
The Department of Physics
in partial fulfillment of the requirements
for the degree of
Doctor of Philosophy
in the subject of

Physics

Harvard University
Cambridge, Massachusetts
May 2006

Thesis advisor
Andrew Strominger

Author
Gregory Chapman Jones

Time-Dependent Solutions of Gravity

Abstract

Several new solutions of Einstein gravity, Einstein-Maxwell, and supergravity are presented. The solutions are derived, often from known solutions via analytic continuation, or generating or transformation methods. Then their properties and global structure are understood. Finally, their rôle in quantum gravity and string theory is described.

First, we describe the card diagram which is used to describe all Weyl-type spacetimes, and can be generalized beyond known Weyl types to include a cosmological constant. Card diagrams are extensions of Weyl half-planes to include time-dependent regions, and display all regions and global structure of a spacetime. Card diagrams have enabled the author and his collaborators to easily understand global structure of spacetime where pictureless methods would result in verbosity, confusion, or error. Additionally, card diagrams teach us about the structure of gravitational equations, sources, and solutions of PDEs/BVPs.

Then, we look at solutions gotten from the black dihole geometry. We review the dihole wave, and the complicated S-dihole $\mathcal{U}$-universes and $\mathcal{E}$-universes. Scaling limits are discussed, and affine coordinates are emphasized for analyzing the complexified non-Killing 2-manifolds.

Third, we give the correct global description of the odd-dimensional S-Kerr universes: $D = 5, 7, 9, \ldots$. All but the first ($D = 5$) yield a new instanton which can be used to describe the semiclassical decay of a simpler spacetime into the S-brane.

Fourth, we discuss the variety of S-branes, bubbles, and anti-bubbles obtainable from charged and spinning black holes in de Sitter and anti-de Sitter space.

Lastly, we use these twisted bubbles in AdS_5 to describe semiclassical decays of AdS_5 orbifolds, and extend the Gibbons-Hawking thermodynamic formalism to the twisted case. We use card diagrams for AdS to argue the global structure in the Kerr-AdS case, and find that a certain non-Killing event horizon remains present in the bubble spacetime for any $a, b \neq 0$, so with a cosmological constant, the nonspinning case is highly nongeneric.

Contents

Acknowledgments

I would like to thank my advisor for beginning me on my research, and giving me the independence to pursue my own ideas with a variety of collaborators both visiting and away from Harvard. This independence aided my own sense of responsibility and gave me an eye towards realities of postdoctoral research. I also thank him for his classes, for a few helpful pieces of advice, and for his excellent modus operandi of making publications and decision making in research.

I thank my research associates A. Maloney, J. E. Wang, D. Astefanesei, B. Julia, V. Balasubramanian and J. Simón, and with J. Levie and K. Larjo, who all had bright ideas for research directions and gave my own ideas serious attention. Special thanks to B. Julia and J. Simón for invites and support to visit ENS, France, and University of Pennsylvania. Extra special thanks to B. Julia for encouraging my career. Thanks to those collaborators for giving permission to include our writings and work based on their ideas.

Special thanks to young professors S. Minwalla and L. Motl in the string theory group for their enthusiasm and overly friendly personalities, journalism, and teaching, and thanks to prof. C. Vafa, to T. Wiseman, and to the rest of the high energy group, and Nancy the secretary. Thanks to N. Arkani-Hamed, S. Coleman, S.-T. Yau, A. Hanany, D. Z. Freedman, P. Kronheimer, D. Allcock, V. Guillemin, D. Podolsky, and D. Nelson who served as teachers. Thanks to Can, Michelle, Joe, and Subhy for the friendly office environment. Thanks to Andy Neitzke, Dave Thompson, Rakhi, Xi, Dan, Gordon, Kirill, Aaron, Josh, Morten, Kyriakos, Monica, Lisa, Wei, Suvrat, Lars, Megha, Jihye, Itay, Jason Gallicchio, and everyone else for self-teaching groups, discussions, the GSS, friendship, company, and presence. Thanks to Carol Davis, Jan Ragusa, Andy Foland, Dave Weitz, Gary Feldman, and Emily Dunkel for teaching-related roles. Lots of thanks to Sheila Ferguson. Thanks to M. Ali Belabbas, Ben Peirce and the Brockett Harvard Robotics Laboratory, and to Dionysis Stefanatos and Emanuele Viola in DEAS. Thanks to Dudley House and to OCS, TECH, Harvard Mathematics Dept, and to MIT. Thanks to my Harvard undergraduate physics and Core students.

Thanks to the HU Physics department for financial support throughout the years, including the Van Vleck fund and White prizes, to the Ford Foundation, and to NSF for their 3-year fellowship.

Thanks to the Strings 2004 (Paris) and 2005 (Toronto) conferences, and Modern Trends in String Theory II (Oporto, Portugal) and to Princeton IAS PITP (2002, 2004).

Thanks to the makers of LaTeX, WinEdt, tkpaint, and Mathematica software, the `RGTC.nb` package, and Alex Barnett for the Harvard thesis template.

Infinite thanks to my parents and family for their unending support and help, and thanks to old friends, musical accomplices, and anyone who told the truth and stayed sane.

"Possibly Gilman ought not to have studied so hard. Non-Euclidean calculus and quantum physics are enough to stretch any brain; and when one mixes them with . . . a strange background of multi-dimensional reality . . . one can hardly expect to be wholly free from mental tension." - H. P. Lovecraft, 1932

Chapter 1

Introduction

Einstein's 1915 theory of general relativity set the stage for much of modern theoretical physics. In addition to setting the basic notions of space and time, and relativity's astrophysical applications, its resistance to a quantum mechanical treatment has led to great questions, great insights, and all but the original motivations of string theory. String theory is still a background-dependent theory, where the backgrounds solve classical field equations that can be corrected order by order. These classical field equations are equations of gravity.

The simplest theory of pure gravity (in Lorentzian or Euclidean signature, and in 4 or higher dimensions) is already highly interesting and nontrivial. Solutions are hard to come by; standard textbooks often derive only those that can be solved by ODEs. Classification of solutions, generating methods, and a large collection of solutions with brief descriptions fill the compendium [1]. Adding to the difficulty is that solutions which are locally well-behaved will have a singularity elsewhere (i.e. they are incomplete), or will have incompatible closing loci of Killing directions with ensuing CTCs or horizon orbifolds. Stationary solutions with multiple objects are difficult to find, and truly dynamical solutions are nigh impossible.

Introduction of 1 Killing vector (for a stationary or brane-type solution) is usually the minimum assumption for the derivation of 4d exact solutions. Einstein's theory then admits an Ehlers $SO(2,1)$ symmetry group [2]. Additionally the Killing vector gives us a notion of Geroch/Hansen/Simon potentials [3, 4, 5] and in asymptotically-flat instances, conserved quantities. Einstein-Maxwell theory admits an $SU(2,1)$ Kinnersley symmetry group [6] including the popular Harrison transformations [7].

The introduction of a second Killing vector to a 4-manifold results in a much more rigid structure, first discovered by Hermann Weyl in 1917 [8, 9]. The resulting problem is still difficult yet tractable. Theoretical gravity takes more of a structure at this stage, and admits a variety of generating techniques and an infinite-dimensional Geroch/Kinnersley group of symmetries [10], as well as the specialized Bonnor transform [11, 12, 13]. Weyl described space as a collection of fields on a 'background' space which is the flat half-plane (or alternatively, axially symmetric flat 3-space).

The non-Killing 2-metric is conformally flat and the half-plane's boundaries close the Killing directions, yielding either horizons or closure (i.e. origin of polar coordinates). When things go wrong, these become horizon orbifolds, or conical singularities. The half-plane's boundary is partitioned into 'rods' and 'rays,' and certain quantities like surface gravities are constant along rods and rays.

After Weyl's seminal work, Achilles Papapetrou extended the static to the stationary case [14], and the Weyl-Papapetrou equations became nonlinear and hence generally nonsolvable. A renaissance came with the modern work of Emparan and Reall [15], generalizing the static Weyl harmonic method to D dimensions, assuming $D-2$ Killing vectors, and then T. Harmark [16, 17] allowed D-dimensional stationary solutions. We include the simple calculation for stationary electromagnetic fields for the D-dimensional static case.

Weyl's half-plane $\rho \geq 0$ gave rise to card diagrams, upon continuation of $\rho \to i\rho'$. Conformally Minkowskian 1+1 'vertical' cards finished out the Weyl description of spacetime. Card diagrams had several interesting properties and depicted spacetime in a way much different from the renowned Penrose diagram. Often, a combination of Penrose and card diagrams is useful to fully understand a spacetime's structure. Card diagrams go beyond Weyl's original ideas though, in that they can still apply in the presence of a cosmological constant. Pure (A)dS$_D$ spacetimes and black holes (or bubbles, anti-bubbles, or S-branes) in (A)dS$_D$ will admit card diagrams despite the failure of Weyl's harmonic method and the lack of a Weyl canonical ρ coordinate.

The development of more complicated supergravity theories in the 1970s gives a more direct injection of Einstein's theory into string theory; various supergravity theories in various dimensions represent the fields of string theory and many are related via dimensional reduction. Solutions in four and five dimensions (some involving a dilaton field) can be lifted to ten- and eleven-dimensional brane solutions in string and M-theory. Generating techniques of 'dilatonization' are important for this lifting, as is the well-known correspondence between the Taub-NUT instanton and D6-branes [18, 19, 20, 21].

One useful fact of gravitational solutions with $\mathbb{Z}_2$ or Lie symmetries is that analytic continuation of the solutions can give new real-valued solutions. Each given solution can generate several solutions, stationary or time-dependent, and each with its own cosmological interpretation, even though the solutions are algebraically identical across the complexified manifold. Imaginary-source solutions [22, 23, 24, 25] become reinterpreted as gravitational waves or S-branes, and black hole solutions also yield bubble-type solutions which result after semiclassical spacetime decay.

These time-dependent solutions have been related to dynamical tachyon solutions of string field theory pioneered by Sen [26, 27, 28] and Strominger/Gutperle [29]. Analytically continued gravitational solutions are thus interpreted as gravitational wave or S-brane solutions, perhaps sourced at imaginary time. The establishment of a (possibly conserved) S-charge for solutions, the issue of their regularity and possible development of horizons, their asymptotics, and scaling limits, guide our description.

Theoretical gravity concerns the finding of solutions and a description of their geometric properties. One is always straddling the line between a geometric description and a coordinate-dependent description. Our theme is to deemphasize coordinate-dependent 'descriptions' of spacetimes and yet to emphasize that spacetimes are in fact naturally written in certain coordinate systems. Our other theme is that horizons and singularities can be understood from the point of view of these canonical coordinate systems, and that spacetime pieces can be trivially patched together to understand a global structure.

This dissertation collects many related works by the author and his collaborators concerning solutions of gravitational equations, their manipulation via analytic continuation, their description and accounting, their relation to stringy objects, and their use in describing spacetime evolution (classical or semiclassical). Some results are published in e-print or journal, some are to be published, and others will appear solely here.

In Chapter 2, we give the concept of the card diagram, a pictorial device used to represent and work with Weyl spacetimes which has been very fruitful. They were developed with J. Wang to keep track of analytic continuation of basic black hole, bubble, and dihole geometries. The idea was to extend the conformal half-plane for stationary regions to time-dependent regions. 'Vertical cards' and 'special null lines' were born and a whole new language and description of Weyl spacetimes emerged. Card diagram methods make most analytic continuations obvious, allow one to keep track of and give names to a host of solutions, and remove the need for long-winded descriptions of horizons and spacetime structure.

Chapter 3 moves on to the dihole solution and analytic continuations thereof (the S-dihole universes). Using both card diagram and spherical prolate/affine coordinates we describe the complexified spacetime, ergosphere and ring singularity loci, and piece together patches to give various universes. The $\mathcal{U}$ and $\mathcal{U}_\pm$ universes are similar in spirit and can be described as an expanding bubble with a vertex in it, stretched out to yield new internal $i^\pm$. The $\mathcal{U}$-universes are drawn as 3-dimensional diagrams and are conjectured to have a complicated alternating sequence of $\mathcal{I}^\pm$ on their conformal boundaries. They are nonsingular and also can be looked at as an evolution of a hyperbolic plane as it collapses to a cigar and then relaxes again to the plane. Closely related are $\mathcal{E}$-universes with ergosphere singularities on their horizontal cards; these can be interpreted as a pair of parallel charged S-branes.

Chapter 4 gives some results on spinning (Kerr) solutions. In odd dimensions $D = 5, 7, 9, \ldots$, the Kerr S-brane with one spin parameter turned off, has an interesting global structure for either a large mass or a small (anomalous) mass range. The anomalous-range solutions continue to give new gravitational instantons. The $D = 5$ case is degenerate with the known instanton but $D = 7, 9, \ldots$ have a new topology and must be new. They describe the semiclassical decay of a space into the new anomalous-mass-range S-brane. A similar structure is present for S-branes deriving from M2-brane solutions and similar solutions with the same codimension. We also

give further solutions gotten from Kerr and a nonsingular S-brane for Taub-NUT.

Chapter 5 adds a cosmological constant. It is here that the form of the metric can get quite complicated. We define procedures to achieve S-branes, bubbles, and anti-bubbles from black holes in AdS or dS space in the spherically symmetric case, and then move to the rotating case. There is a strange occurrence of $W = 0$ coordinate singularities when we include both rotation and Λ that is not present with either turned off. We show these are horizons in many cases and describe spacetimes by skeleton diagrams (they are skeletons for Penrose diagrams, or are the 1d equivalent of a 2d card diagram). We also give the simplest Weyl representations of pure (A)dS$_4$ and (A)dS$_5$. These spacetimes which are asymptotically locally AdS serve in the AdS/CFT correspondence [30, 31, 32]; dominant Euclidean spacetimes satisfying certain boundary conditions are dual to thermal states in the CFT [33, 34]. The solutions here are primarily Lorentzian, possibly without an exterior stationary patch and serve for Lorentzian AdS/CFT [35].

Chapter 6 uses the Kerr-AdS$_5$ bubble as an endpoint for the semiclassical decay of a twisted AdS$_5$ orbifold. To see this, we analyze both geometries and show they have the same asymptotics. One must be careful using spherical vs. spheroidal coordinates, to get a match. In fact, the spheroidal coordinates for pure AdS$_5$ give a natural explanation of the $W = 0$ horizons of S-branes and (anti-)bubbles for Kerr-(A)dS$_D$. These horizons are already present for pure (A)dS$_D$ in the given patched description, and persist for say the Kerr-AdS$_D$ bubble. The bubble formation, which we would expect to seal off these $W = 0$ horizons from the majority of the spacetime, does not; the bubble surface does not expand quickly enough and both the non-Killing horizon and $W = 0$ horizon (or orbifold) are accessible after bubble formation. We also investigate the thermodynamics of the black holes-in-AdS and relate instanton negative modes to specific heat in a constant-Ω ensemble. We also discuss a relation to the flat case of Dowker et al. and the channels for decay.

Chapter 2

Card diagrams

To capture important physical properties of a spacetime we construct a new diagram, the card diagram, which accurately draws generalized Weyl spacetimes in arbitrary dimensions by encoding their global spacetime structure, singularities, horizons, and some aspects of causal structure including null infinity. One of our main results is to describe how Weyl rods can be traversed and the whole spacetime including the interior of horizons can be mapped out. Families of solutions share qualitatively similar card structures. As examples we systematically discuss properties of a variety of solutions including Kerr-Newman black holes, black rings, expanding bubbles, and recent spacelike-brane solutions. Card diagrams draw only non-trivial directions and so provide a clearer picture of the geometric features of spacetimes as compared to Penrose diagrams, and can change continuously as a function of the geometric parameters. In addition we show how card diagrams not only capture information about a geometry but also its analytic continuations. Weyl techniques are also applied to the perturbations of bubble and S-brane solutions by Israel-Khan rods.

This text is based on the paper `hep-th/0506023` with John E. Wang, and some material had already been presented in `hep-th/0409070`.

2.1 A new diagram for spacetime structure

Spacetimes are geometrical objects, independent of the coordinates with which we describe them. However, spacetimes are typically presented and visualized in specific coordinate system. If the coordinates are poorly chosen, many properties of the spacetime such as horizons, causally connected spacetime points, maximal extensions and null infinity are not readily apparent.

A simplification occurs if a D dimensional Lorentzian spacetime has enough fibered directions (like a $(D-2)$-sphere) or other ignorable directions. One can draw two dimensional diagrams for the remaining directions and such Lorentzian $-+$ signature spacetime slices can be conformally compactified leading to Penrose diagrams.

Penrose diagrams are quite useful in understanding spacetime geometry and successful especially in understanding causal structure although there are some limitations to this approach. For instance just knowing the Penrose diagram for the subextremal $Q^2 < M^2$ Reissner-Nordström black hole does not tell us what happens to the spacetime structure in the chargeless or extremal limits. For more complicated spacetimes, Penrose diagrams (which assume symmetry or fibering) can only draw a slice of the spacetime. As a known example, the Penrose diagram for a Kerr black hole does not clearly depict the ring singularity and the possibility of crossing through the interior of the ring into a second universe. In addition, recently analytic continuation has been applied to black hole solutions to yield bubble-type [36, 37, 38, 39, 40, 41] or S-brane [41, 29, 27, 42, 43, 44, 45, 46, 23, 25, 47, 48, 49, 50, 51, 52] solutions. Oftentimes this is done in Boyer-Lindquist type coordinates which are hard to visualize. Again we are not left with a clear picture of the resulting spacetime and the Penrose diagrams are missing important noncompact spatial directions.

It is useful to have an alternative diagram which can also capture important features of a spacetime. For this reason in this paper we expand the notion of drawing spacetimes in Weyl space [53, 15]. Because our diagrams have the appearance of playing cards glued together we will dub them Weyl card diagrams.

To understand the construction of a card diagram we recall that in $D = 4$ dimensions a Weyl solution in canonical coordinates [15, 8, 54] is written as

$$ds^2 = -f dt^2 + f^{-1}[e^{2\gamma}(d\rho^2 + dz^2) + \rho^2 d\phi^2] \tag{2.1}$$

where f and γ are functions of ρ, z. The original Weyl class requires two commuting orthogonal Killing fields $\partial_t, \partial_\phi$ in four dimensions [8], or $D-2$ fields for general D dimensions [15].[1] Sometimes Weyl solutions are called axially-symmetric gravitational solutions although they in fact are more general. We also include the Weyl-Papapetrou class for 2 commuting Killing vectors in $D = 4$ [14], and allow charged static solutions in $D \geq 4$ (see the Appendix to this paper). Furthermore stationary vacuum solutions in $D \geq 4$ are covered with the recent work of [16]. In four and five dimensions this generalized Weyl class includes spinning charged black holes and rings [15, 16, 57, 58] as well as various arrays [25, 51, 59] of black holes, spacelike-branes, and includes backgrounds like Melvin fluxbranes [25, 51, 60, 61, 62, 63, 64] and spinning ergotubes [65].

When constructing card diagrams, we will draw only Weyl's canonical coordinates (ρ, z), or coordinates related to them via a conformal transformation. The Killing coordinates are ignorable and so this diagram is efficient and will show all details of the spacetime. Since there are only two nontrivial coordinates, card diagrams are two dimensional like Penrose diagrams and so are easy to draw. The difference however is that while Penrose diagrams are truly two-dimensional, card diagrams are drawn as if embedded in three dimensions. When a (ρ, z) region of the spacetime

[1] Non-Weyl, axisymmetric spacetimes in $D \geq 4$ are discussed in [53, 56].

has Euclidean ++ signature, we draw the two coordinates (ρ, z) horizontally; and this makes a horizontal card. For Lorentzian signature $+-$ regions we use (ρ', z) or (τ, ρ), and draw the timelike coordinate vertically; this makes a vertical card. Causal structure is automatically built into the vertical cards since the directions (τ, ρ) appear conformally only through the combination $-d\tau^2 + d\rho^2$. Horizontal cards and vertical cards are attached together at Killing horizons and so card diagrams resemble a gluing-together of a house of playing cards.

In this paper we will present card diagrams for the familiar spacetimes of black holes, as well as expanding bubbles, S-branes, and black rings. Many other spacetimes including the S-dihole, infinite periodic universe, C-metric, and multiple-rod solutions in 4 and 5 dimensions are presented in [51], and spacetimes derived from 4 and 5 dimensional Kerr geometries will be presented in [67].

In Section 2 we review the Schwarzschild black hole in the usual coordinates and in Weyl coordinates. By extending through the horizon and properly representing the interior of the black hole we construct the first card diagram. We emphasize the construction of the interior of the black hole as a vertical card comprising four triangles unfolded across special null lines. We then discuss general card diagram properties such as the null lines, list the available card types, and describe the γ-flip analytic continuation procedure.

In Section 3, we discuss the sub/super/extremal Reissner-Nordström black hole card diagrams, the Kerr black hole, and the black ring/C-metric card diagrams. We then show how a spacetime can have multiple card diagrams and as examples present the elliptic, hyperbolic, and parabolic representations of the charged Witten bubble and charged Spacelike brane which we also call S-Reissner-Nordström. Finally, as a newer example we discuss the (twisted) S-Kerr solution [47, 48].

We conclude with a discussion in Section 4. We give an appendix on perturbing Witten bubbles and S-branes by introducing Israel-Khan rods, in their hyperbolic or elliptic representations. We also give an appendix on how the higher dimensional vacuum Weyl Ansatz can be extended to include electromagnetic fields.

This paper is a condensed presentation of the card diagrams in [51].

2.2 Schwarzschild and general card diagrams

In this section we review the Schwarzschild black hole as an example of a Weyl spacetime and then we explain the construction of its associated Weyl card diagram. General features and properties of card diagrams are also developed.

Up to now if a solution such as the Schwarzschild black hole had horizons, then only the regions outside the horizons have been drawn in Weyl coordinates [15, 54]. To go through a nonextremal horizon the Weyl coordinate ρ must be allowed to take imaginary values. We discuss how the horizon can be represented as a junction of four regions which we call four cards. The regions outside the horizon will be drawn as

two horizontal cards while the regions between the horizon and the singularity will be drawn as two vertical cards. The interior vertical cards naively are problematic and have fourfold-covered triangles bounded by 'special null lines'. However the triangles can be unfolded and glued together into a square along the 'special null lines' to achieve a singly covered representation of the spacetime by properly choosing branches of a square root in the solution.

Note that card diagrams represent the spaces on which we solve the Laplace equation (horizontal card) or wave equation (vertical card) to find a Weyl metric. For example, the Schwarzschild black hole has a uniform rod source for the potential $\log f$, and the remainder of its z-axis encodes the vanishing of the ϕ-circle. Thus card diagrams give a full account of the boundary conditions necessary to specify the spacetime.

2.2.1 Schwarzschild black holes

This section will describe the construction of the Schwarzschild black hole card diagram. The Penrose and card diagrams are drawn in comparison in Fig. 2.1.

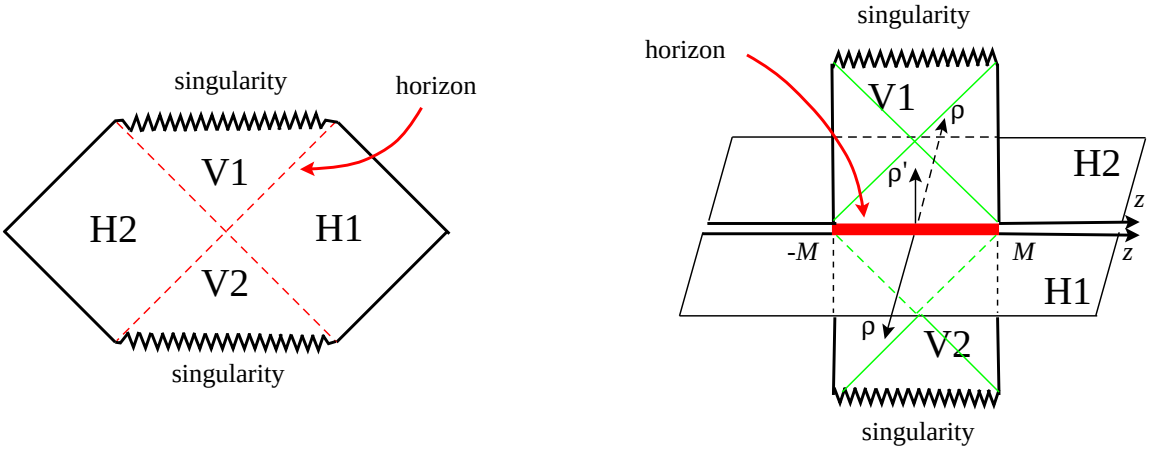

Figure 2.1: The Schwarzschild black hole represented both as a Penrose diagram as on the left and as a Weyl card diagram on the right. The cards V1 and V2 are vertical squares made of four triangles, while the cards H1 and H2 are horizontal and are infinite half-planes. The four cards are joined together along the black hole horizon on the z-axis.

The Schwarzschild metric in spherically symmetric (Schwarzschild) coordinates is

$$ds^2 = -(1-2M/r)dt^2 + (1-2M/r)^{-1}dr^2 + r^2 d\theta^2 + r^2 \sin^2\theta d\phi^2 \ . \qquad (2.2)$$

There is a horizon at $r = 2M$ and a curvature singularity at $r = 0$. On the other hand, in Weyl's canonical coordinates [15, 8, 54] it is

$$ds^2 = -f dt^2 + f^{-1}(e^{2\gamma}(d\rho^2 + dz^2) + \rho^2 d\phi^2)$$

where f and γ are functions of the coordinates ρ and z:

$$\begin{aligned} f &= \frac{(R_+ + R_-)^2 - 4M^2}{(R_+ + R_- + 2M)^2}, \\ e^{2\gamma} &= \frac{(R_+ + R_-)^2 - 4M^2}{4R_+R_-}, \\ R_\pm &= \sqrt{\rho^2 + (z \pm M)^2}. \end{aligned} \tag{2.3}$$

Previously attention was restricted to the half-plane $\rho \geq 0$, $-\infty < z < \infty$, known as Weyl space, which describes the exterior of the black hole and whose horizon is represented by a 'rod' line segment $\rho = 0$, $-M \leq z \leq M$; see Fig. 2.2. Note that the non-Killing 2-metric is conformal to the Euclidean flat space $d\rho^2 + dz^2$. The coordinate transformation between Schwarzschild and Weyl coordinates is

$$\begin{aligned} \rho &= \sqrt{r^2 - 2Mr}\,\sin\theta, \\ z &= (r - M)\cos\theta. \end{aligned} \tag{2.4}$$

Now we wish to ask how Weyl's coordinates draw the spacetime inside the horizon. The Schwarzschild coordinates (2.4) tell us that for $0 < r < 2M$, ρ is imaginary and so we set $\rho' = i\rho$. (In general we must perform an analytic continuation of Weyl coordinates to go through a horizon which are at the zeros of the Weyl functions $f, e^{2\gamma}$.) The analytic continuation gives a region with a conformally Minkowskian metric $-d\rho'^2 + dz^2$ and we will draw this region as being vertical and perpendicularly attached to the horizontal card at the horizon $-M \leq z \leq M$. The vertical direction is always timelike in card diagrams.

Of course the horizon structure is a more complicated than just having two cards joined together. For example we know the Penrose diagram in the t, r coordinates is divided into four regions that meet in a $\times$-horizon structure. In Weyl coordinates, we already saw that we can extend $\rho \to \pm i\rho'$ or go to negative ρ. This gives us the four regions of the Schwarzschild black hole in Weyl coordinates. Two regions will be horizontal at real values of ρ and two regions will be vertical with imaginary values of ρ. So in addition to the first horizontal card in front of the horizon, we also have a copy of the horizontal external universe behind the horizon and attach two vertical cards, one above and one below the horizontal cards (see Fig. 2.1). All together, four different regions attach together at the same $-M \leq z \leq M$ rod horizon.

The four regions labelled H1, H2, V1 and V2 in the Penrose diagram map to the similarly labelled four regions on the card diagram in Fig. 2.1. Note that the Weyl cards show the r, θ coordinates which is different from the Penrose diagram. However

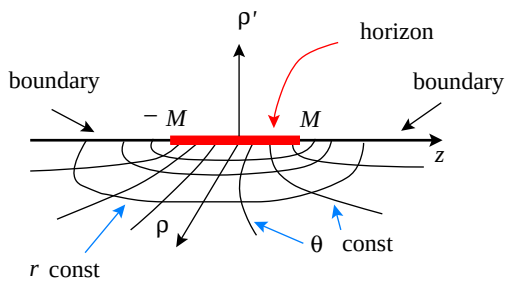

Figure 2.2: In Weyl coordinates the Schwarzschild black hole is typically represented as a ρ, z horizontal half-plane showing one external universe, H1, of $r \geq 2M$. The horizon is represented as a rod along $\rho = 0$ $-M \leq z \leq M$. The $0 < r < 2M$ region will be drawn along the vertical perpendicular ρ'-direction.

the fact that the radial coordinate r describes four distinct regions, two where ∂_r is spacelike and two where it is timelike, is still apparent in the Weyl card diagram. Though a Penrose diagram always has a Lorentzian $-+$ signature, a card diagram will flip from being Euclidean $++$ to Lorentzian $-+$ across a nonextremal Killing horizon.

Let us now examine the construction of the upper vertical card extended in the ρ', z directions. Looking at an r-orbit on the vertical card, we note that $0 \leq \rho' \leq M \pm z$. The bounding lines $R_\pm = \sqrt{-\rho'^2 + (z \pm M)^2} = 0$, we will call 'special null lines,' and they are a general feature of vertical cards with focal points (the rod endpoints $z = \pm M$). Here the special null lines are the envelope of the r-orbits as we vary θ. Thus when inside the horizon the Schwarzschild coordinates apparently fill out a vertical 45-45-90 degree triangle with hypotenuse length $2M$ a total of four times, as shown in Figure 2.3.

Special null lines play an important role in Weyl card diagrams so let us explain their significance. Keep in mind that we have already broken the manifest spherical symmetry when we have written the Schwarzschild metric in Weyl coordinates, so the existence of preferred special null lines is relative to this chosen axis. Consider the two 3-surfaces

$$R_\pm = r - M \pm M\cos\theta = 0, \tag{2.5}$$

which are drawn in Fig. 2.4. These surfaces bound the trajectories of light rays that do not move in the Killing directions. The surfaces intersect at $r = M$ and partition the black hole interior into four subregions. These regions correspond to four Weyl triangles.

It is clear from (2.5) that $R_\pm$ is positive outside the horizon and there is no difficulty going to negative values inside the horizon. On the other hand in terms of Weyl coordinates, the functions $R_\pm = \sqrt{-\rho'^2 + (z \pm M)^2}$ are the square root of

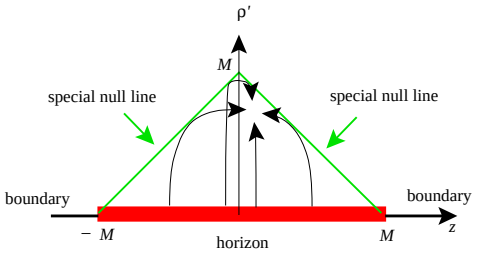

Figure 2.3: The Weyl representation of the interior of the Schwarzschild black hole naively gives a triangle with base length $2M$ and height M. As we illustrate, the triangle interior is covered four times by orbits of r at four different values of θ.

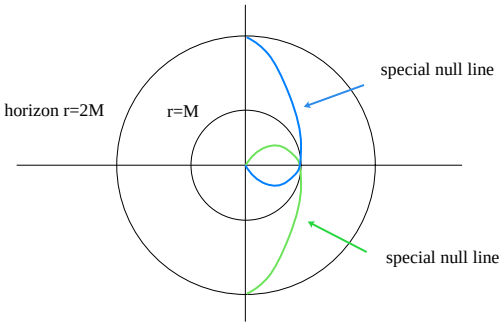

Figure 2.4: The Weyl null lines for the Schwarzschild black hole correspond to two 3-surfaces which partition $0 < r < 2M$ into four subregions.

a positive number when $\rho' < z \pm M$ and imaginary if $\rho' > z \pm M$. Clearly, instead of dealing with imaginary values of $R_\pm$, the way to go 'beyond' the special null line $R_\pm = 0$ is to keep $\rho' < z \pm M$ but use the other square root branch for $R_\pm$ as it enters in the Weyl functions f and γ by explicitly replacing $R_\pm \to -R_\pm$. Since we can pass $R_+ = 0$ and/or pass $R_- = 0$, it is clear that the four different branches of the square root functions differentiate the four copies of the Weyl triangle.

From (2.3), passing each $R_\pm = 0$ null line changes the sign of $e^{2\gamma}$ and hence exchanges the timelike and spacelike nature of ρ' and z. Since the vertical direction on a vertical card always represents time, two of the triangles are drawn turned on their sides, so the hypotenuse is vertical. When the four triangles describing the interior of the black hole $0 \le r \le 2M$ are glued together along the special null lines they fit neatly into a square; see Fig. 2.5. Because of the unfolding of the triangles, the positive z-direction on the top triangle (and any attached horizontal cards) points in the opposite direction compared to that on the original horizontal card.

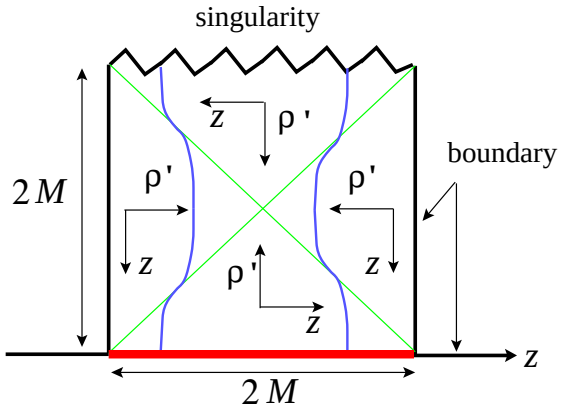

Figure 2.5: Unfolding the four triangles along the 45° special null lines for the Weyl card V1, $0 < r < 2M$, produces a square of side length $2M$. The horizon is at the bottom and the singularity at the top. We also draw two lines of constant θ and varying r.

The upper vertical cards is thus a square of length $2M$. The bottom of the upper card V1 is the black hole horizon which connects to three other cards in a four card junction. The right and left edges of this vertical card correspond to $\theta = 0, \pi$ and are the boundaries where the ϕ-circle vanishes. The top edge of the card represents the $r = 0$ curvature singularity. The second vertical card V2 is built in analogous fashion except the square is built in a downwards fashion towards negative values of ρ'. Additionally there is a second horizontal card plane, H2, identical to H1 at negative values of the ρ coordinate attached to the same horizon along $[-M, M]$ on the z-axis.

One typically stops the construction of the Schwarzschild spacetime with the above four regions, and considers the $r < 0$ regions of the metric to be a separate spacetime. However for reasons which become clear when we look at the Reissner-Nordström and Kerr black holes in Sections 2.3.1 and 2.3.1, we will continue the card diagram past the singularity and attach two horizontal half-plane corresponding to negative-mass (or $r < 0$) universes h3 & h4, and further vertical card above the singularity which is identical to V2. The two new horizontal cards each represent negative mass-universes with a singularity along $-M \leq z \leq M$. Note that while the Penrose diagrams for the $r > 0$ and $r < 0$ regions of Schwarzschild cannot be attached together since the singularity is spacelike in one region and timelike in another, cards can naturally be attached at this rod-singularity. The extended card diagram for Schwarzschild, shown in Fig. 2.6, is an infinite array of repeated cards representing positive and negative mass universes and inside-horizon regions.

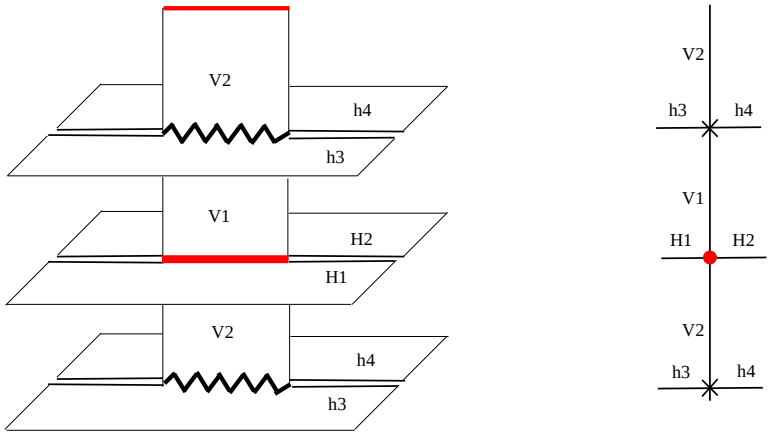

Figure 2.6: The extended card diagram for Schwarzschild includes both positive and negative mass universes half-planes. Its cross-section for $z = 0$ is drawn on the right.

2.2.2 General properties of card diagrams

Having described the construction of the card diagram for Schwarzschild we now turn to a few general remarks about these diagrams. Horizontal cards are conformally Euclidean and represent stationary regions. Vertical cards are always conformally Minkowskian and represent regions with $(D-2)$ spacelike Killing fields. On a vertical card time is always in the vertical direction and a point's causal future lies between 45° null lines. Weyl's coordinates certainly go bad at horizons, so these diagrams are not a full replacement for Penrose diagrams at understanding causal structure or particle trajectories. However, it is clear for example from Fig. 2.1 that two vertical

and two horizontal cards attach together in a orthogonal +-configuration in precisely the sense of the ×-horizon structure of the Penrose diagram.

The prototypical horizon is that of the two Rindler and two Milne wedges of flat space; this spacetime has two horizontal half-plane cards and two vertical half plane cards that meet along the horizon being the whole z-axis. Zooming in on a non-extremal horizon of any card diagram yields this Rindler/Milne picture.

A rod endpoint $(\rho, z) = (0, z_i)$ such as $z = \pm M$ for Schwarzschild is a 'focus' for the Weyl diagram and often represents the end of a black hole or acceleration horizon on a horizontal card. Generally, multi-black hole Weyl spacetimes depend only on distances to foci, such as $R_\pm$ in the case of Schwarzschild [68].

To understand that in general it is natural to change the branch of the distance functions, R_i, when crossing the special null line that emanates from the foci at $z = z_i$, take some Weyl spacetime and imagine moving upwards in a vertical card to meet the special null line at $R_i = 0$ by increasing time $\rho' \geq 0$ for fixed spatial z. Rearranging $R_i = \sqrt{-\rho'^2 + (z + z_i)^2}$ as the semi-ellipse

$$R_i^2 + \rho'^2 = (z + z_i)^2,$$

we see that a smooth traversal of this semi-ellipse across $R_i = 0$ requires a change in the sign of R_i.

In many of our solutions, special null lines are used to reflect vertical triangular cards to create full, rectangular cards. However, in the Bonnor-transformed S-dihole geometry of [51] as well as double Killing rotated extremal geometries and parabolic representations of the bubble and S-Schwarzschild in Sec. 2.3.2, the special null lines will serve as conformal boundaries at null infinity $\mathcal{I}^\pm$.

Boundaries of cards indicate where the metric coefficient along a Killing (circle) direction vanishes. Which circle vanishes is constant over a connected piece of the boundary, even when the boundary turns a right angle onto a vertical card. Furthermore the periodicity to eliminate conical singularities is constant along connected parts of the boundary. For the Schwarzschild, the ϕ-circle vanishes on both the connected boundaries and has periodicity 2π.

It is interesting to consider geodesic trajectories on card diagrams. For example when a light ray is incident from a horizontal card onto a horizon (to enter the upper vertical card), it must turn and meet that horizon perpendicularly. It then appears on the vertical card, again perpendicular to the horizon. Only those light rays which go from the lower vertical card to the upper vertical card directly can meet the horizon rod at a non-right angle; these rays would touch the vertex of the × in a Penrose diagram. When a light ray on a vertical card hits a boundary where a spacelike circle vanishes, it bounces back at the same angle as drawn on the card relative to the perpendicular.

Spacetimes with a symmetry group larger than the minimal Weyl symmetry can have more than one card diagram representation. Multiple diagrams exist when there

is more than one equivalent way to choose $(D-2)$ Killing congruences on the spacetime manifold. Examples we explicitly discuss in Sec. 2.3.2 are the 4d Witten bubble and the 4d S-Reissner-Nordström (S-RN) which have three card diagrams corresponding to the three types of Killing congruences on dS_2 and $\mathbf{H}_2$. These different card diagrams are associated for example with global, patched, and Poincaré coordinates for dS_2 and the different representations will have different applications and reveal different information. The S-Kerr solution, whose card diagram is discussed in Sec. 2.3.1, has symmetry group $U(1) \times \mathbf{R}$ and its unique card representation looks like the 'elliptic' representation of S-RN.

Our deck of cards: The building blocks for Weyl spacetimes

All spacetimes, new and old, in this paper are built from the following card types.

Horizontal cards are always half-planes. They may however have one or more branch cuts which may be taken to run perpendicular to the z-axis. Undoing one branch cut leads to a strip with two boundaries; multiple branch cuts lead to some open subset, with boundary, of a Riemann surface.

Vertical cards may be noncompact: Full planes with or without a pair of special null lines; half-planes with vertical or horizontal (horizon) boundary; or quarter planes at any 45° orientation. Vertical cards may also be compact: Squares with a pair of special null lines; or 45-45-90 triangles at any 45° orientation. All vertical boundaries represent a Killing circle vanishes and hence the end of the card. All horizontal boundaries represent a Killing horizon. All 45° null boundaries represent instances of $\mathcal{I}^{\pm}$.

It is satisfying that for a variety of spacetimes including those in [67, 41], the cards are always of the above rigid types.

There is one basic procedure which can be performed on vertical cards and their corresponding Weyl solutions. It is the analytic continuation $2\gamma \to 2\gamma + i\pi$, which is allowed since γ is determined by first order PDEs and $e^{2\gamma}$ is real of either sign on vertical cards. This continuation is equivalent to multiplying the metric by a minus sign and then analytically continuing the $D-2$ Killing directions. For charged generalizations of Weyl solutions (see Appendix B), this procedure does not affect the reality of the 1-form gauge field. We call this a γ-flip since the way it acts on a card is to flip it about a 45° null line (for example, look at the vertical cards in Figs. 2.18 and 2.19).

2.3 Card diagrams

In this section we construct the card diagrams for a wide assortment of solutions including black holes and S-branes. The card diagrams are shown to be useful in representing continuous changes in the global spacetime structure such as how

Reissner-Nordström black holes change as we take their chargeless and extremal limits. For the superextremal black holes we discuss how to deal with branch points and cuts on horizontal cards. The card diagram also clearly represents the Kerr ring singularity and how traversing the interior of the ring leads to a second asymptotic spacetime. The 5d black ring solution and associated C-metric type solutions are discussed.

Furthermore analytic continuation has an interesting interpretation in terms of card diagrams. We will describe the effect of analytic continuation on the card diagrams by examining two known analytic continuations of the Reissner-Nordström black hole, the charged bubble and the S0-brane which we also call S-RN. These spacetimes each have three card diagram representation and two are obtained via different analytic continuations. The Witten bubble and S-RN are related to each other by what we call a γ-flip.

2.3.1 Black holes

Subextremal $Q^2 < M^2$ Reissner-Nordström black holes

In the usual coordinates the Reissner-Nordström black hole takes the form

$$\begin{aligned} ds^2 &= -\Big(1-\frac{2M}{r}+\frac{Q^2}{r^2}\Big)dt^2+\Big(1-\frac{2M}{r}+\frac{Q^2}{r^2}\Big)^{-1}dr^2+r^2(d\theta^2+\sin^2\theta d\phi^2) \\ A &= Qdt/r \end{aligned} \tag{2.6}$$

Using the coordinate transformation

$$\rho=\sqrt{r^2-2Mr+Q^2}\sin\theta, \qquad z=(r-M)\cos\theta \tag{2.7}$$

we find the Weyl form of Reissner-Nordström black hole

$$ds^2 = -fdt^2+f^{-1}(e^{2\gamma}(d\rho^2+dz^2)+\rho^2d\phi^2) \tag{2.8}$$

$$f = \frac{(R_++R_-)^2-4(M^2-Q^2)}{(R_++R_-+2M)^2} \tag{2.9}$$

$$e^{2\gamma} = \frac{(R_++R_-)^2-4(M^2-Q^2)}{4R_+R_-}$$

$$A = -\frac{2Qdt}{R_++R_-+2M}$$

$$R_\pm = \sqrt{\rho^2+(z\pm\sqrt{M^2-Q^2})^2}=r-M\pm\sqrt{M^2-Q^2}\cos\theta$$

and the card diagram for $Q^2 < M^2$ is shown in Fig. 2.7. The construction of the card diagram proceeds along similar lines to the Schwarzschild card diagram. There are two adjacent horizontal half-planes, H1 and H2, which represent the positive mass asymptotically flat regions. The outer horizon is a rod which lies on the z-axis for

$-\sqrt{M^2-Q^2} < z < \sqrt{M^2-Q^2}$. The vertical cards, V1 and V2, are squares of length $2\sqrt{M^2-Q^2}$ and the diagonal lines connecting opposite corners of the square are special null lines. The top of V2 is the $r = r_-$ rod, a four-card inner horizon. The black hole singularity lies on the boundary of the h1 and h2 regions, at $\rho^2/Q^2 + z^2/M^2 = 1$. The rest of those horizontal cards, regions h3 and h4, are $r < 0$ or equivalently $M < 0$ nakedly singular RN 'black holes.'

At each horizon, the card diagram is continued vertically to obtain an infinite tower of cards. In Fig. 2.8 we show the Penrose diagram for comparison.

Although the chargeless $Q \to 0$ limit is hard to understand using Penrose diagrams, it is easy to understand using the card diagram in Fig. 2.7; the vertical card expands to a $2M \times 2M$ square and the singularity degenerates to a line segment covering the inner horizon. Regions h1 and h2 have collapsed and the singularity is now 'visible' from V1 and V2 as well as h3 and h4. We have achieved the infinite number of cards in the Schwarzschild card diagram Fig. 2.6.

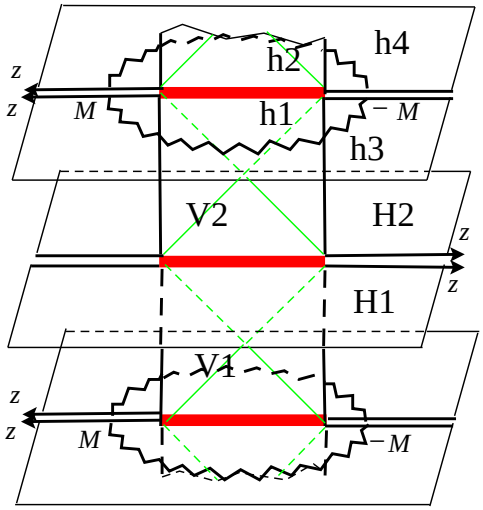

Figure 2.7: The subextremal Reissner-Nordström card diagram. The ellipse singularity has semimajor axes $z = \pm M$ and $\rho = Q$, and the rod endpoints are the foci on the z-axis at $z = \pm\sqrt{M^2-Q^2}$.

Extremal $Q^2 = M^2$ Reissner-Nordström black hole

Starting from the above card diagram we now examine the extremal limit $Q \to \pm M$. In this case the vertical cards which represent the regions between the two horizons get smaller and disappear. When $Q = M$, the horizontal cards are now only attached at point-like extremal-horizons and only half of the horizontal cards remain connected, see Fig. 2.9. The region near the point-horizons are anti-de Sitter throats

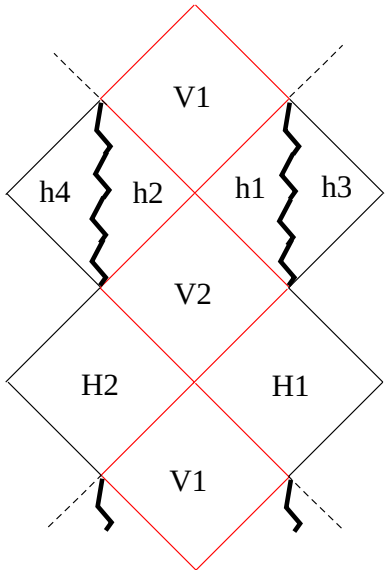

Figure 2.8: The extended Reissner-Nordström Penrose diagram, including negative mass universes.

although cards themselves cannot adequately depict the throat region. The throat is a 'connected' sequence of points on vertically adjacent horizontal cards.

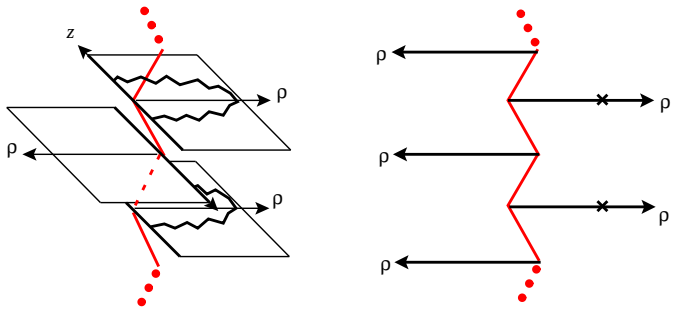

Figure 2.9: Extremal RN horizontal cards are connected in an AdS_2 fashion at their origins. A side-view $z = 0$ cross section is also shown.

To understand how to go across the horizon, it is important to remember that there are special null lines in $r_- < r < r_+$. In the extremal case the focal distances are equal ($R = R_+ = R_-$) and the null lines $R_\pm = 0$ degenerate to the origin. So when we pass through the throat to an adjacent $r < M$ horizontal card, the sign changes for all occurrences of $R = \sqrt{\rho^2 + z^2} = r - M$. The singularity appears as a semicircle on the $r < M$ cards.

For axisymmetric Majumdar-Papapetrou solutions, this 'sign change rule' agrees with that in [53]. Our analysis also applies to non-MP axisymmetric solutions such as the dihole [12, 69, 70].

Superextremal $Q^2 > M^2$ Reissner-Nordström black holes

The superextremal $Q^2 > M^2$ Reissner-Nordström black hole does not have horizons or vertical cards. Its card diagram consists of two horizontal cards, connected along the branch cut $0 \leq \rho \leq \sqrt{Q^2 - M^2}$, $z = 0$. One card has a semi-ellipse singularity passing through the points $(\rho = 0, z = \pm M)$ and $(\rho = Q, z = 0)$ (see Fig. 2.10(a)).

These two horizontal cards are connected in the same sense as a branched Riemann sheet. By choosing Weyl's canonical coordinates (meaning $Z = \rho + iz$ with $-(\mathrm{Coef}\, dt^2)(\mathrm{Coef}\, d\phi^2) = (\mathrm{Re}\, Z)^2$), the solution is no longer accurately represented on the horizontal card. This can be seen by examining the coordinate transformation (2.8) from Schwarzschild coordinates to Weyl coordinates. For fixed r and varying θ, the coordinates from $M < r < \infty$ cover the Weyl plane in semi-ellipses which degenerate to the segment $(0 \leq \rho \leq \sqrt{Q^2 - M^2}, z = 0)$, which serves as a branch cut; and $\rho = \sqrt{Q^2 - M^2}$ is the branch point. The range $-\infty < r < M$ again covers the half-plane with $r = 0$ forming an ellipse singularity. Crossing the branch cut means choosing the opposite signs for $R_\pm = \sqrt{\rho^2 - (z \pm i\sqrt{Q^2 - M^2})^2}$, and indeed we can think of the superextremal 'rod' as being complex-perpendicular to the Weyl Z-plane.

This double cover of the Weyl plane can be fixed by taking a holomorphic square root; this preserves the conformally Euclidean character of the card diagram. By choosing a new coordinate $W = \sqrt{Z - \sqrt{Q^2 - M^2}}$, we map both the positive and negative-mass universes into the region $(\mathrm{Im}\, W)^2 - (\mathrm{Re}\, W)^2 \leq \sqrt{Q^2 - M^2}$ (see Fig. 2.10(b)). The image of the z-axis boundary is a hyperbola where the ϕ-circle vanishes. The origin $W = 0$ is the image of the branch point and the image of the line segment $(0 \leq \rho \leq \sqrt{Q^2 + M^2}, z = 0)$ is a line connecting the two hyperbolas and intersecting the origin of the W-plane. The singular nature of $e^{2\gamma} \propto 1/R_+R_- \propto 1/|\Delta Z| \propto 1/|W|^2$ has been fixed by $e^{2\gamma} dZ d\overline{Z} = 4|W|^2 e^{2\gamma} dW d\overline{W}$. Finally the 'black hole' singularity is mapped to a curved segment stretching from one hyperbola line to the other, to the left of the branch cut.

Alternatively one can use a Schwarz-Christoffel transformation to map the two universes onto the strip $|\mathrm{Im}\, W| \leq W_0$. This is useful when the horizontal card boundaries are horizons as it allows for multiple horizontal cards to be placed adjacent to each other at the horizons (Fig. 2.17). This technique of fixing a horizontal card with a branch point will also be used in more complicated geometries such as the hyperbolic representation of S-RN and multi-rod solutions in four and five dimensions [51].

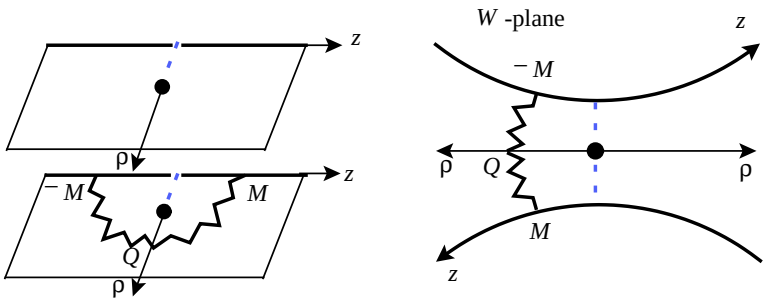

Figure 2.10: (a) The superextremal RN black hole as two half-planes connected along a branch cut; (b) after conformal transformation to the W-plane we obtain a branched, static horizontal card, with two boundaries and one branch point.

Kerr black hole

Written in Weyl-Papapetrou form, the Kerr black hole is

$$\begin{aligned} ds^2 &= -f(dt-\omega d\phi)^2 + f^{-1}(e^{2\gamma}(d\rho^2+dz^2)+\rho^2 d\phi^2), \\ f &= \frac{(R_+ + R_-)^2 - 4M^2 + \frac{a^2}{M^2-a^2}(R_+ - R_-)^2}{(R_+ + R_- + 2M)^2 + \frac{a^2}{M^2-a^2}(R_+ - R_-)^2}, \\ e^{2\gamma} &= \frac{(R_+ + R_-)^2 - 4M^2 + \frac{a^2}{M^2-a^2}(R_+ - R_-)^2}{4R_+R_-}, \\ \omega &= \frac{2aM(M+\frac{R_++R_-}{2})(1-\frac{(R_+-R_-)^2}{4(M^2-a^2)})}{\frac{1}{4}(R_+ + R_-)^2 - M^2 + a^2\frac{(R_+-R_-)^2}{4(M^2-a^2)})}, \end{aligned}$$

where $R_\pm = \sqrt{\rho^2 + (z \pm \sqrt{M^2-a^2})^2} = r - M \pm \sqrt{M^2-a^2}\cos\theta$. The transformation to Boyer-Lindquist coordinates is $\rho = \sqrt{r^2-2Mr+a^2}\sin\theta$, $z = (r-M)\cos\theta$.

For $a^2 < M^2$ the Kerr black hole card diagram (see Figure 2.11) is similar to Reissner-Nordström except that the singularity is a point and lies at $\rho = a$, $z = 0$ on each negative-mass card. The outer and inner ergospheres lie on the positive-and negative-mass cards and are both described by the curve $z^2 = \alpha^2 - (\alpha^2/a^2 - 1)\rho^2 - \rho^4/a^2$ which intersects the rod endpoints at $z = \pm\alpha = \pm\sqrt{M^2-a^2}$. The boundary of the region with closed timelike curves is also described by a quartic polynomial in Weyl coordinates. Once again the vertical card has two special null lines where $R_\pm$ change sign.

The $r = 0$ surface in BL coordinates is a semi-ellipse $\rho^2/a^2 + z^2/M^2 = 1$ on the negative-mass card; but it is not a distinguished locus on the card diagram. Attempting to make one loop around the ring in the Kerr-Schild picture clearly does not make a closed loop in Weyl space, whereas two loops in the Kerr-Schild picture

will form a single loop around the ring singularity on the card diagram. It is also clear that it is possible to find classical trajectories which avoid the singularity and which safely escape into a second asymptotically flat region.

A card diagram for a charged Kerr-Newman solution can similarly be constructed, with $\alpha = \sqrt{M^2 - Q^2 - a^2}$.

The extremal Kerr(-Newman) solution has a card diagram like Fig. 2.9, but the ring singularity is just a point at $z = 0$ and $\rho = M$ on negative-mass cards. Again, $R = R_+ = R_-$ and the special null lines degenerate to the origin; crossing the origin (which is a twisted AdS-type throat) entails changing the sign of R.

The superextremal Kerr(-Newman) solution is similar to the superextremal RN (Fig. 2.10(b)) except that the curved-segment singularity is replaced by a point ($z = 0$), and the ergospheres map to an ∞-looking locus centered at $W = 0$.

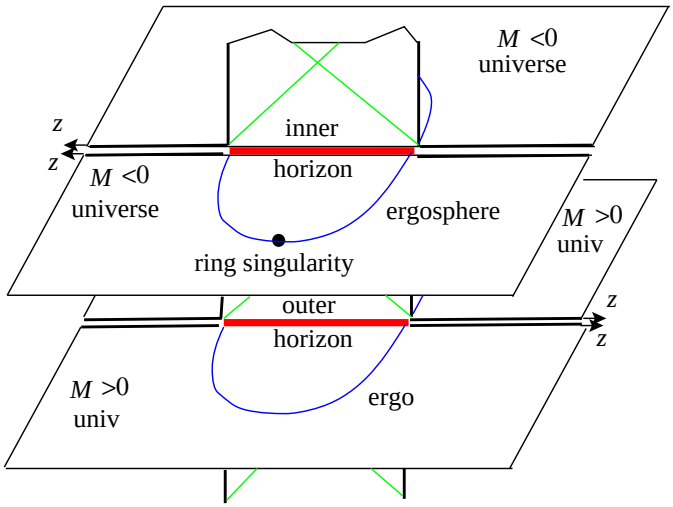

Figure 2.11: The Kerr card diagram.

The black ring

The 5d static black ring solution of [15] is

$$\begin{aligned} ds^2 &= -\frac{F(x)}{F(y)}dt^2 \\ &+ \frac{1}{A^2(x-y)^2}\left[F(x)\Big((y^2-1)d\psi^2 + \frac{F(y)}{y^2-1}dy^2\Big) + F(y)^2\Big(\frac{dx^2}{1-x^2} + \frac{1-x^2}{F(x)}d\phi^2\Big)\right] \end{aligned} \tag{2.10}$$

where $F(x) = 1-\mu x$, $F(y) = 1-\mu y$, and $0 \le \mu \le 1$. The coordinates x, y are 4-focus (including ∞) or C-metric [16, 66, 22, 71] coordinates that parametrize a half-plane

of Weyl space $\rho \geq 0$, $-\infty < z < \infty$:

$$\begin{aligned} \rho &= \frac{1}{A(x-y)^2}\sqrt{F(x)F(y)(1-x^2)(1-y^2)} \\ z &= \frac{(1-xy)(F(x)-F(y))}{2A(x-y)^2} \ . \end{aligned}$$

The foci are on the z-axis at $z = \pm\mu/2A$ and $z = 1/2A$. The black ring horizon is also on the z-axis along $-\mu/2A \leq z \leq \mu/2A$. The ϕ-circle vanishes along $z \leq -\mu/2A$ and $\mu/2A \leq z \leq 1/2A$, and the ψ-circle vanishes along $z \geq 1/2A$. Curves of constant y degenerate to the horizon line segment as $y \to -\infty$, and degenerate to the $(1/2A, \infty)$ ray (better pictured with a conformally equivalent disk) for $y \to -1$. Curves of constant x degenerate to the vanishing ϕ-circle line segment for $x \to 1$ and to the ray $(-\infty, -\mu/2A)$ for $x \to -1$.

The card diagram is easy to construct and is not much different from the four dimensional Schwarzschild case. Past $y = -\infty$ we can go to $y = +\infty$ and hence imaginary $\rho = i\rho'$, and move up a $\mu/A \times \mu/A$ square with two special null lines. At the top of the square, at $y = 1/\mu$ we have the curvature singularity. Continuing again to real ρ and running y down to 1, we map out a (negative-mass) horizontal card. The locus $y = 1$ is the ray $z \geq 1/2A$. The space closes off here as the ψ-circle vanishes, but we formally continue to illustrate how C-metric coordinates run on noncompact vertical cards—this is useful in several applications, such as the Plebański-Demiański solution [72, 73, 74]. Past $y = 1$, we see that for fixed x, reducing y down to x makes a topological half-line in a vertical card with a special null line. Then for $-1 < y < x$, we traverse another vertical card, which we could attach to our original positive-mass horizontal card along $z > 1/2A$ (see Fig. 2.12).

Note that when passing through the black ring horizon at $y = -\infty$, the Weyl conformal factor [15]

$$e^{2\nu} = \frac{1+\mu}{4A}\frac{Y_{23}}{R_1R_2R_3}\sqrt{\frac{Y_{12}}{Y_{13}}}\sqrt{\frac{R_2-\zeta_2}{R_3-\zeta_3}},$$

stays real; $R_3 - \zeta_3$ and Y_{13} go negative. As we pass the special null lines, explicit appearances of R_1 and R_2 in the Weyl functions e^{2U_i}, $e^{2\nu}$ change sign.

The charged ring of [58] is generated by a functional transformation and hence inherits a card diagram structure. In fact, any geometry with $D-2$ Killing directions written in C-metric coordinates has a card diagram.

2.3.2 Charged Witten bubbles and S-branes

The Schwarzschild black hole can be analytically continued to two different time-dependent geometries, the Witten bubble of nothing [36] with a dS_2 element and

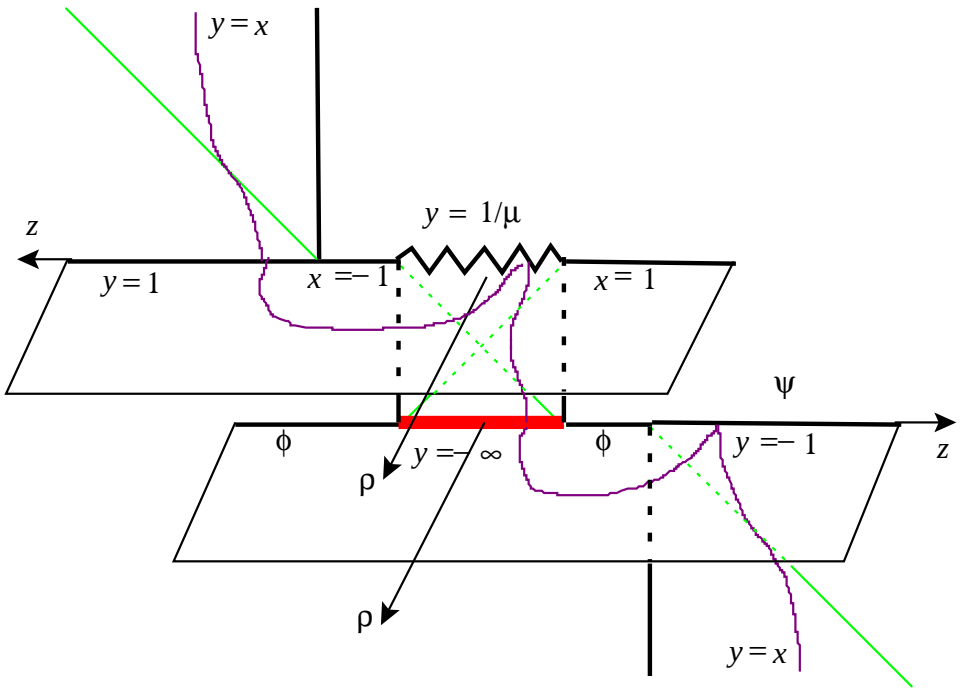

Figure 2.12: An extended card diagram for the black ring, where we have continued past $y =$ constant boundaries for $-1 \leq x \leq 1$. A y-orbit is drawn curving through several cards. Only one of the vertical and horizontal cards are drawn at each four card V-H-H-V card junction to avoid too many overlapping figures.

S-Schwarzschild [42, 43, 44] with an $\mathbf{H}_2$ element, and it is instructive to understand how the card diagram changes.

Unlike the black hole geometries with their unique card diagrams, these geometries can have multiple card diagram representations. Both the bubble and S-Schwarzschild have three different card diagram representations corresponding to three different ways to select Killing congruences. These three types of Killing congruences can be understood by representing $\mathbf{H}_2$ as the unit disk (with its conformal infinity being the unit circle). The orientation-preserving isometries of $\mathbf{H}_2$ are those Möbius transformations preserving the disk, $PSL(2, \mathbf{R})$ [75]. Möbius transformations $z \mapsto \frac{az+b}{cz+d}$ have two complex fixed points, counted according to multiplicity. In the upper half-plane $z = x + i\sigma$ representation, a, b, c, and d are real, so the fixed points are roots of a real quadratic. Hence they may be (i) distinct on the real boundary (hyperbolic), (ii) degenerate on the real boundary (parabolic), or (iii) nonreal complex conjugate pairs, one interior to the upper half-plane $\mathbf{H}_2$ (elliptic). Prototypes of Killing fields are (i) $z \to (1+\epsilon)z$ for the upper half-plane, (ii) $z \to z + \epsilon$ for the upper half-plane; and (iii) $z \to e^{i\epsilon}z$ for the disk $|z| < 1$. These are the striped, Poincaré, and az-

imuthal congruences. In these hyperbolic, parabolic and elliptic representations, the S-Reissner-Nordström (S-RN) and the Witten bubble each have 0, 1, and 2 Weyl foci.

Elliptic representations and extended card diagrams

The bubble of nothing in D dimensions has the interpretation as a semi-classical decay mode of the Kaluza-Klein vacuum. A spatial slice is topologically $S^{D-3} \times \mathbf{R}^2$, where the $\mathbf{R}^2$ is a cigar with the asymptotic-KK S^1 closing at some fixed r, which is an S^{D-3} bubble. As time passes, the bubble increases in size and 'destroys' the spacetime. The solution is obtained as an analytic continuation of a black hole and can be generalized to incorporate gauge fields.

The electrically charged bubble of nothing in its elliptic representation is gotten from (2.6) by sending $t \to ix^4$, $\phi \to i\phi$, and to keep the field strength real we need $Q \to -iQ$. The metric is

$$ds^2 = (1 - \frac{2M}{r} - \frac{Q^2}{r^2})(dx^4)^2 + (1 - \frac{2M}{r} - \frac{Q^2}{r^2})^{-1} dr^2 + r^2(d\theta^2 - \sin^2\theta d\phi^2)$$

At $\theta = 0, \pi$ there are clearly Rindler-type horizons about which we analytically continue θ and obtain the rest of dS_2, $-d\theta^2 + \sinh^2\theta d\phi^2$. These six patches will precisely correspond to the cards of Fig. 2.13.

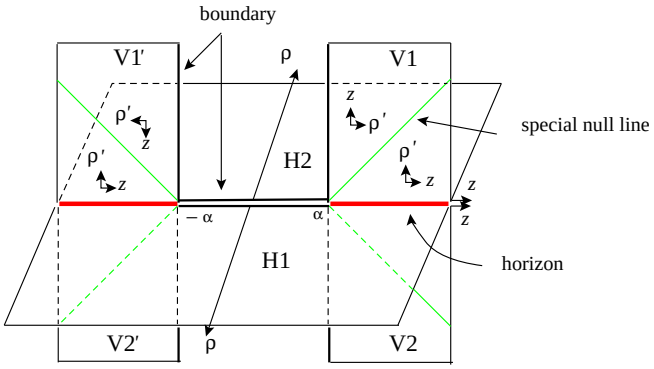

Figure 2.13: The elliptic representation of the non-singular charged Witten bubble contains two horizons and four special null lines. Here, $\alpha = \sqrt{M^2 + Q^2}$.

Let us now turn to the effect of the analytic continuation of the Reissner-Nordström black hole in Weyl coordinates. In Weyl coordinates, the effect of wick rotating $t \to ix^4$ turns the horizon of the Schwarzschild card into an x^4-boundary, while $\phi \to i\phi$ turns the boundaries on the horizontal card into noncompact acceleration horizons along the rays $|z| \geq M$, $\rho = 0$. Sending $\theta \to 0, \pi \pm i\theta$ corresponds to

$\rho \to \pm i\rho'$ along the $|z| \geq \sqrt{M^2+Q^2}$ rays. We find vertical noncompact quarter-plane cards with special null lines along $\rho' = z - M$ for $z \geq M$ and $\rho' = -M - z$ for $z \leq -M$. Each quarter plane is a doubly covered triangle and it is necessary to change branches of the function $R_\pm$ at the null line, as they appear in (2.8).

The elliptic (and as we will shortly see the hyperbolic) representations of the Witten bubble are so trivially obtained because their dS_2 Killing congruences are trivially obtained from those on S^2. Specifically, with $Z = \cos\theta$, $X = \sin\theta\cos\phi$, $Y = \sin\theta\sin\phi$, sending $\phi \to i\phi$, $Y \to iY'$ gives $X^2 - Y'^2 + Z^2 = 1$, or dS_2 with ϕ as an elliptic (azimuthal) congruence. On the other hand, sending $\theta \to \pi/2 + i\theta$, $Z \to iZ'$ gives $X^2 + Y^2 - Z'^2 = 1$, or dS_2 with ϕ as a hyperbolic (striped) congruence.

The S-brane solution of [42, 43, 44]

$$ds^2 = (1 + \frac{2M}{t} - \frac{Q^2}{t^2})(dx^4)^2 - (1 + \frac{2M}{t} - \frac{Q^2}{t^2})^{-1}dt^2 + t^2(d\theta^2 + \sinh^2\theta d\phi^2)$$

can also be gotten from (2.6) by taking $t \to ix^4$, $\theta \to i\theta$, $r \to it$, and $M \to iM$. From (2.7) we see that in Weyl's coordinates we this analytic continuation of RN can be implemented by sending $t \to ix^4$, $z \to i\tau$, $M \to iM$, up to a real coordinate transformation.

The card diagram for elliptic S-RN (Fig. 2.14) has the same structure as the Witten bubble (Fig. 2.13) except that the 6-segment boundary is now $\theta = 0$ where the ϕ-circle vanishes. The right and left horizons are at $t = t_\pm = M \pm \sqrt{M^2+Q^2}$. The $t = 0$ singularity is a hyperbola on the $t_- \leq t \leq t_+$ horizontal cards, $(\rho', \tau) = (|Q|\sinh\theta, -M\cosh\theta)$. Any $Q \neq 0$ gives the same qualitative diagram. The 'smaller' connected universe on the card diagram is the negative-mass version of S-RN. Either sign of the mass gives a universe that is cosmologically singular. The Penrose diagram is given in Fig. 2.15.

In the limit $Q \to 0$, the hyperbola singularity degenerates to cover the horizon at $t = 0$. The two $t > 2M$ vertical cards and two $0 < t < 2M$ horizontal cards then form a positive-mass S-Schwarzschild, while each $t < 2M$ card forms a negative-mass S-Schwarzschild whose singularities begin or end the spacetime.

One can alternatively form the elliptic S-Schwarzschild from the elliptic Witten bubble by performing the γ-flip on any vertical card. This procedure is immediate; the net continuation from Schwarzschild is $\theta \to i\theta$, $g_{\mu\nu} \to -g_{\mu\nu}$, and avoids $r \to it$, $z \to i\tau$, and $M \to iM$.

Note how the card representation of the S-brane is quite different from the black hole card diagram while the Penrose diagrams are related by a simple ninety degree rotation. This is because the card diagram shows the compact or noncompact θ direction.

The elliptic form of the card diagrams show that Schwarzschild S-brane, Witten bubble and Schwarzschild solutions have similar structures and in fact they are all related by γ-flips and trivial Killing continuations.[2] Solutions which are related in this

[2]Perturbed solutions that can only be obtained from $z \to i\tau$ are considered to be less trivial.

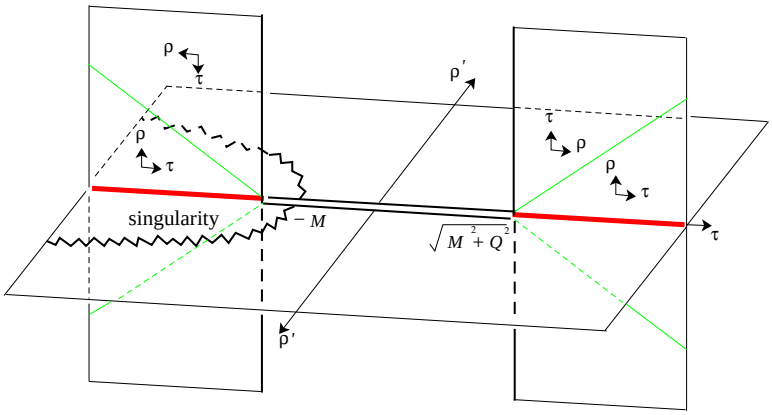

Figure 2.14: The elliptic S-RN card diagram. The singularity is along the hyperbola and it does not intersect the horizons.

manner may be conveniently drawn together in one diagram which simultaneously displays all of their card diagrams. For example in Fig. 2.16 the S-Schwarzschild solution comprises regions $1, 2, 3, 4, 5$, the Witten bubble regions $4, 5, 6$, and the Schwarzschild black hole $6, 7, 8, 9, 10$. Regions $1, 2, 10$ correspond to a singular Witten bubble of negative 'mass.' In this diagram we also see that the unification of the special null lines; we can say $R_+ = 0$ is the long $\diagup$-line and $R_- = 0$ is the long $\diagdown$-line.

The Reissner-Nordström BH/bubble/S-brane solutions cannot be depicted together on such a diagram because $Q \to iQ$ changes $0 < r_- < r_+$ to $r_- < 0 < r_+$. Similar diagrams can be found in [41, 71].

Hyperbolic representations and branch points

The charged Witten bubble can alternatively be obtained from the RN black hole (2.6) by taking $\theta \to \pi/2 + i\theta$ and $t \to ix^4$, $Q \to -iQ$:

$$ds^2 = \Big(1 - \frac{2M}{r} - \frac{Q^2}{r^2}\Big)(dx^4)^2 + \Big(1 - \frac{2M}{r} - \frac{Q^2}{r^2}\Big)^{-1} dr^2 + r^2(-d\theta^2 + \cosh^2\theta d\phi^2) \quad (2.11)$$

Here, θ plays the role of time and $\theta = 0$ is the time where the bubble 'has minimum size.' (This statement has meaning if we break $SO(2,1)$ symmetry.) To achieve this in Weyl's coordinates, we put $z \to i\tau$, $t \to ix^4$, $Q \to -iQ$; the resulting space is equivalent to Witten's bubble by the real coordinate transformation

$$\rho = \sqrt{r^2 - 2Mr}\,\cosh\theta, \qquad \tau = (r - M)\sinh\theta.$$

Thus in Weyl coordinates the only difference between the hyperbolic Witten bubble and the elliptic S-RN is putting $M \to iM$. Witten's bubble universe is represented in Weyl coordinates as a vertical half-plane card, $\rho \geq 0$, $-\infty < \tau < \infty$, where now

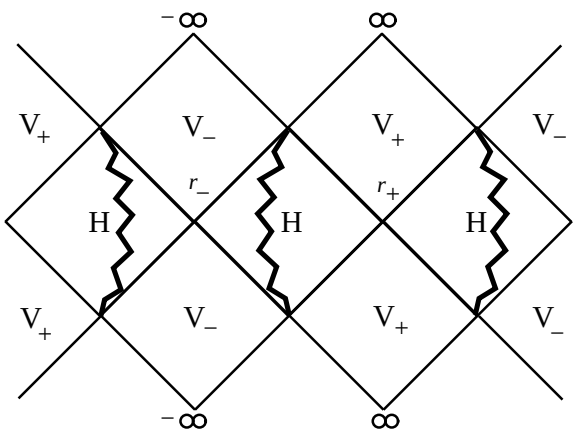

Figure 2.15: The Penrose diagram for S-RN.

the x^4-circle, and not the ϕ-circle, vanishes at $\rho = 0$. Note that the vertical card now has Minkowski signature and is conformal to $-d\tau^2 + d\rho^2$. This vertical card does not have special null lines and is covered only once by the Schwarzschild coordinates. The bubble does have a rod which is along the imaginary τ axis and which intersects the card at the $\rho = 0$, $\tau = 0$ origin. The reason there are no special null lines is that the geometry's foci are at imaginary values $\tau = \pm iM$. The hyperbolic representation of the charged Witten bubble is therefore just a vertical half-plane. In such a case the card diagrams have just as much causal information as a Penrose diagram.

We obtain a hyperbolic representation for S-RN from (2.6) by sending $t \to ix^4$, $M \to iM$, $r \to ir$, $\theta \to \pi/2 + i\theta$, and $\phi \to i\phi$. The fibered directions are now hyperbolic $d\mathbf{H}_2^2 = d\theta^2 + \cosh^2\theta d\phi^2$. In Weyl coordinates, to maintain reality of the solution, we begin with RN (2.8) and send $t \to ix^4$, $\phi \to i\phi$, $M \to iM$, and must explicitly change the branch of the square root introducing the minus sign $R_- \to -R_-$.[3] This has the interpretation of staying on the same horizontal card but rotating the rod in the complex z-plane. The foci are then at $z = \pm i\sqrt{M^2 + Q^2}$, $\rho = 0$ and their special null lines intersect the real half-plane at $z = 0$, $\rho = \sqrt{M^2 + Q^2}$. The half-plane is doubly covered, and we will take $0 \leq \rho \leq \sqrt{M^2 + Q^2}$ as the branch cut. The sign change of R_- has effectively reversed the roles of r and θ so that, after undoing the branch cut with say a square-root conformal transformation, $r = r_+ > 0$ is one boundary-horizon and $r = r_- < 0$ is the other. The hyperbolic angle runs $-\infty < \theta < \infty$.

The doubly-covered half-plane is physically cut into two by the $r = 0$ singularity. At each horizon $r = r_\pm$ we have a four-card junction; the double half-plane horizontal card meets another and two vertical cards. The vertical cards are at $\rho \to \pm i\rho'$ and

[3]The naturalness of this sign change is explained in great detail in [51].

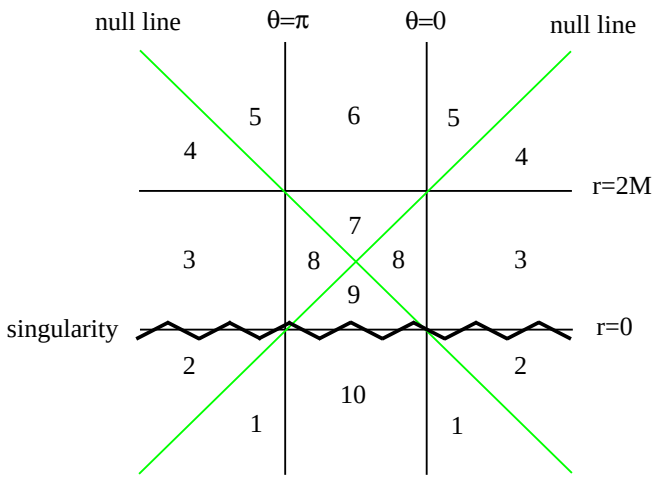

Figure 2.16: The Schwarzschild black hole, Witten bubble and S-Schwarzschild are all related by γ-flips and so their (elliptic) card diagrams may be combined into this one extended diagram.

$-\infty < z < \infty$ and have no special null lines or other features. A full card diagram is shown in Fig. 2.17. Note that there are no boundaries of this card diagram where a spacelike Killing circle vanishes.

Setting $R_\pm = \sqrt{\rho^2 + (z \pm i\sqrt{M^2+Q^2})^2} = 0$ and $R = R_+$, the explicit form of hyperbolic S-RN on the horizontal card is

$$\begin{aligned} ds^2 &= -f(dx^4)^2 + f^{-1}(e^{2\gamma}(d\rho^2 + dz^2) + \rho^2 d\phi^2), \\ f &= \frac{M^2 + Q^2 - (\operatorname{Im} R)^2}{(\operatorname{Im} R + M)^2}, \\ e^{2\gamma} &= \frac{M^2 + Q^2 - (\operatorname{Im} R)^2}{|R|^2}, \\ A &= \frac{Q\, dx^4}{\operatorname{Im} R + M}. \end{aligned} \tag{2.12}$$

We can arrive at this spacetime in a simpler way. Take the RN black hole and continue to get the hyperbolic charged Witten bubbles. These universes are nonsingular for $r \geq r_+$ or $r \leq r_-$. They have boundaries at $r = r_\pm$ where the x^4-circle vanishes. Now, turn these universes on their sides with the γ-flip. We decompactify x^4 and $r = r_\pm$ are now Milne horizons—we are looking precisely at the vertical cards of Fig. 2.17, and they are connected in a card diagram by an $r_- \leq r \leq r_+$ card which is now accessible. We see that generally, vertical half-plane cards parametrized in spherical prolate fashion with no special null lines, when turned on their sides, connect to branched horizontal cards.

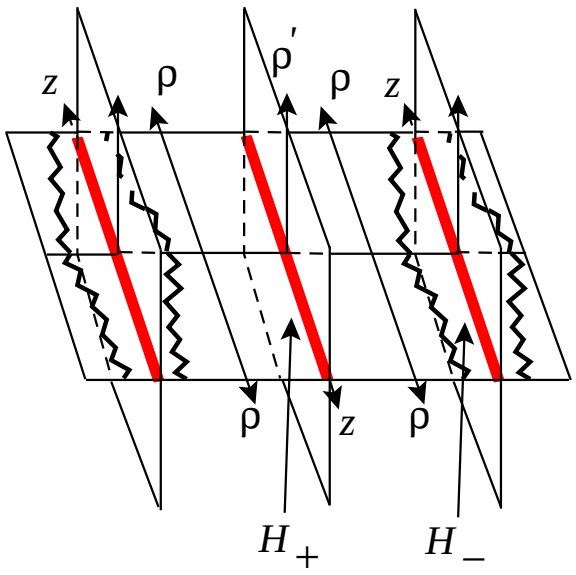

Figure 2.17: Hyperbolic S-RN card diagram after transformation to the W-plane on the horizontal cards. The singularities are closer to the $\mathcal{H}_-$ horizon than to $\mathcal{H}_+$.

The $Q \to 0$ limit (hyperbolic S-Schwarzschild) of the card diagram is easy to picture: The singularities of Fig. 2.17 collapse onto the $r = r_-$ horizon.

One may wonder what happens if we take $z \to i\tau$, on the horizontal card for hyperbolic S-RN, and achieves a vertical card sandwiched between special null lines at $\rho = \sqrt{M^2 + Q^2} + |\tau|$. This must unfold to give a vertical plane with two intersecting special null lines. This card diagram structure is discussed in [51, 67].

Parabolic representations

There is a third way to put a Killing congruence on $\mathbf{H}_2$ or dS_2 using parabolic or Poincaré coordinates. Parametrizing hyperbolic space (which is just Euclideanized AdS_2) as $ds^2 = \sigma^2 dx^2 + \frac{d\sigma^2}{\sigma^2}$, and keeping the Schwarzschild S-brane coordinate r and the usual x^4 we get a Poincaré Weyl representation of S-RN spacetime [29, 42, 43].

It is

$$\begin{aligned} ds^2 &= f(dx^4)^2 - f^{-1}(e^{2\gamma}(-d\rho'^2 + dz^2) + \rho'^2 dx^2), \\ A &= Q dx^4/r, \\ f &= (1 - 2M/r - Q^2/r^2), \\ e^{2\gamma} &= \frac{r^2 - 2Mr - Q^2}{\sigma^2(M^2 + Q^2)}, \\ \rho' &= \sigma\sqrt{r^2 - 2Mr - Q^2}, \\ z &= \sigma(r - M). \end{aligned}$$

In this Weyl representation, ρ' is timelike on $r \geq r_+$ vertical cards which are non-compact 45° wedges, $0 \leq \pm\rho' < z$. This connects along $z > 0$ to an $r_- \leq r \leq r_+$ horizontal card; $r \leq r_-$ vertical cards attaches to $z < 0$. So this is similar to the elliptic representation of S-RN, except the line segment $-\sqrt{M^2 + Q^2} < z < \sqrt{M^2 + Q^2}$ has collapsed and the special null lines are now conformal null infinity (Fig. 2.18). The singularity on the horizontal card is particularly easy to describe in these coordinates. On the first horizontal card it is on a ray $z/\rho = -M/Q$ and on the second card it is on a ray $z/\rho = M/Q$.

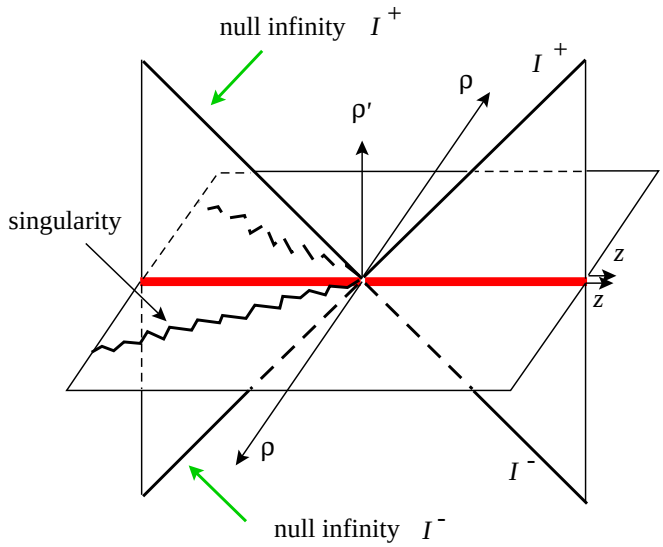

Figure 2.18: The parabolic card diagram representation for S-Reissner-Nordström. The 45° vertical lines represent null infinity.

If we take the $r \geq r_+$ (or $r \leq r_-$) 45° wedges and turn them on their sides via the γ-flip, we get the parabolic version of the $r \geq r_+$ (or $r \leq r_-$) charged Witten bubble. The line which used to be the horizon in the S-brane card diagram becomes

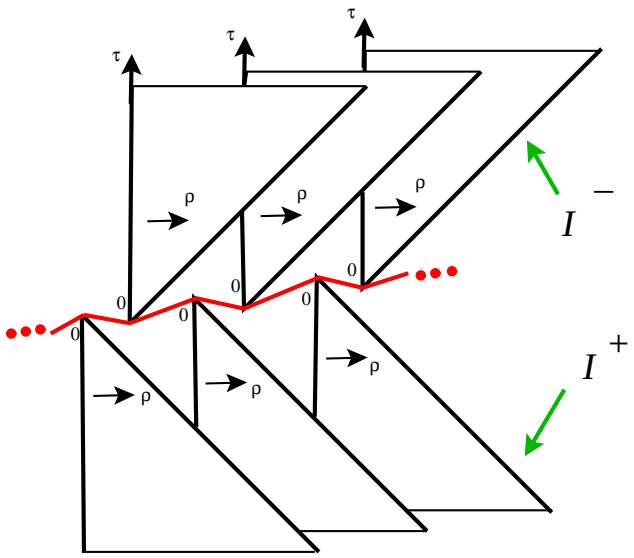

Figure 2.19: The parabolic representation of the Witten bubble contains an infinite number of 45° wedge vertical cards pointing up and down with each wedge joined to two others at the tip in a dS_2 fashion.

a boundary which is the 'minimum volume' sphere, at $\rho = 0$. Time is now purely along the τ direction as in the hyperbolic Witten bubble. The special null line is still $\mathcal{I}^{\pm}$ since $\rho = |\tau|$ corresponds to $r \to \infty$. The vertex of the card is not the end of the spacetime. These wedge cards only represent $\sigma > 0$ and so the card diagram should be extended to $\sigma < 0$. The card diagram is an infinite array of 45° wedge cards pointing up and an infinite number pointing down. The vertex of each upward card is attached to its nearest two downward neighbors (one to the left and one to the right), in the usual dS_2 fashion as shown in Figure 2.19. One can identify cards so only needs one upward and one downward card with two attachments. Although this card diagram is not the most obvious representation of the Witten bubble, it is useful to understand the more complicated S-dihole $\mathcal{U}$, $\mathcal{U}_{\pm}$ universes of [51].

2.3.3 S-Kerr

The twisted S-brane [47], see also [48], is also known as S-Kerr, and is another example of a nonsingular time-dependent solution. It can be obtained from the Kerr black hole using the following card diagram method. Double Killing continue $t \to ix^4$, $\phi \to i\phi$ to achieve a $\mathcal{K}_+$ bubble solution, go to the vertical card via $\theta \to i\theta$, then perform a γ-flip to achieve the S-Kerr. S-Kerr has symmetry group $U(1) \times \mathbf{R}$ and has a unique card diagram. For the parameter range $a^2 < M^2$ there are horizons and the card diagram structure is that of the elliptic S-RN (Fig. 2.14) but is nonsingular. The

foci are at $z = \pm\sqrt{M^2 - a^2}$. The ergosphere lies on the horizontal card and has the same qualitative shape as it does for the Kerr black hole diagram. One can also draw the CTC region. In comparison, the Penrose diagram showing (variably twisted) x^4 and the Boyer-Lindquist coordinate r is shown in Fig. 2.20.

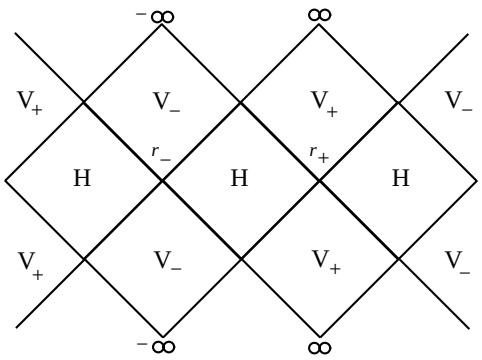

Figure 2.20: Subextremal $a^2 < M^2$ S-Kerr Penrose diagram. $V_\pm$ map to vertical cards of positive and negative 'mass,' while all H diamonds give identical horizontal cards. It is possible to identify cards (say, every other H diamond) so there are only a finite number of regions in the spacetime.

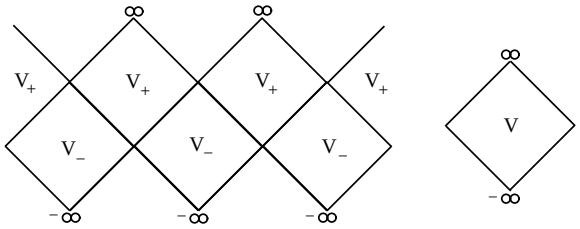

Figure 2.21: The extremal $a^2 = M^2$ (left) and superextremal $a^2 > M^2$ (right) S-Kerr Penrose diagrams.

In the extremal limit $\pm a \to M$, θ-orbits on the vertical card shift up relative to the special null line, and any fixed (r, θ) point is sent above the null line. The region below the null line disappears in this limit and the horizontal card collapses to a point. Furthermore, those geodesics in the upper-right card can only reach the lower-left card (and the same with upper-left and lower-right), splitting the universe into connected 45° wedges just like the parabolic representation for the Witten bubble (Fig. 2.19), where the connections for dS_2 were added for clarity.

The case $a^2 > M^2$ for S-Kerr does not have horizons and can be represented as a single vertical half-plane card with $\rho \geq 0$ and with no special null lines. Just like the

hyperbolic Witten bubble, superextremal S-Kerr can be turned on its side with the γ-flip, to yield a new spacetime [67]. In the limit where $|a| \to \infty$, the θ-orbits flatten out on the card, and the solution becomes flat space.

The Penrose diagrams for extremal and superextremal S-Kerr are given in Fig. 2.21.

2.4 Discussion

In this chapter we have examined the utility of the Weyl Ansatz and constructed an associated card diagram. The card diagram conveniently captures most of the interesting properties of a spacetime including its singularities, horizons, and some aspects of its causal structure and null infinity. Weyl coordinates provide a standard reference against which we can describe geometric features. Card diagrams for families of solutions such as charged and rotating black holes (and bubbles and S-branes) share similar features, change continuously with parameters and help to keep track of various analytic continuations. The only technical issues that arise involve dealing with branches of Weyl distance square-root functions, special null lines, and branched horizontal cards.

Here we give a summary of the solutions we have discussed in this paper. The card diagrams correctly capture the different regions of the charged Reissner-Nordström black hole and its various charged and chargeless limits, and its negative mass complement. We also analyzed the Kerr black hole and its singularity structure. In particular the safe passage through the interior of the ring to the second asymptotic universe through $r = 0$ is clearly depicted.

The Witten bubbles and S-branes each have three card diagrams representations corresponding to the three different choices of Killing congruence on dS_2 or $\mathbf{H}_2$. The elliptic representations has two foci and six cards. S-RN has a cosmological singularity on the horizontal card splitting the card diagram into two connected universes, whereas the charged bubbles are nonsingular. The hyperbolic representations have no foci and hyperbolic S-RN has a branched horizontal card which we fixed by a conformal mapping of the half-plane. Finally the parabolic representation of the bubble is an infinite array of 45° triangle wedges connected pointwise while S-RN had a 6-card butterfly shape. This parabolic representation showcases special null lines serving as null infinity, and this will be useful for us in the investigation of the S-dihole in the next chapter.

S-Schwarzschild can be obtained from the bubble in two ways. One may start with the bubble and analytically continue $M \to iM$ in Weyl coordinates. In this case the hyperbolic/elliptic representation of the bubble maps to the elliptic/hyperbolic representation of the S-brane. There was also a second way to relate these two solutions which we termed the γ-flip and which was conveniently visualized as a flip of the associated cards about a null line. This procedure maintains the number of Weyl foci on the card and so maps the elliptic/parabolic/hyperbolic bubble to the

elliptic/parabolic/hyperbolic S-brane. The γ-flip provides a very simple and interesting way to relate Schwarzschild with its analytic continuations the bubble and the S-brane. In fact all spacetimes related in this way by γ-flips can be simultaneously drawn together in a spherical prolate (or affine) diagram.

Just as we used the γ-flip to turn the hyperbolic Witten bubble on its side and got hyperbolic S-RN, we can take the vertical half-plane card diagrams for the Kerr bubble, dihole wave, superextremal S-Kerr and superextremal S-dihole and apply the γ-flip to yield new spacetimes. These solutions are not identical to any previously described solutions and are described in Chapters 3 and 4.

2.5 Appendix: Perturbed bubbles and S-branes

The chargeless Schwarzschild black hole is easily perturbed as a Weyl solution by adding more rod-horizons, to form Israel-Khan arrays. We can use these solutions to smoothly perturb the Witten bubble in two different ways and also the S-Schwarzschild in two different ways. Addition of charge can be done via Weyl's electrification method [51, 8, 76].

The analytic continuation in Weyl space to obtain the hyperbolic Witten bubble is precisely the same as in [25], except here the Schwarzschild rod crosses $z = 0$. Solutions which are even-in-z Israel-Khan arrays where no rod crosses $z = 0$ can be analytically continued to gravitational wave solutions sourced by imaginary black holes, ie rods at imaginary time. We can thus generalize the Witten bubble by adding additional waves by symmetrically placing more rods in addition to the one which crosses $z = 0$. We dub such an array the 'hyperbolic-perturbed Witten bubble.' As these additional rods are made to cover more of the z-axis and are brought closer and closer to the principal rod, the deformed Witten bubble solution hangs longer with a minimum-radius ϕ-circle. In the limit where rods occupy the entire z-axis, we get a static flat solution, which is Minkowski 3-space times a fixed-circumference ϕ-circle.

The hyperbolic-perturbed Witten bubble can be turned on its side, yielding a hyperbolic-perturbed S-Schwarzschild. It has the card diagram structure of Fig. 2.17.

We can also perturb S-Schwarzschild by adding rods before analytically continuing $z \to i\tau$, $M \to iM$. We dub this the 'elliptic-perturbed S-Schwarzschild.' It is different than hyperbolic-perturbed S-Schwarzschild, and has the card diagram structure of Fig. 2.14. Turned on its side, it yields an elliptic-perturbed Witten bubble, with the card diagram structure of Fig. 2.13. It is different than the hyperbolic-perturbed Witten bubble.

In any of the cases, we can choose to analytically continue the mass parameters of the additional rods or not. Additionally, we can displace some rods in the imaginary z-direction which affects the τ-center of their disturbance. If we do everything in an even fashion, i.e. we respect $\mathrm{Im}\,\tau \to -\mathrm{Im}\,\tau$, the resulting geometry (at real τ) will be real. In particular, rotating a rod at $z > 0$ counterclockwise means rotating its image

at $z < 0$ clockwise. We see in the discussion of the 2-rod example [51] that there may be several choices for branches.

The card diagram techniques allow us to easily construct these two inequivalent families of perturbed Witten bubble and perturbed S-Schwarzschild solutions. These and other multi-rod, S-dihole, and infinite-periodic-universe solutions are described in [51] and cannot be easily described or understood without Weyl coordinates and the construction and language of card diagrams. The nontrivial $z \to i\tau$ continuation is essential.

2.6 Appendix: Electrostatic Weyl formalism

The formalism of [15] can be extended for general D to include an electrostatic potential. This is somewhat surprising since the electromagnetic energy-momentum tensor

$$T_{\mu\nu} = F_{\mu\rho}F_{\nu}{}^{\rho} - \frac{1}{4}g_{\mu\nu}F^2$$

is traceless only in $D = 4$ and so Einstein's equations are more complicated. Nevertheless, a cancellation does occur and one may sum the diagonal Killing frame components of the Ricci tensor to achieve a harmonic condition.

Follow the notation of [15] and add a 1-form potential $A(Z,\overline{Z})dt$ where $t = x^1$ is timelike ($\epsilon_1 = -1$) and all other x^i, $i = 2,\ldots,D-2$ are spacelike (with $\epsilon_i = +1$). The metric takes the form

$$ds^2 = -e^{2U_1}dt^2 + \sum_{i=2}^{D-2} e^{2U_i}(dx^i)^2 + e^{2C}dZd\overline{Z},$$

from which we extract the frame metric

$$g_{\hat{\mu}\hat{\nu}} = \mathrm{diag}(-1,+1,\ldots,+1) \oplus \begin{bmatrix} 0 & 1/2 \\ 1/2 & 0 \end{bmatrix}.$$

For $F = dA$ we have $F_{\hat{Z}\hat{t}} = -F_{\hat{t}\hat{Z}} = \partial A\, e^{-U_1-C}$ and $F_{\hat{\overline{Z}}\hat{t}} = -F_{\hat{t}\hat{\overline{Z}}} = \overline{\partial}A\, e^{-U_1-C}$, all other components vanishing. We compute $F^2 = -8\partial A\overline{\partial}A\, e^{-2U_1-2C}$ and

$$\begin{aligned}
T_{\hat{t}\hat{t}} &= 2\partial A\overline{\partial}A\, e^{-2U_1-2C} \\
T_{\hat{i}\hat{i}} &= 2\partial A\overline{\partial}A\, e^{-2U_1-2C} \quad (i \neq 1) \\
T_{\hat{Z}\hat{Z}} &= -(\partial A)^2 e^{-2U_1-2C} \\
T_{\hat{\overline{Z}}\hat{\overline{Z}}} &= \overline{T_{\hat{Z}\hat{Z}}} \\
T_{\hat{Z}\hat{\overline{Z}}} &= 0.
\end{aligned}$$

The field equations are $R_{\hat{\mu}\hat{\nu}} - \frac{1}{2}g_{\hat{\mu}\hat{\nu}}R = T_{\hat{\mu}\hat{\nu}}$; taking the trace, we get

$$R = -\frac{4(D-4)}{D-2}\partial A\overline{\partial}A\, e^{-2U_1-2C}$$

and Einstein's equations are then

$$R_{\hat{\mu}\hat{\nu}} = T_{\hat{\mu}\hat{\nu}} - \frac{2(D-4)}{D-2} g_{\hat{\mu}\hat{\nu}} \partial A \overline{\partial} A \, e^{-2U_1 - 2C}. \tag{2.13}$$

Form the sum $\sum_{i=1}^{D-2} R_{\hat{i}\hat{i}} \epsilon_i$; the right side of (2.13) gives

$$(D-4) 2 \partial A \overline{\partial} A \, e^{-2U_1-2C} - \frac{2(D-4)}{D-2}(D-2) \partial A \overline{\partial} A \, e^{-2U_1-2C} = 0.$$

Hence (following (2.4)-(2.5) of [15]) we get

$$\partial \overline{\partial} \exp\left(\sum_{i=1}^{D-2} U_i \right) = 0,$$

the Weyl harmonic condition.

One can add magnetostatic potentials along spatial Killing directions as well. We skip remaining details and give the equations. Let us assume x^1 is timelike and x^i are spacelike for $i = 2, \ldots, D-2$, the potential is $A_1 = \sum_{i=1}^{D-2} A_i dx^i$, and the metric is $ds^2 = -e^{2U_1}(dx^1)^2 + \sum_{i=2}^{D-2} e^{-2U_i}(dx^i)^2 + e^{2\nu}(d\rho^2 + dz^2)$ and $w = \rho + iz$, $\partial_w = \frac{1}{2}(\partial_\rho - i\partial_z)$. Einstein's equations are

$$\begin{aligned}
\Delta U_1 &= \frac{1}{2}\Big(\sum_{i=1}^{D-2} (\nabla A_i)^2 e^{-2U_i} + \frac{D-4}{D-2} \sum_{i=1}^{D-2} (\nabla A_j)^2 e^{-2U_i}, \\
\Delta U_k &= \frac{1}{2}\Big(- (\nabla A_1)^2 e^{-2U_1} - (\nabla A_k)^2 e^{-2U_k} + \sum_{i \neq k,1} (\nabla A_i)^2 e^{-2U_i} \\
&\qquad - \frac{D-4}{D-2} \sum_{i \neq 1} (\nabla A_i)^2 e^{-2U_i} + \frac{D-4}{D-2} (\nabla A_1)^2 e^{-2U_1} \Big),
\end{aligned}$$

and

$$\partial_w \sum_{i=1}^{D-2} \nu = -2\rho \Big(\sum_{i<j} \partial_w U_i \partial_w U_j + \frac{(\partial_w A_1)^2 e^{-2U_1}}{2} - \sum_{i=2}^{D-2} \frac{(\partial_w A_i)^2}{2} e^{-2U_i} \Big).$$

Maxwell's equations are

$$\nabla \cdot \big(\nabla A_i e^{-2U_i} \big).$$

All Laplacians and divergences are with respect to a flat 3d axisymmetric auxiliary space with coordinates ρ, z.

2.7 Appendix: Möbius transformations on horizontal and vertical cards

Weyl's canonical coordinates on a horizontal half-plane card have

$$f_t f_\phi = \rho^2 \tag{2.14}$$

with conformal element $d\rho^2 + dz^2$. (For Weyl-Papapetrou, we set $\rho^2 = -\det_{2\times 2} g_{\alpha\beta}$.) This has the Möbius symmetries of translation $z \to z + \epsilon$ as well as uniform rescaling $(\rho, z) \to (1+\epsilon)(\rho, z)$, if we allow Killing rescaling. There is a third (elliptic) generator of $PSL(2, \mathbf{R})$ that does not leave (2.14) invariant and it is a rotation in the conformally equivalent disk picture. If we let $W = \frac{Z-1}{Z+1}$, $\tilde{W} = e^{i\alpha} W$, and $\tilde{Z} = \frac{1+\tilde{W}}{1-\tilde{W}}$, then with $Z = \rho + iz$, $\tilde{Z} = \tilde{\rho} + i\tilde{z}$, we have

$$\begin{aligned} \tilde{\rho} &= \frac{4\rho}{(2-2\cos\alpha)(\rho^2+z^2) + 2 + 2\cos\alpha + 4z\sin\alpha} \\ \tilde{z} &= \frac{2\sin\alpha(-1+\rho^2+z^2) + 4z\cos\alpha}{(2-2\cos\alpha)(\rho^2+z^2) + 2 + 2\cos\alpha + 4z\sin\alpha}. \end{aligned} \tag{2.15}$$

One might ask how it affects vertical (say square) cards and special null lines. So put $\rho = i\rho'$, $\tilde{\rho} = i\tilde{\rho}'$ in (2.15). The point $0 \mapsto -i\tan\alpha/2$ and one can check that $\rho'^2 = z^2$ then maps to $\tilde{\rho}'^2 = (\tilde{z} + i\tan\alpha/2)^2$, so special null lines are preserved. Square vertical cards with their two intersecting special null lines, being built from four copies of a 45-45-90 triangle, are thus also preserved assuming their base does not then touch $\tilde{Z} = \infty$; but they are scaled in size.

This α-rotation maps $Z = \infty \mapsto \tilde{z}_\infty$. Spherical prolate coordinates are degenerate at ∞ and their α-rotation is then degenerate at $\tilde{z}_\infty$.

Take for example the elliptic Witten bubble card diagram with rod endpoints $z_\pm \pm M = 0$, and α-rotate it for some small $\alpha > 0$. The degenerate point $\tilde{z}_\infty$ emits special null lines that serve as $\mathcal{I}^\pm$ (see Fig. 2.22). So no new interior special null lines are generated in this process. The special null line from $\tilde{z}_-$ goes and meets the left $\mathcal{I}^\pm$ null line. The 45-45-90 triangle with base $\tilde{z}_- \le z \le \tilde{z}_\infty$ is unfolded just once across the $\tilde{z}_-$ null line to form a larger 45-45-90 triangle with horizontal and vertical legs and a null $\mathcal{I}^+$ hypotenuse. This interesting card structure could also occur as the double Killing rotation to E-brane solution [77] of a two charged-BH solution where just one is extremal.

Now there is the issue of the $z > \tilde{z}_\infty$ and $z < \tilde{z}_+$ horizons and their vertical cards, which are connected across $\tilde{z} = \infty$ which is not infinitely far away. We note the totality of the vertical-cards region must have the features of the already-drawn $\tilde{z}_- < \tilde{z} < \tilde{z}_\infty$ region: a vertical boundary, a null boundary, and a special null line that meets the null boundary. To complete this, we need two additional cards (Fig. 2.23). This figure shows a compactification of four vertical cards to see how they attach to

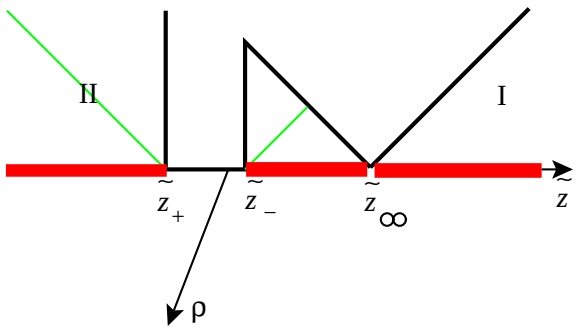

Figure 2.22: Möbius-transformed bubble. This is not the whole spacetime; there are additional vertical cards that connect the $\tilde{z} > \tilde{z}_\infty$ and $\tilde{z} < \tilde{z}_+$ vertical card regions.

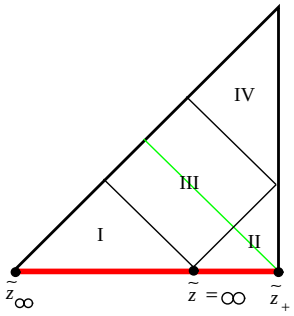

Figure 2.23: A compactified representation of the vertical cards in the $\tilde{z}$ coordinate for the $-\infty < z < z_+$ vertical card of the original elliptic Witten bubble. The lower two triangles are the cards shown in Fig. 2.22. Region III is half of a vertical full-plane card with two special null lines; the spacetime lies to the lower-right of the $\diagup$ null line. Region IV is a vertical wedge with a vertical boundary.

each other. New card III, uncompactified, is everything below a null boundary on a vertical plane, and new card IV, uncompactified, is a 45° wedge with a vertical and null boundary. We wee that card diagrams, though unwieldy, are sufficient for these Möbius-transformed card coordinates.

Real Möbius transformations preserve intersections of the lines and circles with the boundary, including the point at infinity. Those curves normally intersecting the boundary can be continued to vertical lines and hyperbolas which are asymptotically null; on vertical cards then, the action of Möbius transformations preserves this set.

2.8 Appendix: Extension of card diagrams and the notion of Weyl spacetime

History has shown increased applicability of Weyl techniques and card diagrams to a more general class of spacetimes. The original 1917 work expanded with Papapetrou [14], Emparan and Reall [15], and Harmark [16]. The idea was to look at Einstein's equations and use a harmonic condition to find special coordinates, namely $\rho^2 = -\det_{(D-2)\times(D-2)} g_{\alpha\beta}$. The ensuing card diagram description, which includes vertical card regions and attachments, came in 2004-2006. The main obstacle to the extension of the whole program was that the analytical techniques were not compatible with a nonzero cosmological constant.

We write the Einstein equation with cosmological constant Λ in D dimensions as $R_{\mu\nu} = (D-1)\Lambda g_{\mu\nu}$. Then following [15], in the static case we have

$$R_{i\hat{j}} = -2e^{-2C}\Big(2\partial\overline{\partial}U_i + \partial U_i \sum_k \overline{\partial}U + k + \overline{\partial}U_i \sum_k \partial U_k\Big)\epsilon_i\delta_{ij},$$

and $g_{\hat{i}\hat{j}} = \epsilon_i\delta_{ij}$. Summing $i = 1, \ldots, D-2$ of Einstein's $R_{\hat{i}\hat{i}} = (D-1)\Lambda g_{\hat{i}\hat{i}}$ gives

$$-2e^{-2C}e^{-\Sigma_i U_i}\partial\overline{\partial}\big(e^{\Sigma_i U_i}\big) = (D-1)(D-2)\Lambda.$$

The RHS is nonzero and we cannot conclude that $e^{\Sigma_i U_i}$ is harmonic. Thus the Weyl formalism which worked in [15] does not hold for $\Lambda \neq 0$.

In spite of this, it seemed clear that for certain spacetimes with $D-2$ symmetries, one could still change to Weyl-type coordinates and construct card diagrams with well-behaved properties, without regard for Einstein's field equations. The idea of the card diagram was axiomatized and it is merely assumed that a horizontal card (stationary) region of a spacetime can have its non-Killing 2-metric conformally mapped to the half-plane, or a multiple branched cover of the half-plane. It is also a requirement that all closures of Killing directions, spacelike or timelike, occur at the boundary of that half-plane. The half-plane admits a group of symmetries $PSL(2,\mathbf{R})$, and so the Weyl coordinates (ρ, z) are well-defined for the given Killing$\oplus$non-Killing representation of the metric, up to this group. One then continues onto vertical cards and hopes for ensuing good properties of the card diagram. (As we saw in the previous Appendix, the elliptic generator of $PSL(2,\mathbf{R})$ acts on vertical cards in an interesting way.)

This was first applied to (A)dS$_4$ and (A)dS$_5$, each of which has non-minimal Killing symmetry and thus admits many different card diagram representations. A simple change of coordinate reverted the $dr^2/(1 \pm r^2)$ piece to Reissner-Nordström-like form, and then into spherical prolate and card diagram coordinates. Examples of the simplest forms of these spaces are shown in the appendix to Chapter 5. Furthermore, various AdS orbifolds [78] will be compatible with certain card diagram structures. However, not all putative card representations of AdS space yield good card diagrams—ensuing vertical cards can have horizon loci which are not at $\rho = 0$

(such as the Kruskal representation of the AdS_5 constant curvature black hole of [79] and Chapter 6). For standard card diagrams, setting $\rho^2 = -\det g_{\alpha\beta}$ for the Killing submetric ensures the horizons always occur at $\rho^2 = 0$, but after relaxing this condition, it is not clear why some card diagram attempts succeed and others fail.

It was also eminently clear that any metric writable in C-metric (or black ring [57, 58]) coordinates [22, 71, 66, 16, 55] would have a card diagram description, which follows Fig. 2.12. The C-metric Ansatz involves a piece

$$dZ^2/p(Z) - dC^2/p(C),$$

where p is a polynomial of fourth degree or less. (Missing degrees can be reinterpreted as extra zeros at infinity. In the case of $\Lambda \neq 0$, the condition degree ≤ 4 is tied to the condition $R =$constant [80].) For p of degree 2 with distinct roots, this reduces to spherical prolate coordinates; for p of degree 3 with distinct roots, this gives us standard black ring coordinates with a single zero at infinity. The order of the zero of p, if one or two, translates in the card diagram to the appearance of a vertical card: there is a 90° turn from the horizontal boundary, or a 45° turn, respectively. The key limitation in the C-metric Ansatz is that there is a symmetry exchanging C and Z in the conformal 2-metric; each uses the same polynomial p.

The next extension of card diagram applications would then be the famous 7-parameter Demiański-Plebański solution [72, 73, 74, 1] in 4d (with a mass, nut, cosmological constant, electric charge, magnetic charge, spin and boost parameter):

$$\begin{aligned} ds^2 &= (1-pq)^{-2}\Big((p^2+q^2)\big(\frac{dp^2}{X(p)} + \frac{dq^2}{Y(q)}\big) + \frac{X(d\tau + q^2 d\sigma)^2}{p^2+q^2} - \frac{Y(d\tau - p^2 d\sigma)^2}{p^2+q^2}, \\ & X(p) = (-g^2 + \gamma - \Lambda/6) + 2lp - \epsilon p^2 + 2Mp^3 - (e^2 + \gamma + \Lambda/6)p^4, \\ & Y(q) = (e^2 + \gamma - \Lambda/6) - 2Mq + \epsilon q^2 - 2lq^3 + (g^2 - \gamma - \Lambda/6)q^4, \\ \Phi_{\text{Ernst}} &= (e+ig)/(q+ip). \end{aligned}$$

Also in five dimensions, we could try to extend card diagrams to spinning or charged black holes in 5d with a cosmological constant [81, 82]. These all involve metrics with non-Killing piece of the form $dZ^2/p(Z) + dC^2/q(C)$, where p and q are different polynomials. These spacetimes, at least naively, *will admit* a card diagram description, and the description is unique up to the $PSL(2,\mathbf{R})$ symmetry. The construction follows: Integrate

$$d\zeta = dZ/\sqrt{p(Z)} \tag{2.16}$$

and $d\theta = dC/\sqrt{q(C)}$, so the non-Killing metric is $\propto d\zeta^2 + d\theta^2$. If p and q have simple zeros, then (ζ, θ) form a finite-sized rectangle. The map from a rectangle to the half-plane is given by the Schwarz-Christoffel transformation [83],

$$f'(z) = \frac{A}{(z-z_1)^{1/2}(z-z_2)^{1/2}(z-z_3)^{1/2}}, \tag{2.17}$$

where A is a constant, and is unique up to $PSL(2,\mathbf{R})$. This gives $\zeta(\rho,z)$ and $\theta(\rho,z)$ directly; the pre-image points of the Schwarz-Christoffel transformation become the locations on the z-axis which serve as vertices in the card diagram. Two of them may be chosen arbitrarily (say $z_1=-1$, $z_2=+1$), and the third's location is nontrivial; it is tied to the shape of the $\zeta\theta$ rectangle. Solving the integral equation for z_3 in general is hard; in the C-metric case of $p=q$ it has already been solved for because the same square root appears in (2.16) and (2.17).

We can then write the metric in Weyl form (there is no need to do the difficult inversion of the Schwarz-Christoffel transformation). The metric is rewritten in terms of ρ, z and the vertices z_i, and all instances $z-z_i$ can be eliminated in favor of $R_i=\sqrt{\rho^2+(z-z_i)^2}$; there is perhaps no unique way to do this. One then hopes that $e^{2\gamma}$, the coefficient of $d\rho^2+dz^2$ has simple poles in all the R_i, which would result in a γ-flip for vertical cards as one approaches special null lines, just like for ordinary card diagrams. One also hopes that Killing closure or horizon loci occur only at $\rho^2=0$.

Apart from a graphical representation of the spacetimes, which would aid in understanding their global structure (for example, the strange nature of the Kerr-AdS$_5$ bubble, described in Chapter 6), these Weyl coordinates may give a clue as to a reformulation of the elliptic system of Einstein-Maxwell-Λ (or supergravity) equations. The nonlinear equations could be understood as being sourced on the boundary $\rho=0$, and being solved on an auxiliary axisymmetric 3-space. This new understanding could possibly lead to finding multi-object axisymmetric solutions in the given theory.

It remains to be seen whether the card diagrams for Demiański-Plebański solutions and black holes in AdS$_5$ can be completed in general, and whether the new coordinates give a useful new way to understand or solve the field equations.

Chapter 3

S-dihole

We construct a variety of S-brane solutions from the black dihole geometry. We look at the complexified spacetimes and the global structure of real sections. Spherical prolate, card, and Penrose diagrams are used to depict all spacetimes. These spacetimes have complicated yet understandable structure and many interesting features. The solutions admit several scaling limits to Melvin, S-Melvin, asymptotic cones, and a surprising near-vertex limit to a charged expanding bubble. The expanding bubble is related via Bonnor transformation to flat space in a special coordinate system, at the north pole of the Kerr horizon. All systems of extremal 4d black holes, when dilatonized, lift to D6-$\bar{\text{D}}$6 systems in M-theory.

This chapter is based on a forthcoming paper with John E. Wang, and much of the material has already been published in `hep-th/0409070`. The e-print `hep-th/0409070` also contains a generalization to infinite arrays and a periodic-in-time universe.

3.1 Introduction

S-branes have been a topic of interest in the last several years, both in string theory and its supergravity limit. Sen's construction [26] of BPS and non-BPS branes as solitons inside larger-dimension branes and the Gutperle/Strominger extension to the timelike case [29] show the existence of these objects in string theory, as purely spacelike-extended analogs of ordinary (timelike-extended) branes. References include [27, 28, 42, 43, 44, 45, 46, 52, 48, 50, 84].

The closed string or gravitational description of these S-branes (valid at small string coupling and small curvature) gives a cosmological evolution of a universe, either nonsingular or possibly with some singularity behind one, or two or more horizons. Time-dependent gravitational solutions, like S-branes and expanding bubbles [36, 37, 38, 39, 40, 41, 85, 86, 87, 61], are often related to stationary-exterior solutions [88] by double analytic continuation. The continued directions need not be Killing, and the complexified manifold with a time-dependent real section will have interesting

structure (such as sources for the wave equation) off the real section.

For D-dimensional spacetimes with $D-2$ commuting Killing vectors, the Weyl formalism [8, 15] and card diagrams [89] are the standard technique to represent these spacetimes and follow the analytic continuations. In [89], card diagrams were given for the Kerr black hole and can be easily constructed for the Kerr bubble and S-Kerr spacetimes. Under the Bonnor transformation [12, 13, 1], which maps a stationary vacuum solution to a magnetostatic solution in 4d, these solutions are mapped to the black dihole [12, 69, 70], dihole wave [25], and new S-dihole solutions. Specifically, in the subextremal case we find three nonsingular solutions $\mathcal{U}$, $\mathcal{U}_\pm$ with purely vertical cards, and three solutions $\mathcal{E}$, $\mathcal{E}_\pm$ with horizontal and vertical cards, and an 'ergosphere' singularity. In the superextremal case, we find a nonsingular vertical-card solution, and also find that solution 'turned on its side' via the γ-flip [89].

The S-dihole $\mathcal{U}$-type and $\mathcal{E}$-type universes admit several scaling limits, which help us give their physical interpretation. We find early- and late-time flat limits, large-distance asymptotic conical deficits, near-origin limits to Melvin or S-Melvin (Melvin on its side), a near-special null line intersection flat limit, and a surprising near-vertex limit to the Reissner-Nordström (RN) bubble.

These Kerr-type solutions have an algebraic simplicity: Their card diagrams are intimately related to spherical prolate coordinates, and then affine coordinates for the complexified non-Killing manifold $\mathbb{C}^2 \subset \mathbb{P}^1 \times \mathbb{P}^1$. We investigate the role of (degree 1 and 2) complex hypersurfaces such as ergospheres, ring singularities, and Killing-degenerate (horizon) loci. The Bonnor transform maps ergospheres to 'ergosphere singularities' and the rigid properties of these singularities are described, along with the fact that their intersection with $\rho^2 = 0$ generates extremal black holes or sources at imaginary time.

This paper is organized as follows. In Section 2, we give the Kerr solution and its Bonnor transform, the black dihole. In Section 3, we review the dihole wave solution and its scaling limits. In Section 4, we write down the S-dihole geometry generally, and then analyze the subextremal case. This yields six universes, and we investigate their scaling limits. The superextremal case is then investigated. We compute S-charge when possible, discuss global structure, and give a prescription for writing the solutions in terms of Weyl distance functions with branch choices. In Section 5, we relate the Bonnor transformation to KK reduction, discuss the nontrivial nature of its application, and lift certain solutions to D6-brane solutions of IIA string theory and M-theory. In Section 6, we give conclusions.

Appendix 3.7 features the dihole wave and superextremal S-dihole turned on their sides. Appendix 3.8 discusses hypersurfaces in the complexified non-Killing manifold. Appendix 3.9 compares the Bonnor transforms of ergospheres and ring singularities. Lastly, Appendix 3.10 analyzes the wave propagation of the dihole wave in Weyl coordinates.

3.2 Kerr, Bonnor transformation, and dihole

The 4d Kerr black hole in Boyer-Lindquist coordinates is

$$\begin{aligned} ds^2 &= -\frac{\Delta}{\Sigma}(dt - a\sin^2\theta d\phi)^2 + \frac{\sin^2\theta}{\Sigma}(a\,dt - (r^2+a^2)d\phi)^2 \\ &\quad +\Sigma(\frac{dr^2}{\Delta} + d\theta^2), \end{aligned}$$

where $\Delta = r^2 - 2Mr + a^2$ and $\Sigma = r^2 + a^2\cos^2\theta$. This solution has symmetry group $\mathbf{R}\times U(1)$ and hence qualifies as Weyl-Papapetrou (a stationary axisymmetric vacuum solution) [14, 16, 17]. Setting

$$\rho = \sqrt{r^2 - 2Mr + a^2}\sin\theta, \qquad z = (r-M)\cos\theta,$$

the solution can be written in Weyl-Papapetrou form

$$ds^2 = -f(dt + \omega d\phi)^2 + f^{-1}(e^{2\gamma}(d\rho^2 + dz^2) + \rho^2 d\phi^2). \tag{3.1}$$

The formulas for the functions are in [51, 89]. The Kerr black hole has a card diagram, drawn in [51, 89]; for the subextremal case, the foci are at $z = \pm\sqrt{M^2 - a^2}$. There is a nonsingular 'ergosphere' locus where $g_{tt} = 0$ or $\Sigma - 2Mr = 0$; this appears as a semicircle-like locus on each horizontal card. There is also a ring singularity at $\Sigma = 0$ which appears as a point on the negative-mass horizontal card, and a region of CTCs on that card.

Bonnor [12, 13] gave a transformation from a Weyl-Papapetrou metric to a magnetically charged static Weyl metric[1]. The Bonnor transformation takes the Weyl-Papapetrou (3.1) to the magnetostatic Weyl

$$\begin{aligned} ds^2 &= -f^2 dt^2 + f^{-2}(e^{8\gamma}(d\rho^2 + dz^2) + \rho^2 d\phi^2), \\ A &= B(\rho, z)d\phi, \end{aligned} \tag{3.2}$$

where $\omega = iB$ and ω is proportional to a parameter (a in the case of Kerr) which must be analytically continued to make B real.

The black magnetic dihole [12, 69, 70] is the Bonnor transform of Kerr. For any $M > 0$ and $a \neq 0$ it represents two oppositely charged, extremal (degenerate horizon) black holes[2] We can write it in the inherited Boyer-Lindquist coordinates as

$$\begin{aligned} ds^2 &= \big(1 - \frac{2Mr}{\Sigma}\big)^2\Big(-dt^2 + \frac{\Sigma^4}{(\Delta + (a^2+M^2)\sin^2\theta)^3}\big(\frac{dr^2}{\Delta} + d\theta^2\big)\Big) + \frac{\Delta\sin^2\theta}{(1-\frac{2Mr}{\Sigma})^2}d\phi^2 \\ A &= \frac{2aMr\sin^2\theta}{\Delta + a^2\sin^2\theta}d\phi \\ \Delta &= r^2 - 2Mr - a^2, \qquad \Sigma = r^2 - a^2\cos^2\theta\ . \end{aligned} \tag{3.3}$$

[1]For electromagnetic Weyl solutions, see [8, 76] or appendices of [51, 89].

[2]For $a = 0$ the solution degenerates to the singular vacuum Darmois solution [1]. For $M = 0$, the solution is again vacuum, and flat, though in general a Bonnor transform of flat space is not flat.

The black hole horizons appear at $z = \pm\sqrt{M^2 + a^2}$, $\rho = 0$ on the Weyl half-plane. For $\phi \simeq \phi + 2\pi$, there is a conical excess strut on the z-axis between the horizons; one can recompactify ϕ to eliminate this in favor of conical deficit strings for $|z| > \sqrt{M^2 + a^2}$. We will see that generally, Bonnor transforms of ergospheres $g_{tt} = 0$ are singular when on the interior of cards, but here the ergosphere $\Sigma - 2Mr = 0$ only intersects the Weyl half-plane at the horizons, and is in fact responsible for them. If one passes through the extremal black hole horizon at $z = \pm\sqrt{M^2 + a^2}$, one must change the sign of $R_\pm$ in the Weyl form of the dihole solution [54, 51], and the $\Sigma = 0$ 'ring singularity' gives the black hole singularity in the ensuing horizontal card.

Since the horizon function $\Delta(r) = r^2 - 2Mr \pm a^2$ with roots $r = r_\pm$ is quadratic for Kerr/dihole, the Weyl coordinates (and card diagrams) for these solutions are intimately related to the spherical prolate coordinates. We will draw spherical prolate diagrams to show different regions of the complexified spacetime. For dihole (M^2+a^2) or subextremal Kerr ($M^2 - a^2$), define

$$r - M = \sqrt{M^2 \pm a^2}Z, \qquad Z = \pm\cosh\zeta,\ \cos\zeta$$

and set $C = \cos\theta$, allowing $\theta \to i\theta$ and $\theta \to \pi + i\theta$ to give $C = \pm\cosh\theta$. Then Z and C are real variables with the lines $Z = \pm 1$ ($r = r_\pm$), $C = \pm 1$ ($\theta = 0, \pi$) distinguished. In Weyl coordinates,

$$\rho^2 = (M^2 \pm a^2)(Z^2 - 1)(1 - C^2),$$

so $Z, C = \pm 1$ correspond to $\rho^2 = 0$.[3] The 2-metric is conformal to $\pm d\zeta^2 + d\theta^2 \propto \frac{dZ^2}{Z^2-1} - \frac{dC^2}{C^2-1}$.[4] When both $|Z|, |C| \geq 1$ or both are ≤ 1, these are vertical card (time-dependent) regions. We know from card diagrams that these regions are cut into triangles by special null lines (see Figs. 3.1-3.2).

The spherical prolate diagram for subextremal Kerr is drawn in Fig. 3.1, and shows $\rho^2 = 0$, special null lines, the ergosphere, and the ring singularity. Due to the $C \to -C$ symmetry, regions IV and IV$'$ are identical, etc. The Kerr black hole occupies regions I, II, III. The subextremal S-Kerr of [47] occupies regions IV, V, and VI.

The spherical prolate diagram for the dihole is drawn in Fig. 3.2. The region exterior to both black holes is I, regions exterior to one but interior to another are II and III, and the region interior to both is IV.

Some discussion of these singularity loci are given in Appendix 3.8 and 3.9.

[3] We remind the reader that $\rho^2 = -\det_{2\times 2} g_{\alpha\beta}$ and that this is invariant under Bonnor transformation.

[4] Spherical prolate coordinates are a special case of C-metric coordinates; see [72, 22, 16] and references therein. Our spherical prolate diagrams are analogs of C-metric diagrams in [71]. Complex $\zeta \in \cos^{-1}[\mathbb{R}]$ is the basis for the skeleton diagrams of [41].

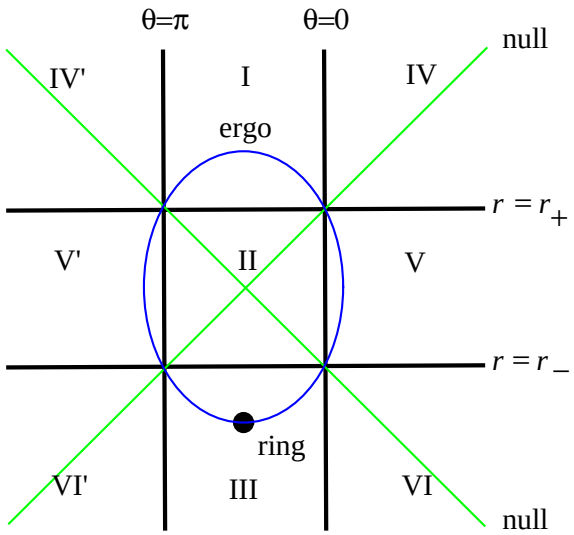

Figure 3.1: The spherical prolate diagram for the Kerr black hole. The ergosphere, ring singularity, and special null lines are labelled.

3.3 Dihole wave

Before deriving and discussing the new S-dihole solutions, we review the dihole wave solution of [25]. It is gotten from the dihole (3.3) by sending $t \to ix^4$, $\theta \to \pi/2 + i\theta$. Then $\Sigma = r^2 + a^2 \sinh^2\theta$, and shifting A_ϕ to remove the Dirac string, the solution is

$$\begin{aligned} ds^2 &= \big(1 - \frac{2Mr}{\Sigma}\big)^2 \Big((dx^4)^2 + \frac{\Sigma^4}{(\Delta + (a^2+M^2)\cosh^2\theta)^3} \big(\frac{dr^2}{\Delta} - d\theta^2\big)\Big) \\ &\quad + \frac{\Delta \cosh^2\theta}{(1 - \frac{2Mr}{\Sigma})^2} d\phi^2 \\ A &= \Big(\frac{2aMr\cosh^2\theta}{\Delta + a^2\cosh^2\theta} - \frac{2Mr_+}{a} \Big) d\phi \ . \end{aligned} \tag{3.4}$$

Periodically identifying $\phi \simeq \phi + 2\pi a^4/(M^2+a^2)^2$ eliminates the conical singularity at $r = r_+$. The analytic continuation $\theta \to \pi/2 + i\theta$ is equivalent to $C \to iS$, where $S = \sinh\zeta$ and $S = 0$ is a symmetric line (just like $C = 0$ was a symmetric line) but there is no other distinguished S. We draw a spherical prolate diagram (Fig. 3.3). The dihole wave occupies region I, where time points right. The rest of the diagram is realized as the dihole wave on its side (see Appendix 3.7).

In Weyl coordinates, one obtains the dihole wave by $z \to i\tau$, $t \to ix^4$. The card diagram is a vertical half-plane $\rho \geq 0$, $-\infty < \tau < \infty$. The sources (the extremal black hole horizons, which appear as points in Weyl coordinates) are located at $\rho = 0$

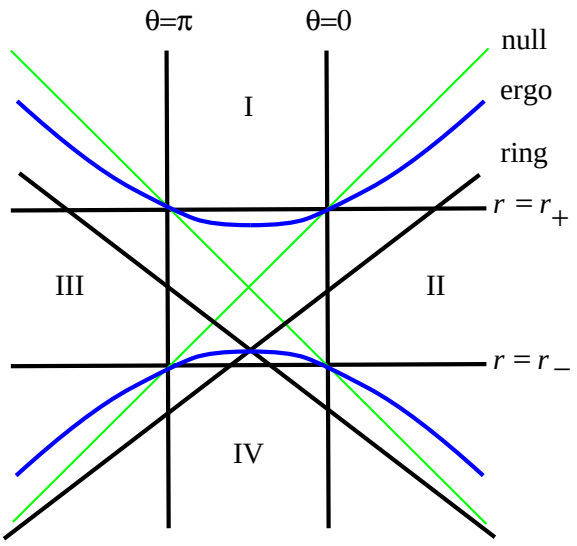

Figure 3.2: The spherical prolate diagram for the black dihole. The ergosphere singularity, 'ring' singularity, and special null lines are labelled.

and $\tau = \pm i\sqrt{M^2 + a^2}$. These are interpreted as the intersection of $\rho^2 = 0$ with the nonsingular ergosphere hypersurface $\Sigma - 2Mr = 0$ (see Appendix 3.8).

The wave-like character of this solution and the asymptotic fall-off on a null line on the card diagram are described in Appendix 3.10.

Upon dilatonization [90, 91, 92, 54] with $\alpha = \sqrt{3}$ (for a $4 \to 5$ lift [61, 93, 94]), and then adding six flat directions, the dihole wave solutions can be interpreted as a background of type IIA string theory with Euclidean D6- and $\bar{\text{D}}$6-branes located at imaginary time [23, 24, 25]. The 11d supergravity approximation will hold as long as curvatures are small and distances between objects are small. Specifically, in the IIA description, the distance between D-brane horizons must be much larger than a critical distance $\propto l_s$ at which the lowest string mode of an open string between a neighboring D- and $\bar{\text{D}}$-branes becomes tachyonic. (In the case of an infinite alternating array, this is known to create an S-brane for Sen's rolling tachyon [23].) From simple dimensional analysis considerations, there are no decoupling limits for D6-branes, so more objects would have to be included to obtain any type of AdS/CFT correspondence from these kind of geometries. Since there are no horizons or special null lines in the dihole wave geometry, the dilatonization procedure does not affect the global structure of the solution, and the dilatonized and undilatonized solutions have a similar physical interpretation.

The continuation to get the dihole wave is very similar to that to get the Kerr $\pi/2$-bubble [37], which is $t \to ix^4$, $\theta \to \pi/2 + i\theta$, $a \to ia$; there is then a twisted circle closing at $r = r_+$. We can think of the dihole wave as the Bonnor transform of

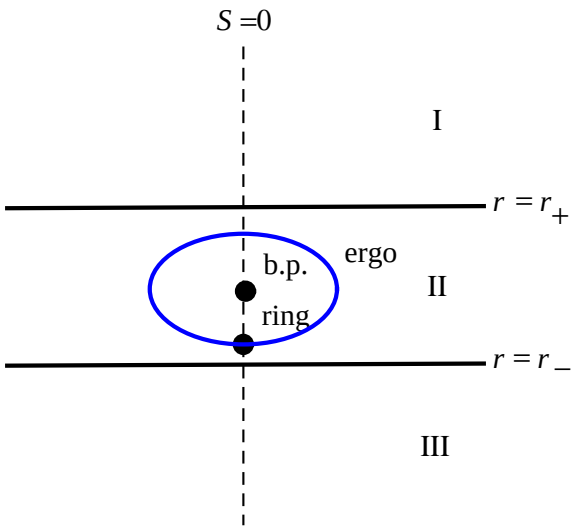

Figure 3.3: The spherical prolate diagram for the dihole wave (region I). Positive $S = \sinh\theta$ (time) points to the right.

the Kerr bubble (there is no relative $a \to ia$ between them, since the associated 5d Killing submetrics have signature $+++$; see Sec. 3.5).

3.3.1 Scaling limits

The scaling limit to find a Melvin [60, 62] region near the origin $\rho, \tau \approx 0$ of the dihole wave was found in [25]. This is the same region in the complexified spacetime as the Melvin scaling near $\rho, z \approx 0$ for the black dihole, in [63]. The Melvin scaling and analytic continuation from dihole to wave, commute, and Melvin itself is invariant under the continuation.

There is another, long-distance spatial scaling limit of the dihole wave. In Boyer-Lindquist (r, θ) coordinates, r is space and we can put $r \to \lambda r$, $x^4 \to \lambda x^4$, $g_{\mu\nu} \to g_{\mu\nu}/\lambda^2$, $A_\mu \to A_\mu/\lambda$, and send $\lambda \to \infty$. Then the vector potential scales to zero and we get the vacuum solution

$$ds^2 = (dx^4)^2 + dr^2 - r^2 d\theta^2 + r^2 \cosh^2\theta d\phi^2.$$

The constraint $r \geq r_+$ scales to $r \geq 0$, and we have a Rindler wedge of $\mathbf{R}^{2,1}$ flat space. Changing to Weyl coordinates, the metric is

$$ds^2 = (dx^4)^2 + d\rho^2 - d\tau^2 + \rho^2 d\phi^2, \qquad \rho \geq |\tau|.$$

This is locally flat space, but there is an asymptotic conical deficit, since we earlier identified $\phi \simeq \phi + 2\pi \frac{a^4}{(M^2+a^2)^2}$ to avoid a conical singularity at $\rho = 0$. This solution is

therefore interpreted as the creation of an S0-brane with energy per unit length equal to the deficit angle over 8π, so $E/L = \frac{1}{4}(1-(1+M^2/a^2)^{-2})$ [95]. The dihole wave universe with $r \leq r_-$ gives the same result.

3.4 The S-Dihole Universes

We will discover several different universes that can be achieved from the black dihole solution. Roughly, these are analogs of the Kerr double Killing bubbles, Kerr $\pi/2$-bubble, and S-Kerr solutions.

3.4.1 Subextremal

We give a quick overview of the subextremal S-dihole solutions, then write them generally, and then construct the six universes.

S-dihole has the horizon function $\Delta(r) = r^2 - 2Mr + a^2$ and in the subextremal case $a^2 < M^2$, its spherical prolate diagram is identical to that of the Kerr black hole, which we repeat in Fig. 3.4 with some new labellings. The Bonnor transform has changed some powers and the Weyl special null lines (which appear as the $\times$ in Fig. 3.1) become physically infinitely far away from the bulk of cards II, III, IV; and serve as subsets of $\mathcal{I}^{\pm}$. These Weyl null lines cut up the regions and we will find six universes: $\mathcal{U}$ and $\mathcal{U}_{\pm}$ are 3-vertical-card universes (Fig. 3.5) that are nonsingular and connected in a dS_2 fashion at their vertices, while $\mathcal{E}$ and $\mathcal{E}_{\pm}$ are 6-card universes (Figs. 3.6,3.7) with an ergosphere singularity on the two horizontal cards.

We now write down the solution, and then cut it up into pieces and assemble the regions into our six S-dihole universes. The S-dihole is gotten from the black dihole (3.3) by

$$\theta \to i\theta, \qquad a \to ia, \qquad t \to ix^4, \qquad \phi \to i\phi, \qquad \gamma\text{-flip}.$$

Here, the γ-flip of [51, 89] means we flip the sign of the 2×2 non-Killing metric in (3.2) via $e^{8\gamma} \to -e^{8\gamma}$. Equivalently, we change the sign of the entire metric and continue $\phi \to i\phi$, $x^4 \to ix^4$. The γ-flip procedure preserves the reality of the magnetostatic gauge field. The solution is then

$$\begin{aligned} ds^2 &= \big(1-\frac{2Mr}{\Sigma}\big)^2\Big((dx^4)^2 + \frac{\Sigma^4}{(\Delta-(M^2-a^2)\sinh^2\theta)^3}\big(-\frac{dr^2}{\Delta}+d\theta^2\big)\Big) \\ &\qquad + \frac{\Delta\sinh^2\theta}{(1-\frac{2Mr}{\Sigma})^2}d\phi^2 \\ A &= \Big(\frac{2aMr\sinh^2\theta}{\Delta+a^2\sinh^2\theta} - A_{\text{bndry}}\Big)d\phi. \end{aligned} \tag{3.5}$$

where $\Sigma = r^2 + a^2\cosh^2\theta$. To change to spherical prolate coordinates, we set $r - M =$

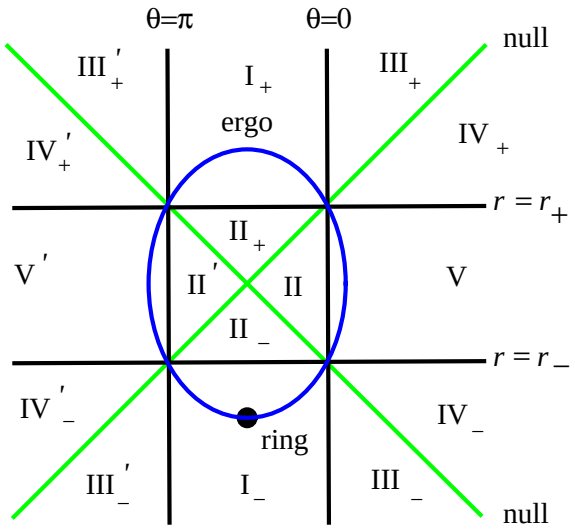

Figure 3.4: The regions of the S-dihole universe (subextremal). Regions III_+ and III'_+, etc. are isometric. Each region will correspond to one card in some S-dihole universe(s).

$\sqrt{M^2-a^2}\cosh\zeta$, so the solution is

$$\begin{aligned} ds^2 &= \big(1-\frac{2Mr}{\Sigma}\big)^2\Big((dx^4)^2+\frac{\Sigma^4(-d\zeta^2+d\theta^2)}{(M^2-a^2)^3(\sinh^2\zeta-\sinh^2\theta)^3}\Big) \\ &\quad +\frac{(M^2-a^2)\sinh^2\zeta\sinh^2\theta d\phi^2}{(1-\frac{2Mr}{\Sigma})^2} \\ A &= \frac{2aMr\sinh^2\theta}{\Sigma-2Mr}d\phi, \end{aligned} \tag{3.6}$$

where $\Sigma-2Mr=\Delta+a^2\sinh^2\theta=(M^2-a^2)\sinh^2\zeta+a^2\sinh^2\theta$ and $\Sigma=r^2+a^2\cosh^2\theta$.

These coordinates cover regions III_+ and IV_+; the null line which separates them is $\zeta=\theta$. In region III_+, ζ is larger than θ and hence ζ is timelike. In region IV_+, ζ is smaller than θ and hence θ is timelike.

$\mathcal{U}$, $\mathcal{U}_\pm$ universes

Let us focus on region III_+, which will be part of the $\mathcal{U}$ universe.

To see that the line $\theta=\zeta$ serves as $\mathcal{I}^-$, the relevant non-Killing part of the metric is

$$\frac{-d\zeta^2+d\theta^2}{(\sinh^2\zeta-\sinh^2\theta)^3}.$$

Let us change variables so $U = \frac{\zeta+\theta}{2}$, $V = \frac{\zeta-\theta}{2}$ where $U \geq V > 0$. For small V and staying away from $U = 0$, we have $ds^2 \sim -dUdV/V^3$. Next define $v = -1/V^2$, $u = -1/U^2$, so the metric is $ds^2 \sim -dudv$ for $v \leq u < 0$. From these coordinate transformations it is clear that region III_+ extends infinitely far into the negative v direction. The uv chart for region III_+ looks like region III_- in Fig. 3.4, with $\mathcal{I}^+$ drawn explicitly as $u = 0$.

We will see later (Sec. 3.4.1) that there is a scaling limit towards the vertex $\theta, \zeta \approx 0$ that yields a fibered dS_2-type Poincaré (planar) horizon. Beyond this, there is another time-dependent region where we conclude ζ is still timelike. This must then be region II. Applying the same argument at the bottom vertex of II ($r \approx r_-, \theta \approx 0$) connects us to region III_-. These are the three cards that form the $\mathcal{U}$ universe. We know from the Penrose diagram of dS_2 that a horizontally-infinite array of regions accompanies each dS_2 horizon. Thus the card diagram for $\mathcal{U}$ actually has an infinite number of cards, shown in the right diagram in Fig. 3.5. In Weyl coordinates ($\propto -d\tau^2 + d\rho^2$) the vertices are located at $\rho = 0$, $\tau = \pm\sqrt{M^2 - a^2}$. This universe is nonsingular and not time-symmetric. Sending $M \to -M$ gives the time-reverse.

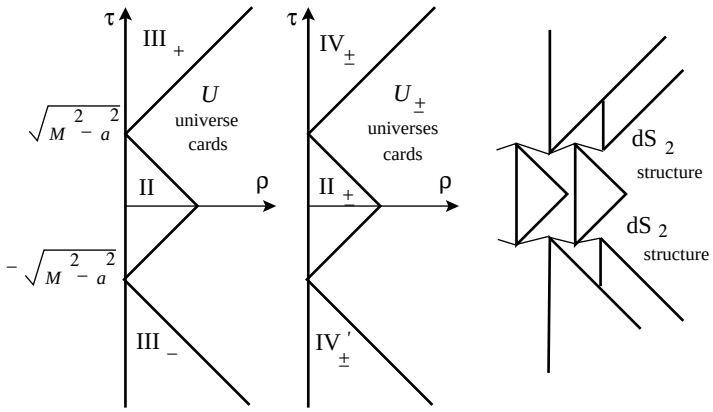

Figure 3.5: The $\mathcal{U}$ universes. Each pointlike dS_2 horizon connects each card to two adjacent regions which are isometric, as illustrated on the right. The zig-zag connections are suggestive of the Poincaré horizons.

Now, start in region IV_+, where θ is time. A similar near-vertex scaling limit shows dS_2 horizons, and that we must pass to region II_+ and then IV'_+. This universe, $\mathcal{U}_+$ is nonsingular and is time-symmetric.

Lastly, start in region IV_-, where θ is time. The vertex gives dS_2 horizons, and we pass to regions II_- and IV'_-. This universe, $\mathcal{U}_-$ is nonsingular and is time-symmetric. It is related trivially to $\mathcal{U}_+$ by $M \to -M$. The cards for the $\mathcal{U}$ universes are summarized in Fig. 3.5.

$\mathcal{E}$, $\mathcal{E}_\pm$ universes

We can turn any of the cards of the $\mathcal{U}, \mathcal{U}_\pm$ universes on their sides via the γ-flip, and achieve the following universes:

$$\begin{aligned} \mathcal{E} &: \quad \text{II, V, IV}_+, \text{IV}_- \\ \mathcal{E}_\pm &: \quad \text{I}_\pm, \text{II}_\pm, \text{III}_\pm, \text{III}'_\pm. \end{aligned}$$

These regions are fitted together in 8-card diagrams, as shown in Figs. 3.6, 3.7. They have ergosphere singularities on the horizontal cards, connecting the vertices $z = \pm\sqrt{M^2 - a^2}$ and separating each $\mathcal{E}$-type universe into an interior and exterior universe. Upon dilatonization and lifting to 5d, these ergosphere singularities are lifted (and the special null lines are then traversable).

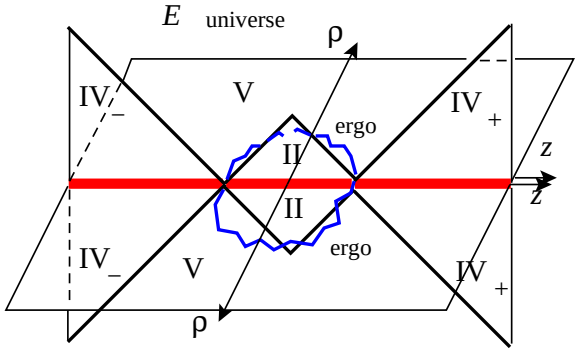

Figure 3.6: The $\mathcal{E}$ card diagram consists of eight cards and a singular ergosphere on the horizontal cards V.

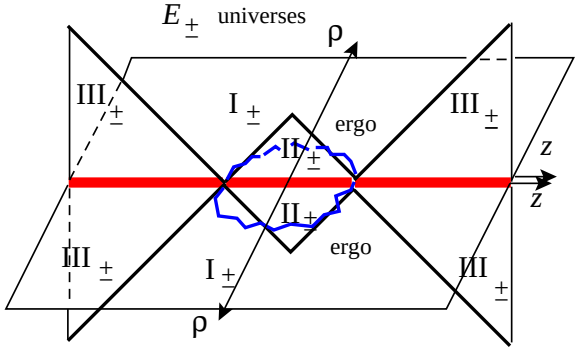

Figure 3.7: The $\mathcal{E}_\pm$ card diagrams are similar to $\mathcal{E}$'s. The $\mathcal{E}_-$ universe has a ring singularity atop the ergosphere at $z = 0$ (not pictured).

Scaling limit to Melvin, flat space

Like the black dihole [63] and dihole wave [25], we can achieve a Melvin scaling limit for some S-dihole universes. The Melvin universe has cylindrical symmetry, with a magnetic field which decays to zero in the transverse direction. The quantity $\Sigma - 2Mr$, whose zero locus yields the ergosphere singularity, is the quantity of interest yielding the nontrivial spatial dependence. Both the parameters M, a, and $\theta - \pi/2$, ζ must be scaled such that $(\theta - \pi/2) \sim \zeta \to 0$ and $M\zeta \sim a$ (hence $M \gg a$).

The dihole and S-dihole (and dihole wave) are related by analytic continuation, and the Melvin universes which come from the dihole and dihole wave are actually from the same neighborhood of their complexified 4-manifolds. Since the $r \geq r_+$ dihole is region I_+, and II_+ is directly adjacent (near $\rho = 0$, $z = 0$), we must also have a Melvin scaling limit in II_+. For $r \leq r_-$, similar remarks apply to I_- and II_-. As part of the $\mathcal{U}_\pm$ universes, $\mathrm{II}_\pm$ scale to

$$\begin{aligned} ds^2 &= \Big(\frac{a^2+\rho^2}{4M^2}\Big)^2 \Big(\frac{4M^2}{a^2}\Big)^4 \big((dx^4)^2 - d\tau^2 + d\rho^2\big) + \big(\frac{4M^2}{a^2+\rho^2}\big)^2 \rho^2 d\phi^2 \qquad (3.7) \\ A &= -a\tau dx^4/2M^2. \end{aligned}$$

As part of the $\mathcal{E}_\pm$ universes, we must turn (3.7) on its side, changing

$$-d\tau^2 + d\rho^2 \to d\tau^2 - d\rho^2$$

and going through the $\rho = 0$ horizon by $\rho \to i\rho'$ to yield a 4-card S-Melvin scaling limit, with an ergosphere singularity at $\rho' = a$ on the horizontal cards [64].

There is no corresponding (S-)Melvin scaling limit for regions II or V. The $M \gg a$ requirement makes the ergosphere ellipse in Fig. 3.4 very wide, so that on the horizontal card V, it becomes infinitely far away from the $\rho = 0$ horizon at $\theta = 0$. Hence $\mathcal{U}$ and $\mathcal{E}_\pm$ have no Melvin scaling limit. There is also no Melvin limit for the superextremal S-dihole (Sec. 3.4.2).

Now, we look at a scaling limit towards the future. Taking the $\mathcal{U}$ universe and sending $\zeta \to \infty$ (or $r \sim \sqrt{M^2 - a^2}\cosh\zeta \to \infty$), we get the flat scaling limit in the far future

$$ds^2 \sim (dx^4)^2 - dr^2 + r^2(d\theta^2 + \sinh^2\theta d\phi^2). \qquad (3.8)$$

This is interpreted to hold for $r > 0$, i.e. above the null cone in $\mathbf{R}^{2,1}$, times a spatial line. The $\mathcal{U}_\pm$ universes also have flat space limits in the future and past, as $r \to \pm\infty$.

There is also a scaling limit towards the center vertex of Fig. 3.4, where the special null lines meet. It is

$$ds^2 = (dx^4)^2 + \frac{M^8(-d\theta^2 + d\zeta^2)}{(M^2-a^2)^3((\pi/2-\theta)^2 + (\pi/2-\zeta)^2)^3} + (M^2 - a^2)d\phi^2, \qquad A = 2ad\phi.$$

Picking a sign for each of $\pi/2 - \theta$, $\pi/2 - \zeta$ (there are four choices) gives us a complete metric $\propto -dx^+dx^-$ for each wedge card that meets at the vertex. It is clear that special null lines act as $\mathcal{I}^\pm$ here. We have $\mathbf{R}^{2,1} \times S^1$, where the proper circumference of the S^1 is $2\pi\sqrt{M^2 - a^2}$ and the Wilson line (as approached from Region II) is $4\pi a$.

Scaling limit to RN-bubble, S-RN

Next we examine the corner of the Weyl wedge card for say the $\mathcal{U}$ universe, where θ and ζ are small, and find in this limit a magnetic, dS_2-fibered geometry. It is just the RN-bubble. Define $\theta = \sqrt{\sigma}\sinh\eta$, $\zeta = \sqrt{\sigma}\cosh\eta$ and scale the coordinates as $\sigma \to \sigma/\lambda$, $x^4 \to \lambda x^4$, $\lambda \to \infty$. This gives the $\sigma > 0$ half of a universe

$$\begin{aligned} ds^2 &= (M^2\cosh^2\eta - a^2)^2\Big(\frac{\sigma^2(dx^4)^2}{\Sigma_+^2} + \frac{\Sigma_+^2}{(M^2-a^2)^3}(-d\sigma^2/4\sigma^2 + d\eta^2)\Big) \\ &\quad + \frac{(M^2-a^2)\Sigma_+^2\cosh^2\eta\sinh^2\eta d\phi^2}{(M^2\cosh^2\eta - a^2)^2}, \\ A &= \frac{2aMr_+ d\phi}{a^2 + (M^2-a^2)\coth^2\eta} \end{aligned} \tag{3.9}$$

where the constant $\Sigma_+ = r_+^2 + a^2 = 2Mr_+$. The $\eta \to \infty$ limit gives a proper ϕ-circumference of $2\pi\sqrt{M^2-a^2}\Sigma_+/M^2$. The card diagram consists of an upper and lower noncompact wedge, connected in a dS_2 fashion. This is like the parabolic (Poincaré) representation of the RN (charged Witten) bubble [51, 89]. Putting $g_{\mu\nu} \to g_{\mu\nu}(M^2-a^2)^3/M^2\Sigma_+^2$, $A_\mu \to A_\mu(M^2-a^2)^{3/2}/M\Sigma_+$, $\phi \to \phi M^3/(M^2-a^2)^2$, and setting $2Mr = M^2\cosh^2\eta - a^2$, we achieve the RN bubble

$$\begin{aligned} ds^2 &= f d\phi^2 + \frac{dr^2}{f} + r^2 d\mathrm{dS}_2^2, \qquad d\mathrm{dS}_2^2 = -\frac{d\sigma^2}{\sigma^2} + \sigma^2(dx^4)^2, \\ A &= \pm Q\big(\frac{1}{r_+} - \frac{1}{r}\big)d\phi, \end{aligned} \tag{3.10}$$

with

$$M_{\mathrm{RN}} = \frac{M}{4}(1 - 2a^2/M^2), \qquad Q^2 = \frac{a^2}{4}(1 - a^2/M^2), \qquad f = 1 - \frac{2M_{\mathrm{RN}}}{r} - \frac{Q^2}{r^2}.$$

The ϕ-direction is the RN bubble's Euclidean time. Recalling that $0 \le a^2 < M^2$, we generate all shapes (parametrized by Q^2/M_{RN}^2) of bubbles of positive and negative mass.

One can also perform near-vertex scaling on $\mathcal{U}_\pm$ universes and achieve RN bubbles. The formulas are the same as for $\mathcal{U}$ up to $a^2 \to M^2 - a^2$, a rescaling of Einstein-Maxwell, and fixing ϕ's periodicity.

One can turn the RN bubble on its side via the γ-flip and achieve S-RN, which in its parabolic card description is a 'butterfly' diagram with two horizontal half-plane cards and four vertical noncompact wedge cards. The γ-flip and the small-σ scaling limit commute, and so one can achieve S-RN as a near-vertex scaling limit of the $\mathcal{E}$-universes.

We see that the S-RN curvature singularity (and since it is formally the same, the RN curvature singularities) now has an interpretation as an 'ergosphere' singularity.

(See Appendix 3.9, where we discuss the character of such a singularity and also show how the Kerr 'ring' singularity can be interpreted as an ergosphere singularity.) By ergosphere singularity, we mean one that can be eliminated via an appropriate inverse Bonnor transformation or appropriate dilatonization and KK lift (see Sec. 3.5). Indeed, if one interchanges the roles of t, ϕ and inverse Bonnor transforms the negative mass card for the RN black hole, the curvature singularity becomes a nonsingular ergosphere. Unfortunately, $\rho = 0$ (where the ϕ-circle had vanished) becomes singular.

It is not clear how general and useful this idea may be—which familiar and unfamiliar curvature singularities in D dimensions can be easily lifted by an analogous procedure, and what spacetimes result. A generalization of the Bonnor transform or dilatonization procedures should yield interesting results.

3.4.2 Superextremal case

For the superextremal case $a^2 > M^2$, Δ has no roots and there are no horizons. We set $r - M = \sqrt{a^2 - M^2}\sinh\zeta$, $Z = \sinh\zeta$. The spherical prolate diagram is shown in Fig. 3.8; superextremal S-dihole is region I, and time runs up.

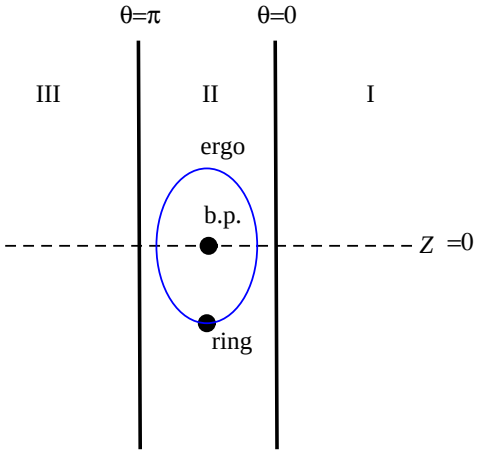

Figure 3.8: The spherical prolate diagram for the superextremal S-dihole (Region I). Time runs up the right column. The other regions will appear in the superextremal S-dihole on its side (see Appendix 3.7).

The coordinate θ is noncompact and spacelike. The ϕ-circle vanishes along $\theta = 0$ around which the metric has the expansion

$$ds^2 \supset \frac{(r^2 + a^2)^2}{\Delta}(d\theta^2 + \theta^2 d\phi^2) \ .$$

This is smooth if $\phi \simeq \phi + 2\pi$; this is the same periodicity for the black dihole on the axis outside the black holes.

The superextremal S-dihole solution is the Bonnor transform of the superextremal S-Kerr [47], which has the same spherical prolate diagram as in Fig. 3.8; it is also region I, time running up. These superextremal solutions can be represented by one vertical half-plane card with a vertical boundary.

We turn the superextremal S-dihole on its side in Appendix 3.7.

Scaling limits to (locally) flat space

The large-time (large-r) scaling limit for superextremal S-dihole is flat space, just like for the late-time wedge of the $\mathcal{U}$ subextremal S-dihole universe.

On the other hand, just as for the dihole wave (which has the same card structure), we can take a large-θ spatial scaling limit to recover an asymptotic conical deficit. We scale $e^\theta \to \lambda e^\theta$, $x^4 \to \lambda x^4$, $g_{\mu\nu} \to g_{\mu\nu}/\lambda^2$, $A \to A/\lambda$. In this limit the solution again simplifies to a vacuum solution

$$ds^2 = (dx^4)^2 + \frac{a^8}{(a^2-M^2)^3}(-R^2 d\zeta^2 + dR^2) + (a^2-M^2)R^2 \cosh^2\zeta d\phi^2, \qquad (3.11)$$

where $r - M = \sqrt{a^2-M^2}\sinh\zeta$ and $-\infty < \zeta < \infty$ parametrizes a Rindler wedge. Changing to dimensionless Weyl coordinates, the metric becomes

$$ds^2 = (dx^4)^2 + \frac{a^8}{(a^2-M^2)^3}(-d\tau^2 + d\rho^2) + (a^2-M^2)\rho^2 d\phi^2, \qquad \rho \geq |\tau|. \qquad (3.12)$$

The angular ϕ was previously periodically identified with $\phi \simeq \phi + 2\pi$ to avoid a conical singularity at the origin so superextremal S-dihole has an asymptotic conical singularity. We have created an S0-brane with $E/L = \frac{1}{4}(1-(1-M^2/a^2)^2)$.

Extremal limit

Let us examine the extremal case $a^2 = M^2$ for the S-dihole. The metric near the degenerate vertex is

$$ds^2 = \frac{T^4}{M^4}(dx^4)^2 - \frac{M^4}{T^4}dT^2 + \frac{M^4}{T^2}(d\theta^2 + \sinh^2\theta d\phi^2),$$

where $T = r - M$. We find a metric singular at $T = 0$. This extremal case does not have the de Sitter space of extremal S-Kerr ([47, 49] and see [96]) but a singular metric. The Bonnor transformation has changed the powers of the coordinate T in the metric components. Coming from the subextremal side, we see that two dS_2-fibered horizons are becoming coincident. One can use the Tx^4 part of the metric to show one can reach $T = 0$ by a null geodesic in finite affine parameter; and the blowing up of the $\mathbf{H}_2$ part of the metric indicates a singularity. Note that the near-vertex limit and extremal limits do not commute: Putting $a^2 = M^2$ in the RN bubble (3.10) yields a negative-mass chargeless bubble with a timelike singularity.

Coming from the superextremal side, we can interpret this as a Euclidean D6- and $\bar{\text{D}}$6-brane becoming closer together in imaginary time. They are separated by a distance of $\Delta z = 2\sqrt{a^2 - M^2}$. When the distance is dialed down to the critical distance $\propto l_s$, the lowest stretched open string mode will become tachyonic and string loop effects will dominate [23, 24, 25]. So the extremal S-dihole supergravity solution (which has unbounded curvature) should be replaced with some other, stringy description.

3.4.3 S-charge

For an S-brane solution with electromagnetic field, the magnetic S-charge [29, 23] is defined as the integral of F over a two dimensional surface $\mathcal{S}$ which is spacelike and transverse to the brane (or Killing) direction. In the absence of sources or singularities and with sufficient decay of fields at infinity, the S-charge is conserved in the sense that it does not depend on $\mathcal{S}$. (Care must be taken to distinguish those $\mathcal{S}$ which asymptote purely to i^0 and those which hit $\mathcal{I}^{\pm}$.

In [25] the S-charge of the dihole wave for $r \geq r_+$ was computed in Weyl coordinates over a constant-τ slice to be $Q_s = \frac{M}{a}(M + \sqrt{M^2 + a^2})$ and was shown to be conserved. The S-charge along a constant-t slice in BL coordinates can be shown to give the same result. The result for the dihole wave with $r \leq r_-$ is the same, up to putting $M \to -M$ in the above formula.

S-dihole (3.5) has a vector potential

$$A = \frac{2aMr\sinh^2\theta}{r^2 - 2Mr + a^2\cosh^2\theta}d\phi.$$

The superextremal $a^2 > M^2$ spacetime has a simple card diagram—it is free of horizons, singularities and special null lines. To compute the S-charge on a BL slice, we fix r and integrate $F_{\theta\phi}$

$$Q_s = \frac{1}{4\pi}\int_0^{2\pi} d\phi \int_0^{\infty} d\theta \frac{\partial}{\partial\theta}\Big(\frac{2aMr\sinh^2\theta}{r^2 - 2Mr + a^2\cosh^2\theta}\Big) = Mr/a.$$

This is not conserved, and is due to the fact that $F_{r\phi}$ does not decay fast enough; as $\theta \to \infty$ the $drd\phi$ flux integral is $d\Phi_\infty = \frac{4\pi M}{a}dr$.

On the other hand, we can compute S-charge for superextremal S-dihole at fixed Weyl time τ. In this case $A|_{\rho=0} = 0$ and $A|_{\rho\to\infty} = -2M^2/a$ so the S-charge is $Q_s = M^2/a$. This result is independent of τ and so superextremal S-dihole has a 'conserved' S-charged in a quite limited sense.

The difference between the BL and Weyl S-charges can be seen from looking at the surfaces $\mathcal{S}$ in Weyl coordinates: The BL constant-r slice asymptotes to a finite, nonzero slope at large values of θ as shown in Fig. 3.9. We stress that $r =$constant slices tend to i^0 as $\theta \to \infty$.

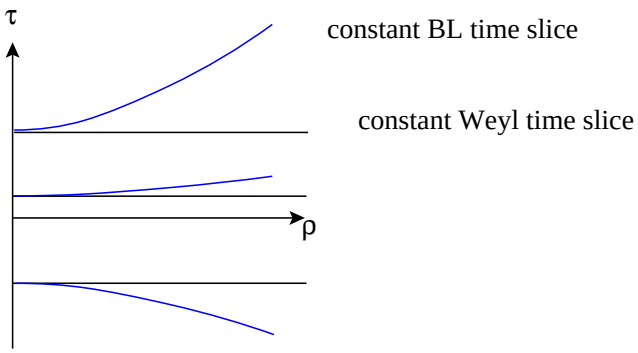

Figure 3.9: Calculation of S-charge on Boyer-Lindquist versus Weyl time slices can lead to different results.

The S-charges at $r =$ and $\tau =$ constant are the same for $r = M$ ($\tau = 0$) which is in a sense the center of the cone of the Einstein-Maxwell waves (this is like a null cone in $\mathbf{R}^{2,1}$); we could say this is where the solution experiences a 'bounce,' but there is no time-symmetry since $M \neq 0$.

Examining the EM field strength for the $\mathcal{E}$ universe, we notice the following fact. On the horizontal card (region V) there is an electric field in the r direction, and for large values of θ, $F_{\phi r} = 2M/a$ is constant. One can then interpret this as a background electric field which is related to the two-dimensional object lying along the ergosphere singularity. As time passes (we eventually go up the vertical $\mathrm{IV}_\pm$ cards) the electric field eventually goes to zero so this gives support for the interpretation of the S-dihole $\mathcal{E}$-universe as the creation of a localized two-dimensional unstable object. In contrast, the dihole wave is the formation and decay of a localized fluxbrane, which is one-dimensional object.

The subextremal case $\mathcal{U}$-universes are less directly amenable to S-charge than the superextremal S-dihole. The noncompact wedge universes which are regions $\mathrm{III}_\pm$ and $\mathrm{IV}_\pm$ have finite but nonconserved S-charge as we compute along a constant-time (say BL time r) slice out to the boundary. However, these surfaces $\mathcal{S}_r$ asymptote to the conformal infinity $\mathcal{I}^\pm$, not to i^0. One can compactify the noncompact wedge à la Penrose, and the emergent i^0 has infinite S-charge, being the limit as one runs up $\mathcal{I}^-$. (i^0 is treated merely the singular boundary between $\mathcal{I}^\pm$; it can have more structure as in [97, 98].)

On the other hand, the compact wedge cards have a clear i^0 on the card diagram. S-charges are conserved and finite; one evaluates A_ϕ at i^0 and subtracts A_ϕ evaluated anywhere on the $\rho = 0$ boundary. Keeping in mind that $\phi \simeq \phi + 2\pi$ for $\mathcal{U}$ and $\phi \simeq \phi + 2\pi a^4/(M^2 - a^2)^2$ for $\mathcal{U}_\pm$, the S-charges are $Q_s = a$, and $Q_s^\pm = \frac{a^4}{(M^2-a^2)^2}(a - Mr_\pm/a)$. The S-charge suggests that the i^0 in the upper, middle, and lower cards are disjoint, and helps us to conclude the global structure (see Fig. 3.13).

3.4.4 A desingularizing change of coordinates

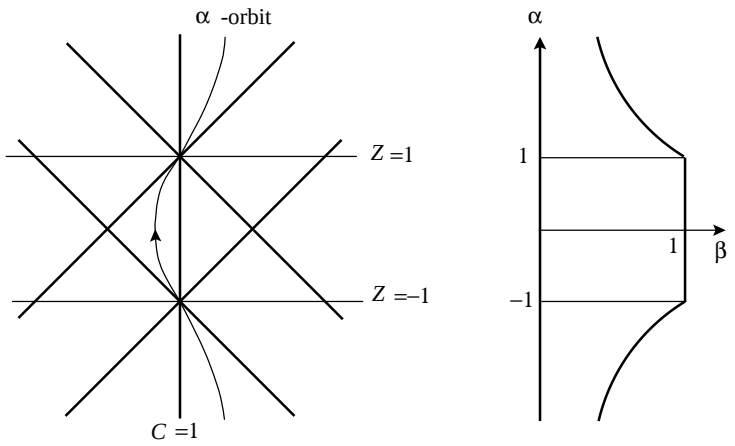

Figure 3.10: The shown patch for α, β, on the right, fills out three triangles on the CZ diagram, left, for the three cards of the S-dihole $\mathcal{U}$-universe.

The three vertical cards for the $\mathcal{U}$-universe, lie on the irregular patches $0 \leq \rho < \min(|z - \sqrt{M^2 - a^2}|, |z + \sqrt{M^2 - a^2}|)$, which are not easily amenable to finding a cross-patch or global description. As the first step to a better global spacetime coordinates, we give a desingularizing transformation, which re-renders the degenerate vertex (where the complex ergosphere locus pierces the vertical cards at $\rho = 0$, and where the RN bubble scaling limit is to be found) as a line segment.

One must find equations for orbits as drawn in Fig. 3.10. The answer has been given implicitly by Penrose's ideas for compactifying the 1+1 half-plane, using the hyperbolic tangent, and by analytically continuing to achieve the noncompact wedges with the hyperbolic cotangent. The derivation is omitted. In terms of the dimensionless spherical prolate coordinates, the transformation is

$$Z = \frac{\alpha(1-\beta^2)}{1-\alpha^2\beta^2}, \qquad C = 1 - \frac{\beta(1-\alpha^2)}{1-\alpha^2\beta^2}.$$

We require $0 \leq \beta < 1$, and also $\beta < 1/|\alpha|$. For fixed β, an α-orbit for $-1/\beta < \alpha < 1/\beta$ snakes through all three vertical cards, hitting each vertex with slope $\Delta C/\Delta Z = 2\beta/(1+\beta^2)$. The resulting $\alpha\beta$ coordinate system is not Penrosian in the sense of drawing light cones on the coordinate patch; there is a cross-term; but ∂_α and ∂_β do have timelike and spacelike signature. To get the stated RN scaling limit, near the vertex, use $\alpha - 1 \approx \sigma/2$.

Note then how the degenerate vertices have become the segment $0 \leq \beta < 1$ for $\alpha = \pm 1$. This coordinate system is *not* adapted to the full spherical prolate diagram, merely to the three given cards for the $\mathcal{U}$-universe and their reflections about $C = 1$.

If one likes, one can rectangularize the coordinate patch via

$$\alpha_{\rm final} = \tanh^{-1}(\beta\alpha)/\tanh^{-1}(\beta).$$

Then the patch is $0 \leq \beta < 1$, $-\infty < \alpha_{\rm final} < \infty$.

We can make a direct assault on noncontractible loops. To directly check for an nontrivial loop around dS_2 from the near-vertex scaling limit, we make a change of variables motivated from dS_2 formulas

$$X^0 = \frac{\sigma^{-1}-\sigma}{2} - \frac{\sigma 4(M^2-a^2)^3}{2\Sigma_+^4}(x^4)^2 = \sinh\tau \tag{3.13}$$

$$X^1 = 2(M^2-a^2)^{3/2}x^4\sigma/\Sigma_+^2 = \cosh\tau\sin\psi \tag{3.14}$$

$$X^2 = \frac{\sigma^{-1}+\sigma}{2} - \frac{\sigma 4(M^2-a^2)^3}{2\Sigma_+^4}(x^4)^2 = \cosh\tau\cos\psi, \tag{3.15}$$

and $\theta = \sqrt{\sigma}\sinh\eta$, $\zeta = \sqrt{\sigma}\cosh\eta$. Thus $\sigma = \cosh\tau\cos\psi - \sinh\tau$, and x^4 can be solved from the X^1 equation. Plugging into the formula for the S-dihole, one can then check the existence of nontrivial ψ-loops in the S-dihole geometry. This description holds for small η.

As we see from the 2d Penrose diagram (Fig. 3.11), the loops obtained from the vicinity of the upper vertex and the lower vertex, are not homotopic. The whole spacetime has the topology of the tangent bundle to the 2-cylinder, minus one base point and its plane fiber; Thus $(S^1 \times \mathbf{R}^3) \setminus \mathbf{R}^2$. The fundamental group is the same as a cylinder minus a point (or the plane minus two points).

A combination of the above coordinate transformations may yield further insight, but the topology has been identified, and the ensuing complicated form of the metric after such transformations defies any analysis by mere inspection. The real goal is then to find coordinates near conformal null infinity to show its (patched) regularity.

3.4.5 Penrose diagram of $\mathcal{U}$ universe

Take the $\mathcal{U}$ universe with $\theta = \sqrt{\sigma}\sinh\eta$ and $\zeta = \sqrt{\sigma}\cosh\eta$. If one takes the σ and x^4 coordinates (that is, ignores azimuthal ϕ and fixes an η-slice), then the small-σ limit gives dS_2. The large-σ limit (the flat space future limit (3.8)) gives $ds^2 \sim (dx^4)^2 - e^\sigma d\sigma^2/\sigma^2$, which is flat $\mathbf{R}^{1,1}$. One then concludes that the Penrose diagram for $\mathcal{U}$ in these two coordinates should be three rows of diamonds (Fig. 3.11). However, this Penrose diagram is inadequate in two senses. First, it ignores the important noncompact η-direction and hence misses out on some parts of $\mathcal{I}^\pm$.[5] These are represented as the special null lines or an ordinary (at infinity) $\mathcal{I}^\pm$ for the card diagram. Second, the interior vertices, across the center of the Penrose diagram, are

[5]The often-drawn Penrose diagram for S-Schwarzschild is similarly inadequate for that solution, since it does not draw noncompact directions.

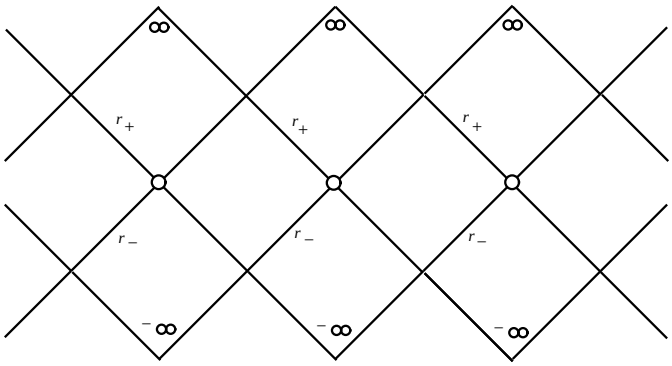

Figure 3.11: The Penrose diagram for the $\rho = 0$ slice of the $\mathcal{U}$ universe. The interior vertices are at an infinite distance and cannot be traversed. Anticipating a sensible 3-diagram, it is canonical à la dS_2 to identify every other diamond horizontally, giving the Penrose diagram the topology of a 2-cylinder minus a point.

an infinite distance away and cannot be traversed. They should be interpreted as part of the missing i^0 or $i^\pm$. So we have drawn them as blown-up circles on the Penrose diagram. (See [99] for a similar feature, in the cut-up multi-diamond Penrose diagrams.)

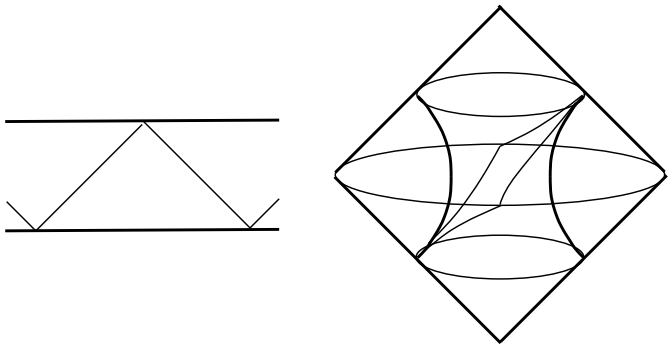

Figure 3.12: (a) The Penrose diagram for dS_2. (b) A 3-diagram of the Witten bubble; the spacetime lies spatially outside dS_2, and is cut into two patches by the parabolic coordinates for dS_2.

A conjunction of both the Penrose diagram (in σ, x^4) and card diagram (in σ, η) highlights the features of the spacetime, but it would be nice to have a 3-diagram (where only ϕ is ignored) to show the global properties of the spacetime, like its topology and the conformal structure at infinity [100]. For the near-vertex limit which is the RN bubble, its fibered dS_2 has the Penrose diagram in Fig. 3.12(a) and a 3-diagram (ignoring the bubble circle ϕ) in Fig. 3.12(b).

For the $\mathcal{U}$ universe, the 3-diagram is as shown in Fig. 3.13, where the nondrawn ϕ-direction closes the spacetime in a warped bubble locus. The bubble has a vertex which is stretched to infinite distance, and serves as $i^{\pm}$ for the lower and upper cards, and part of i^0 for the middle card. This is the vertex appearing on Fig. 3.11. S-charge is finite along any curve in the diagram extending from the bubble surface to a point between the lower i^0 and the upper i^0, at and beyond which it becomes infinite.

Dashed lines are drawn to indicate the Poincaré horizons for the near-horizon dS_2. These lines must extend as null planes and pierce $\mathcal{I}$. These piercings must be interpreted as another (spacelike-extended) i^0, with $\mathcal{I}^+$ below it and $\mathcal{I}^-$ above it.

One may object that the given diagram is not Penrosian (causal as drawn) in that the $\mathcal{I}^{\pm}$, if they are null cones at 45°, cannot intersect in an i^0 as depicted. Actually, the 3-metric for the S-dihole is not conformally flat, so no 3-diagram can be Penrosian. This lack of conformal flatness of the 3-metric persists with $a = 0, M$. The thing to check is the vanishing of the 3-tensor [101, 102])

$$R_{abc} = R_{ab|c} - R_{ac|b} + \frac{1}{4}(g_{ac}R_{|b} - g_{ab}R_{|b}),$$

where all quantities are for the 3-manifold and the stroke indicates covariant differentiation. We conclude that the S-dihole's 3-diagram can only be considered schematic, and find no further objections to Fig. 3.13. (The charged Witten bubble's 3-metric

$$ds_3^2 = \frac{dr^2}{f(r)} + r^2 d\mathrm{dS}_2{}^2$$

is conformally flat.)

Fig. 3.13 is missing the ϕ-direction, so we discuss its evolution. As one passes from the infinite past (drawn as a ring) forward through the two dS_2 horizons and to the infinite future, the $\theta\phi$ directions start as an ordinary hyperbolic space in (3.8), and then close to a test-tube shape in the $\eta\phi$ coordinates in (3.9) at each dS_2 horizon. In the middle, we know that the near-i^0 scaling limit also gives a finite ϕ-circumference. This evolution is depicted in Fig. 3.14. Note that it is sensible to identify early and late-time θ with near-vertex η, since both have hyperbolic trajectories on noncompact wedge cards that do not intersect the special null line; we could also describe this with the desingularized coordinate β.

A full description of the $\mathcal{E}$-universes is lacking; they can be described near their foci, as two S-branes; these S-branes are connected in the bulk of the $\mathcal{E}$-type universe. We desire a more complete description and 3-diagram.

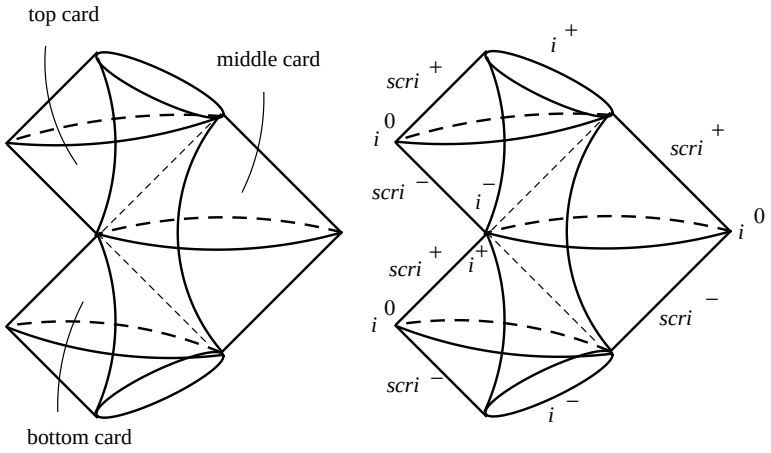

Figure 3.13: The 3-diagram, analogous to that for the Witten bubble, for the $\mathcal{U}$-universe. The azimuthal symmetry of the Witten bubble is broken to a nonobvious Poincaré translation symmetry. There are three disjointed sets of ordinary i^0, and three each of $\mathcal{I}^{\pm}$. The Poincaré horizons extend as 2-planes in the diagram to pierce null infinity and cause a singularity in its conformal structure (two additional i^0's). The $\mathcal{U}_{\pm}$ universes have an additional timelike $\mathbb{Z}_2$ isometry as suggested by the picture.

3.4.6 Weyl coordinates and branches

The magnetic dihole in Weyl coordinates is $ds^2 = -f^2dt^2 + f^{-2}(e^{8\gamma}(d\rho^2 + dz^2) + \rho^2 d\phi^2)$ with

$$\begin{aligned} f^2 &= \left[\frac{(R_+ + R_-)^2 - 4M^2 - \frac{a^2}{M^2+a^2}(R_+ - R_-)^2}{(R_+ + R_- + 2M)^2 - \frac{a^2}{M^2+a^2}(R_+ - R_-)^2}\right]^2 \\ e^{8\gamma} &= \left[\frac{(R_+ + R_-)^2 - 4M^2 - \frac{a^2}{M^2+a^2}(R_+ - R_-)^2}{4R_+R_-}\right]^4 \qquad (3.16) \\ A &= \frac{aM(R_+ + R_- + 2M)(1 - \frac{(R_+-R_-)^2}{4(M^2+a^2)})}{\frac{1}{4}(R_+ + R_-)^2 - M^2 - a^2\frac{(R_+-R_-)^2}{4(M^2+a^2)})}d\phi, \\ R_{\pm} &= \sqrt{\rho^2 + (z \pm \sqrt{M^2+a^2})^2}. \qquad (3.17) \end{aligned}$$

To achieve the dihole universe where either of the two black holes or both are replaced by negative-mass objects, the card diagram rule [53, 51, 89] is just to explicitly change the sign of the branches of $R_{\pm}$ in (3.16). This gives a Weyl description of regions II, III, and IV in Fig. 3.2. The sign of R_- corresponds with the object at $\theta = 0$, and the sign of R_+ corresponds with the object at $\theta = \pi$.

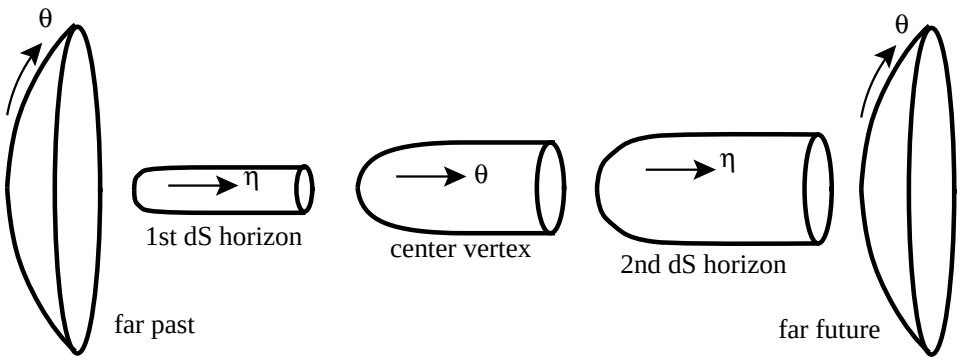

Figure 3.14: Time-evolution of spacelike 2-surfaces involving the ϕ-circle, for the S-dihole $\mathcal{U}$ universe. This is drawn for small a, where $\Sigma_- < M^2 < \Sigma_+$ and so the asymptotic proper circumference of the ϕ circle increases for the bubble-type fiberings.

Let us move to region III_+ of the $\mathcal{U}$-universe of subextremal S-dihole. Starting from the black dihole, we first continue $a \to ia$, $t \to ix^4$, $\phi \to i\phi$—this puts us in region I on Fig. 3.4. Then we then keep $z \geq \sqrt{M^2 - a^2}$ and put $\rho \to i\rho'$, to pass to region III_+, and then perform a γ-flip. The signs of (R_+, R_-) for III_+ are thus $(+,+)$. When we pass down through the vertex in the $\mathcal{U}$ universe to region II, we pass over the special null line for R_-, and hence change the sign of R_- in (3.16). As we go farther into the past and pass the R_+ vertex into region III_-, we must change the sign of R_+ as well. Thus the time-evolution of the $\mathcal{U}$ universe from past to future (from noncompact to compact to noncompact wedge card) is

$$\mathcal{U}: \qquad (-,-), \qquad (+,-), \qquad (+,+).$$

Similarly, the $\mathcal{U}_\pm$ time evolve according to branches

$$\begin{aligned} \mathcal{U}_+ &: \qquad (-,+), \qquad (+,+), \qquad (+,-), \\ \mathcal{U}_- &: \qquad (+,-), \qquad (-,-), \qquad (-,+). \end{aligned}$$

The $\mathcal{E}_+$ universe can be gotten directly from the dihole's exterior universe. Then $\mathcal{E}$ is gotten by sending $R_- \to -R_-$, and $\mathcal{E}_-$ is gotten by further sending $R_+ \to -R_+$.

3.5 KK interpretation and Bonnor Transform

The ergosphere singularity of a dilatonized version of S-Melvin was found and discussed in [64]. Just as dilatonized Melvin can be obtained by twisting a completely flat KK direction with an azimuthal angle [61], S-Melvin can be obtained by twisting a completely flat KK direction with a boost parameter. The ergosphere singularity

is then where the twisted KK direction becomes null. On one side of the ergosphere singularity (small ρ on the horizontal card), the twisted KK direction is spacelike whereas on the other side (large ρ on the horizontal card) it is timelike yielding a KK CTC.

Actually, this is a general feature of ergosphere singularities: The singularity occurs when the KK Killing direction goes null. This also occurs in the Bonnor transformation (see Appendix 3.9). We wish to emphasize the following connection: The 'ergosphere,' where a timelike Killing direction of say Kerr becomes null and switches to spacelike, maps via the Bonnor transformation to an ergosphere singularity of say the S-dihole $\mathcal{E}_+$, where a dilatonized version has a KK circle changing signature. The precise connection is that the Bonnor transformation can be understood from the KK perspective in reducing from five to four dimensions.[6] If we take a magneto-Weyl (MW) solution (3.2) and dilatonize it with $\alpha = \sqrt{3}$ [91, 92, 54] we get

$$\begin{aligned} ds^2_{\rm dil} &= -f^{1/2} dt^2_{\rm MW} + f^{-1/2}\big(e^{2\gamma}(d\rho^2+dz^2)+\rho^2 d\phi^2\big) \\ A_{\rm dil} &= \frac{1}{2} B d\phi \\ e^{2\phi} &= f^{\sqrt{3}/2}. \end{aligned} \tag{3.18}$$

Lifting to 5 dimensions [61, 25], we get

$$ds^2_{\rm 5d} = f(dx^5 + B d\phi)^2 - dt^2_{\rm MW} + f^{-1}\big(e^{2\gamma}(d\rho^2+dz^2)+\rho^2 d\phi^2\big),$$

and the Killing $t_{\rm MW}$ becomes completely flat. It may be dropped and the resulting 4d solution is a Kerr-type instanton. Upon Wick rotating $x^5 \to i t_{\rm Kerr}$ and $B \to -i\omega$, the x^5 direction becomes Kerr time. Hence x^5 and $t_{\rm Kerr}$ change signature on the same complexified locus, the 'ergosphere.'

For a time-dependent Weyl-Papapetrou geometry, we can add a trivial *space* direction and then KK reduce along a different space direction, and undilatonize. There is no analytic continuation in this case and this is why S-dihole, as the Bonnor transform of S-Kerr, does not have $a \to ia$ relative to it.

3.5.1 Generating nontrivial geometries from trivial ones

We have seen how the near-vertex scaling limit of the $\mathcal{U}$ universe gives us the RN bubble. Turned on its side, this gives us the Reissner-Nordström S-brane (S-RN). This should be the Bonnor transform of a near-vertex scaling limit of Kerr's double Killing bubble, $\mathcal{K}_+$ for $r \geq r_+$. Specifically, we want to zoom in on the north pole of the Kerr horizon, i.e. $\theta = 0$ for $\mathcal{K}_+$'s rod, at $z = \sqrt{M^2 - a^2}$, $\rho = 0$. Such focusing limits on nonextremal geometries always give flat space, albeit in a strange coordinate

[6] This has been known; see comments in e.g. [70, 92].

system. For $\mathcal{K}_+$'s north pole, flat space is written on the horizontal card $0 \leq 2\eta \leq \pi$ as

$$\begin{aligned} ds^2 &= d\epsilon^2 + \epsilon^2 d\eta^2 - \epsilon^2(M^2\cos^2\eta - a^2)(dt + a\sin^2\eta d\phi/(M^2\cos^2\eta - a^2))^2 \\ &\quad + \frac{\epsilon^2(M^2 - a^2)\cos^2\eta\sin^2\eta d\phi^2}{M^2\cos^2\eta - a^2}. \end{aligned}$$

The corresponding instanton ($t \to ix^5$, $a \to ia$) has a self-dual nut [103] at $\epsilon = 0$ for the Killing vector $\partial/\partial x^5$.

The point is then that since the Bonnor transform relies on (i) a choice of two Killing directions to put the metric in Weyl-Papapetrou form and (ii) and choice of one of those two Killing directions to be 'time,' it is not unique, and we can have a nontrivial Bonnor transform of flat space. In the present example, the near-north-pole limit of $\mathcal{K}_+$, with its Killing time t and azimuth ϕ, transforms to give us the S-RN solution in Poincaré/parabolic coordinates [51, 89], where $t \to ix^5$ is reduced and ϕ becomes the bubble Euclidean circle. Kerr's ergosphere has become the S-RN singularity.

3.5.2 D6-brane interpretation

Upon dilatonization and lifting to 5d, six extra flat directions can be added to give a solution to 11d supergravity (or M-theory). The local characterization of each black hole as a self-dual/anti-self-dual nut gives it a (Euclidean) D6-brane interpretation in the lifted theory [18, 19]. These objects may be located off the real manifold; in Appendix 3.8 we describe how they may be located in Weyl coordinates in terms of intersection of an ergosphere locus with $\rho^2 = 0$.

The formulas for reducing the 11d metric to the 10d IIA string metric are almost identical to $\text{Einstein}_5 \to \text{Einstein}_4$ reduction [93, 94]. To the metric in (3.18) we merely add $f^{1/2}(d\mathbf{R}^6)^2$, with an $ISO(6,1)$ symmetry. Removing the dilaton here could potentially yield S-brane solutions like the $\mathcal{U}$-universes with fibered dS_8 scaling limits.

3.6 Summary

The Kerr and Kerr $\pi/2$-bubble solutions, under Bonnor transform, become the black dihole and dihole wave solutions. Acting on S-Kerr or the double-Killing bubbles of Kerr, Bonnor gives us new solutions which we refer to collectively as S-dihole solutions.

There are six subextremal S-dihole universes which we called $\mathcal{U}, \mathcal{U}_\pm$ and $\mathcal{E}, \mathcal{E}_\pm$. The three $\mathcal{U}$-type universes were nonsingular and had a near-vertex limit to the Reissner-Nordström bubble. Through a combination of card and Penrose diagram, we understand the features of the spacetimes, and have attempted to depict their global

structure. The $\mathcal{E}$ universes had ergosphere singularities, represented the decay of two-dimensional unstable objects, and had a near-vertex limit giving the S-Reissner-Nordström solution.

The superextremal S-dihole has a simple card diagram. Physically it shows the creation and decay of an asymptotic conical deficit, and it has an S-charge that is conserved only in a limited sense (on constant-time Weyl slices). This is in contrast with the dihole wave which has a robustly conserved S-charge. Both solutions turn on their sides (see Appendix 3.7).

The roles of card, spherical prolate, and affine coordinates have been clarified, as has the location of the ergosphere, ring singularity, and special $\rho^2 = 0$ loci, and their intersections (Appendix 3.8). The Bonnor transform of ergospheres and ring (i.e. usual curvature) singularities are shown to have identical properties (Appendix 3.9).

The Bonnor transform is related to $5 \to 4$ KK reduction and Weyl dilatonization procedures. These dilatonization procedures will not change spacetimes with simple card diagrams, but will destroy the interesting structure of those card diagrams where the special null line serves as conformal null infinity, such as the $\mathcal{U}$-type and $\mathcal{E}$-type universes. Dilatonized solutions lift to IIA string theory and M-theory as configurations of D6- and $\bar{\text{D}}$6-branes.

3.7 Appendix: More universes by turning cards on their sides

Taking the half-plane vertical cards that are the dihole wave and the superextremal S-dihole, we can turn them on their sides via the γ-flip, namely $e^{8\gamma} \to -e^{8\gamma}$ [51, 89]. Vertical cards are then connected by a horizontal card which is a doubly covered half-plane, like the superextremal RN black hole in 4 dimensions [51, 89]. The geometries we get have ergosphere singularities appearing as circular loci on the horizontal cards, as well as a 'ring' singularity at a point. The ergosphere singularities can be gotten rid of by dilatonization [92, 54] and lifting to 5d. The vertical cards are nonsingular.

3.7.1 Dihole wave on its side

The dihole wave of [25] exists for $r \geq r_+$ and $r \leq r_-$; both can be put on their sides to give the vertical cards of this universe. It is

$$\begin{aligned} ds^2 &= \big(1-2Mr/\Sigma\big)^2\Big((dx^4)^2+\frac{\Sigma^4}{(\Delta+(a^2+M^2)\cosh^2\theta)^3}(-dr^2/\Delta+d\theta^2)\Big) \\ &\quad +\frac{\Delta\cosh^2\theta}{(1-2Mr/\Sigma)^2}d\phi^2, \\ A &= \frac{2aMr\cosh^2\theta}{\Delta+a^2\cosh^2\theta}d\phi, \end{aligned}$$

where $\Sigma = r^2 + a^2\sinh^2\theta$ and $\Delta = r^2 - 2Mr - a^2$. This spacetime comprises all three regions in the spherical prolate diagram in Fig. 3.3. Both Killing directions are noncompact. It has an ellipse ergosphere singularity on the horizontal card and a point $\Sigma = 0$ curvature singularity. A dilatonized version lifts to a 5d solution with just the $\Sigma = 0$ singularity. Our solution is the Bonnor transform of the Kerr $\pi/2$-bubble (gotten from Kerr by $t \to ix^4$, $\theta \to \pi/2 + i\theta$, $a \to ia$), turned on its side [67].

3.7.2 S-dihole superextremal on its side

Take the superextremal S-dihole, and turn it on its side via the γ-flip. Written for real θ on the vertical half-plane cards, we have

$$\begin{aligned} ds^2 &= \big(1-2Mr/\Sigma\big)^2\Big((dx^4)^2+\frac{\Sigma^4}{(\Delta+(a^2-M^2)\sinh^2\theta)^3}(\frac{dr^2}{\Delta}-d\theta^2)\Big) \\ &\quad +\frac{\Delta\sinh^2\theta}{(1-2Mr/\Sigma)^2}d\phi^2, \\ A &= \frac{2aMr\sinh^2\theta}{\Delta+a^2\sinh^2\theta}d\phi, \end{aligned}$$

where $\Delta = r^2 - 2Mr + a^2$ and $\Sigma = r^2 + a^2\cosh^2\theta$. This spacetime comprises all three regions in the spherical prolate diagram in Fig. 3.8. Both Killing directions are noncompact. It has an ellipse ergosphere singularity on the horizontal card and a point $\Sigma = 0$ curvature singularity. A dilatonized version lifts to a 5d solution with just the $\Sigma = 0$ singularity. Our solution is the Bonnor transform of the superextremal S-Kerr, turned on its side [67].

3.8 Appendix: Ergosphere and ring singularity as affine loci

The Kerr, black dihole, and related manifolds have two non-Killing directions which can be complexified. We now study the ergosphere and ring singularity loci

in terms of natural affine coordinates C, Z for $\mathbb{C}^2 \subset \mathbb{P}^1 \times \mathbb{P}^1$. Here, $C = \pm\cosh\theta$ or $\cos\theta$, and for subextremal Kerr, $Z = (r - M)/\sqrt{M^2 - a^2}$. The dihole has $a \to ia$ relative to Kerr.

Take subextremal Kerr or the black dihole. The family of polynomials $P_\rho(C, Z) = (M^2 \pm a^2)(Z^2 - 1)(1 - C^2) - \rho^2$ vanish to define $\rho^2 = -\det_{2\times 2} g_{\alpha\beta} \in \mathbf{C}$ in terms of the complex affine coordinates. The locus $P_\rho = 0$ is only algebraically singular for $\rho^2 = 0$, i.e. $C, Z = \pm 1$, or for $\rho^2 = -(M^2 \pm a^2)$, i.e. $C = Z = 0$. These are the five vertices in Figs. 3.1,3.4.

Killing circles become null or vanish at $\rho^2 = 0$, i.e. $Z = \pm 1$ or $C = \pm 1$. The real manifold's card diagram is in some sense a square-root-fold over those $C, Z = \pm 1$ which serve as horizons.

For the Kerr black hole (or the S-dihole), the ring singularity is

$$(\sqrt{M^2 - a^2}Z + M)^2 + a^2C^2 = 0.$$

This quadric is reducible to the union of two complex lines. They meet at the algebraically singular vertex, $C = 0$, $Z = -M/\sqrt{M^2 - a^2}$, which happens to lie on the real manifold.

The ergosphere, on the other hand, is

$$Z^2 + \frac{a^2C^2}{M^2 - a^2} = \frac{M^2}{M^2 - a^2}.$$

This is an irreducible hyperboloid. It is fitting that this geometrically nonsingular locus (for Kerr) is also algebraically nonsingular. It forms an ellipse on the real CZ plane; it circumscribes the square and the distinguished points of this ellipse are where the ergosphere hits the $C, Z = \pm 1$ vertices (see Fig. 3.1). The ergosphere asymptotes to $(M^2 - a^2)Z^2 + a^2C^2 = 0$ and the ring singularity is a shift of this so that its vertex lies atop the ergosphere.

For the dihole, the ring singularity is

$$(\sqrt{M^2 + a^2}Z + M)^2 - a^2C^2 = 0.$$

which is now reducible in the reals: The singularity cuts two lines across the real CZ diagram, as shown in Fig. 3.2. Note then that the top region I is free of singularities, being the exterior to both black holes. The bottom region IV is has two singularities, each cutting off its black hole horizon ($C, Z = \pm 1$ vertex) from the negative-mass complement. The side regions II and III each have one ring singularity locus, cutting off the appropriate black hole interior from the negative-mass complement (which then also has a nonsingular black hole).

The ergosphere is at $Z^2 - a^2C^2/(M^2 + a^2) = M^2/(M^2 + a^2)$, which intersects the real manifold as a hyperbola. This hits the vertices $C, Z = \pm 1$ and does not enter the horizontal card regions I, II, III, IV. Thus the only effect on the 'ergosphere

singularity' on the physical black dihole spacetime is to pierce the real Weyl half-planes at vertices $z = \pm\sqrt{M^2 + a^2}$, $\rho = 0$ and to create the extremal horizons.

For superextremal Kerr or S-dihole, we set $r = M + \sqrt{a^2 - M^2}Z$, $Z = \sinh\zeta$; see Fig. 3.8. The polynomial

$$P_\rho(C, Z) = (a^2 - M^2)(1 + Z^2)(1 - C^2) - \rho^2$$

gives algebraic singularities at $C = Z = 0$ (the branch point) as well as $Z = \pm i$, $C = \pm 1$. The latter coincide with the intersection of the ergosphere singularity with $\rho^2 = 0$, which are the imaginary 'locations' of the Euclidean D6-branes (or black holes) in the superextremal S-dihole. Similar considerations apply to the dihole wave (Fig. 3.3) and give the imaginary locations of the branes.

For all Kerr and derived solutions, it is satisfying that the features of the geometry admit such a simple description in terms of hyperbolas and intersecting lines, and that distinguished points occur at the intersection with special surfaces $\rho^2 = 0$, or at algebraically singular points.

The use of these affine coordinates may have further uses. For example, it can be proved in 4d Weyl-Papapetrou that any ergosphere locus that intersects $\rho^2 = 0$ transversally, must do so where ρ^2 is algebraically singular. This gives additional explanation to why Kerr's ergosphere hits $Z = \pm 1$, $C = \pm 1$, even though we already know physically that the ergosphere must touch a spinning horizon at the poles.

Furthermore, loci such as ergosphere and ring singularity are always expressible in terms of certain-degree polynomials in a compactified $\mathbf{P}^1 \times \mathbf{P}^1$. A variable-$\Omega$ ergosphere defining polynomial will be reducible when $\Omega = \Omega_\pm$ is the angular velocity at the horizon; then $(Z \mp 1)$ factors out. There may be other, physical or nonphysical, values of parameters such as Ω that result in reducibility of these loci. The application of polynomial or algebraic geometry to these loci may yield further insights into Weyl spacetimes.

3.9 Appendix: Character of ergosphere and ring singularities

We give a brief characterization of ergospheres and their Bonnor-transforms, and compare them with the 'ring' singularity. Given a 2×2 Killing metric in the Weyl-Papapetrou form (3.1) with the understanding that ∂_t is a distinguished direction for an ensuing Bonnor transformation, we can define its ergosphere locus to be the nonsingular locus where f vanishes. Then ω must have a pole like f^{-1} so that

$$\begin{pmatrix} -f & f\omega \\ f\omega & f^{-1}\rho^2 - f\omega^2 \end{pmatrix} \to \begin{pmatrix} 0 & \text{finite} \neq 0 \\ \text{finite} \neq 0 & \text{finite} \end{pmatrix},$$

where we have nondegeneracy away from $\rho^2 = 0$. In the interior of a card, from (3.1) we see that $e^{2\gamma} \sim f$ to keep the coefficient of $d\rho^2 + dz^2$ finite. Thus in the Bonnor-transformed geometry (3.2) we see that the coefficients of $-dt^2$ and $d\rho^2 + dz^2$ vanish like f^2, the coefficient of $d\phi^2$ blows up like f^{-2}, and the magnetic potential A_ϕ blows up like f^{-1}. (At the card boundary $\rho = 0$, we have seen for the dihole that instead, the ergosphere gives nonsingular extremal black holes which are locally $\mathrm{AdS}_2 \times S^2$.) This characterization of ergosphere singularities will help us to identify them—because upon dilatonization and a KK lift to 5d, they are resolved (see Sec. 3.5).

When the Weyl-Papapetrou geometry is singular, we do not have much to say in general, but we will look at the Bonnor transform of the Kerr ring singularity and find a surprise. There, $f \sim 1/\Sigma$ blows up, and $e^{2\gamma}$ stays finite. Then, the Bonnor-transformed geometry has non-Killing $d\rho^2 + dz^2$ as well as $d\phi^2$ vanish like f^{-2} and the $-dt^2$ direction blows up like f^2. Also, one can compute the electric EM-dual potential for the black dihole:

$$A_t = \frac{2Ma\cos\theta dt}{(r^2 - a^2\cos^2\theta)},$$

and this blows up like f. (It is not surprising that the electric potential blows up at the curvature singularity of a charged black hole.) Thus the Bonnor transform of a ring singularity is just like that for an ergosphere, but with the roles of ϕ and t exchanged. It them seems possible that $\Sigma = 0$ could be made nonsingular with the right inverse transform, but in the present case, the locus intersects the real spacetime at a vertex point where it is algebraically singular, and also is a subset of the ergosphere singularity. So we do not immediately expect any new nonsingular geometries from this idea.

3.10 Appendix: Dihole wave fall-off

The magneto-gravitational wave decay for the dihole wave geometry [25, 51] can be analyzed by setting $\tau = \rho + \text{constant}$, and looking at the decay of say g_{44}. The result is $g_{44} \sim 1 + \mathcal{O}(1/\tau^{1/2})$.

We can understand this power-law decay in Weyl coordinates with the following linearized model, using x, y, z, τ coordinates in Minkowski 4-space. A codimension 3+1 source for the wave equation gives precisely causal wave fronts, and a codimension $2+1$ source can be gotten by dimensional reduction. Hence we may write a wave as

$$\delta g_{44}(x, y, \tau) = \int_{-\infty}^{\infty} \Big(\frac{dz}{x^2 + y^2 + z^2 - \tau^2 + i\epsilon} + \text{c.c.} \Big)$$

where ϵ is a regulator. Along $x^2 + y^2 - \tau^2 = 0$, $\delta g_{44} = \frac{1}{\sqrt{\epsilon}} \int_{-\infty}^{\infty} \frac{\zeta^2 d\zeta}{\zeta^4 + 1}$. If the wave is regulated by displacing the source into imaginary time, $\tau \to \tau \pm i\alpha$, we find that $\epsilon \propto \tau$. Therefore the behavior for such time-displaced wave sources is $\delta g_{44} \sim 1/\tau^{1/2}$.

Chapter 4

Kerr S-brane and Instanton

The S-brane for the higher-dimensional Kerr (Myers-Perry) black holes [104] is correctly analyzed in odd dimensions. Key issues of the global structure have been missed in previous descriptions [49]. We find that in the 'anomalous range' of large a_i compared to small but positive mass μ, for $D = 7, 9, \ldots$ there is a new instanton of topology $S^3 \times \mathbf{R}^{D-3}$, in contrast to the usual Kerr instanton of topology $\mathbf{R}^2 \times S^{D-2}$. Note that for $D = 5$ there is a putative 'new instanton' of $\mathbf{R}^2 \times S^3$, but in this case it is isometric to the usual one. There are indications that these new instantons mediate the decay of simpler spacetimes with the same asymptotics, a work which has not been completed.

Card diagrams are used to illustrate the $D = 5$ case. Unfortunately the $D = 5$ S-brane is identically a bubble, and the new instanton is the usual one, but the constructions are markedly different and showcase the method, which applies in $D = 7, 9, \ldots$. We also give the 5d black hole 'on its side' solution, which is new and nonsingular. We also give some other solutions like the Kerr bubble on its side, superextremal S-Kerr on its side, the S-brane for Taub-NUT in $\pi/2$- (nonsingular) and double Killing- (CTCs) versions. We discuss Taub-NUT on its side and generating techniques.

The S-Kerr work was done with J. E. Wang and may be forthcoming as a publication. For earlier S-Kerr work, see [47, 48].

4.1 Odd D with one a_i turned off: Global structure of the solution

Take $D = 2n + 1$, and take $a_n = 0$, with other $a_i \neq 0$. The Myers-Perry black hole solution is

$$ds^2 = -dt^2 + \sum_{i=1}^{n}(r^2 + a_i^2)(d\mu_i^2 + \mu_i^2 d\phi_i^2) + \frac{\mu r^2}{\Pi F}(dt + \sum_{i=1}^{n} a_i \mu_i^2 d\phi_i)^2 + \frac{\Pi F}{\Pi - \mu r^2} dr^2 \quad (4.1)$$

and we set $a_n = 0$. Here,

$$\Pi = \prod_{i=1}^{n}(r^2 + a_i^2), \qquad F = \sum_{i=1}^{n} \frac{r^2\mu_i^2}{r^2 + a_i^2}.$$

To Wick rotate, we send

$$t \to iz, \quad r \to it, \quad a_i \to ia_i, \quad \mu_i \to i\mu_i \ (i = 1, \ldots, n-1), \quad \phi_n \to i\phi_n,$$

and we determine ϕ_n's compactness later. We also make the conventional change $\mu \to -\mu$ for $D = 5,\ 9,\ 13,\ \ldots$ but not for $D = 7,\ 11,\ \ldots$. The relation $\sum_{i=1}^{n} \mu_i^2 = 1$ becomes $\mu_n^2 - \sum_{i=1}^{n-1} \mu_i^2 = 1$. We get

$$\begin{aligned} ds^2 = dz^2 - t^2 d\mu_n^2 + t^2\mu_n^2 d\phi_n^2 + \sum_i (t^2 + a_i^2)(d\mu_i^2 + \mu_i^2 d\phi_i^2) \\ - \frac{\mu}{\prod_i (t^2 + a_i^2)\big(\mu_n^2 - \sum_i \frac{\mu_i^2}{1 + a_i^2/t^2}\big)} \big(dz + \sum_i a_i \mu_i^2 d\phi_i\big)^2 \\ - \frac{\prod_i (t^2 + a_i^2)\big(\mu_n^2 - \sum_i \frac{\mu_i^2}{1 + a_i^2/t^2}\big)}{\prod_i (t^2 + a_i^2) - \mu} dt^2 \end{aligned} \tag{4.2}$$

where all products and sums are over $i = 1, \ldots, n-1$. The S-brane solution has a global structure which was missed in [49].

There is a single horizon (where $g_{tt} = \infty$) for $\mu > \prod_i a_i^2$, at some $t_H > 0$. This is a horizon in the coordinates t and $\tilde{z}$, where $\tilde{z}$ is z twisted with ϕ_i's. Near $t = 0$, the metric contains pieces that look like

$$t^2\mu_n^2 d\phi_n^2 + \frac{(\prod_i a_i^2)\mu_n^2}{\mu - \prod_i a_i^2} dt^2.$$

This is a ϕ_n-boundary, and we can avoid a conical singularity by compactifying

$$\phi_n \simeq \phi_n + 2\pi \sqrt{\frac{\prod_i a_i^2}{\mu - \prod_i a_i^2}}. \tag{4.3}$$

The tz Penrose diagram, drawn for a $\mu_n = 1$ slice, is then four regions, all with $t > 0$; they are connected in a $\times$-pattern at $t = t_H$. The upper and lower regions are diamonds. The left and right regions are triangles; the universe is closed on their timelike $t = 0$ boundaries; and CTCs can be found in these regions. See Fig. 4.1(a).

For $0 < \mu < \prod_i a_i^2$, there is no tz horizon. Near $t = 0$, we have

$$t^2\mu_n^2 d\phi_n^2 - \frac{(\prod_i a_i^2)\mu_n^2}{\prod_i a_i^2 - \mu} dt^2.$$

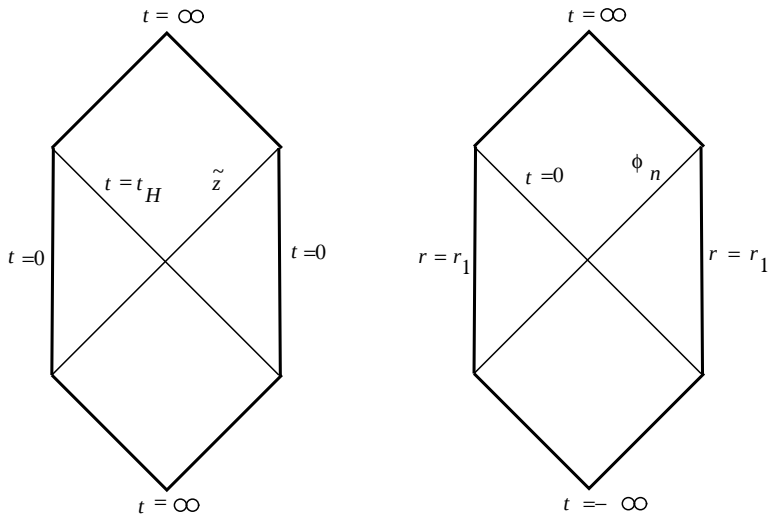

Figure 4.1: (a) On the left, the Penrose diagram for the ordinary $\mu > \prod_i a_i^2$ nonsingular S-Kerr. (b) On the right, the Penrose diagram for the anomalous $\mu < \prod_i a_i^2$ nonsingular S-Kerr.

We want ϕ_n noncompact: This is a Milne horizon. The prototypical Milne embedding is of $t > 0$, ϕ into the upper wedge of Minkowski 2-space $ds^2 = -dT^2 + dX^2$ as

$$\begin{aligned} X &= t \sinh \phi \\ T &= t \cosh \phi. \end{aligned}$$

Setting $t < 0$ gives the lower Milne wedge, and continuing $t \to \pm ir$, $\phi \to \phi + i\pi/2$ gives the Rindler wedges. Thus $t > 0$ is the upper diamond of our Penrose diagram, $t < 0$ is the lower diamond, and imaginary t gives right and left diamonds, which we now investigate.

So put $t \to ir$ in (4.2); we get

$$\begin{aligned} ds^2 = dz^2 + r^2 d\mu_n^2 - r^2 \mu_n^2 d\phi_n^2 + \sum_i (a_i^2 - r^2)(d\mu_i^2 + \mu_i^2 d\phi_i^2) \\ - \frac{\mu}{\prod_i (a_i^2 - r^2)\big(\mu_n^2 - \sum_i \frac{\mu_i^2}{1 - a_i^2/r^2}\big)} \big(dz + \sum_i a_i \mu_i^2 d\phi_i\big)^2 \\ + \frac{\prod_i (a_i^2 - r^2)\big(\mu_n^2 - \sum_i \frac{\mu_i^2}{1 - a_i^2/r^2}\big)}{\prod_i (a_i^2 - r^2) - \mu} dr^2 \end{aligned} \tag{4.4}$$

Now, ϕ_n is a time direction, under which the metric is static. The rest of the Killing directions have purely Riemannian (positive definite) signature, so there are no CTCs. The next possible singularity occurs at $\prod_i (a_i^2 - r^2) - \mu = 0$, which has precisely one

simple root $0 < r_1 < a_1$, with negative slope, where we take $a_1 \leq \cdots \leq a_{n-1}$. Here, $g_{rr} = \infty$; nothing else goes wrong and in particular Coef dz^2 has not gone negative since $\mu_n^2 - \sum_i \frac{\mu_i^2}{1-a_i^2/r^2} \geq \mu_n^2 \geq 1$. We have a twisted $\tilde{z}$-boundary at $r = r_1$.

The surface gravity in [104] is

$$\kappa = \left. \frac{\partial_r \Pi - 2\mu r}{2\mu r^2} \right|_{r=r_1},$$

and we compute it (ignoring overall signs) in our present scenario to be

$$\kappa = \left. \frac{1}{2\mu} \frac{\partial}{\partial r} \prod_{i=1}^{n-1} (a_i^2 - r^2) \right|_{r=r_1},$$

where we used $\prod_{i=1}^{n-1}(a_i^2 - r_1^2) - \mu = 0$. For $D = 5$ this simplifies to $\kappa = \sqrt{a^2 - \mu}/\mu$. Following [61] we can twist to new variables

$$\tilde{z} = z, \qquad \tilde{\phi}_i = \phi_i - \Omega_i z, \qquad \Omega_i = \frac{a_i}{a_i^2 - r_1^2}$$

and compactify $\tilde{z} \simeq \tilde{z} + 2\pi/\kappa$ to close off the spacetime at $r = r_1$. Note that this makes $l = \frac{\partial}{\partial z} + \sum_{i=1}^{n-2} \Omega_i \frac{\partial}{\partial \phi_i} = \frac{\partial}{\partial \tilde{z}}$ null at $r = r_1$.

It is appropriate to draw a $t\phi_n$ Penrose diagram (drawn for the $\mu_n = 1$ slice). It again has four regions connected in a $\times$-pattern at $t = 0$. The upper and lower diamonds are at $t > 0$ and $t < 0$, and the right and left triangles are at $r > 0$ and $r < 0$. The triangles end at their timelike boundary $r = r_1$. See Fig. 4.1(b).

We do not consider the details of singular $\mu < 0$ for general odd D.

4.1.1 A simpler continuation

Usually in the construction of an S-brane, some continuation $r \to it$ is done. Solutions have functions which depend on r and it is not a priori clear that a real S-brane geometry can be obtained this way. Often times other parameters, M or a_i are continued, and the end result is that horizon functions and other functions take the same functional form as in the black hole solution. As the reader may guess, much of this analytic continuation is unnecessary.

We give a simpler analytic continuation for $D = 2n + 1$ S-Kerr. This is a generalization of the idea of the γ-flip for 4d and 5d solutions ([51], and below for 5d S-Kerr). Take the $D = 2n + 1$ Kerr geometry (4.1) with $a_n = 0$, and continue

$$\mu_i \to i\mu_i, \ i = 1, \ldots, n-1, \qquad \phi_n \to i\phi_n, \qquad g_{\mu\nu} \to -g_{\mu\nu}.$$

The last step, being the sign flip of the metric, emphasizes that charged solutions solve Einstein-anti-Maxwell (where the gauge field is imaginary) after this procedure.

In the presence of a gauge field, a further $Q \to iQ$ or some other transformation is needed; this $Q \to iQ$ does change horizon functions. Additionally, if the cosmological constant Λ is nonzero, it will flip sign. The constraint is now $\mu_n^2 - \sum_{i=1}^{n-1} \mu_i^2 = 1$.

For $D = 2n + 2$ Kerr, there is $-1 \leq \mu_0 \leq 1$ in addition to $\mu_i \geq 1$, $i = 1, \ldots, n$. Keep all the a_i, $i = 1, \ldots, n$ turned on. Then the continuation [49] to S-Kerr is just

$$\mu_i \to i\mu_i, \ i = 1, \ldots, n, \qquad g_{\mu\nu} \to -g_{\mu\nu}.$$

The constraint is now $\mu_0^2 - \sum_{i=1}^{n} \mu_i^2 = 1$.

4.1.2 A New Kerr Instanton

For the range $0 < \mu < \prod_i a_i^2$, one can take the right diamond $0 < r < r_1$ and continue $\phi_n \to i\phi_n$. This region is now a D-dimensional instanton, and one can compactify according to

$$\phi_n \simeq \phi_n + 2\pi \sqrt{\frac{\prod_i a_i^2}{\prod_i a_i^2 - \mu}}$$

to close off the spacetime at $r = 0$. Thus the coordinate r runs over $[0, r_1]$, the ϕ_n-circle closes at $r = 0$ and the $\tilde{z}$-circle closes at $r = r_1$. The topology of the instanton is thus

$$S^3 \times \mathbf{R}^{D-3},$$

where S^3 is parametrized by variables r, $\tilde{z}$, and ϕ_n, and $\mathbf{R}^{D-3}$ is parametrized by variables μ_i and ϕ_i for $i = 1, \ldots, n-1$. (Note that μ_n is a redundant variable.) This is in contrast to the usual Kerr instanton which has topology

$$\mathbf{R}^2 \times S^{D-2}, \tag{4.5}$$

where $\mathbf{R}^2$ is parametrized by r and $\tilde{z}$, and S^{D-2} is parametrized by cosines and azimuthal angles μ_i, $i = 1, \ldots, n-1$, and ϕ_i including ϕ_n. What happens when we make analytic continuation from the regular Kerr instanton, is that the ϕ_n circle no longer closes at a special locus in the second factor of (4.5) but instead closes at a special locus in the first factor of (4.5), giving us an S^3, and the second factor decompactifies to a hyperbolic sheet, or $\mathbf{R}^{D-3}$ (it is really half of a hyperboloid of two sheets: $\mu_n^2 = 1 + \sum_i \mu_i^2$, $\mu_n \geq 1$).

We attempt to draw this instanton. Note that as $\mu_i \to \infty$, the ϕ_n-circle gets very large. Keeping in mind that $\mathbf{R}^{D-3}$ is like a hyperbolic sheet, we are led to Fig. 4.2. For $D = 5$, we have a card diagram, presented in Fig. 4.8.

The asymptotic region of the instanton is gotten by sending $\mu_i \to \infty$. We get in this limit a fibering of a twisted $S^3 \ltimes S^{D-4}$ over $\varrho = \sqrt{\sum_i \mu_i^2}$ where the radii of the spheres are proportional to ϱ. The details have not been finished in general D, describing how this instanton mediates the decay of a spacetime.

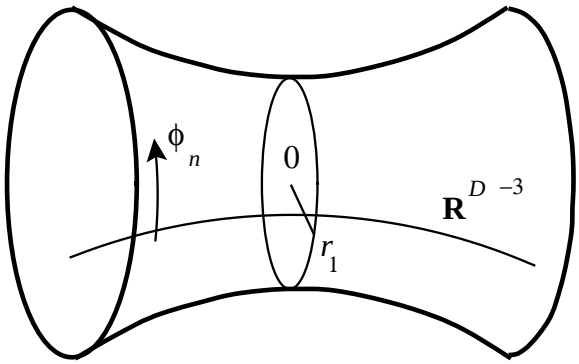

Figure 4.2: The new Kerr instanton. Here, $0 \le r \le r_1$, and ϕ_n generates the axial symmetry of the diagram. The coordinate $\tilde{z}$ is not drawn but its circle vanishes at the boundary $r = r_1$. A particular $\mathbf{R}^{D-3}$ hyperbolic slice is drawn.

4.1.3 Extremal

For $\mu = \prod_i a_i^2$ we have an extremal situation. Then the ordinary tz horizon coincides with the vanishing ϕ_n direction (we have $r_1 = 0$). Twist to $\tilde{z}$, $\tilde{\phi}_i$ ($i = 1, \ldots, n-1$) with $\Omega_i = 1/a_i$, and both $\tilde{z}$ and ϕ_n noncompact. We take a near-horizon scaling limit: Put $t \to t/\lambda$, $\tilde{z} \to \lambda\tilde{z}$, and send $\lambda \to \infty$. We find a dS_3 in this small-t limit:

$$\begin{aligned} ds^2 &= \mu_n^2 \left(\alpha^2 t^2 d\tilde{z}^2 + t^2 d\phi_n^2 - \frac{dt^2}{t^2(1/a_1^2 + \cdots + 1/a_{n-1}^2)} \right) \\ &\quad + \sum_i a_i^2 (d\mu_i^2 + \mu_i^2 d\tilde{\phi}_i^2) - \frac{1}{\mu_n^2} \big(\sum_i a_i \mu_i^2 d\tilde{\phi}_i \big)^2 . \end{aligned} \tag{4.6}$$

where α is some constant that depends on the a_i. So not only do we have the nonsingular $t > 0$ region, but we have an isomorphic $t < 0$ copy. The full solution is nonsingular. Since the Killing directions always have Riemannian signature, there are no CTCs.

The appearance of dS_3 is in contrast to the even-dimensional extremal S-Kerr, which has dS_2 [49]. The presence of these fibered dS_2, dS_3 geometries in the near-horizon limit is interesting in light of certain no-go theorems [105].

4.1.4 Kerr bubbles

For completeness, we describe the types of Kerr bubbles available.

In odd dimensions $D = 2n+1$, there are μ_i and ϕ_i, $i = 1, \ldots, n$. By taking $t \to iz$ and $\phi_j \to i\phi_j$ for one particular j, and continuing all angular momenta $a_i \to ia_i$

except a_j, we achieve the $\mathcal{K}_i$ bubble. The non-stationary part of the spacetime is gotten to by going through the Rindler horizon $\mu_j = 0$ to imaginary μ_j.

In even dimensions $D = 2n + 2$, there is μ_0 as well as μ_i, ϕ_i, $i = 1, \ldots, n$. We can find a $\mathcal{K}_i$ bubble as above, but there is also the possibility of a $\mathcal{K}_0$ (or $\pi/2$-) bubble by taking $\mu_0 \to \pi/2 + i\mu_0$. If rotations are turned on, this is different from the $\mathcal{K}_i$, $i = 1, \ldots, n$.

4.2 5D case and card diagrams

The simplest nontrivial example of D odd is $D = 5$. Since this spacetime has three commuting Killing vectors, it is of generalized Weyl type [16] and we can use canonical coordinates to draw a card diagram [51]. We start with the black hole and the old instanton, turn a black hole solution on its side, then move onto bubbles, S-branes and the new instanton.

4.2.1 Two turned on

The solution, writing $a_1 \to a$, $a_2 \to b$, $\phi_1 \to \phi$, $\phi_2 \to \psi$, $\mu_1 \to \cos\theta$, $\mu_2 \to \sin\theta$, is

$$\begin{aligned} ds^2 &= -dt^2 + \frac{\mu(dt + a\cos^2\theta d\phi + b\sin^2\theta d\psi)^2}{r^2 + a^2\sin^2\theta + b^2\cos^2\theta} + (r^2 + a^2)\cos^2\theta d\phi^2 \\ &\quad + (r^2 + b^2)\sin^2\theta d\psi^2 + (r^2 + a^2\sin^2\theta + b^2\cos^2\theta) \\ &\quad \times\Big(\frac{r^2 dr^2}{r^4 + r^2(a^2 + b^2 - \mu) + a^2b^2} + d\theta^2\Big). \end{aligned} \tag{4.7}$$

Using the canonical coordinates of [16], or just by solving an appropriate change of variables with a spherical prolate coordinate Ansatz, the Weyl coordinates are

$$\begin{aligned} \rho &= \frac{1}{2}\sin 2\theta\sqrt{r^4 + (a^2 + b^2 - \mu)r^2 + a^2b^2} \\ z &= \frac{1}{2}(r^2 - \frac{\mu - a^2 - b^2}{2})\cos 2\theta. \end{aligned} \tag{4.8}$$

The relevant horizon function is $\Delta = r^4 + (a^2 + b^2 - \mu)r^2 + a^2b^2$, with roots $r_\pm^2 = \frac{\mu - a^2 - b^2 \pm \sqrt{(\mu - a^2 - b^2)^2 - 4a^2b^2}}{2}$. We first take the case where both angular momenta are turned on, and assume $a > b > 0$. Treating a, b as fixed and viewing the discriminant as a quadratic in μ, there are three special values $\mu = (a \pm b)^2$ (each extremal) and $\mu = 0$ (the solution is flat). There are then four parameter ranges, $\mu > (a + b)^2$ (ordinary), $(a - b)^2 < \mu < (a + b)^2$ (superextremal), $0 < \mu < (a - b)^2$ (anomalous), and $\mu < 0$ (negative mass). In the ordinary, anomalous, and negative mass ranges, Δ has two distinct roots; these are all subextremal. There are rod horizons of half-length $\alpha = \frac{1}{4}\sqrt{(\mu - a^2 - b^2)^2 - 4a^2b^2}$.

The horizon function minimizes at the 'central' value of $r^2_{\rm cent} = \frac{\mu - a^2 - b^2}{2}$. There is just one (outer) ergosphere, where $g_{tt} = 0$, at $r^2_{\rm ergo} = \mu - \frac{a^2+b^2}{2} + \frac{a^2-b^2}{2}\cos 2\theta$. Since both a, b are turned on, the metric is not singular at $r^2 = 0$ and can be continued to negative values of r^2, as can be seen by setting $2l = r^2$ [104]. Then there is a singularity locus where $g_{tt} = \infty$, at $r^2_{\rm sing} = -\frac{a^2+b^2}{2} + \frac{a^2-b^2}{2}\cos 2\theta$.

In the 4d Kerr case the inner and outer ergospheres had identical shapes and were right on top of each other, but on different horizontal cards [51]. For the 5d case the ergosphere and the singularity occupy the same locus up to reflection $\theta \to \pi/2 - \theta$ (see Fig. 4.3). This can be seen from the spherical prolate coordinates and the fact that

$$r^2_{\rm ergo}(\theta) - r^2_{\rm center} = r^2_{\rm center} - r^2_{\rm sing}(\pi/2 - \theta).$$

Since the z direction points opposite directions on the two horizontal cards, this means the loci actually do coincide in ρ, z coordinates. For the example shown, $a > b > 0$, the ergosphere hugs closer to the horizon at $\theta = \pi/2$ and the singularity hugs closer to the horizon at $\theta = 0$.

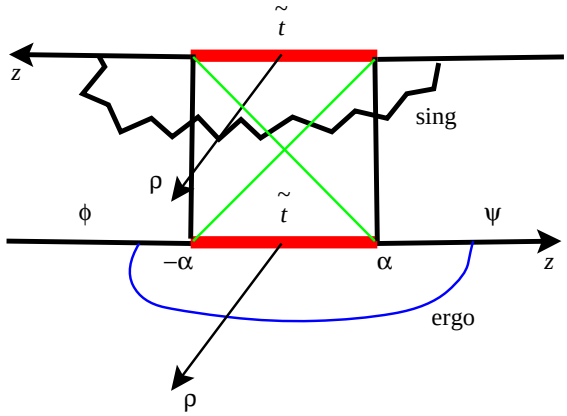

Figure 4.3: The Myers-Perry black hole card diagram, with both turned on, $a > b > 0$; and in the ordinary range $\mu > (a+b)^2$. The labelling ϕ, ψ, $\tilde{t}$ indicate boundaries where circles vanish and a spinning horizon. Of course, there are four cards that meet at each horizon and an infinite stack of cards, that are not drawn [51].

Beyond the singularity we have a negative-r^2 solution; however, it has signature $-----$. This can be seen by checking the signature as $r^2 \to -\infty$ which is clearly $-----$, and using some facts about the determinant of the metric. From [82] the 3×3 determinant of the $t\phi\psi$ Killing directions is $-\Delta\cos^2\theta\sin^2\theta$, and so the full 5×5 determinant is $-(r^2 + a^2\sin^2\theta + b^2\cos\theta)^2\cos^2\theta\sin^2\theta$, when it is expressed in terms of $dl^2 = r^2 dr^2$. The 5×5 determinant is negative except where it vanishes, at the singularity. The metric signature cannot change unless the determinant passes through zero.

The extremal solution $\mu = (a+b)^2$ has its rod degenerate to a point. The two horizons are now $r_\pm^2 = ab$, and the ergosphere is $r_{\rm ergo}^2 = 2ab + \frac{a^2+b^2}{2} + \frac{a^2-b^2}{2}\cos 2\theta$ which is nearest the horizon at $\theta = \pi/2$, $r^2 = 2ab + b^2$, and farthest at $\theta = 0$, $r^2 = 2ab + a^2$. The ergosphere stays away from the horizon just like the 4d case. The solution written explicitly is

$$\begin{aligned} ds^2 &= -dt^2 + \frac{(a+b)^2(dt + a\cos^2\theta d\phi + b\sin^2\theta d\psi)^2}{r^2 + a^2\sin^2\theta + b^2\cos^2\theta} + (r^2+a^2)\cos^2\theta d\phi^2 \\ &\quad + (r^2+b^2)\sin^2\theta d\psi^2 + (r^2 + a^2\sin^2\theta + b^2\cos^2\theta)\Big(\frac{r^2 dr^2}{(r^2-ab)^2} + d\theta^2\Big). \end{aligned} \tag{4.9}$$

To check near the horizon, we twist to $\tilde\phi = \phi - \Omega_\phi t$, $\tilde\psi = \psi - \Omega_\psi t$, $\tilde t = t$ where both angular velocities are equal: $\Omega_\phi = \Omega_\psi = -1/(a+b)$. After twisting, it is easy to take a near-horizon limit: Put $r^2 = ab + \epsilon^2$ and send $\epsilon \to 0$ holding $\epsilon d\tilde t$ fixed. Since the $d\tilde t^2$, $d\tilde t d\tilde\phi$, and $d\tilde t d\tilde\psi$ are all $\mathcal{O}(\epsilon^2)$, the latter two vanish in this limit and the resulting spacetime is static. We are left with

$$\begin{aligned} ds^2 &= -\epsilon^2 d\tilde t^2 \frac{ab + a^2\cos^2\theta + b^2\sin^2\theta}{(a+b)^2(ab + a^2\sin^2\theta + b^2\cos^2\theta)} \\ &+ \frac{(a+b)^2(a\cos^2\theta d\tilde\phi + b\sin^2\theta d\tilde\psi)^2}{ab + a^2\sin^2\theta + b^2\cos^2\theta} + (a+b)(a\cos^2\theta d\tilde\phi^2 + b\sin^2\theta d\tilde\psi^2) \\ &+ (ab + a^2\sin^2\theta + b^2\cos^2\theta)(d\epsilon^2/\epsilon^2 + d\theta^2). \end{aligned}$$

Superextremal solutions $(a-b)^2 < \mu < (a+b)^2$ have a branch cut on the horizontal card and are nakedly singular.

The extremal $\mu = (a-b)^2$ solution we will call 'anomalous extremal.' It is extremal in that the rod horizon has degenerated into a point. However, unlike the $\mu = (a+b)^2$ extremal solution, on the main horizontal card, the ergosphere and singularity locus are both present and enter into the point-horizon. Setting $r_{\rm ergo}^2 = r_{\rm cent}^2 = -ab$ we get $\cos 2\theta = -(a-b)/(a+b)$, the asymptotic angle where the ergosphere threads through the horizon. The singularity threads through at angle $\cos 2\theta = (a-b)/(a+b)$. Both the singularity and ergosphere emerge on the secondary horizontal card.

The anomalous (subextremal) region $0 < \mu < (a-b)^2$ has the ergosphere and singularity each running from one horizontal card up the vertical card to the other horizontal card. They do not intersect. The horizon rod is actually cut into two pieces by the ergosphere; the rod which is immediately accessible to the outside-ergo region is actually a twisted $\tilde x^5$ boundary, whereas the rod part which is inside the ergosphere is a $\tilde x^5$-horizon. The ergosphere locus on the vertical card, where the Killing directions have signature $+++$, is a singularity.

As $\mu \downarrow 0$ the ergosphere approaches (from below) the special null line that goes from $r^2 = r_+^2$, $\theta = 0$ to $r = r_-^2$, $\theta = \pi/2$. The singularity approaches this null line from above. This null line is preferred over the other because $a > b$. At $\mu = 0$ we

have a strange parametrization of flat space (it is not singular). The main horizontal card has signature $-++++$ and has the ψ-circle vanish along the rod as well as the right semi-infinite ray. The vertical card is split into two triangles; the triangles and the secondary horizontal card represent flat space of various signatures.

For the region $\mu < 0$, the ergosphere lies above the singularity and both are purely on the vertical card. The ergosphere on the vertical card is again a singularity. However, the $r^2 \to \infty$ universe is not nakedly singular. It does have CTCs. The $r^2 \to -\infty$ horizontal card has signature $-----$ and has r_-^2 as boundary, where we must twist ϕ and ψ to close an $\tilde{x}^5$ circle. Flipping the sign of the metric, we have a $+++++$ Kerr instanton. To see that this is the regular Kerr instanton, note that (i) sending $a \to ia$, $b \to ib$, $t \to ix^5$ is the same as (ii) sending $r^2 \to -r^2$, $\mu \to -\mu$, and $g_{\mu\nu} \to -g_{\mu\nu}$ in (4.7). In particular, performing either (i) or (ii), the horizon function becomes $\Delta = r^4 - r^2(a^2 + b^2 + \mu) + a^2b^2$. This has two roots for all $\mu > 0$, and the special values are $\mu = -(a \pm b)^2$ and of course $\mu = 0$. So the ranges for μ for the Kerr instanton map via $\mu \to -\mu$ to the ranges for the black hole, and every $\mu > 0$ nonsingular instanton is the secondary horizontal card for a $\mu < 0$ black hole.

For $a = b > 0$, we do not have the anomalous region or the anomalous extremal solution, but we have all other solutions. They have the additional feature that the ergosphere and singularity loci are invariant under $\theta \to \pi/2 - \theta$.

4.2.2 One turned on

The case of one angular momentum turned on and the other turned off is substantially different from the case of both turned on. For the black hole, we turn off the ψ-rotation. The solution is

$$\begin{aligned} ds^2 &= -dt^2 + \frac{\mu(dt + a\cos^2\theta d\phi)^2}{r^2 + a^2\sin^2\theta} + (r^2 + a^2)\cos^2\theta d\phi^2 \\ &\quad + r^2\sin^2\theta d\psi^2 + (r^2 + a^2\sin^2\theta)\big(\frac{dr^2}{r^2 + a^2 - \mu} + d\theta^2\big). \end{aligned} \tag{4.10}$$

and

$$\rho = \frac{1}{2}\sin 2\theta\sqrt{r^4 + (a^2 - \mu)r^2} \tag{4.11}$$

$$z = \frac{1}{2}\cos 2\theta(r^2 - \frac{\mu - a^2}{2}). \tag{4.12}$$

The horizon function is $r^4 + (a^2 - \mu)r^2$, with roots $r^2 = \mu - a^2, 0$. Extremality is when $\mu = a^2$, and we call this solution 'half-anomalous.' The $\mu = 0$ solution is flat and so we have three parametric ranges, $\mu > a^2$ (ordinary), $0 < \mu < a^2$ (anomalous), and $\mu < 0$ (negative mass). Note that though the spherical prolate coordinates respect $r^2 = 0$ as a 'rod horizon/boundary,' the metric does not have $g_{rr} = \infty$ there and it is not a horizon.

Take the ordinary $\mu > a^2$ case. The card diagram is drawn in Fig. 4.4. The center is $r^2 = \frac{\mu - a^2}{2}$, the ergosphere is $r^2 = \mu - \frac{a^2}{2} + \frac{a^2}{2}\cos 2\theta$ which touches $r_+^2 = \mu - a^2$ at $\theta = \pi/2$, and the singularity is $r^2 = -\frac{a^2}{2} + \frac{a^2}{2}\cos 2\theta$ which touches r_-^2 at $\theta = 0$. The $r^2 \to \infty$ universe is well behaved through the ergosphere, through the r_+^2 horizon, but as we approach the r_-^2 rod, the ψ-direction vanishes as timelike r^2 decreases to zero. We had already compactified $\psi \simeq \psi + 2\pi$ at $\theta = 0$, so this is a Milne orbifold. Furthermore there is a curvature singularity at $r^2 = 0$, $\theta = 0$ where the singular locus on the top horizontal card meets the rod's endpoint.

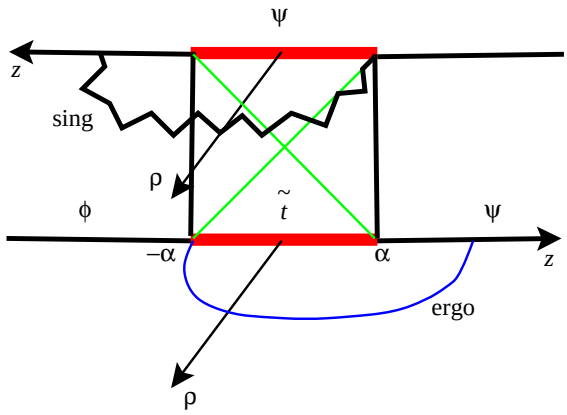

Figure 4.4: The Myers-Perry black hole card diagram, with one turned on, $a > b = 0$; and in the ordinary range $\mu > a^2$. This time, the top of the square is not a spinning $\tilde{t}$ horizon, but is a special locus of ψ-vanishing. It is a Milne orbifold. The curvature singularity touches the upper-right corner.

The half-anomalous extremal case can be gotten by putting $\mu = a^2$ in (4.10). The singularity on the secondary horizontal card goes into the extremal horizon $r^2 = 0$ and stops at $\theta = 0$; it does not go into the primary horizontal card and so we call the solution half-anomalous. There is no near-horizon limit because, even if one could rescale the compact ψ, the whole $\theta = 0$ ray would become singular. One might wonder whether to call the extremal spacetime nakedly singular. The spacetime is nonsingular for all $r^2 > 0$, but the curvature invariant is unbounded on this open set as can be seen by taking a path approaching $r^2 = 0$, $\theta = 0$. From the point of view of string theory, α'-corrections to Einstein's equations mean that the written solution is not valid for all $r^2 > 0$.

The anomalous case with $b = 0$ is similar to the anomalous case for $a > b > 0$. When we set $b = 0$, the edge of the ergosphere and singularity that had been closest to the rod endpoints get stuck on the rod endpoint. Note that the $r^2 = 0$ horizon is now 'outer,' i.e. it has a larger value of r^2, and $r^2 = 0$ is the rod-horizon on the principal horizontal card. So the ψ-circle vanishes there and it has a conical

singularity because this rod boundary requires a different periodicity than the $\theta = 0$ ray. The ergosphere runs from the primary horizontal card into the vertical card and terminates at $\theta = \pi/2$ in the upper-left corner. The singularity runs from the secondary horizontal card down into the vertical card and terminates at $\theta = 0$ in the lower-right corner.

The negative mass case has a singularity purely on the vertical card which touches the outer horizon $r^2 = 0$, $\theta = 0$, and an ergosphere purely on the vertical card. The interior of the principal horizontal card is then nonsingular, but its rod horizon is $r^2 = 0$, where the ψ-circle vanishes with different periodicity than on the right semi-infinite ray. So it has a conical singularity. The secondary horizontal card is nonsingular and signature $- - - - -$, giving the known Kerr instanton, related to the usual formulation by $\mu \to -\mu$.

4.2.3 Turning on its side

The operation known as a γ-flip [51] amounts to continuing all Killing directions and also sending $g_{\mu\nu} \to -g_{\mu\nu}$. This takes a vertical card and turns it on its side, switching the timelike and spacelike (non-Killing) directions. Let us take the vertical square card for the $\mu > a^2$ 5d black hole with one angular momentum on, and turn it on its side, so that $r^2 = 0$ is the left boundary and $r^2 = \mu - a^2$ is the right boundary, the ϕ-direction closes on the bottom and the ψ direction closes at the top (with Euclidean periodicity 2π). Rename $t \to x^5$. The card diagram is in Fig. 4.5.

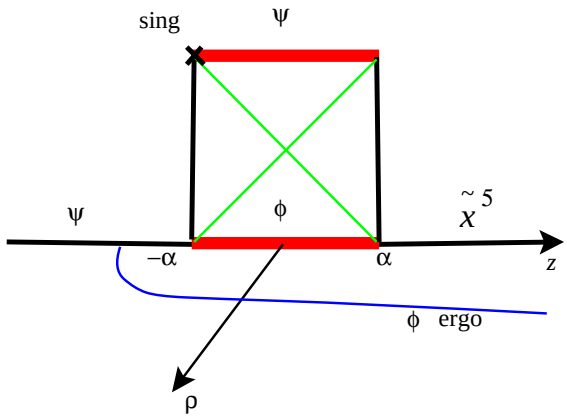

Figure 4.5: The Myers-Perry black hole with $a > b = 0$, $\mu > a^2$ turned on its side. The special locus of vanishing ψ is the left boundary, so ψ is compact, and the top of the square is a Milne orbifold.

Then the horizontal card on its left semi-infinite ray has the special $r^2 = 0$ closing of the ψ-direction with periodicity $2\pi a/\sqrt{\mu - a^2}$. On the right semi-infinite ray $r^2 =$

$\mu - a^2$, we twist to $\tilde{\phi} = \phi - \Omega x^5$ with $\Omega = -a/\mu$ and then compactify $\tilde{x}^5$ at fixed $\tilde{\phi}$. We leave $\tilde{\phi}$ noncompact so the rod is a nonsingular horizon. At the top of the vertical card we have a Milne orbifold again, and at the top-left we have a curvature singularity.

Since $\theta = \pi/2$ is the rod horizon, we continue $\theta \to \pi/2 + i\theta$ in (4.10) in addition to the γ-flip to get the horizontal card solution,

$$ds^2 = -(dx^5)^2 + \frac{\mu(dx^5 - a\sinh^2\theta d\phi)^2}{r^2 + a^2\cosh^2\theta} - (r^2+a^2)\sinh^2\theta d\phi^2 \qquad (4.13)$$

$$+r^2\cosh^2\theta d\psi^2 + (r^2 + a^2\cosh^2\theta)\Big(\frac{dr^2}{\mu - a^2 - r^2} + d\theta^2\Big) \qquad (4.14)$$

There is a ϕ-ergosphere where $g_{\phi\phi} = 0$,

$$(r^2+a^2)(r^2 + a^2\cosh^2\theta) = \mu a^2\sinh^2\theta,$$

which is a topological semi-infinite ray which touches the special ψ-boundary at $a^2/\mu = \tanh^2\theta$, and bends around the horizon to go parallel to the positive z+axis.

Since ψ is compact, there does not seem to be a large-θ scaling limit.

4.2.4 Kerr bubbles

We can make bubble universes $\mathcal{K}_+$ by analytically continuing an angle to time. Without loss of generality, we consider $a, b \geq 0$ and continue

$$t \to ix^5, \qquad \psi \to i\psi, \qquad a \to ia.$$

The solution, written on the horizontal card for real $0 \leq \theta \leq \pi/2$, is

$$\begin{aligned} ds^2 &= (dx^5)^2 - \frac{\mu(dx^5 + a\cos^2\theta d\phi + b\sin^2\theta d\psi)^2}{r^2 - a^2\sin^2\theta + b^2\cos^2\theta} + (r^2-a^2)\cos^2\theta d\phi^2 \\ &\quad -(r^2+b^2)\sin^2\theta d\psi^2 + (r^2 - a^2\sin^2\theta + b^2\cos^2\theta) \\ &\quad \times\Big(\frac{r^2dr^2}{r^4 + r^2(b^2-a^2-\mu) - a^2b^2} + d\theta^2\Big). \end{aligned}$$

The horizon function is then $\Delta = r^4 + (b^2 - a^2 - \mu)r^2 - a^2b^2$. If $a, b > 0$ then this always has two roots $r_\pm^2 = -\frac{b^2-a^2-\mu}{2} \pm \frac{1}{2}\sqrt{(b^2-a^2-\mu)^2 + 4a^2b^2}$ and $r_+^2 > 0$ and $r_-^2 < 0$. Note that $\Delta|_{a^2} = -\mu a^2$ and $\Delta|_{b^2} = b^2(2(b^2-a^2) - \mu)$. We have the card diagram structure as shown in Fig. 4.6. We twist to $\tilde{\phi} = \phi - \Omega_\phi x^5$, $\tilde{\psi} = \psi - \Omega_\psi x^5$, $\tilde{x}^5 = x^5$ and compactify $\tilde{x}^5$ on the rod and the adjacent vertical boundary.

The singularity on the horizontal card is $r^2_{\rm sing} = a^2\sin^2\theta - b^2\cos^2\theta$. The most positive value is $r^2 = a^2$ at $\theta = \pi/2$, where $\Delta = -\mu a^2$, so for $\mu > 0$, $a^2 < r_+^2$ and this stays away from the spacetime. On the vertical card, $r^2_{\rm sing} = -a^2\sinh^2\theta - b^2\cosh^2\theta <$

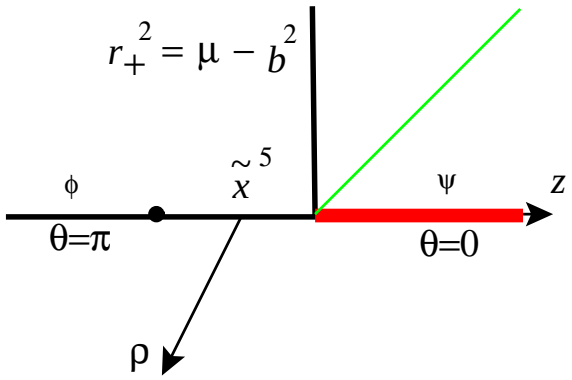

Figure 4.6: The Myers-Perry bubble, where we took ψ to be time. This diagram applies for $a, b > 0$, or for $a = 0$ and the ordinary range $\mu > b^2$.

0 stays away from the spacetime. There is no nonsingular $\mathcal{K}_-$ universe at negative r^2 because $r^2_{\rm sing}$ runs on the vertical cards.

If we have $a = 0$ and $b > 0$, then the horizon function is identical to that of the black hole, $\Delta = r^2(r^2 + b^2 - \mu)$. We again have three ranges, 'ordinary,' 'anomalous,' and 'negative-mass'; they are separated by the half-anomalous extremal $\mu = b^2$ and the flat $\mu = 0$. The singularity is $r^2_{\rm sing} = -b^2 \cos^2\theta$ with most positive value 0. In the ordinary case $\mu > b^2$, this means $0 = r_-^2 < r_+^2 = \mu - b^2$ so the singularity stays away. In the half-anomalous extremal case, the singularity touches $r^2 = 0$, $\theta = \pi/2$; but for $\theta < \pi/2$, $r \downarrow 0$ gives an infinite nonsingular throat. For either the anomalous case or the negative-mass case, the singularity touches the point $r^2 = 0$, $\theta = \pi/2$; this is the left endpoint of the rod.

If instead $b = 0$ and $a > 0$, then $\Delta = r^2(r^2 - a^2 - \mu)$. We go ahead and term the three ranges 'ordinary' $\mu > 0$, 'anomalous' $-a^2 < \mu < 0$, and 'negative-mass' $\mu < -a^2$. The singularity is $r^2_{\rm sing} = a^2 \sin^2\theta$. The most positive value is a^2 at $\theta = \pi/2$. In the ordinary case $\mu > 0$, $r_+^2 = \mu + a^2$ is larger than this so the singularity stays away from the spacetime. For any of the cases of $\mu < 0$, the singularity is on the horizontal card.

4.2.5 S-Kerr

Taking all the bubble solution' vertical cards and turning them on their sides with a γ-flip, we achieve the S-Kerr solutions. This demonstrates concretely the global properties already discussed in Sec. 4.1. We are always now at noncompact

hyperbolic θ; the solution is

$$\begin{aligned} ds^2 &= (dx^5)^2 - \frac{\mu(dx^5 + a\cosh^2\theta d\phi - b\sinh^2\theta d\psi)^2}{r^2 + a^2\sinh^2\theta + b^2\cosh^2\theta} + (r^2 - a^2)\cosh^2\theta d\phi^2 \\ &\quad + (r^2 + b^2)\sinh^2\theta d\psi^2 + \Big(r^2 + a^2\sinh^2\theta + b^2\cosh^2\theta\Big) \\ &\quad \times\Big(-\frac{r^2 dr^2}{r^4 + r^2(b^2 - a^2 - \mu) - a^2 b^2} + d\theta^2\Big) \end{aligned}$$

and the singularity is $r^2_{\rm sing} = -a^2\sinh^2\theta - b^2\cosh^2\theta$.

With both turned on, $a, b > 0$, we always have an ordinary subextremal card diagram with two x^5 horizons and a ψ boundary. The most positive value of $r^2_{\rm sing}$ is $-b^2$. The horizon function $\Delta|_{-b^2} = b^2(2(b^2 - a^2) + \mu)$ so if $\mu > 2(a^2 - b^2)$ then the singularity lies purely on the secondary vertical quarter-plane cards. If μ is smaller than this, the singularities also stretch to the horizontal cards.

If $a = 0$, we have

$$\begin{aligned} ds^2 &= (dx^5)^2 - \frac{\mu(dx^5 - b\sinh^2\theta d\psi)^2}{r^2 + b^2\cosh^2\theta} + r^2\cosh^2\theta d\phi^2 \\ &\quad + (r^2 + b^2)\sinh^2\theta d\psi^2 + (r^2 + b^2\cosh^2\theta)\Big(-\frac{dr^2}{r^2 + b^2 - \mu} + d\theta^2\Big) \end{aligned} \tag{4.15}$$

Now $r^2_{\rm sing} = -b^2\cosh^2\theta$ with most positive value $-b^2$. For the ordinary range $\mu > b^2$ (Fig. 4.7), this is always less than $r^2_- = 0$. There is a twisted x^5 horizon at $r^2_+ = \mu - b^2$ and $r^2_- = 0$ is the special closing of the ϕ-circle. The ψ-circle closes on the rod and the adjacent vertical boundary. This is a nonsingular spacetime, ordinary 5d S-Kerr.[1] There are CTCs on the horizontal card; to see this one can look at large θ.

The anomalous $0 < \mu < b^2$ case (Fig. 4.8) has $r^2_- = \mu - b^2$ so the singularity still stays away. This is a twisted $\tilde{x}^5$ boundary. The right ray of the horizontal card is $r^2_+ = 0$ making ϕ into the special Rindler/Milne horizon. The ψ circle closes on the rod and the adjacent vertical boundary. This is a nonsingular spacetime, anomalous 5d S-Kerr. Since the $x^5\psi$ directions have signature $++$, there are no CTCs.

There is an extremal case for $\mu = b^2$:

$$\begin{aligned} ds^2 &= (dx^5)^2 - \frac{b^2(dx^5 - b\sinh^2\theta d\psi)^2}{r^2 + b^2\cosh^2\theta} + r^2\cosh^2\theta d\phi^2 \\ &\quad + (r^2 + b^2)\sinh^2\theta d\psi^2 + (r^2 + b^2\cosh^2\theta)\Big(-dr^2/r^2 + d\theta^2\Big). \end{aligned}$$

Then the horizontal card collapses and we have an upper $r^2 > 0$ triangular wedge vertical card, with the $\psi \simeq \psi + 2\pi$ circle closing on the vertical boundary. We twist

[1] We apologize for our conventions for which to turn off: Both the nonsingular S-Kerr's we get have $a = 0$, so x^5 is twisted with ψ which was the bubble time. For the black hole with one turned off, in our presentation we arbitrarily chose $b = 0$. In our general odd-D S-brane treatment, we turned off ϕ_n which would be $b = 0$.

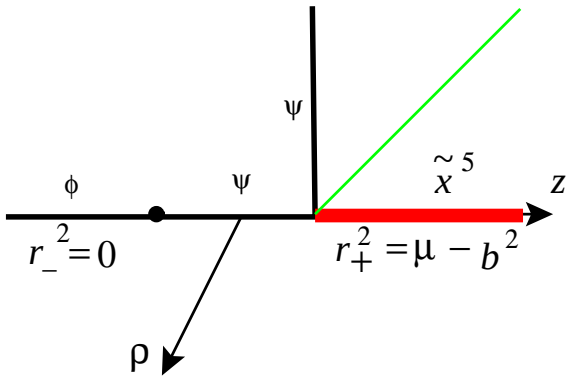

Figure 4.7: The ordinary $\mu > b^2$ nonsingular S-brane solution.

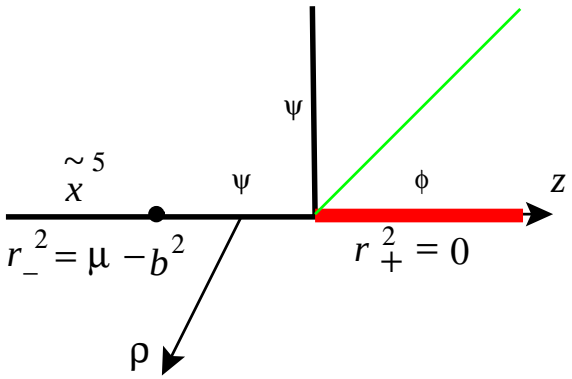

Figure 4.8: The anomalous range $0 < \mu < b^2$ nonsingular S-brane solution. This horizontal card of this solution, upon $\phi \to i\phi$, gives us the new instanton.

to $\tilde{\psi} = \psi - \Omega x^5$ where $\Omega = -1/b$, and then take a near-horizon limit $r^2 \to 0$ dilating $\tilde{x}^5$. The twist vanishes and we get a 'little' dS_3 region:

$$ds^2 = \cosh^2\theta\Big(r^2\big((d\tilde{x}^5)^2/b^2 + d\phi^2\big) - dr^2/r^2\Big) + b^2\sinh^2\theta d\psi^2 + b^2\cosh^2\theta d\theta^2.$$

At the vertex, the triangle wedge attaches to an identical $r < 0$ lower triangle wedge in a dS_3 fashion, just like the parabolic-parabolic card diagram representation of the 5d Witten bubble of [51]. We thus avoid any singularities at $r^2 < 0$.

We emphasize that while extremal S-Kerr with one turned on has a near-horizon scaling limit, the black hole does not. This may be confusing because such solutions all occur at the same 'point' in the card diagrams. The key issue is that extremality means that the $r_-^2 \le r^2 \le r_+^2$ region collapses, but contrary to the card picture, $0 \le \theta \le \pi/2$ does not collapse at the horizon. The Myers-Perry 5d singularity touches

the horizon only at $\theta = \pi/2$ and stays away from the extremal S-Kerr solution.

The $a = 0$, $\mu < 0$ case has a singularity on the horizontal card.

Now, we instead try $b = 0$. Then $r^2_{\text{sing}} = -a^2 \sinh^2\theta$ with most positive value 0. For the $\mu > 0$ or $-a^2 < \mu < 0$ cases, $r_-^2 = 0$ and $r_+^2 = \mu + a^2$ so the singularity touches the rod's left endpoint at $r^2 = 0$, $\theta = 0$. Furthermore ψ closes on the rod but closes also on the left ray $r^2 = 0$, so there are conical singularities. The case $\mu < -a^2$ is singular on the horizontal card. It still has $\psi \simeq \psi + 2\pi$ from the rod, but puts $r_+^2 = 0$ on the right ray, where ψ closes to give a Rindler/Milne orbifold.

4.2.6 Instantons and Spacetime Decay

Let us take the horizontal cards of S-Kerr and try to make nonsingular instantons. If both a, b are turned on, we have $\Omega_+ \neq \Omega_-$ at $r^2 = r_\pm^2$ and cannot in general close twisted $\tilde{x}^5$, $\tilde{\tilde{x}}^5$ circles.

The new Kerr instanton can be easily gotten from the $a = 0$, $0 < \mu < b^2$ 'anomalous' nonsingular 5d S-Kerr. Simply take $\phi \to i\phi$ in (4.15) which turns the right-ray Rindler horizon into a boundary of the horizontal card.[2]

No new nonsingular instantons are gotten from setting $b = 0$.

It is now obvious that the horizontal card of the S-Kerr (with $a = 0$) coincides with that of Sec. 4.2.3 up to Killing continuation. It was nontrivial to discover that for $D = 5$, this new instanton is in fact identical to the ordinary Kerr instanton. This comes from an interesting algebraic symmetry between radial and angular direction for Kerr_5 with one angular momentum turned on. Using affine coordinates, we refer to this as $C \leftrightarrow Z$ symmetry. This flips the spherical prolate diagram about its 45° line. As such, this instanton mediates decay of a simpler, flat orbifold spacetime, as described in [61]. The initial spacetime is 'simpler' in that the finite-sized ψ-rod is deleted as a source from Fig. 4.8. This deleting of a finite source is typical; since the semi-infinite sources are preserved, the leading asymptotics of solutions to the elliptic Weyl-Papapetrou(-Harmark) equations are unchanged.

It is quite likely that the addition of a cosmological constant will lift the remarkable $C \leftrightarrow Z$ symmetry, yielding a new S-brane and new instanton in $D = 5$.

Although card diagrams do not generalize to $D \geq 6$ Myers-Perry black holes, we hope that they have made the structure of the $D = 5$ (which is eminently different from $D = 4$) black hole, bubble, S-brane, and instantons clear. In the case, of the anomalous S-brane mediating spacetime decay via a new instanton for $D = 7, 9, \ldots$, the idea of deleting a finite-sized locus of source for elliptic equations holds. In principle this describes the simpler spacetime which decays into the S-brane.

Details of the $D = 7, 9, \ldots$ decay are forthcoming from the present author and J. E. Wang.

[2]One might note that one could also take $b \to ib$, $x^5 \to ix^5$, $\phi \to i\phi$, and flip the sign of $g_{\mu\nu}$; this gives the same instanton.

4.3 Global Structure of SM2-brane, etc.

We give here the complete global structure of the SM2-brane, which is analogous to the 9d S-Kerr; the solution was given in [49]. This analysis also applies to SD3-branes, analogous to the 7d S-Kerr, and Sp-branes with $D-p$ odd, also found in [49]. The SM5-brane is analogous to the even-dimensional 6d S-Kerr solution, and has already been properly discussed.

The spinning M2-brane solution has a corresponding S-brane with the same interesting global structure as the odd-dimensional black hole. It has the possibility of extremality and a dS_3 scaling limit (after twisting) at the extremal horizon. The M2-brane solution is [106, 107, 49]

$$\begin{aligned} ds^2 &= H^{-2/3}\big(-(1-2M/r^6\Delta)dt^2+dE_2^2\big) \\ &\quad +H^{1/3}\Big(\frac{\Delta dr^2}{H_1H_2H_3H_4-2M/r^6}+r^2\sum_{i=1}^4 H_i(d\mu_i^2+\mu_i^2d\phi_i^2) \\ &\quad -\frac{4M\cosh\alpha}{r^6H\Delta}\sum_{i=1}^4 l_i\mu_i^2d\phi_i dt+\frac{2M}{r^6H\Delta}\big(\sum_{i=1}^4 l_i\mu_i^2d\phi_i\big)^2\Big). \end{aligned}$$

where $dE_2^2=dx_1^2+dx_2^2$, $H_i=1+l_i^2/r^2$, $\Delta=H_1H_2H_3H_4\sum_{i=1}^4\mu_i^2/H_i$, and $H=1+2M\sinh^2\alpha/r^6\Delta$. Note that Δ should be compared to ΠF in the Myers-Perry notation, and is not the horizon function, which is the reciprocal of the coefficient of dr^2. The constraint is $\mu_1^2+\mu_2^2+\mu_3^2+\mu_4^2=1$ and each $\mu_i\geq 0$. The gauge field is

$$A_{\mathcal{J}}=\frac{1-H^{-1}}{\sinh\alpha}(-\cosh\alpha dt+\sum_{i=1}^4 l_i\mu_i^2d\phi_i)\wedge dx_1\wedge dx_2.$$

To get the nice nonsingular structure we want to set $l_4=0$; $H_4=1$. As $r\downarrow 0$, we have $ds^2\supset l_1^2l_2^2l_3^2\mu_4^2dr^2/(l_1^2l_2^2l_3^2-2M)+\mu_4^2d\phi_4^2$ and $H\sim 1$, much like the black hole case.

The analytic continuation to S-brane is $\mu_i\to i\mu_i$, $i=1,2,3$, $\phi_4\to i\phi_4$, $dE_2^2\to -dE_2^2$ via $x_i\to ix_i$, and then a sign flip $g_{\mu\nu}\to -g_{\mu\nu}$. The stress tensor $T_{\mu\nu}^{4-\text{form}}\supset(\#)g_{\mu\nu}\|F_4\|^2$ has an odd number of metrics appearing and $A_{\mathcal{J}}$ has an even number of dx_i, so we must continue $\alpha\to i\alpha$. We also rename $t\to z$. The S-brane geometry is

$$\begin{aligned} ds^2 &= H^{-2/3}\big((1-2M/r^6\Delta)dz^2+dE_2^2\big) \\ &\quad +H^{1/3}\Big(-\frac{\Delta dr^2}{H_1H_2H_3H_4-2M/r^6}+r^2\sum_{i=3}^4 H_i(d\mu_i^2+\mu_i^2d\phi_i^2) \\ &\quad -r^2d\mu_4^2+r^2\mu_4^2d\phi_4^2 \\ &\quad -\frac{4M\cos\alpha}{r^6H\Delta}\sum_{i=1}^3 l_i\mu_i^2d\phi_i dt-\frac{2M}{r^6H\Delta}\big(\sum_{i=1}^3 l_i\mu_i^2d\phi_i\big)^2\Big). \end{aligned}$$

Here, $\Delta = H_1H_2H_3(\mu_4^2 - \sum_{i=1}^3 \mu_i^2/H_i)$ and $H = 1 - 2M\sin^2\alpha/r^6\Delta$.

Note that $\Delta > 0$ for $r^2 > 0$. The horizon function is then $(r^2+l_1^2)(r^2+l_2^2)(r^2+l_3^2)-2M$, just like the 7d black hole case. There is a regular range, $2M > l_1^2l_2^2l_3^2$, where we have a spinning horizon at $r^2 > 0$ and then the ϕ_4-circle closes at $r = 0$. There is an extremal case $l_1^2l_2^2l_3^2 = 2M$ where we can twist and find a dS_3 scaling limit. There is an anomalous range $0 < 2M < l_1^2l_2^2l_3^2$, where we first have the ϕ_4-horizon at $r^2 = 0$ and then pass to negative r^2, and find a $\tilde{z}$-boundary at $r^2 = -r_1^2 > -l_1^2$.

As in Myers-Perry, define $F = \mu_4^2 - \sum_{i=1}^3 \mu_i^2/H_i$, $\Pi = H_1H_2H_3$. An $H = 0$ singularity occurs when $r^6\Pi F = 2M\sin^2\alpha$. In the ordinary case, the left side minimizes at $r^2 = 0$, $\mu_4 = 1$ to $l_1^2l_2^1l_3^2$. So actually we need $2M\sin^2\alpha < l_1^2l_2^2l_3^2 < 2M$. In the extremal case, we need $\sin^2\alpha < 1$. In the anomalous case, we go to negative r^2 where $H_i < 0$; we still have $F \geq 1$. But $r^6H_1H_2H_3 \geq 2M$ for $r^2 \geq -r_1^2$ so again we only need $\sin^2\alpha < 1$. All $2M < 0$ solutions are singular; as r^2 decreases from ∞, we hit $r^6H_1H_2H_3 = 2M\sin^2\alpha$ before $r^6H_1H_2H_3 = 2M$.

One can repeat the above analysis for the SD3-brane case and for Sp-branes where $D-p$ is odd.

4.4 More universes by turning cards on their sides

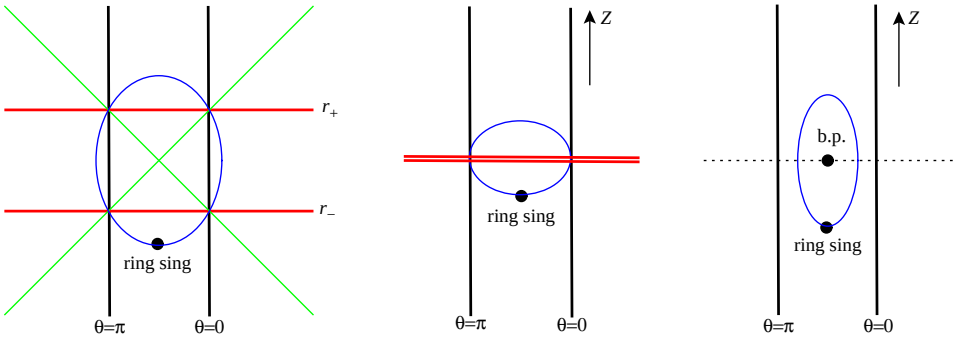

Figure 4.9: Subextremal, extremal, and superextremal spherical prolate diagrams for the Kerr, Kerr bubbles $\mathcal{K}_\pm$, and S-Kerr universes. The black hole (or superextremal massive stationary object) is the middle column. The $\mathcal{K}_\pm$ bubbles are the top and bottom rows (in the superextremal case they are joined). The S-Kerr is either the right or left column. These diagrams are drawn in affine coordinates, $C = \pm\cosh\theta, \cos\theta$, and $Z = (r-M)/\sqrt{M^2-a^2}, (r-M)/M, (r-M)/\sqrt{a^2-M^2}$.

We understand from [51] or the right-hand superextremal diagram in Fig. 4.9, how a vertical half-plane card with spherical prolate coordinates attaches to a branched half-plane horizontal card, we are in a position to take all the vertical half-plane cards we know and turn them on their sides via $2\gamma \to 2\gamma + i\pi$. Some of the geometries

have ugly features on their horizontal cards, but none are nakedly singular on vertical cards. In the following examples all derived in some sense from Kerr geometry, we borrow the term 'ring singularity' to refer to the obvious singularity $\Sigma = 0$, where Coef $(dx^4)^2$ blows up.

4.4.1 Kerr bubble on its side

The $r \geq r_+$ and $r \leq r_-$ Kerr $\pi/2$-bubbles (gotten from $z \to i\tau$ or $\theta \to \pi/2 + i\theta$) are put on their sides to give the vertical cards of this universe. It is

$$ds^2 = \frac{\Delta}{\Sigma}(dx^4 + a\cosh^2\theta d\phi)^2 + \frac{\cosh^2\theta}{\Sigma}(-adx^4 + (r^2 - a^2)d\phi)^2 - \frac{\Sigma dr^2}{\Delta} + \Sigma d\theta^2,$$

where $\Sigma = r^2 + a^2\sinh^2\theta$, $\Delta = r^2 - 2MR - a^2$. There is an ergosphere which is a topological circle on the horizontal card, and a ring singularity which is a point $r = 0$, $\theta = 0$ on the ergosphere. But keep in mind here that ϕ can be taken to be noncompact, so the ring singularity is really a 1-brane singularity.

4.4.2 S-Kerr superextremal on its side

We write the solution for real θ meaning on the vertical card; one runs θ from 0 to $i\pi$ on the horizontal card and then from $i\pi$ to $i\pi + \infty$ on the other (identical) vertical card. We have

$$ds^2 = \frac{\Sigma dt^2}{\Delta} + \frac{\Delta}{\Sigma}(dx^4 + a\sinh^2\theta d\phi)^2 + \frac{\sinh^2\theta}{\Sigma}(adx^4 - (t^2 + a^2)d\phi)^2 - \Sigma d\theta^2,$$

where $\Delta = t^2 - 2Mt + a^2$ and $\Sigma = t^2 + a^2\cosh^2\theta$. This geometry has an ergosphere (which is fine—and keep in mind that ϕ is noncompact) and the ring singularity also appears at $t = 0$, $\theta = i\pi/2$. In principle we already know this geometry; it is the superextremal Kerr bubble $\mathcal{K}_\pm$; it occupies the entire superextremal diagram in Fig. 4.9.

4.5 Taub-NUT, bubbles, and S-branes

The Brill-charged Taub-NUT spacetime ([108, 109, 110, 111, 1]) with metric

$$\begin{aligned} ds^2 &= -\frac{r^2 - 2Mr - l^2 + Q^2}{r^2 + l^2}(dt + 2l\cos\theta d\phi)^2 + \frac{r^2 + l^2}{r^2 - 2Mr - l^2 + Q^2}dr^2 \\ &\quad + (r^2 + l^2)(d\theta^2 + \sin^2\theta d\phi^2) \end{aligned}$$

has a card diagram like Kerr except ergospheres sit atop the horizons and there is no ring singularity. The Taub-NUT space is problematic because there are too many

types of boundaries. On the semi-infinite ray $\theta = 0$, one must twist to $\tilde{t} = t + 2l\phi$ to close the ϕ-circle, but on the semi-infinite ray $\theta = \pi$, one must twist to $\tilde{\tilde{t}} = t - 2l\phi$ to close the ϕ-circle. This means $\tilde{t} \simeq \tilde{t} + 4\pi l$ must be compactified and the horizon rod then is a Rindler orbifold.

If $Q^2 > m^2 + l^2$ then the Brill-charged Taub-NUT is superextremal; there is no horizon hence no Rindler orbifold; and no singularity. The time is still compactified however.

Besides the $Q = 0$ Taub-NUT instanton [112], which exists only for the special value of $l = \pm iM$, and the special Taub-bolt instanton of Page [113], there are a number of other solutions that are easily obtainable and not problematic because they have fewer types of Euclidean boundaries.

First, there is the Taub-NUT $\pi/2$-bubble, obtained by $t \to ix^4$, $\theta \to \pi/2 + i\theta$ (or $z \to i\tau$ in Weyl coordinates), $Q \to iQ$. It is important here, that l is left alone; the solution is always subextremal. This gives a vertical half-plane card without special null lines, like the hyperbolic Witten bubble [51] or dihole wave of [25, 51]. One can also get a negative-r bubble or equivalently a negative-mass bubble. 'Nutty bubbles' have been described by Mann et al. [85, 87].

The Taub-NUT $\pi/2$-bubbles of positive and negative mass can be turned on their sides, like the solutions of the previous section. They are connected by a branched horizontal card. The solution is

$$\begin{aligned} ds^2 &= \frac{r^2 - 2Mr - l^2 - Q^2}{r^2 + l^2}(dx^4 - 2l\sinh\theta d\phi)^2 + (r^2 + l^2)\cosh^2\theta d\phi^2 \\ &\quad + (r^2 + l^2)\Big(\frac{-dr^2}{r^2 - 2Mr - l^2 - Q^2} + d\theta^2\Big). \end{aligned}$$

There are no singularities anywhere. There are also no boundaries, so both x^4 and ϕ are left noncompact, and hence the horizontal card has no CTCs. A fuller investigation to the physical description or application of this nonsingular $\pi/2$-S-Taub-NUT spacetime and its orbifolds might merit its own publication.

If we did not continue $Q \to iQ$ then we have an E-bubble which can be superextremal if $Q^2 > l^2 + M^2$. The superextremal Taub-NUT E-bubble has a card diagram structure like superextremal E-RN; a vertical full-plane card with two intersecting special null lines [51]. Furthermore it is nonsingular. It can be turned on its side to yield a non-time-symmetric universe of the same card diagram structure.

On the other hand, we can take Taub-NUT and just do the Killing rotation $t \to ix^4$, $\phi \to i\phi$, and $Q \to iQ$. Then $\theta = 0, \pi$ are both horizons with ϕ noncompact. The Taub-NUT rod closes the x^4 circle (no twisting is needed) and this gives us a nonsingular NUT bubble universe. It turns out this is the same as the solution gotten from $\theta \to \pi/2 + i\theta$. To prove this, instead of constructing the map explicitly, one need only analyze the representation of the Killing $SO(3) \to SO(2,1)$ algebra, which makes the spacetime homogeneous on an $r =$constant slice. Here is the proof: the

Killing algebra of Taub-NUT is generated by

$$\begin{aligned}\xi_1 &= \sin\phi\partial_\theta + \cos\phi\Big(\cot\theta\partial_\phi + \frac{2l}{\sin\theta}\partial_t\Big)\\ \xi_2 &= \cos\phi\partial_\theta - \sin\phi\Big(\cot\theta\partial_\phi + \frac{2l}{\sin\theta}\partial_t\Big)\\ \xi_3 &= \partial_\phi\\ \xi_4 &= 2l\partial_t,\end{aligned}$$

where $[\xi_i, \xi_j] = \epsilon_{ijk}\xi_k$ and ξ_4 is invariant. Under the continuation to get the $\pi/2$-bubble, we continue all but ξ_3 by i; whereas to get the double Killing bubble, we continue all but ξ_2 by i. The point $t = 0$, $\phi = 0$, $\theta = \pi/2$ is shared between the two continuations, and at that point the contravariant metric at constant r takes the form

$$(ds_3^2)^{-1} = (f/4l^2)\xi_1^2 + (r^2 + l^2)(\mp\xi_2^2 \pm \xi_3^2),$$

where $\pm$ is for the two choices for continuation. Since this point can generate the entire $r =$constant hypersurface by Lie dragging, the 3-metrics are isometric. Since they are fibered in an identical way over the r-coordinate, the 4-metric Taub-NUT bubbles are isometric. This is an extension of the equivalence of hyperbolic and elliptic card diagrams for Schwarzschild or RN bubbles.

The double Killing bubble's vertical card can be turned on its side. We must then twist to close at $\theta = 0$, and the ensuing horizontal card for this S-Taub-NUT always has CTCs on its horizontal card. However, it must be locally isometric to the $\pi/2$ S-Taub-NUT. It turns out the present S-Taub-NUT is a nontrivial quotient of the $\pi/2$ S-Taub-NUT, gotten by 2π-parametric identifications along orbits of

$$K = \cos\phi\partial_\theta - \sin\phi\Big(\tanh\theta\partial_\phi + \frac{2l}{\cosh\theta}\partial_{x^4}\Big) + 2l\partial_{x^4}.$$

This vector field partitions $\mathbf{R}^3$ into separate regions of two types, and the double Killing S-Taub-NUT comes from one of these region. There may be another (possibly well-behaved) quotient from the other region.

Their also then exist parabolic representations for the NUT-bubble and S-Taub-NUT; the card structure will look just like for the Schwarzschild/RN case.

It can be noted that $M = 0$ for Taub-NUT gives an additional $\mathbb{Z}_2$ isometry for some extension of the full spacetime. Then, upon turning the vertical card on its side, we achieve Taub-NUT on its side. The principal horizontal card has the same closure data on the left and right rays and hence has good properties. Including a cosmological constant and gauge field, Taub-NUT on its side thus has apart from an overall scale parameter, two additional parameters, l and Q. Also, we can reconsider adding M back into the game: The asymmetry provided by the mass parameter could be fixed by a generalized Harrison transformation, where the electric potential Q/r at $r = r_1, r_2$ could be used to fix the conical singularities. This may be forthcoming from the author.

Chapter 5

S-branes and (Anti-)Bubbles in (A)dS Space

We describe the construction of new locally asymptotically (A)dS geometries with relevance for the AdS/CFT and dS/CFT correspondences. Our approach is to obtain new solutions by analytically continuing black hole solutions. A basic consideration of the method of continuation indicates that these solutions come in three classes: S-branes, bubbles and anti-bubbles. A generalization to spinning or twisted solutions can yield spacetimes with complicated horizon structures. Interestingly enough, several of these spacetimes are nonsingular.

This chapter is based on the e-print `hep-th/0502162` with Dumitru Astefanesei.

5.1 Introduction

Time-dependent backgrounds in string theory provide an interesting arena for exploring intrinsically dynamical issues such as black hole evaporation, cosmological evolution or the possible formation and resolution of singularities. An essential ingredient in understanding quantum gravity in asymptotically Anti-de Sitter (AdS) spacetimes is the Maldacena conjecture (or the AdS/Conformal Field Theory (CFT) correspondence) [30, 33, 31].[1] In this framework, a *large* black hole in AdS is described as a thermal state of the dual conformal field theory. A remarkable property of the AdS/CFT correspondence is that it works even far from the conformal regime [114, 115]. This result is consistent with the interpretation of the radial coordinate of AdS space as a energy scale of the dual CFT. In other words, timelike D-branes lead to a spacelike holography.

Inspired by the fact that the microphysical statistical origin of cosmological horizon entropy may well be associated with a holographic dual theory, some authors

[1] It is referred to as a duality in the sense that the supergravity (closed string) description of D-branes and the field theory (open string) description are different formulations of the same physics.

conjectured a de Sitter/CFT correspondence [116, 117, 118] — the bulk time translation is dual to the boundary scale transformation and so the time is holographically reconstructed. Using the analogy with D-branes, one expects new (spacelike) objects S-branes to be at the heart of the dS/CFT correspondence. An S-brane [29] is a topological defect for which time is a transverse dimension and so it exists only for a moment (or brief period) of time. In the same way that (for $\Lambda = 0$) p-branes are stationary solutions of supergravity and string theory, S-branes are time-dependent backgrounds of the theory.

In this paper we find three families of exact solutions: S-branes, bubble-like solutions and the newly coined anti-bubble solutions. Roughly speaking, in D dimensions, these solutions involved a $(D-2)$-dimensional hyperbolic space, de Sitter, or anti-de Sitter component, respectively. The solutions are classified according to the technique of their construction. (See also [119].)

The first is the S-brane type [120, 25, 47, 48, 49, 50, 51, 67, 122, 121, 123] describing a shell of radiation coming in from infinity and creating an unstable brane which subsequently decays.[2] Nonspinning S-branes solutions involve $\mathbf{H}_{D-2}$ which can be quotiented, to yield topological (A)dS black holes — these have been known (see e.g. [99, 125] and references therein). For example, a spherical black hole with $\Lambda > 0$, under analytic continuation and sign flip of metric, gives a black solution with $\Lambda < 0$ and a hyperbolic component. We may refer to this as a (topological) black hole in AdS, or as the corresponding S-brane solution to a black hole in dS. On the other hand, a BHAdS with $\Lambda < 0$ yields a cosmologically singular S-BHAdS with $\Lambda > 0$; this solution has an exterior region [88] which is time-dependent, like de Sitter space itself.[3] The S-BH(A)dS solutions have timelike singularities and the Penrose diagrams are related to a $\pi/2$-rotation of the corresponding black hole Penrose diagrams [99]. However, in the Reissner-Nordström case, the inmost horizon is moved to negative r and the $r > 0$ S-brane Penrose diagram has fewer regions. The solutions we describe here are analogs of the S-branes found previously (with $\Lambda = 0$) and that justifies the terminology.

With $\Lambda = 0$, a black hole is stationary and an S-brane is time-dependent, but a $\Lambda \neq 0$ will dominate at large r and its sign determines the signature of the Killing vector. Black holes and S-branes in AdS are both stationary, and black holes and S-branes in dS are both time-dependent.

The second family are of bubble type [36, 37, 38, 39, 40, 124]. A bubble is a $(D-3)$-sphere which exists only for $r \geq r_{\min}$. An x^D Killing circle vanishes at $r = r_{\min}$. These bubbles are time-dependent since the $(D-3)$-sphere expands in a

[2]The solutions in [25] do not have horizons and are better described as gravitational wave solutions, describing the creation and decay of a fluxbrane. They were constructed by analytic continuation keeping in mind Sen's rolling tachyon solution for unstable D-branes [27].

[3]We emphasize a solution being time-dependent if it does not have an exterior/asymptotic region with a timelike Killing vector. Thus the Schwarzschild black hole is not time-dependent even though there is no global timelike Killing vector, and de Sitter space is time-dependent.

de Sitter fashion. We also define 'double bubbles' as solutions where an expanding $(D-3)$-sphere exists over an interval $r_{\min} \leq r \leq r_{\max}$ and the x^D-circle closes at both endpoints (hence two 'bubbles of nothing').

The third family is the newly coined anti-bubbles, which must be distinguished from expanding bubbles. Here, we have AdS_{D-2} whose spatial section is not a sphere but a noncompact 'anti-bubble.' This spatial section exists only for $r \geq r_{\min}$. We also find double anti-bubbles where the AdS_{D-2} runs over $r_{\min} \leq r \leq r_{\max}$.

When rotation parameters are added (hence looking at Kerr-(A)dS solutions), there is an additional complication to the solution where a quantity W (or Δ_θ) can vanish. This can generate additional horizons changing the time-dependent or stationary nature of various regions in the solution. Also, sometimes this will close the spacetime creating boundary conditions with inconsistent Killing compactifications.

In some cases involving rotation, there are two types of S-branes. For example, the $D = 4$ Kerr solution admits a usual S-brane [47] and also a $\pi/2$-S-brane [67]. This is analogous to the double Killing Kerr bubble (with horizons and CTCs) as opposed to the $\theta \to \pi/2 + i\theta$ Kerr bubble (without horizons or CTCs). The idea is that in even dimensions, one direction cosine is not associated with a rotation and hence it is different; in any dimension, direction cosines with rotations turned off are different from those with rotations turned on. We will be careful to emphasize when such different solutions are available.

The rest of the paper is organized as follows: In Sec. 5.2 we look at the simple case of RN(A)dS black holes in $D = 4$ and find the bubbles, S-branes and anti-bubbles (as well as interior double bubbles and anti-bubbles) using card diagram[4] techniques and using $r\theta$ diagrams. Then in Sec. 5.3 we look at the general-D RN(A)dS solutions, finding bubbles, S-branes and anti-bubbles. We see how the conformal boundary geometry of the S-brane fits nicely with that for the bubble to give the global boundary of AdS.

In Sec. 5.4 we move to the Kerr solutions. These solutions are sometimes plagued by what we call $W = 0$ coordinate singularities [82] (also called $\Delta_\theta = 0$ singularities [39]). We find that these are just spinning Killing horizons (or twisted closures of spatial Killing circles), which complicate the structure of the spacetime. We allow general rotation parameters and try to avoid $W = 0$ singularities. Then, in Sec. 5.5, we only turn one rotation on and allow $W = 0$ singularities. Here we find extremely interesting global structures for bubble geometries with $W = 0$ singularities and illustrate them by drawing skeleton diagrams[5] for the θ coordinate.

[4]Card diagrams are applicable for $D = 4$ or 5 black hole spacetimes which have the requisite 2 or 3 Killing fields. Card diagrams and the technique of the γ-flip were used to understand S-branes in [51].

[5]A skeleton diagram is a 1-dimensional analog of a card diagram; it shows only the coordinate which determines where the horizons are. The skeleton diagram for the Schwarzschild black hole is a +, where the horizontal legs are where r is spacelike and the vertical legs where r is timelike. Four legs meet at a nonextremal horizon.

We conclude in Sec. 5.6 by outlining the role of these solutions in the holographic AdS/CFT correspondence (or the putative dS/CFT correspondence). Lastly we give a short appendix on generalized card diagrams as they apply to pure (A)dS$_D$ space for $D = 4, 5$.

We will not look at genus-zero planar or toroidal black holes or their generalizations — see [99, 125] and references contained therein.

5.2 4d Examples

Before writing down the general analytic continuation, we look at the simple case of four dimensions. Here (as well as in five dimensions) black holes in (A)dS are of Weyl type: in D dimensions they have $D-2$ commuting Killing fields. Methods of obtaining bubbles, anti-bubbles and S-branes are then very evident (see Figs. 5.1-5.4). Unlike previous approaches to analytic continuation to S-branes (involving continuations like $r \to it$), we will find all the spacetimes by only performing simple analytic continuations involving real sections of hyperboloids, by making sign flips in the metric and sometimes continuing to imaginary charge.

We begin discussing the variety of solutions we will obtain starting with the 4d Reissner-Nordström-(A)dS black hole solution. From the 4d RNdS black hole with $\Lambda > 0$ we can obtain an S-brane with $\Lambda < 0$ as well as a static 'anti-bubble' (which is to an expanding bubble what AdS$_2$ is to dS$_2$) with $\Lambda < 0$. From the 4d RNAdS black hole $\Lambda < 0$ we can obtain a bubble solution with $\Lambda < 0$ as well as an S-brane with $\Lambda > 0$.

5.2.1 De Sitter

The RNdS$_4$ solution with $\Lambda = (D-1)/l^2$, $\Lambda > 0$ is

$$\begin{aligned} ds^2 &= -f(r)(dx^4)^2 + dr^2/f(r) + r^2 d\Omega_2^2, \\ A &= Q dx^4/r \end{aligned} \tag{5.1}$$

where $f(r) = 1 - 2M/r + Q^2/r^2 - r^2/l^2$. We take the horizon function to be the quartic polynomial $r^2 f(r) = -r^4/l^2 + r^2 - 2Mr + Q^2$, which can have up to four roots[6] $r_1 < 0 < r_2 \leq r_3 \leq r_4$. The root r_4 is the cosmological horizon of de Sitter, and r_3 and r_2 are the outer and inner black hole horizons, which can coincide in an 'extremal' case. The singularity is at $r = 0$, and $r < 0$ with its single (cosmological) horizon r_1 represents a negative-mass black hole in dS$_4$. We can draw the two non-Killing directions r, θ on the diagram in Fig. 5.1. The RNdS$_4$ black hole solution occupies the middle row, to the right of the singularity. On this and also Fig. 5.2

[6]See [99] for a discussion of roots and parameters. However, the triple root $r_2 = r_3 = r_4$ is singular.

we anticipate several solutions that can be obtained from RNdS_4 by trivial analytic continuation.

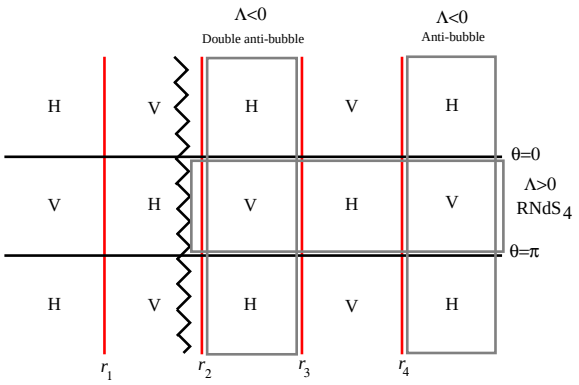

Figure 5.1: Those regions of the extended RNdS_4 spacetime, where we do not send $Q \to iQ$. We have the black hole with $\Lambda > 0$, the anti-bubble with $\Lambda < 0$, and the $r_2 \leq r \leq r_3$ double anti-bubble with $\Lambda < 0$. This $r\theta$ diagram is similar to the C-metric diagrams in [71].

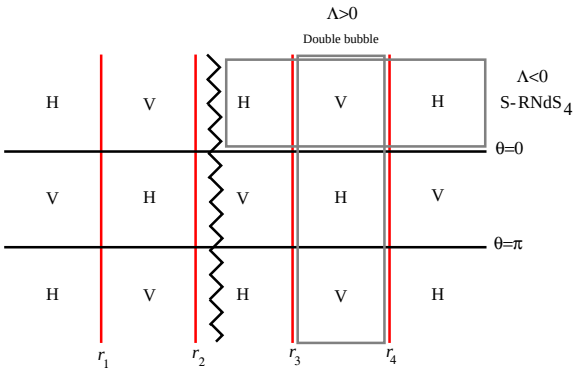

Figure 5.2: Those regions of the extended RNdS_4 spacetime, where we send $Q \to iQ$. We have the $r_3 \leq r \leq r_4$ double bubble with $\Lambda > 0$, and the S-RNdS_4 with $\Lambda < 0$.

We can explicitly give $d\Omega_2^2 = d\theta^2 + \sin^2\theta d\phi^2$. An alternative way to write it (to make contact with later formulas) is to set $-1 \leq \mu_0 = \cos\theta \leq 1$ and $0 \leq \mu_1 = \sin\theta \leq 1$; we have the constraint $\mu_0^2 + \mu_1^2 = 1$.

This 4d spacetime has two commuting Killing vectors (say, the x^4 and ϕ directions) and so is of generalized Weyl type. The regions in Fig. 5.1 are labelled H(orizontal) and V(ertical) in analogy with Weyl card diagrams [51] (and see Appendix A to this paper). Horizontal cards are stationary regions of spacetimes, whereas vertical cards

are time-dependent and have $D-2$ commuting spatial Killing fields. There are two basic operations one can perform on cards. On a horizontal card, one can do a double Killing continuation to pick a new time direction. On vertical cards, one can perform an operation known as a γ-flip which exchanges the timelike and spacelike character of the two non-Killing directions. The γ-flip can be realized by changing the sign of the metric $g_{\mu\nu} \to -g_{\mu\nu}$ and analytically continuing all Killing directions; here $x^4 \to ix^4$ and $\phi \to i\phi$. Along with the sign flip of the metric, from the Einstein-Maxwell-Λ equation we must flip the sign of Λ. Our conventions are to leave the parameter l alone but now interpret the solution to solve a $\Lambda < 0$ equation. The sign flip of the metric also forces the gauge field strength to become imaginary; but we also continue the 1-form $dx^4 \to idx^4$, so the net result is a real field strength. In summary, the γ-flip takes a signature $(D-1,1)$ vertical card with a real field strength and given Λ and turns it 'on its side' to yield a signature $(D-1,1)$ vertical card with a real field strength and opposite sign of Λ.

It is clear then that we can take the vertical-card $r \geq r_4$ region and turn the card on its side with a γ-flip. We now occupy the right column of Fig. 5.1. The solution is

$$\begin{aligned} ds^2 &= -f(r)(dx^4)^2 - \frac{dr^2}{f(r)} - r^2 d\theta^2 + r^2 \sin^2\theta d\phi^2 \\ &\to -f(r)(dx^4)^2 - \frac{dr^2}{f(r)} + r^2 d\theta^2 - r^2 \sinh^2\theta d\phi^2. \end{aligned}$$

We decompactify ϕ to get horizons at $\theta = 0, \pi$; the $0 \leq \theta \leq \pi$ variable can be continued $\theta \to i\theta$, $\theta \to \pi + i\theta$ to give a patched representation of AdS_2. We must compactify $x^4 \simeq x^4 + 4\pi|f'(r_4)|^{-1}$ to avoid a conical singularity at $r = r_4$. In summary, we have AdS_2 and an x^4-circle fibered over $r \geq r_4$. At $r = r_4$ the x^4-circle closes in a fashion very similar to well-known expanding bubble solutions giving a minimum-size AdS_2. In analogy with 'bubble' terminology we shall call this solution [38] the $RNdS_4$ anti-bubble, with $\Lambda < 0$.

Note that we could also perform the γ-flip on $r_2 \leq r \leq r_3$. Now the spacetime has two boundaries $r = r_2, r_3$ where the x^4-circle closes. We must then match $f'(r_2) + f'(r_3) = 0$ to eliminate conical singularities at both ends; then of the parameters M, Q and l, one is dependent — one can also be eliminated by a global conformal transformation, leaving one true dimensionless shape parameter. This solution occupies the center column in Fig. 5.1, and we call it the $r_2 \leq r \leq r_3$ $RNdS_4$ double anti-bubble. Since it does not have an $r \to \infty$ asymptotic region, it is not useful for holography.

The region $r_3 \leq r \leq r_4$ is a stationary region (horizontal card) and we may perform a double Killing continuation $x^4 \to ix^4$, $\phi \to i\phi$ to get a new solution. We must also continue $Q \to iQ$ to make the field strength real. Then the horizon function $r^2 f(r) = 1 - 2M/r - Q^2/r^2 + r^2/l^2$ is changed and its roots are generically $r_1 \leq r_2 < 0 < r_3 \leq r_4$. We now reference solutions to Fig. 5.2; note that positive-

and negative-mass solutions are qualitatively similar. The solution is

$$\begin{aligned} ds^2 &= f(r)(dx^4)^2 + \frac{dr^2}{f(r)} + r^2(d\theta^2 - \sin^2\theta\, d\phi^2) \\ &\to f(r)(dx^4)^2 + \frac{dr^2}{f(r)} + r^2(-d\theta^2 + \sinh^2\theta\, d\phi^2). \end{aligned} \tag{5.2}$$

We see now a patched dS_2; and the x^4 circle vanishes at $r = r_3, r_4$, so we require $f'(r_3) + f'(r_4) = 0$ and have the $r_3 \leq r \leq r_4$ $RNdS_4$ double bubble. It solves $\Lambda > 0$ Einstein-Maxwell-Λ. Since it does not have an $r \to \infty$ asymptotic region, it is not useful for holography.

We can however take the vertical card at hyperbolic θ on the $RNdS_4$ double bubble and perform a γ-flip. The resulting solution has $\Lambda < 0$ and we call it S-$RNdS_4$, since it is the S-brane gotten from the $RNdS_4$ geometry. It occupies the top row of Fig. 5.2, to the right of the singularity. It is

$$ds^2 = f(r)(dx^4)^2 - \frac{dr^2}{f(r)} + r^2(d\theta^2 + \sinh^2\theta d\phi^2).$$

We see $\mathbf{H}_2$, azimuthally parametrized. Note that just as the $RNdS_4$ black hole is not stationary, its S-brane is not time-dependent.

The $RNdS_4$, $RNdS_4$ anti-bubble and S-$RNdS_4$ all have $r \to \infty$ asymptotic regions where they are locally asymptotic to (A)dS_4, depending on their sign of Λ.

We summarize the five spacetimes gotten from $RNdS_4$ in the following table.

Name	Λ	Hyp.	iQ?	ϕ cpct	x^4 cpct	Asym.
$RNdS_4$	+	S^2	No	Yes	No	dS_4
$RNdS_4$ anti-bub.	−	AdS_2	No	No	Yes	AdS_4
$RNdS_4$ doub. bub.	+	dS_2	Yes	No	Double	
$RNdS_4$ doub. anti-bub.	−	AdS_2	No	No	Double	
S-$RNdS_4$	−	$\mathbf{H}_2$	Yes	Yes	No	AdS_4

Here we give the name, the sign of the cosmological constant, the real section of the complex 2-hyperboloid, whether Q has been continued with $Q \to iQ$, whether ϕ is compact, whether x^4 is compact, whether x^4 has two boundaries instead of just one since this is a nontrivial condition and whether the manifold asymptotes locally to (A)dS_4. The isometry group of the solution is the isometry of the hyperbolic space ($SO(3)$, $SO(2,1)$ or $SO(1,2)$) times $\mathbf{R}$ (if x^4 is noncompact) or $U(1)$ (if x^4 is compact).

5.2.2 Anti-de Sitter

To achieve $RNAdS_4$, take $l \to il$ in (5.1). We have

$$\begin{aligned} ds^2 &= -f(r)(dx^4)^2 + dr^2/f(r) + r^2 d\Omega_2^2, \\ A &= Q dx^4/r \end{aligned} \tag{5.3}$$

where $f(r) = 1 - 2M/r + Q^2/r^2 + r^2/l^2$. Then $r^2 f(r)$ can have at most two roots; we assume $Q \neq 0$ and M is large enough so that this happens. Then $0 < r_1 \leq r_2$ — see Fig 5.3. Looking ahead, when we will have to send $Q \to iQ$, we will have $r_1 < 0 < r_2$ — see Fig. 5.4.

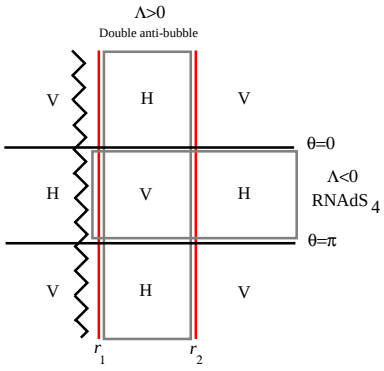

Figure 5.3: Those regions of the extended RNAdS_4 spacetime, where we do not send $Q \to iQ$.

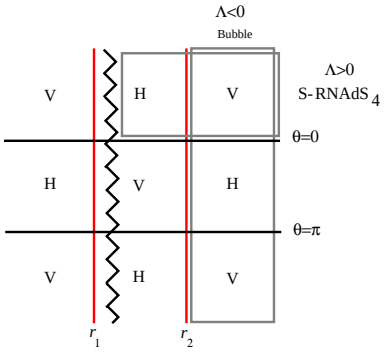

Figure 5.4: Those regions of the extended RNAdS_4 spacetime, where we send $Q \to iQ$.

Since our discovery of solutions parallels the RNdS_4 case, we will be brief. We can take $r \geq r_2$ which is static, and double Killing rotate $x^4 \to ix^4$, $\phi \to i\phi$, $Q \to iQ$. We then get the RNAdS_4 bubble solution with a patched description of dS_2 fibered over $r \geq r_2$, and an x^4-circle which closes at $r = r_2$ to give the bubble. This is the right column of Fig. 5.4.

We can perform a γ-flip on the upper (vertical card) region of the RNAdS_4 bubble to achieve S-RNAdS_4, which is the top row of Fig. 5.4, to the right of the singularity. It has azimuthally parametrized $\mathbf{H}_2$ and $\Lambda < 0$.

Finally we can perform a γ-flip on $r_1 \leq r \leq r_2$ of the RNAdS$_4$ black hole to achieve a double anti-bubble. It has AdS$_2$, $\Lambda > 0$, and appears as the central column in Fig. 5.3.

The RNAdS$_4$ black hole, bubble and S-brane asymptote to (A)dS$_4$ locally.

Again we summarize

Name	Λ	Hyp.	iQ?	ϕ cmpct	x^4 cmpct	Asym.
RNAdS$_4$	$-$	S^2	No	Yes	No	AdS$_4$
RNAdS$_4$ bub.	$-$	dS$_2$	Yes	No	Yes	AdS$_4$
RNAdS$_4$ doub. anti-bub.	$+$	AdS$_2$	No	No	Double	
S-RNAdS$_4$	$+$	$\mathbf{H}_2$	Yes	Yes	No	dS$_4$

The fact that all the listed solutions are different from each other is evident just by looking at where they stand in relation to their neighbors and the singularity, in Figs. 5.1-5.4. One can also use the symmetry groups to prove they are different.

These 4d solutions with $SO(3)$ symmetry can also yield bubbles, anti-bubbles or S-branes based on the continuation $\theta \to \pi/2 + i\theta$ instead of $\theta \to i\theta$. These solutions are not different from those solutions just described. However, even-dimensional Kerr solutions admit $\theta \to \pi/2 + i\theta$ solutions which are different from those gotten by taking the analog of $\theta \to i\theta$. This distinction has been emphasized in [51, 67] and we will revisit it below.

The card-diagram method of the γ-flip also applies in 5d. Card diagrams of (A)dS$_4$ and (A)dS$_5$ spacetime can be drawn; in fact due to their extra symmetries, many different card diagram representations exist. These diagrams are also useful for visualizing the local-(A)dS$_4$, AdS$_5$ asymptotia of the black hole, bubble, anti-bubble, and S-brane solutions. For some details and diagrams, see Appendix A to this paper.

However, card diagram methods do not apply in $D \geq 6$. Nonetheless, analogs of these RN solutions do exist in all $D \geq 4$, and we give them in the next section.

5.3 General Reissner-Nordström-(A)dS$_D$ Solutions

We construct the S-branes for the general RN(A)dS$_D$ solution, along with the bubbles and anti-bubbles. We will not have Figs. 5.1-5.4 to guide us, but again we will only do simple analytic continuations involving cos(h)-type quantities, metric sign flips, and $Q \to iQ$. We will not focus on double (anti-)bubble solutions, only on those solutions with $r \to \infty$ asymptotia. We also give the $r \to \infty$ conformal boundary geometry (CBG) gotten from the given coordinates.

5.3.1 De Sitter

The RNdS_D black hole is

$$\begin{aligned} ds^2 &= -f(r)(dx^D)^2 + \frac{dr^2}{f(r)} + r^2 d\Omega_{D-2}^2, \\ A &= \sqrt{\frac{D-2}{2(D-3)}}\frac{Q dx^4}{r}, \end{aligned} \tag{5.4}$$

where $f(r) = 1 - 2M/r^{D-3} + Q^2/r^{2(D-3)} - r^2/l^2$, $\Lambda = (D-1)/l^2 > 0$. The horizon function is the polynomial $r^{2(D-3)}f(r)$. For D even, an appropriate parameter subdomain gives roots $r_1 < 0 < r_2 \leq r_3 \leq r_4$ — we consider the solution for $r > 0$. For D odd we let r^2 be the independent variable and allow it to go negative. Then for the appropriate parameter subdomain the horizon function has roots which we call $0 < r_2^2 \leq r_3^2 \leq r_4^2$ and we consider $r^2 > 0$ (there is no r_1^2 root in our notation).

Take $D = 2n + 2$ even first; we can write

$$d\Omega_{D-2}^2 = d\mu_0^2 + d\mu_1^2 + \cdots + d\mu_n^2 + \mu_1^2 d\phi_1^2 + \cdots + \mu_n^2 d\phi_n^2, \tag{5.5}$$

where $-1 \leq \mu_0 \leq 1$ and $0 \leq \mu_i \leq 1$ $i = 1, \ldots, n$. The constraint is $\mu_0^2 + \sum_{i=1}^n \mu_i^2 = 1$.

To get the S-brane, we send $\mu_i \to i\mu_i$, $i = 1, \ldots, n$, send $g_{\mu\nu} \to -g_{\mu\nu}$, and $Q \to iQ$. The line element (5.5) becomes, including the sign flip, the (still spacelike)

$$d\mathbf{H}_{D-2}^2 = -d\mu_0^2 + d\mu_1^2 + \cdots + d\mu_n^2 + \mu_1^2 d\phi_1^2 + \cdots + \mu_n^2 d\phi_n^2 \tag{5.6}$$

with constraint $\mu_0^2 - \sum_{i=1}^n \mu_i^2 = 1$. The solution is

$$\begin{aligned} ds^2 &= f(r)(dx^D)^2 - \frac{dr^2}{f(r)} + r^2 d\mathbf{H}_{D-2}^2, \\ A &= \sqrt{\frac{D-2}{2(D-3)}}\frac{Q dx^4}{r}, \end{aligned}$$

which has $\Lambda < 0$. As $r \to \infty$, the solution is asymptotically locally AdS_D. The conformal boundary geometry (CBG) in these coordinates is $ds^2 = -(dx^D)^2/l^2 + d\mathbf{H}_{D-2}^2$, which is $\mathbf{R}_{\text{time}} \times \mathbf{H}_{D-2}$. There is no invariant relating the size of these two components. The horizon function now has roots $r_1 \leq r_2 < 0 < r_3 \leq r_4$ like the S-RNdS_4 case. Our $r \to \infty$ gets the asymptotia gotten from one Rindler wedge of the r_4 horizon — there is another Rindler wedge ignored in this procedure.

Taking the S-brane, we can take $x^D \to ix^D$, continue back $Q \to -iQ$, so $r_1 < 0 < r_2 \leq r_3 \leq r_4$. We compactify $x^D \simeq x^D + 4\pi|f'(r_4)|^{-1}$ to form an anti-bubble at $r = r_4$, and then take for example $\phi_1 \to i\phi_1$. Thus

$$ds^2 = -f(r)(dx^D)^2 - \frac{dr^2}{f(r)} + r^2 d\mathrm{AdS}_{D-2}^2.$$

Here,

$$d\mathrm{AdS}^2_{D-2} = -d\mu_0^2 + d\mu_1^2 + \cdots + d\mu_n^2 - \mu_1^2 d\phi_1^2 + \mu_2^2 d\phi_2^2 + \cdots + \mu_n^2 d\phi_n^2$$

is a patched description; we can go through the μ_1 Rindler horizon to $\mu_1 \to i\mu_1$. This anti-bubble solution was discovered in planar coordinates in [126] where they were termed fluxbranes. In planar coordinates the solutions resemble branes but keeping in mind their global structure, we choose not to think of them as branes, the term anti-bubble (for the AdS_{D-2} factor) being more appropriate.

The CBG is $ds^2 \propto (dx^D)^2/l^2 + d\mathrm{AdS}^2_{D-2}$, which is $S^1 \times \mathrm{AdS}_{D-2}$. Since x^D is compact, there is a dimensionless invariant, the ratio of the circumference of the x^D-circle to the unit-sized AdS_{D-2}.

In odd dimension $D = 2n + 1$ the idea is the same, but the cosines are set up differently. We have μ_i, $i = 1, \ldots, n$, with $0 \leq \mu_i \leq 1$ and

$$d\Omega^2_{D-2} = d\mu_1^2 + \cdots + d\mu_n^2 + \mu_1^2 d\phi_1^2 + \cdots + \mu_n^2 d\phi_n^2. \tag{5.7}$$

To get the S-brane, take $\mu_i \to i\mu_i$ $i = 1, \ldots, n-1$, $g_{\mu\nu} \to -g_{\mu\nu}$, $Q \to iQ$, flip the sign of Λ, and $\phi_n \to i\phi_n$. Then we have

$$d\mathbf{H}^2_{D-2} = d\mu_1^2 + \cdots + d\mu_{n-1}^2 - d\mu_n^2 + \mu_1^2 d\phi_1^2 + \cdots + \mu_n^2 d\phi_n^2, \tag{5.8}$$

and the geometry is

$$ds^2 = f(r)(dx^D)^2 - \frac{dr^2}{f(r)} + r^2 d\mathbf{H}^2_{D-2}.$$

The horizon function now has roots $r_2^2 < 0 < r_3^2 \leq r_4^2$.

To go to the anti-bubble, send $x^D \to ix^D$, return $Q \to -iQ$, and send say $\phi_1 \to i\phi_1$. Then

$$d\mathrm{AdS}^2_{D-2} = d\mu_1^2 + \cdots + d\mu_{n-1}^2 - d\mu_n^2 - \mu_1^2 d\phi_1^2 + \mu_2^2 d\phi_2^2 + \cdots + \mu_n^2 d\phi_n^2.$$

This is in the 'real' μ_1 patch where the constraint reads $\mu_n^2 - \mu_1^2 - \mu_2^2 - \cdots - \mu_{n-1}^2 = 1$, but going through the Rindler horizon at $\mu_1 = 0$, we send $\mu_1 \to i\mu_1$ and get $\mu_n^2 + \mu_1^2 - \mu_2^2 - \cdots - \mu_{n-1}^2 = 1$. The anti-bubble is

$$ds^2 = -f(r)(dx^D)^2 - \frac{dr^2}{f(r)} + r^2 d\mathrm{AdS}^2_{D-2}.$$

The CBG is $ds^2 \propto (dx^D)^2/l^2 + d\mathrm{AdS}^2_{D-2}$, which is $S^1 \times \mathrm{AdS}_{D-2}$. Since x^D was compactified at the largest r-root, there is a dimensionless invariant, the circumference of the x^D-circle over the unit AdS size.

5.3.2 Anti-de Sitter

From the RNAdS$_D$ solution we will make a $\Lambda < 0$ bubble and $\Lambda > 0$ S-brane. The solution is like for RNdS$_D$ except $f(r) = 1 - 2M/r^{D-3} + Q^2/r^{2(D-3)} + r^2/l^2$, with roots $0 < r_1 \leq r_2$.

For $D = 2n + 2$, $d\Omega^2_{D-2}$ is as in (5.5). To get the bubble, send $x^D \to ix^D$, compactify at r_2, and send say $\phi_1 \to i\phi_1$. The solution is

$$ds^2 = f(r)(dx^D)^2 + \frac{dr^2}{f(r)} + d\mathrm{dS}^2_{D-2}, \tag{5.9}$$

where

$$d\mathrm{dS}^2_{D-2} = d\mu_0^2 + d\mu_1^2 + \cdots + d\mu_n^2 - \mu_1^2 d\phi_1^2 + \mu_2^2 d\phi_2^2 + \cdots + \mu_n^2 d\phi_n^2.$$

Of course we can go through the Rindler horizon at $\mu_1 = 0$ and send $\mu_1 \to i\mu_1$. This bubble was described in [38, 39].

The CBG is $ds^2 \propto (dx^D)^2/l^2 + d\mathrm{dS}^2_{D-2}$ which is $S^1 \times \mathrm{dS}_{D-2}$. There is a dimensionless invariant, the ratio of the sizes of these factors.

To get the S-brane from the black hole, send $\mu_i \to i\mu_i$, $i = 1, \ldots, n$, $g_{\mu\nu} \to -g_{\mu\nu}$, $Q \to iQ$, and flip the sign of Λ. Now $r_1 < 0 < r_2$; the solution is

$$ds^2 = f(r)(dx^D)^2 - \frac{dr^2}{f(r)} + r^2 d\mathbf{H}^2_{D-2}, \tag{5.10}$$

where

$$d\mathbf{H}^2_{D-2} = -d\mu_0^2 + d\mu_1^2 + \cdots + d\mu_n^2 + \mu_1^2 d\phi_1^2 + \cdots + d\mu_n^2.$$

The constraint is $\mu_0^2 - \sum_{i=1}^n \mu_i^2 = 1$. Since the singularity is just protected by a cosmological horizon r_2, this solution is nakedly singular, like the S-Schwarzschild geometry of pure Einstein theory.

The CBG is $ds^2 \propto (dx^D)^2/l^2 + d\mathbf{H}^2_{D-2}$, which is $\mathbf{R} \times \mathbf{H}_{D-2}$. This is a Euclidean geometry, so this would serve to investigate the putative dS/CFT correspondence.

In odd dimensions $D = 2n + 1$, we have $d\Omega^2_{D-2}$ given by (5.7). The bubble is gotten by sending $x^D \to ix^D$, $Q \to iQ$ and say $\phi_1 \to i\phi_1$. The solution is (5.9), where

$$d\mathrm{dS}^2_{D-2} = d\mu_1^2 + \cdots + d\mu_n^2 - \mu_1^2 d\phi_1^2 + \mu_2^2 d\phi_2^2 + \cdots + \mu_n^2 d\phi_n^2.$$

The odd-dimensional S-brane on the other hand is gotten from $\mu_i \to i\mu_i$ $i = 1, \ldots, n-1$, $g_{\mu\nu} \to -g_{\mu\nu}$, $\phi_n \to i\phi_n$. The solution is (5.10) with the hyperbolic space given by (5.8).

5.3.3 Extremal S-RNdS$_D$

Take S-RNdS$_D$,

$$ds^2 = f(r)(dx^D)^2 - dr^2/f(r) + r^2 d\mathbf{H}^2_{D-2} \tag{5.11}$$

$$A = \sqrt{\frac{D-2}{2(D-3)}}\frac{Q dx^D}{r}. \tag{5.12}$$

Here, $f(r) = 1 - 2M/r^{D-3} - Q^2/r^{2(D-3)} - r^2/l^2$. For D even we normally assume four roots $r_1 \leq r_2 < 0 < r_3 \leq r_4$. For D odd we have $r_2^2 < 0 < r_3^2 \leq r_4^2$. In either case, one can find an extremal solution where $r_3 = r_4$. Here, 'extremal' refers just to degenerate horizons; this solution is the analog of the $r_3 = r_4$ maximal RNdS$_D$ black hole solution where the outer black hole horizon coincides with the cosmological (de Sitter) horizon. Then $f(r) \sim -A(r - r_4)^2$, and letting $\epsilon = r - r_4$, we can take a scaling limit where $\epsilon \to 0$, ϵx^D fixed, which is

$$ds^2 = -A\epsilon^2 (dx^D)^2 + \frac{d\epsilon^2}{A\epsilon^2} + r_4^2 d\mathbf{H}^2_{D-2},$$

and $F \propto \frac{Q}{r_4^{D-2}} dx^D \wedge d\epsilon$. This solution is AdS$_2 \times \mathbf{H}_{D-2}$. Thus extremal S-RNdS$_D$ interpolates between AdS$_2 \times \mathbf{H}_{D-2}$ at the extremal horizon to local AdS$_D$ at $r = \infty$ and the latter can have a CBG of $\mathbf{H}_{D-2} \times \mathbf{R}_{\text{time}}$.

Solutions which interpolate between spacetimes with similar $\mathbf{H}_{D-2}$ factors were found in [127]. For de Sitter bounces, see [121].

5.3.4 Embedding the Conformal Boundary Geometry of Bubbles and S-branes

In [39] the conformal boundary of the RNAdS$_D$ bubble was given as a subset of $S^1_{\text{time}} \times S^{D-2}$ which is the global conformal boundary of AdS$_D$ — we have identified the time-circle in the canonical fashion. There, it was found that in the $x^D\theta$ strip, where $0 \leq \theta \leq \pi$ is the polar angle for the S^{D-2} of RNAdS$_D$, the bubble asymptotes to the open set $|\theta - \pi/2| < |x^D - \pi/2|$; each bubble asymptotes to one diamond in Fig. 5.5. We now complete the picture by showing that S-RNdS$_D$ asymptotes to the remainder triangles.

First, take $D = 2n + 1$ odd. The embedding of dS$_D$ into $\mathbf{R}^{D,1}$ is

$$\begin{aligned} X'^0 &= \sqrt{1 - r^2}\sinh x^D \\ X^1 &= r\mu_1 \cos\phi_1 \\ X^2 &= r\mu_1 \sin\phi_1 \\ &\vdots \\ X^D &= \pm\sqrt{1 - r^2}\cosh x^D. \end{aligned}$$

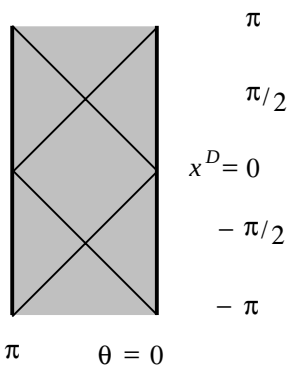

Figure 5.5: Penrose diagram for the global conformal boundary of AdS_D. The top and bottom $x^D = \pm\pi$ are identified. Each diamond is filled in by the asymptotia of an RNAdS_D bubble, and S-RNdS_D gives triangles. Four triangles and two diamonds neatly fit together so their closure gives the whole global boundary.

Here, a prime denotes a timelike coordinate. We want to send $\mu_i \to i\mu_i$ for $i = 1, \ldots, n-1$, $\phi_n \to i\phi_n$, and flip the sign of $g_{\mu\nu}$. Then we get, upon also taking $r > 1$,

$$\begin{aligned} X'^0 &= \sqrt{r^2-1}\sinh x^D \\ X^1 &= r\mu_1 \cos\phi_1 \\ X^2 &= r\mu_1 \sin\phi_1 \\ &\vdots \\ X'^{D-2} &= r\mu_n \cosh\phi_n \\ X^{D-1} &= r\mu_n \sinh\phi_n \\ X^D &= \pm\sqrt{r^2-1}\cosh x^D. \end{aligned}$$

Then $X'^{D-2} > 0$ and we let $X'^0/X'^{D-2} = T$. The global-time angle $\tan^{-1} T$ runs from $-\pi/2$ to $\pi/2$. Then $\tan|\theta - \pi/2| = |X^D|/\sqrt{(X^{D-1})^2 + (X^1)^2 + (X^2)^2 + \cdots} = (\cosh x^d)/(\mu_n \cosh\phi_n) > |T|$, so we have precisely two triangles from this description.

For $D = 2n+2$ even, we have

$$\begin{aligned} X'^0 &= \sqrt{1-r^2}\sinh x^D \\ X^1 &= r\mu_1 \cos\phi_1 \\ X^2 &= r\mu_1 \sin\phi_1 \\ &\vdots \\ X^{D-1} &= r\mu_0 \\ X^D &= \pm\sqrt{1-r^2}\cosh x^D. \end{aligned}$$

Sending $\mu_i \to i\mu_i$ for $i = 1, \ldots, n$ and flipping the sign of $g_{\mu\nu}$, and going to $r > 1$, we get

$$\begin{aligned} X'^0 &= \sqrt{r^2-1}\sinh x^D \\ X^1 &= r\mu_1 \cos\phi_1 \\ X^2 &= r\mu_1 \sin\phi_1 \\ &\vdots \\ X'^{D-1} &= r\mu_0 \\ X^D &= \pm\sqrt{r^2-1}\cosh x^D. \end{aligned}$$

We have $X'^{D-1} > 0$ so set $X'^0/X'^{D-1} = (\sinh x^D)/\mu_0 = T$, and $-\infty < T < \infty$. Furthermore, $|X^D|/\sqrt{(X^1)^2 + (X^2)^2 + \cdots} = (\cosh x^D)/\mu_0 > |T|$.

5.4 Kerr-(A)dS$_D$ And Related Solutions which avoid $W = 0$

We now find S-branes, bubbles and anti-bubbles from the Kerr-(A)dS solutions. In the notation of [82], for bubbles, S-branes and anti-bubbles, a quantity W defined below has the possibility to zero along certain hypersurfaces which are r-independent — they depend on the cosines and hyperbolic functions.

In this section, we will look for solutions which avoid $W = 0$, which are clearly good solutions, with an expected global structure. The $W = 0$ coordinate singularity for the Kerr-AdS$_4$ bubble was a source of some confusion in [39]; actually it is a regular spinning horizon with a constant angular velocity. Following their approach, in Sec. 5.5 we will look at the case of general D with one angular momentum turned on, and explore solutions where we allow $W = 0$. In this case there are two nontrivial Killing directions and one nontrivial cosine, like the $D = 4$ case. A treatment of general D, general a_i will not be given here.

5.4.1 Black Holes, S-branes: Odd dimensions

In odd dimensions $D = 2n + 1$, there are n angular momentum parameters a_i, $i = 1, \ldots, n$ for a spinning black hole, and we want to turn off just one of them, $a_n = 0$. This will force a horizon/polar-origin/orbifold for both the black hole and S-brane at $r^2 = 0$.

For $\lambda = 1/l^2$ for $\Lambda = (D-1)\lambda > 0$, the Kerr-dS solution of [82] is

$$\begin{aligned} ds^2 &= -W(1-\lambda r^2)(dx^D)^2 + \frac{U dr^2}{V-2M} + \frac{2M}{U}\Big(dx^D - \sum_{i=1}^{n-1}\frac{a_i\mu_i^2 d\phi_i}{1+\lambda a_i^2}\Big)^2 \\ &\quad + \sum_{i=1}^{n}\frac{r^2+a_i^2}{1+\lambda a_i^2}\big(d\mu_i^2 + \mu_i^2(d\phi_i - \lambda a_i dx^D)^2\big) \\ &\quad + \frac{\lambda}{W(1-\lambda r^2)}\Big(\sum_{i=1}^{n}\frac{(r^2+a_i^2)\mu_i d\mu_i}{1+\lambda a_i^2}\Big)^2. \end{aligned} \tag{5.13}$$

where $V = \frac{1}{r^2}(1-\lambda r^2)\prod_{i=1}^{n}(r^2+a_i^2)$, $W = \sum_{i=1}^{n}\frac{\mu_i^2}{1+\lambda a_i^2}$ and $U = \sum_{i=1}^{n}\frac{\mu_i^2}{r^2+a_i^2}\prod_{j=1}^{n}(r^2+a_j^2)$. The constraint is $\sum_{i=1}^{n}\mu_i^2 = 1$ and for reference, $F = U/V = \frac{r^2}{1-\lambda r^2}\sum_{i=1}^{n}\frac{\mu_i^2}{r^2+a_i^2}$. The thermodynamics of these black holes are discussed in [128].

To get the S-brane, continue $\mu_i \to i\mu_i$ for $i = 1, \ldots, n-1$, $\phi_n \to i\phi_n$ and perform a flip $g_{\mu\nu} \to -g_{\mu\nu}$. The change in the sign of the metric necessitates a change in the cosmological constant — our notation will be $\Lambda < 0$ but $1/l^2 = \lambda > 0$. So the S-Kerr-dS$_D$ solves Einstein's equations with $\Lambda < 0$. The constraint is now $\mu_n^2 - \sum_{i=1}^{n-1}\mu_i^2 = 1$. The solution is

$$\begin{aligned} ds^2 &= W(1-\lambda r^2)(dx^D)^2 - \frac{U dr^2}{V-2M} - \frac{2M}{U}\Big(dx^D + \sum_{i=1}^{n-1}\frac{a_i\mu_i^2 d\phi_i}{1+\lambda a_i^2}\Big)^2 \\ &\quad + \sum_{i=1}^{n-1}\frac{r^2+a_i^2}{1+\lambda a_i^2}\big(d\mu_i^2 + \mu_i^2(d\phi_i - \lambda a_i dx^D)^2\big) - r^2(d\mu_n^2 - \mu_n^2 d\phi_n^2) \\ &\quad - \frac{\lambda}{W(1-\lambda r^2)}\Big(r^2\mu_n d\mu_n - \sum_{i=1}^{n-1}\frac{(r^2+a_i^2)\mu_i d\mu_i}{1+\lambda a_i^2}\Big)^2. \end{aligned} \tag{5.14}$$

Now, W and U are given in terms of μ_i by

$$W = \mu_n^2 - \sum_{i=1}^{n-1}\frac{\mu_i^2}{1+\lambda a_i^2}$$

and

$$U = \Big(\mu_n^2 - \sum_{i=1}^{n-1}\frac{\mu_i^2}{1+a_i^2/r^2}\Big)\prod_{j=1}^{n-1}(r^2+a_j^2).$$

Note that all elements in the solution that are functions of r, a_i and λ have not changed and so it is clear that the S-brane has the same parameter regions and ensuing horizon structure as the black hole. However, the description of each r-interval as stationary or time-dependent is flipped. In particular, horizons are still located at $V - 2M = 0$. The determinant of the $(n+1)\times(n+1)$ Killing submetric

has $\det g_{\alpha\beta} = r^2(V-2M)W\prod_{i=1}^{n}\frac{\mu_i^2}{1+\lambda a_i^2}$, which has opposite sign from the black hole case [82].

Consider the horizon function

$$r^2(V-2M) = r^2\Big((1-\lambda r^2)\prod_{i=1}^{n-1}(r^2+a_i^2) - 2M\Big).$$

The geometry depends only on r^2, which we take to be the independent variable, and allow to be negative. In the ordinary parameter range $2M > \prod_{i=1}^{n-1} a_i^2 = A^2$ then for sufficiently small λ, there are two positive roots $0 < r_1^2 \le r_2^2$. For $r^2 > r_2^2$, the solution is stationary as we expect for asymptotically AdS_D space. With $r_1^2 < r^2 < r_2^2$ the solution is time-dependent and for $r_1^2 = r_2^2$, there is an extremal horizon with an AdS_2 scaling limit. For $0 < r^2 < r_1^2$ the solution is stationary. At $r^2 = 0$, the solution is not singular and the ϕ_n-circle closes with periodicity[7]

$$\phi_n \simeq \phi_n + 2\pi\sqrt{A^2/(A^2-2M)}.$$

Since $r^2 \ge 0$, there is no $U = 0$ singularity.

For the anomalous parameter range $0 < 2M < A^2$ (described for $\lambda = 0$ in [67] (Chapter 4) and in great detail for $D = 5$ black holes and S-branes), any $\lambda > 0$ is allowed and we have a root $r^2 = r_2^2 > 0$, a ϕ_n Milne horizon at $r^2 = 0$ and another root at $r^2 = -r_1^2 < 0$. Without loss of generality we assume $0 < a_1 \le a_2 \le \cdots \le a_{n-1}$ and so $-a_1^2 < -r_1^2 < 0$. The spacetime closes at $r^2 = -r_1^2$ — the twisting and periodicity can be gotten by continuing the angular momentum and surface gravity of [82]. In particular, just put $r_{\text{horizon}} \to ir_1$ ($r_{\text{horizon}} \to -ir_1$ also gives the right answer) and $\kappa \to \pm i\kappa$. We have

$$\Omega^i = \frac{a_i(1+\lambda a_i^2)}{a_i^2 - r_1^2}, \qquad \kappa = r_1(1+\lambda r_1^2)\sum_{i=1}^{n}\frac{1}{a_i^2-r_1^2} + \frac{1}{r_1}.$$

For $n = 2$, $\lambda = 0$, this reduces to $\Omega = a/2M$, $\kappa = \frac{\sqrt{a^2-2M}}{2M}$, which matches [67]. Since $-r^2 < a_1^2 \le a_2^2 \le \cdots$, there is no $U = 0$ singularity.

The region $-r_1^2 \le r^2 \le 0$ for an anomalous range S-Kerr-dS gives upon $\phi_n \to i\phi_n$ the new S-Kerr instanton of [67] (or Chapter 4). The extremal case $2M = A^2$ is nonsingular at $r^2 = r_1^2 = 0$ and has a dS_3 scaling limit as described in Chapter 4.

For the Kerr-dS black hole, $\lambda > 0$ and $W = \sum_{i=1}^{n}\frac{\mu_i^2}{1+\lambda a_i^2}$ never zeroes. For λ a little negative, namely $-\min_i(a_i^{-2}) < \lambda < 0$, W is still positive. This is the Kerr-AdS black hole which avoids $W = 0$. For $\lambda < -\min_i(a_i^{-2})$, there is a mixture of positive and negative terms and we will find a $W = 0$ coordinate singularity (moreover, a priori the spacetime has the wrong signature).

[7] The global structure here for D odd is just like the $\lambda = 0$ case, which was first discovered by Jones and Wang (Chapter 4).

For S-Kerr-dS, we have $W = \mu_n^2 - \sum_{i=1}^{n-1} \frac{\mu_i^2}{1+\lambda a_i^2}$. For $\lambda > 0$, from the constraint $\mu_n^2 - \sum_{i=1}^{n-1} \mu_i^2 = 1$, this never zeroes; we have a good S-Kerr-dS with $\Lambda < 0$. However, any $\lambda < 0$ will give us a $W = 0$ coordinate singularity.

5.4.2 Black holes and S-branes: Even dimensions

The even-dimensional case $D = 2n+2$ is quite different from the odd-dimensional case. Here we have n rotation parameters and we want to leave them all on, so the black hole has an equatorial 'ring' singularity and the S-brane is nonsingular at $r = 0$.[8] The black hole solution is

$$\begin{aligned} ds^2 &= -W(1-\lambda r^2)(dx^D)^2 + \frac{U dr^2}{V-2M} + \frac{2M}{U}\Big(dx^D - \sum_{i=1}^{n} \frac{a_i \mu_i^2 d\phi_i}{1+\lambda a_i^2}\Big)^2 \\ &\quad + d\mu_0^2 + \sum_{i=1}^{n} \frac{r^2+a_i^2}{1+\lambda a_i^2} d\mu_i^2 + \sum_{i=1}^{n} \frac{r^2+a_i^2}{1+\lambda a_i^2} \mu_i^2 (d\phi_i - \lambda a_i dx^D)^2 \\ &\quad + \frac{\lambda}{W(1-\lambda r^2)}\Big(r^2 \mu_0 d\mu_0 + \sum_{i=1}^{n} \frac{(r^2+a_i^2)\mu_i d\mu_i}{1+\lambda a_i^2}\Big)^2 . \end{aligned}$$

The constraint is $\mu_0^2 + \sum_{i=1}^{n} \mu_i^2 = 1$, where $-1 \le \mu_0 \le 1$ has no rotation parameter and $0 \le \mu_i \le 1$ for $i = 1, \ldots, n$ has rotation parameter ϕ_i. We have $V = \frac{1}{r}(1-\lambda r^2)\prod_{i=1}^{n}(r^2+a_i^2)$, $W = \mu_0^2 + \sum_{i=1}^{n} \frac{\mu_i^2}{1+\lambda a_i^2}$, $U = \frac{1}{r}\Big(\mu_0^2 + \sum_{i=1}^{n} \frac{\mu_i^2}{1+a_i^2/r^2}\Big)\prod_{i=1}^{n}(r^2+a_i^2)$, and for reference $F = U/V = \frac{r^2}{1-\lambda r^2}\big(\mu_0^2 + \sum_{i=1}^{n} \frac{\mu_i^2}{r^2+a_i^2}\big)$.

For the even-dimensional case, the solution depends properly on r, not r^2. It has the symmetry $r \to -r$, $M \to -M$. For the right range of parameters, the horizon function $rV(r) - 2Mr$ has four roots, $r_1 < 0 < r_2 \le r_3 \le r_4$; an extremal black hole occurs for $r_2 = r_3$. Since all a_i are turned on, at $r = 0$ there is only a $U = 0$ S^{D-3} 'ring' singularity at $\mu_0 = 0$ — hence we can go to negative r.

The continuation to S-brane is $\mu_i \to \mu_i$, $i = 1, \ldots, n$, and $g_{\mu\nu} \to -g_{\mu\nu}$. We then have Λ with sign opposite to λ.

$$\begin{aligned} ds^2 &= W(1-\lambda r^2)(dx^D)^2 - \frac{U dr^2}{V-2M} - \frac{2M}{U}\Big(dx^D + \sum_{i=1}^{n} \frac{a_i \mu_i^2 d\phi_i}{1+\lambda a_i^2}\Big)^2 \\ &\quad - d\mu_0^2 + \sum_{i=1}^{n} \frac{r^2+a_i^2}{1+\lambda a_i^2} d\mu_i^2 + \sum_{i=1}^{n} \frac{r^2+a_i^2}{1+\lambda a_i^2} \mu_i^2 (d\phi_i - \lambda a_i dx^D)^2 \\ &\quad - \frac{\lambda}{W(1-\lambda r^2)}\Big(r^2 \mu_0 d\mu_0 - \sum_{i=1}^{n} \frac{(r^2+a_i^2)\mu_i d\mu_i}{1+\lambda a_i^2}\Big)^2 \end{aligned}$$

[8] The global structure of this solution for the $\lambda = 0$ case was worked out by Lü and Vázquez-Poritz [49]. The $D = 4$ S-Kerr-dS with $\Lambda < 0$ is in [99].

The quantity V is as for the black hole, $W = \mu_0^2 - \sum_{i=1}^n \frac{\mu_i^2}{1+\lambda a_i^2}$ and $U = \frac{1}{r}\Big(\mu_0^2 - \sum_{i=1}^n \frac{\mu_i^2}{1+a_i^2/r^2}\Big)\prod_{i=1}^n (r^2+a_i^2)$. The constraint is now $\mu_0^2 - \sum_{i=1}^n \mu_i^2 = 1$ and this implies $\mu_0 \geq 1$. Since there is no ring singularity, we may follow $r \to -\infty$ and so the solution is nonsingular.

S-Kerr-dS with $\lambda > 0$ avoids $W = 0$. S-Kerr-AdS with $\lambda < 0$ hits a $W = 0$ coordinate singularity.

The $r_2 = r_3$ extremal case of the S-brane is nonsingular at the extremal horizon and has a dS_2 scaling limit [49]. The $r_3 = r_4$ extremal case has an AdS_2 scaling limit.

5.4.3 Asymptotics

Take say the odd D case. Sending $r \to \infty$ for the black hole, we get a CBG

$$\begin{aligned} ds^2 \;\propto\; & \lambda W (dx^D)^2 + \sum_{i=1}^n \frac{1}{1+\lambda a_i^2}\big(d\mu_i^2 + \mu_i^2 (d\phi_i - \lambda a_i dx^D)^2\big) \\ & - \frac{1}{W}\Big(\sum_{i=1}^n \frac{\mu_i d\mu_i}{1+\lambda a_i^2}\Big)^2. \end{aligned}$$

This appears to be spinning, but the spinning is a pure coordinate effect. If we let $\phi_i = \tilde{\phi}_i + \lambda a_i x^D$, we get

$$ds^2 \propto \lambda W (dx^D)^2 + \sum_{i=1}^n \frac{1}{1+\lambda a_i^2}\big(d\mu_i^2 + \mu_i^2 d\tilde{\phi}_i^{\,2}\big) - \frac{1}{W}\Big(\sum_{i=1}^n \frac{\mu_i d\mu_i}{1+\lambda a_i^2}\Big)^2.$$

This is the same CBG as we get from the $M = 0$ case, which was identically $(\mathrm{A})\mathrm{dS}_D$. In fact these are just the 'spheroidal coordinates' of [82]. This boundary is conformal to $\mathbf{R}_{\text{space}} \times S^{D-2}$ for $\lambda > 0$ and $\mathbf{R}_{\text{time}} \times S^{D-2}$ for $\lambda < 0$.

The S-brane we know has no $W = 0$ locus for $\lambda > 0$ ($\Lambda < 0$) and has CBG

$$\begin{aligned} ds^2 \;\propto\; & \lambda W (dx^D)^2 + \sum_{i=1}^{n-1} \frac{1}{1+\lambda a_i^2}\big(d\mu_i^2 + \mu_i^2 (d\phi_i - \lambda a_i dx^D)^2\big) \\ & - d\mu_n^2 + \mu_n^2 d\phi_n^2 + \frac{1}{W}\Big(\mu_n d\mu_n - \sum_{i=1}^{n-1} \frac{\mu_i d\mu_i}{1+\lambda a_i^2}\Big)^2. \end{aligned}$$

Again sending $r \to \infty$ has dropped out the M parameter, so this CBG should be conformal to $\mathbf{R}_{\text{time}} \times \mathbf{H}_{D-2}$.

5.4.4 The μ_0-negative S-Kerr-dS for even dimensions

There is another S-brane obtainable from Kerr-dS_D for D even. This is the analog of the 4d 'Kerr $\pi/2$-bubble on its side' of Chapter 4. A sphere in even D is written

as

$$d\Omega_{D-2}^2 = d\mu_0^2 + d\mu_1^2 + \cdots + d\mu_n^2 + \mu_1^2 d\phi_1^2 + \cdots + \mu_n^2 d\phi_n^2,$$

where the constraint is $\mu_0^2 + \sum_{i=1}^n \mu_i^2 = 1$. Send $\mu_0 \to i\mu_0$ and $\mu_i \to i\mu_i$ $i = 2, \ldots, n$, $\phi_1 \to i\phi_1$, and flip the sign of the metric. We then get

$$d\mathbf{H}_{D-2}^2 = d\mu_0^2 - d\mu_1^2 + \cdots + d\mu_n^2 + \mu_1^2 d\phi_1^2 + \cdots + \mu_n^2 d\phi_n^2,$$

where $-\mu_0^2 + \mu_1^2 - \mu_2^2 - \cdots - \mu_n^2 = 1$. In the Kerr case along with $\phi_1 \to i\phi_1$ we must do $a_1 \to ia_1$. We call the resulting solution the μ_1-positive S-Kerr-dS, or a μ_0-negative S-Kerr-dS. This emphasizes that in the $\mathbf{H}_{D-2}$ constraint, it is not μ_0 but rather a μ_i that has a rotation angle, that has the plus sign. The full Kerr S-brane is

$$\begin{aligned} ds^2 &= W(1-\lambda r^2)(dx^D)^2 - \frac{U dr^2}{V-2M} - \frac{2M}{U}\Big(dx^D + \frac{a_1\mu_1^2 d\phi_1}{1-\lambda a_1^2} \\ &\quad + \sum_{i=2}^n \frac{a_i \mu_i^2 d\phi_i}{1+\lambda a_i^2}\Big)^2 + d\mu_0^2 - \frac{r^2 - a_1^2}{1-\lambda a_1^2} d\mu_1^2 + \sum_{i=2}^n \frac{r^2+a_i^2}{1+\lambda a_i^2} d\mu_i^2 \\ &\quad + \frac{r^2-a_1^2}{1-\lambda a_1^2}\mu_1^2 (d\phi_1 - \lambda a_1 dx^D)^2 + \sum_{i=2}^n \frac{r^2+a_1^2}{1+\lambda a_i^2}\mu_i^2 (d\phi_i - \lambda a_i dx^D)^2 \\ &\quad - \frac{\lambda}{W(1-\lambda r^2)}\Big(- r^2 \mu_0 d\mu_0 + \frac{r^2-a_1^2}{1-\lambda a_1^2}\mu_1 d\mu_1 - \sum_{i=2}^n \frac{r^2+a_i^2}{1+\lambda a_i^2}\mu_i d\mu_i\Big)^2. \end{aligned}$$

Here, $W = -\mu_0^2 + \frac{\mu_1^2}{1-\lambda a_1^2} - \sum_{i=2}^n \frac{\mu_i^2}{1+\lambda a_i^2}$. For $0 < \lambda < 1/a_1^2$, this does not zero, and we never go to imaginary μ_1. There is no $U = 0$ singularity at $r = a_1$, because $\mu_1 \geq 1$. Horizons are given by $r_1 \leq r_2 < 0 < r_3 \leq r_4$. This solution is also important for constructing even-dimensional anti-bubbles.

5.4.5 Spinning Λ bubble or anti-bubble solutions

It was noticed in [39] that Kerr-AdS bubbles are 'problematic' from the $W = 0$ singularity, even in the simple 4d case. We now check that $W = 0$ always occurs in Kerr-AdS bubbles and find ways to avoid $W = 0$ for anti-bubbles constructed from Kerr-dS.

Bubbles with large-r asymptotia can only come from $\lambda < 0$ ($\Lambda < 0$) black holes, where the large-r region is stationary. Then in even $D = 2n + 2$,

$$W = \mu_0^2 + \sum_{i=1}^n \frac{\mu_i^2}{1+\lambda a_i^2}.$$

One way to get a bubble is to send $\mu_0 \to i\mu_0$, $x^D \to ix^D$, and $a_i \to ia_i$ $i = 1, \ldots, n$. This is the analog of the Kerr $\pi/2$-bubble in 4d gotten from $\theta \to \pi/2 + i\theta$, which has

no Killing horizons or CTCs. Then

$$W = -\mu_0^2 + \sum_{i=1}^{n} \frac{\mu_i^2}{1-\lambda a_i^2}, \qquad \text{where} \qquad -\mu_0^2 + \sum_{i=1}^{n} \mu_i^2 = 1.$$

We see that the terms with + signs in W are divided to make them smaller; the $-\mu_0^2$ can dominate and make $W = 0$.

Another type of bubble[9] is gotten by picking one angle from $\phi_1, \ldots, \phi_n$, for example ϕ_1. Take $x^D \to ix^D$, $\phi_1 \to i\phi_1$, $a_i \to ia_i$ $i = 2, \ldots, n$. This is the analog of the $\mathcal{K}_+$ bubble of [51, 67] in 4d obtained from double Killing continuation, which has Killing horizons and CTCs. In our present case, we can continue past $\mu_1 = 0$ to $\mu_1 \to i\mu_1$ and get

$$W = \mu_0^2 - \frac{\mu_1^2}{1+\lambda a_1^2} + \sum_{i=2}^{n} \frac{\mu_i^2}{1-\lambda a_i^2}, \qquad \text{where} \qquad \mu_0^2 - \mu_1^2 + \sum_{i=1}^{n} \mu_i^2 = 1.$$

Even if $a_1 = 0$, if some a_i is turned on, $W = 0$ still occurs.

For odd D, there is no μ_0. One can check that in any case except no angular momentum, $W = 0$ occurs.[10]

For anti-bubbles, the situation is better — we find Kerr-dS$_D$ anti-bubbles that avoid $W = 0$ for all $D \geq 4$, and an extra one in $D = 4$. The idea is to make the term with the + coefficient in W to have a denominator smaller than the denominator of all − terms. Recall that to take an anti-bubble we start with Kerr-dS$_D$ with $\lambda > 0$. Take D even and first go to the usual S-brane with $\Lambda < 0$:

$$W = \mu_0^2 - \sum_{i=1}^{n} \frac{\mu_i^2}{1+\lambda a_i^2}, \qquad \text{where} \qquad \mu_0^2 - \sum_{i=1}^{n} \mu_i^2 = 1.$$

Then pick say the angle ϕ_1. Send $x^D \to ix^D$, $\phi_1 \to i\phi_1$, $a_i \to ia_i$ $i = 2, \ldots, n$. We have

$$W = \mu_0^2 - \frac{\mu_1^2}{1+\lambda a_1^2} - \sum_{i=2}^{n} \frac{\mu_i^2}{1-\lambda a_i^2}, \qquad \text{where} \qquad \mu_0^2 - \sum_{i=1}^{n} \mu_i^2 = 1.$$

This hits $W = 0$ unless we turn off a_i (with $i = 2, \ldots, n$), but in that case going through the horizon to $\mu_1 \to i\mu_1$,

$$W = \mu_0^2 + \frac{\mu_1^2}{1+\lambda a_1^2} - \sum_{i=2}^{n} \mu_i^2.$$

[9] These two types of bubbles are not the same as the two solutions presented at the beginning of [86], in the context of one angular momentum on. There, the first is a bubble with $W = 0$, and the second is an anti-bubble with $W = 0$; its dS$_{D-5}$ is part of an AdS$_{D-4}$ which is part of a perturbed AdS$_{D-2}$. The construction of an anti-bubble by continuing from hyperbolic space suggests those authors also considered the S-brane.

[10] In [39], (31)-(34) should be corrected to have $\Delta_\tau = 1 - \frac{\alpha^2}{l^2}\sinh^2\tau - \frac{\beta^2}{l^2}\cosh^2\tau$, so $W \propto \Delta_\tau = 0$ also occurs.

This still hits zero unless $D = 4$ where $i = 2, \ldots, n$ don't exist. So the $D = 4$ case with a turned on, works. This solution can be easily obtained by card diagram methods using Fig. 5.1 by performing a γ-flip on the $r \geq r_4$, $0 \leq \theta \leq \pi$ region (and extending to $\theta \to i\theta$ or $\theta \to \pi + i\theta$).

In even D, we can also find a whole family of anti-bubbles from μ_0-negative S-branes. Picking μ_1 to have the + sign, this S-brane has

$$W = -\mu_0^2 + \frac{\mu_1^2}{1 - \lambda a_1^2} - \sum_{i=2}^{n} \frac{\mu_i^2}{1 + \lambda a_i^2}, \qquad \text{where} \qquad -\mu_0^2 + \mu_1^2 - \sum_{i=2}^{n} \mu_i^2 = 1.$$

Then double Killing $x^D \to ix^D$, $\phi_1 \to i\phi_1$, $a_i \to ia_i$ (with $i = 2, \ldots, n$), we have

$$W = -\mu_0^2 + \frac{\mu_1^2}{1 - \lambda a_1^2} - \sum_{i=2}^{n} \frac{\mu_i^2}{1 - \lambda a_i^2}, \qquad \text{where} \qquad -\mu_0^2 + \mu_1^2 - \sum_{i=2}^{n} \mu_i^2 = 1.$$

For $0 < 1 - \lambda a_1^2 < 1 - \lambda a_i^2$ $i = 2, \ldots, n$, we avoid $W = 0$. Note that we never get to a $\mu_1 = 0$ ϕ_1-horizon, so the above distribution of hyperbolic pieces is global. So for general even D we have this Kerr-dS anti-bubble. We stress that the $D = 4$ solution of this is different from the one gotten from the ordinary S-brane. This present $D = 4$ solution can be obtained from the black hole by $\theta \to \pi/2 + i\theta$, performing a γ-flip to make the non-Killing directions ++, and then $\phi \to i\phi$, $a \to ia$. To avoid the $U = 0$ 'ring' singularity, taking $a_1 > a_2 \geq \cdots$, we want the largest horizon root (the anti-bubble) to occur at $r_4 > a_2$. This can always be arranged for large enough l.

In odd dimension $D = 2n + 1$, the S-brane with a_n turned back on has

$$W = \frac{\mu_n^2}{1 - \lambda a_n^2} - \sum_{i=1}^{n-1} \frac{\mu_i^2}{1 + \lambda a_i^2}, \qquad \text{where} \qquad \mu_n^2 - \sum_{i=1}^{n-1} \mu_i^2 = 1.$$

To get a good anti-bubble, we send $x^D \to ix^D$, $\phi_n \to i\phi_n$, $a_i \to ia_i$ $i = 1, \ldots, n-1$, hence

$$W = \frac{\mu_n^2}{1 - \lambda a_n^2} - \sum_{i=1}^{n-1} \frac{\mu_i^2}{1 - \lambda a_i^2}.$$

For $0 < 1 - \lambda a_n^2 < 1 - \lambda a_i^2$, we avoid $W = 0$. Again, we never reach a $\mu_n = 0$ ϕ_n-horizon so the above characterization is global. The $D = 5$ solution can be obtained by γ-flipping the $r \geq r_4$, $0 \leq \theta \leq \pi/2$ of the black hole, going to $\mu_1 \to i\mu_1$ where $\mu_1 = \sin\theta$, then continuing $\phi_i \to i\phi_i$, $a_i \to ia_i$ (with $i = 1, 2$). Taking $a_n^2 > a_1^2 \geq \cdots$, the largest root (anti-bubble) is at $r_4^2 > a_1^2$ for large l, so the solution is nonsingular.

5.5 Kerr-(A)dS$_D$: One a_i on, and allow $W = 0$

When a $W = 0$ coordinate singularity occurs, an extra horizon-like locus will be present. We will just look at the case of one angular momentum on, where the Kerr-(A)dS$_D$ solution simplifies considerably [81]. For bubbles, we find that in $D \geq 4$ there

is one family of nonsingular solutions and in $D = 4$ there is an additional solution. For S-Kerr-AdS, $D \geq 4$ we find one family. There are no other generically nonsingular solutions.

5.5.1 Bubbles

Let's examine bubbles; take $D = 4$ first. The Kerr-AdS$_4$ black hole solution [134] is

$$\begin{aligned} ds^2 &= \rho^2\big(\frac{dr^2}{\Delta} + \frac{d\theta^2}{1-(a^2/l^2)\cos^2\theta}\big) - \frac{\Delta}{\rho^2}\big(dx^4 - \frac{a\sin^2\theta}{1-a^2/l^2}d\phi\big)^2 \\ &\quad + \frac{\sin^2\theta(1-(a^2/l^2)\cos^2\theta)}{\rho^2}\big(a dx^4 - \frac{r^2+a^2}{1-a^2/l^2}d\phi\big)^2, \end{aligned} \tag{5.15}$$

where $\Delta = (r^2+a^2)(1+r^2/l^2) - 2Mr$, $\rho^2 = r^2 + a^2\cos^2\theta$, and $0 \leq \theta \leq \pi$.

The $\pi/2$-bubble is gotten from $\theta \to \pi/2 + i\theta$, $a \to ia$, $x^4 \to ix^4$. Then

$$\begin{aligned} ds^2 &= \rho^2\big(\frac{dr^2}{\Delta} - \frac{d\theta^2}{1-(a^2/l^2)\sinh^2\theta}\big) + \frac{\Delta}{\rho^2}\big(dx^4 - \frac{a\cosh^2\theta}{1+a^2/l^2}d\phi\big)^2 \\ &\quad + \frac{\cosh^2\theta(1-(a^2/l^2)\sinh^2\theta)}{\rho^2}\big(a dx^4 + \frac{r^2-a^2}{1+a^2/l^2}d\phi\big)^2, \end{aligned} \tag{5.16}$$

where $\Delta = (r^2-a^2)(1+r^2/l^2) - 2Mr$ has roots $r_1 < 0 < r_2$, and $\rho^2 = r^2 + a^2\sinh^2\theta$. At $r = r_2$, $\Delta = 0$ and the differential displacement $a dx^4 + \frac{r_2^2-a^2}{1+a^2/l^2}d\phi = 0$ is null. So let $\tilde{\phi} = \phi - \Omega x^4$, $\tilde{x}^4 = x^4$, $\Omega = -a(1+a^2/l^2)/(r_2^2-a^2)$. Then $d\tilde{\phi} = 0$ is null so the vector $(\partial/\partial\tilde{x}^4)_{\tilde{\phi}}$ is null at $r = r_2$. We can compactify $\tilde{x}^4 \simeq \tilde{x}^4 + \beta$ for some periodicity to make $r = r_2$ the origin of polar coordinates. We must leave $\tilde{\phi}$ noncompact to get a horizon at $W = 0$ (and make no reference to the previous $x^4\phi$ Killing coordinates).[11] The metric is now

$$\begin{aligned} ds^2 &= \rho^2\big(\frac{dr^2}{\Delta} - \frac{d\theta^2}{1-(a^2/l^2)\sinh^2\theta}\big) + \frac{\Delta}{\rho^2}\big(dx^4 - \frac{a\cosh^2\theta}{1+a^2/l^2}(d\tilde{\phi} + \Omega d\tilde{x}^4)\big)^2 \\ &+ \frac{\cosh^2\theta(1-(a^2/l^2)\sinh^2\theta)}{\rho^2}\big(a d\tilde{x}^4 + \frac{r^2-a^2}{1+a^2/l^2}(d\tilde{\phi} + \Omega d\tilde{x}^4)\big)^2. \end{aligned} \tag{5.17}$$

Setting $\sinh\theta_0 = l/|a|$, this metric has expected bubble properties for $-\theta_0 < \theta < \theta_0$. Following [39], set $\sinh\theta = l/a - \epsilon^2$; then for small real ϵ, we have

$$\begin{aligned} ds^2 &\approx (r^2+l^2)\frac{dr^2}{\Delta} - \frac{2la(l^2+r^2)}{l^2+a^2}d\epsilon^2 + \frac{\Delta}{r^2+l^2}\big(d\tilde{x}^4 - \frac{l^2}{a}(d\tilde{\phi} + \Omega d\tilde{x}^4)\big)^2 \\ &\quad + \epsilon^2\frac{2(l^2+a^2)}{la(l^2+r^2)}\big(a d\tilde{x}^4 + \frac{r^2-a^2}{1+a^2/l^2}(d\tilde{\phi} + \Omega d\tilde{x}^4)\big)^2. \end{aligned} \tag{5.18}$$

[11] The differentials dx^4, $d\phi$ are still well defined and it is still acceptable to write the metric in terms of them.

At $\epsilon = 0$, $d\tilde{x}^4 - \frac{l^2}{a}(d\tilde{\phi} + \Omega d\tilde{x}^4) = 0$ is null. That is a regular spinning horizon — the angular velocity of a regular spinning horizon must be constant [88, 82]. On this side of the horizon the Killing submetric has signature $++$ and on the other side it will have $+-$. We let $\tilde{\tilde{x}}^4 = \tilde{x}^4 - \mho\tilde{\phi}$, $\tilde{\tilde{\phi}} = \tilde{\phi}$, where $\mho = \Omega^{-1}(1 - a^2/l^2)$. Then $d\tilde{\tilde{x}}^4 = 0$ is null, or the vector $(\partial/\partial\tilde{\tilde{\phi}})_{\tilde{\tilde{x}}^4}$ gives us the Milne trajectories.

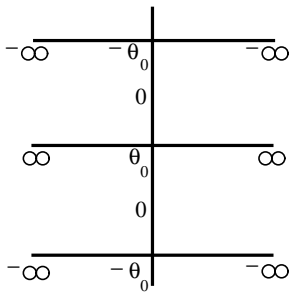

Figure 5.6: A skeleton diagram for the θ coordinate of the Kerr-AdS$_4$ $\pi/2$-bubble. Horizontal segments are where θ is spacelike and vertical where θ is timelike. Here, four-segment intersections are spinning $\tilde{x}^4\tilde{\phi}$ horizons.

This horizon is then just like a Kerr horizon except the role of the two Killing metric squares is reversed and r is replaced by θ. If we repress the Killing directions and $r \geq r_2$, we arrive at a spacetime skeleton diagram for just the θ coordinate — see Fig. 5.6. The vertical legs have θ timelike and the horizontal legs have θ spacelike. The spacetime is periodic in time; each dS$_{D-2}$-type region gives way to horizons beyond which are stationary regions. The $r \to \infty$ limit gives a CBG which can be represented by the same skeleton diagram — the metric is

$$ds^2 \propto \frac{1}{l^2}\big(d\tilde{x}^4 - \frac{a\cosh^2\theta}{1 + a^2/l^2}(d\tilde{\phi} + \Omega d\tilde{x}^4)\big)^2 + \frac{\cosh^2\theta}{1 + a^2/l^2}(d\tilde{\phi} + \Omega d\tilde{x}^4)^2 - \frac{d\theta^2}{1 - \frac{a^2}{l^2}\sinh^2\theta}.$$

On the other hand, we can form the double Killing bubble from (5.15). We take $x^4 \to ix^4$ and $\phi \to i\phi$ and then the metric becomes

$$\begin{aligned} ds^2 \;\; &= \;\; \rho^2\big(\frac{dr^2}{\Delta} + \frac{d\theta^2}{1 - \frac{a^2}{l^2}\cos^2\theta}\big) + \frac{\Delta}{\rho^2}\big(dx^4 - \frac{a\sin^2\theta}{1 - a^2/l^2}d\phi\big)^2 \\ &\quad - \frac{\sin^2\theta(1 - (a^2/l^2)\cos^2\theta)}{\rho^2}\big(adx^4 - \frac{r^2 + a^2}{1 - a^2/l^2}d\phi\big)^2, \end{aligned} \tag{5.19}$$

where $\Delta = (r^2 + a^2)(1 + r^2/l^2) - 2Mr$, $\rho^2 = r^2 + a^2\cos^2\theta$.

We must twist like before: $\tilde{\phi} = \phi - \Omega x^4$, $\tilde{x}^4 = x^4$, $\Omega = a(1 - a^2/l^2)/(r_2^2 + a^2)$, $\tilde{x}^4 \simeq \tilde{x}^4 + \beta$ for some β, $\tilde{\phi}$ noncompact. So replace $d\phi \to d\tilde{\phi} + \Omega d\tilde{x}^4$ and $dx^4 \to d\tilde{x}^4$ in (5.19).

Take the case $l^2 > a^2$. Then $0 \le \theta \le \pi$ is fine, and we can continue $\theta \to i\theta$:

$$\begin{aligned} ds^2 &= \rho^2\big(\frac{dr^2}{\Delta} - \frac{d\theta^2}{1-\frac{a^2}{l^2}\cosh^2\theta}\big) + \frac{\Delta}{\rho^2}\big(d\tilde{x}^4 + \frac{a\sinh^2\theta}{1-a^2/l^2}(d\tilde{\phi} + \Omega d\tilde{x}^4)\big)^2 \\ &+ \frac{\sinh^2\theta(1-(a^2/l^2)\cosh^2\theta)}{\rho^2}\big(ad\tilde{x}^4 - \frac{r^2-a^2}{1-a^2/l^2}(d\tilde{\phi} + \Omega d\tilde{x}^4)\big)^2, \end{aligned} \quad (5.20)$$

where $\Delta = (r^2+a^2)(1+r^2/l^2) - 2Mr$, $\rho^2 = r^2 + a^2\cosh^2\theta$. With $\cosh^2\theta_0 = l^2/a^2$, $\theta = \theta_0$ is a horizon as before, and beyond it we have stationary regions of $\theta > \theta_0$. The skeleton diagram is shown in Fig. 5.7(a). It is canonical to identify every other $0 \le \theta \le \pi$ horizontal segment. If on the other hand $a^2 > l^2$, then with $\cos^2\theta = l^2/a^2$, we imagine expanding out from $\theta = \pi/2$, we have θ_0 occurring before $\theta = 0, \pi$ and the skeleton diagram is shown in Fig. 5.7(b). These solutions are nonsingular.

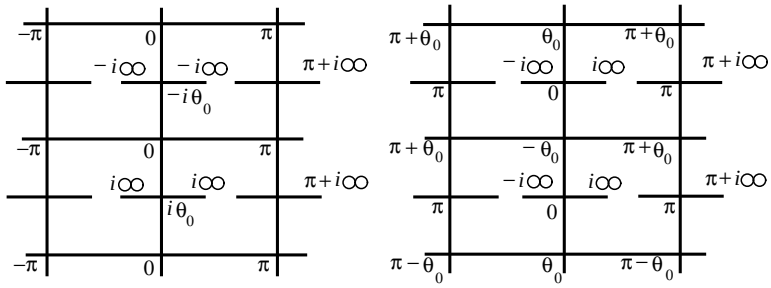

Figure 5.7: Skeleton diagram for the θ coordinate of the Kerr-AdS$_4$ double Killing bubble. Horizontal segments are where θ is spacelike and vertical where θ is timelike. (a) The figure on the left is the case where $l^2 > a^2$. (b) The figure on the right is the case where $l^2 < a^2$.

For $D \ge 5$, we must add $r^2\cos^2\theta d\Omega_{D-4}^2$ to the metric as in (5.15) [81] and also set $\Delta = (r^2+a^2)(1+r^2/l^2) - 2M/r^{D-5}$. The motivation is

$$d\Omega_{D-2}^2 = d\theta^2 + \sin^2\theta d\phi^2 + \cos^2\theta d\Omega_{D-4}^2,$$

where $0 \le \theta \le \pi/2$. To get the $\pi/2$-bubble, send $\theta \to \pi/2 + i\theta$, $x^D \to ix^D$, $a \to ia$, and $d\Omega_{D-4}^2 \to -d\mathbf{H}_{D-4}^2$. Our motivating element becomes

$$d\mathrm{dS}_{D-2}^2 = -d\theta^2 + \cosh^2\theta d\phi^2 + \sinh^2\theta d\mathbf{H}_{D-4}^2.$$

Alternatively, we could have done $d\Omega_{D-4}^2 \to d\mathrm{dS}_{D-4}^2$, $x^D \to ix^D$, $a \to ia$, where our motivating element becomes

$$d\mathrm{dS}_{D-2}^2 = d\theta^2 + \sin^2\theta d\phi^2 + \cos^2\theta d\mathrm{dS}_{D-4}^2. \quad (5.21)$$

These two representations of dS_{D-2} are connected together where either hyperbolic space or dS_{D-4} degenerates to the null cone. A skeleton diagram is drawn in Fig. 5.8. This spacetime, however, is problematic — we have a compactification at $\theta = 0$ of (5.21) and another compactification condition at $r = r_2$. Generically, both Killing directions are compact, and the horizon at $\theta = \pi/2 \pm i\theta_0$ is thus an orbifold.

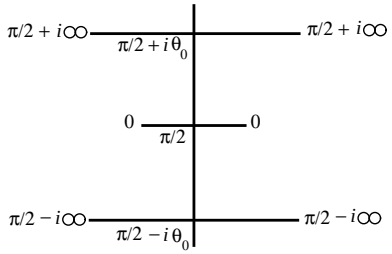

Figure 5.8: A skeleton diagram for the θ coordinate of the Kerr-AdS_D $\pi/2$-bubble for $D \geq 5$, one turned on. At $\theta = 0$, a Killing direction closes the spacetime. (For $D \geq 6$, there is only one dS_{D-4} leg and we have a $\vdash$ junction instead of + junction at $\theta = \pi/2$.) At $\theta = \pi/2$, dS_{D-4} becomes null and becomes $\mathbf{H}_{D-4}$. At $\theta = \pi/2 \pm i\theta_0$, there is a spinning horizon orbifold — this solution is singular.

The double-Killing bubble, gotten from $x^D \to ix^D$, $\phi \to i\phi$, is nonsingular. There are two cases, $l^2 > a^2$ and $a^2 > l^2$. The skeleton diagrams are different from the $D = 4$ case and are shown in Figs. 5.9(a,b).

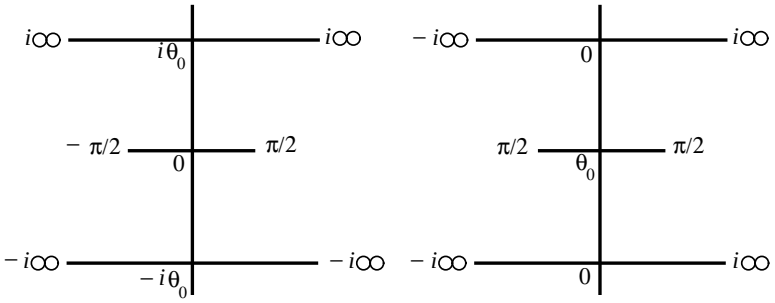

Figure 5.9: Skeleton diagrams for the θ coordinate of the Kerr-AdS_D double-Killing bubble for $D \geq 5$, one turned on. At $\theta = \pm\pi/2$, the S^{D-4} closes the spacetime. The four-leg junctions are all spinning horizons. (a) The diagram on the left is for $l^2 > a^2$. (b) The diagram on the right is for $l^2 < a^2$.

5.5.2 S-branes and anti-bubbles

The $\pi/2$-S-Kerr-AdS with one on can be motivated from the continuation and sign flip

$$\begin{aligned} d\Omega_{D-2}^2 &= d\theta^2 + \sin^2\theta d\phi^2 + \cos^2\theta d\Omega_{D-4}^2 \\ \to d\mathbf{H}_{D-2}^2 &= d\theta^2 + \cosh^2\theta d\phi^2 + \sinh^2\theta d\Omega_{D-4}^2. \end{aligned}$$

The full continuation of Kerr-AdS is $\theta \to \pi/2 + i\theta$, $g_{\mu\nu} \to -g_{\mu\nu}$, $\phi \to i\phi$, $a \to ia$. The result has $\Lambda > 0$ and is

$$\begin{aligned} ds^2 &= \rho^2\big(-\frac{dr^2}{\Delta} + \frac{d\theta^2}{1-(a^2/l^2)\sinh^2\theta}\big) + \frac{\Delta}{\rho^2}\big(dx^D + \frac{a\cosh^2\theta}{1+a^2/l^2}d\phi\big)^2 \\ &+ \frac{\cosh^2\theta}{\rho^2}(1-(a^2/l^2)\sinh^2\theta)\big(adx^D - \frac{r^2-a^2}{1+a^2/l^2}d\phi\big)^2 + r^2\sinh^2\theta d\Omega_{D-4}^2, \end{aligned} \tag{5.22}$$

where $\rho^2 = r^2 + a^2\sinh^2\theta$ and $\Delta = (r^2-a^2)(1+r^2/l^2) - 2M/r^{D-5}$. This has $W = 0$ at $\theta = \pm\theta_0$ where $\sinh\theta_0 = l/|a|$; θ is spacelike and for $r > r_2$, the Killing directions are $++$, so this closes the spacetime. The conditions at $\pm\theta_0$ are identical hence compatible and one Killing direction is noncompact to give a horizon at $r = r_2$. This solution is nonsingular.

The $\pi/2$-S-Kerr-dS solution has no $W = 0$ and has already been discussed, but we use $\pi/2$-S-Kerr-dS to construct anti-bubbles. The $\pi/2$-S-Kerr-dS$_D$ solution with one on is

$$\begin{aligned} ds^2 &= \rho^2\big(-\frac{dr^2}{\Delta} + \frac{d\theta^2}{1+(a^2/l^2)\sinh^2\theta}\big) + \frac{\Delta}{\rho^2}\big(dx^D + \frac{a\cosh^2\theta}{1-a^2/l^2}d\phi\big)^2 \\ &+ \frac{\cosh^2\theta}{\rho^2}(1+(a^2/l^2)\sinh^2\theta)\big(adx^D - \frac{r^2-a^2}{1-a^2/l^2}d\phi\big)^2 + r^2\sinh^2\theta d\Omega_{D-4}^2, \end{aligned} \tag{5.23}$$

where $\rho^2 = r^2 + a^2\sinh^2\theta$ and $\Delta = (r^2-a^2)(1-r^2/l^2) - 2M/r^{D-5}$.

One anti-bubble is gotten from $x^D \to ix^D$, $\phi \to i\phi$, with motivating element

$$d\mathrm{AdS}_{D-2}^2 = d\theta^2 - \cosh^2\theta d\phi^2 + \sinh^2\theta d\Omega_{D-4}^2.$$

This solution does not have $W = 0$ so it was already covered in the last section.

For $D \geq 5$, another anti-bubble is gotten from $x^D \to ix^D$, $a \to ia$, $d\Omega_{D-4}^2 \to d\mathrm{dS}_{D-4}^2$. Since $W \propto 1-(a^2/l^2)\sinh^2\theta$, the space closes at $\theta = \pm\theta_0$. But the space also closes at $r = r_2$ and these two conditions are not compatible, orbifolding the horizon that occurs at $\theta = \pm i\pi/2$.

We now investigate the usual S-Kerr-AdS and Kerr-dS anti-bubbles instead of the $\pi/2$-versions and find that generically they are all problematic, though there may be lower-dimensional parametric families or special cases that work.

The usual S-brane is gotten from the black hole by $g_{\mu\nu} \to -g_{\mu\nu}$, $\theta \to i\theta$, $d\Omega_{D-4}^2 \to -d\mathbf{H}_{D-4}^2$. S-Kerr-AdS$_D$ with one on is

$$\begin{aligned} ds^2 &= \rho^2\big(-\frac{dr^2}{\Delta}+\frac{d\theta^2}{1-(a^2/l^2)\cosh^2\theta}\big)+\frac{\Delta}{\rho^2}\big(dx^4+\frac{a\sinh^2\theta}{1-a^2/l^2}d\phi\big)^2 \\ &+ \frac{\sinh^2\theta(1-(a^2/l^2)\cosh^2\theta)}{\rho^2}\big(adx^4-\frac{r^2+a^2}{1-a^2/l^2}d\phi\big)^2+r^2\cosh^2\theta d\mathbf{H}_{D-4}^2, \end{aligned} \tag{5.24}$$

where $\rho^2 = r^2 + a^2\cosh^2\theta$ and $\Delta = (r^2+a^2)(1+r^2/l^2) - 2M/r^{D-5}$. Here $W = 0$ occurs, and this solution is problematic. Assuming $l^2 > a^2$ to get the right signature, the $\theta = 0$ and $\theta = \theta_0$ conditions are incompatible, forcing x^D to be compact and the $r = r_2$ horizon to be an orbifold.

S-Kerr-dS$_D$ is

$$\begin{aligned} ds^2 &= \rho^2\big(-\frac{dr^2}{\Delta}+\frac{d\theta^2}{1+(a^2/l^2)\cosh^2\theta}\big)+\frac{\Delta}{\rho^2}\big(dx^4+\frac{a\sinh^2\theta}{1+a^2/l^2}d\phi\big)^2 \\ &+ \frac{\sinh^2\theta(1+(a^2/l^2)\cosh^2\theta)}{\rho^2}\big(adx^4-\frac{r^2+a^2}{1+a^2/l^2}d\phi\big)^2+r^2\cosh^2\theta d\mathbf{H}_{D-4}^2, \end{aligned} \tag{5.25}$$

where $\rho^2 = r^2 + a^2\cosh^2\theta$ and $\Delta = (r^2+a^2)(1-r^2/l^2) - 2M/r^{D-5}$.

The double Killing anti-bubble is gotten from (5.25) by $x^D \to ix^D$, $\phi \to i\phi$. The solution as written is then good down to $\theta = 0$ where we have a spinning Rindler horizon; then move up to $\theta = \pm i\pi/2$ where $\mathbf{H}_{D-4}$ becomes dS$_{D-4}$ and then to $\theta = \pm i\pi/2 \pm \theta_0$ with $\sinh\theta_0 = l/|a|$, where the space closes. The space closing here is generally incompatible with the $r = r_2$ condition, making the $\theta = 0$ horizon into an orbifold. The exception is $D = 4$ where there is no $\mathbf{H}_{D-4}$; this has no $W = 0$ and has already been discussed.

On the other hand, for $D \geq 5$, making an anti-bubble from $x^D \to ix^D$, $a \to ia$, $d\mathbf{H}_{D-4}^2 \to d\text{AdS}_{D-4}^2$ gives $W \propto 1 - (a^2/l^2)\cosh^2\theta$. Assuming $l^2 > a^2$, the spacetime closes at $\theta = 0$ as well as $\theta = \theta_0$ and in general this is not compatible with the $r = r_2$ condition. Also there may be a 'ring' singularity $\rho^2 = 0$, although it does not propagate to large r.

5.6 Conclusions and Relation to Holography

In this paper we presented a procedure to generate time-dependent (and other black and anti-bubble) backgrounds starting from black holes solutions in (A)dS spacetime. We hope that our unified treatment of S-branes, bubbles and anti-bubbles with an emphasis on which solutions are possible, which are distinct, and what is their global structure including horizons and singularities, is useful to the reader. Some solutions in this paper are already known; several have been reexamined, reinterpreted or renamed (the 'anti-bubble') and several new solutions have been presented.

We have emphasized $D = 4, 5$ $r\theta$-diagrams and θ-skeleton diagrams to keep track of spacetime regions and for pure (A)dS$_D$ for $D = 4, 5$ we present various card diagrams in Appendix A. Our analytic continuation has been simple, involving only Killing directions and cosine directions. For $D = 4, 5$ analytic continuation has been restated in terms of the card diagram technique of the γ-flip.

We find six types of spacetimes with a characteristic expected conformal boundary geometry. Black holes in AdS have $S^{D-2} \times \mathbf{R}_{\text{time}}$, bubbles have $\text{dS}_{D-2} \times S^1$, anti-bubbles have $\text{AdS}_{D-2} \times S^1$ and S-branes with $\Lambda < 0$ have $\mathbf{H}_{D-2} \times \mathbf{R}_{\text{time}}$. Black holes in dS have conformal boundary geometry $S^{D-2} \times \mathbf{R}_{\text{space}}$ and S-branes with $\Lambda > 0$ have $\mathbf{H}_{D-2} \times \mathbf{R}_{\text{space}}$. Solutions from Kerr-(A)dS which have $W = 0$ horizons, if they are good spacetimes, have a more complicated global structure for themselves and for their conformal boundaries.

Since many of the presented solutions are locally asymptotically (A)dS, it would be interesting to study them in the context of gauge/gravity dualities — the holographic results concerning some of the new spacetimes are forthcoming. The main tool that we use is the counterterm method proposed by Balasubramanian and Kraus in [135]. That is, to regularize the boundary stress tensor and the gravity action by supplementing the quasilocal formalism [136] with counterterms depending of the *intrinsic* boundary geometry. This way, the infrared divergencies of quantum gravity in the bulk are equivalent to ultraviolet divergences of dual theory living on the boundary. This method was also generalized to locally asymptotically dS spacetimes [137, 138]. However, unlike the AdS/CFT correspondence, the conjectured dS/CFT correspondence is far from being understood (see, e.g., [139] for a nice review).

Recently, Ross and Titchener [140] used the counterterm method to show that the AdS/CFT may teach us how to choose the right vacuum for the strongly-coupled CFT living on a dS background. A blowing up of 2-point correlators at null separation in the constant curvature orbifold (non-Killing horizon black hole) suggests the Euclidean vacuum for de Sitter space. Also, Balasubramanian et al. [79] investigate the semiclassical decay of a class of orbifolds of AdS space via a bubble of nothing.

Using similar 'holographic' reasoning[12] to investigate some of the solutions presented in this paper, we hope to shed light on different aspects of the gauge/gravity correspondence for time-dependent backgrounds.

5.7 Generalized card diagrams for (A)dS$_4$, (A)dS$_5$

Some of the solutions in this paper were found in analogy with card diagram techniques [51] (see also [8, 15, 54, 25, 16]). Furthermore the asymptotia of these solutions can be understood from the card diagram perspective. It is thus appropriate

[12]Other interesting examples of time-dependent AdS/CFT and dS/CFT correspondences can be found in [39, 86, 141, 142, 143, 85, 144, 145]. It is also worth mentioning that, in a different context [146], some unexpected results were obtained for asymptotically AdS Taub-NUT spacetimes.

to give a small application of card diagrams to (anti-)de Sitter space in dimensions 4 and 5, where they have the requisite 2 and 3 commuting Killing fields. The Weyl technique for Einstein's dynamical equation fails with a nonzero Λ. Nonetheless these spacetimes still have satisfying card diagrams. Here, we will not give a theory of generalized card diagrams, but rather just some examples which we can obtain by formal analogy to the 4d Reissner-Nordström black hole. More conventional Penrose diagrams for (A)dS may be found in [147, 148].

The massless RN black hole of imaginary charge (to make it subextremal) has line element $\propto \frac{dr^2}{r^2-Q^2} + d\theta^2$. Once the non-Killing directions are of this form, we can immediately go to spherical prolate coordinates via $r = Q\cosh\zeta$; then $ds^2 \propto d\zeta^2 + d\theta^2$; and then to card diagram coordinates via $\rho = Q\sinh\zeta\sin\theta$, $z = Q\cosh\zeta\cos\theta$.

De Sitter 4-space has $\frac{dr^2}{1-r^2/l^2} + d\theta^2$. Set $u = 1/r$. Then we get $\propto \frac{du^2}{u^2-l^2} + d\theta^2$ and can proceed as above. The result is an elliptic card diagram with a rod horizon $-1/l < z < 1/l$, and the vertical square card above it is bisected halfway up at $u = 0$ (see Fig. 5.10(a)). Please note that for simplicity we have only drawn two cards at each 4-card horizon; see [51].

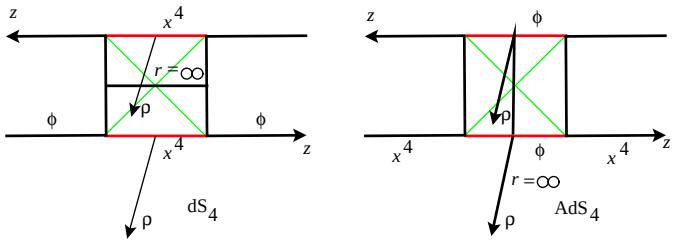

Figure 5.10: (a) On the left, we have dS_4 fibered by S^2. Turning the vertical square card on its side, we get (b) the diagram on the right; it is AdS_4 fibered by patched AdS_2. This is the same fibering as the $RNdS_4$ anti-bubble.

Turning the vertical card on its side via the γ-flip, we achieve AdS_4 in a coordinate system similar to the $RNdS_4$ anti-bubble solution (see Fig. 5.10(b)). An infinite stack of cards give periodic time. The $RNdS_4$ anti-bubble asymptotes to all the $r = \infty$ asymptotia drawn here. Fig. 5.10(b) can be double Killing continued to give a card diagram suitable for understanding S-$RNdS_4$; this will be skipped for brevity.

To get AdS_4 fibered with spheres, we start with $\frac{dr^2}{1+r^2/l^2} + d\theta^2$. Let $u = 1/r$ as for de Sitter, and we get $\propto \frac{du^2}{u^2+l^2} + d\theta^2$. Now, the solution is superextremal and on a branched horizontal card. To go to spherical prolate coordinates, let $u = l\sinh\zeta$. The resulting card diagram is shown in Fig. 5.11. This card diagram can be double Killing continued to give AdS_4 fibered by dS_2, like the $RNAdS_4$ bubble; this will be skipped for brevity.

We give one more example of an interesting 4d de Sitter card diagram: the purely time-dependent one where dS_4 is fibered by azimuthal dS_2 and $\mathbf{H}_2$; see Fig. 5.12. Each

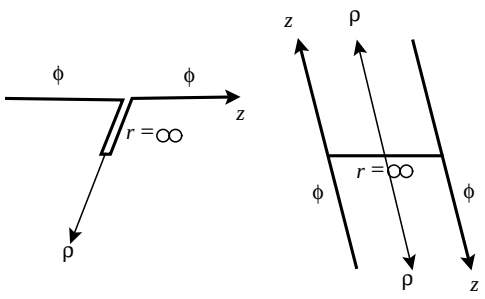

Figure 5.11: AdS_4 fibered by S^2. Shown as a doubly covered half-plane and then in a conformally fixed picture.

45-45-90 triangle with a vertical hypotenuse is a compactified representation of a half-plane vertical card without special null lines. The cards are compactified in precisely the same way as for a Penrose diagram. The S-RNAdS_4 solution asymptotes down through the $\mathbf{H}_2$-fibered region to the two $r = \infty$ regions drawn, with the exception of the 'point' on the right side (actually a ϕ-circle) where the x^4-circle would vanish.

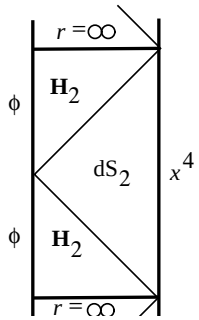

Figure 5.12: dS_4 fibered by azimuthal $\mathbf{H}_2$, dS_2. These vertical cards have been compactified.

Lastly we look at 5d case and find a card diagram which has both 5d de Sitter and anti-de Sitter in the same diagram. Take dS_5 fibered by S^3 with $d\Omega_3^2 = d\theta^2 + \cos^2\theta d\phi^2 + \sin^2\theta d\psi^2$; it has $\frac{dr^2}{1-r^2/l^2} + r^2 d\theta^2$ just like the 4d case. We will get an elliptic card diagram. We want the rightward z-ray boundary to be $\theta = 0$ and now we want the leftward z-ray boundary to be $\theta = \pi/2$, not π. So in analogy with 4d RN, we need the metric to look like $\frac{dv^2}{v^2 - v_0^2} + 4d\theta^2$.

To this end, let $u = 1/r^2$ and then $u = v + 1/2l^2$. The metric is $\propto \frac{dv^2}{v^2 - 1/4l^4} + 4d\theta^2$ and we let $v = (1/2l^2)\cosh\zeta$. The card diagram is then as follows: take the card diagram structure of the Schwarzschild black hole [51]; call the positive-mass

external universe the 'primary' horizontal card and the negative-mass universe the 'secondary' horizontal card. Alternatively, take Fig. 5.10 and label the alternating levels of horizontal cards primary and secondary. Two primary horizontal cards and two vertical cards which connect at an $r = l$ horizon form a dS_5 of signature $++++-$. Each secondary horizontal card forms an AdS_5 of opposite signature $+----$. The horizontal edges of the vertical cards which are not horizons give $r = \infty$ regions for the dS_5 and AdS_5 universes that 'meet' there. Note that both $++++-$ dS_5 and $----+$ AdS_5 satisfy the Einstein-Λ equation with the same $\Lambda > 0$, and hence can appear on the same card diagram.

These diagrams also apply to orbifolds of pure (A)dS space, such as the constant-curvature black hole of [78], which has a non-Killing horizon, and bears certain resemblance to a BHAdS bubble.

Chapter 6

Semiclassical decay of the twisted AdS_5 orbifold

Semiclassical decay of spacetime orbifolds via bubble production has been known since [36]. The analog of Witten's decay of the KK vacuum, in the $\Lambda < 0$ case, is the decay of the constant-curvature black hole (or AdS_5 orbifold), and was described in [79]. This is the analog of the BTZ black hole [78]; the horizon is non-Killing; the bubble formation seals off the non-Killing horizon from the majority of the spacetime (the stationary patch of spacetime which survives the bubble formation).

Here, we extend this to the spinning black hole, or Kerr case. The black hole orbifold generalizes the twisted flat case of [61]. We generalize the Laplace transform argument of Hawking and Page [149] for the connection of instanton negative modes and negative specific heat (at constant extensive J, i.e. 'volume'). Furthermore, the card diagram for AdS_5 compatible with the given orbifold, as covered by spheroidal coordinates, shows us the nature of the singularities in the skeleton diagrams for the Kerr-AdS_5 bubble. We find that if $a \neq 0$, then the non-Killing horizon *is not shielded from the majority of the spacetime.*

The AdS case is especially interesting because the Lorentzian semiclassical evolution, valid at small curvatures, should be dual via AdS/CFT to a decay in the boundary, nongravitational theory.

This work grew from the idea of J. Simón and was in collaboration with V. Balasubramanian, D. Astefanesei, and K. Larjo, and may be forthcoming from those authors.

6.1 The Kerr-AdS$_5$ black hole, instanton, and bubble

The Kerr-AdS$_5$ black hole, with $\lambda = 1/l^2 > 0$, taken from [82] is

$$\begin{aligned} ds^2 &= -W(1+\lambda r^2)dt^2 + \frac{U dr^2}{V-2M} + \frac{2M}{U}(dt - \frac{a\mu^2 d\phi_0}{1-\lambda a^2} - \frac{b\nu^2 d\psi_0}{1-\lambda b^2})^2 \\ &+\frac{r^2+a^2}{1-\lambda a^2}(d\mu^2 + \mu^2(d\phi_0 + \lambda a dt)^2) + \frac{r^2+b^2}{1-\lambda b^2}(d\nu^2 + \nu^2(d\psi_0 + \lambda b dt)^2) \\ &-\frac{\lambda}{W(1+\lambda r^2)}(\frac{r^2+a^2}{1-\lambda a^2}\mu d\mu + \frac{r^2+b^2}{1-\lambda b^2}\nu d\nu)^2. \end{aligned}$$

Note: we have changed the sign convention of λ from [82, 41]. Here, $V = \frac{1}{r^2}(1+\lambda r^2)(r^2+a^2)(r^2+b^2)$, $W = \frac{\mu^2}{1-\lambda a^2} + \frac{\nu^2}{1-\lambda b^2}$, $\mu^2+\nu^2 = 1$, $U = r^2 + \mu^2 b^2 + \nu^2 a^2$. The function $r^2(V-2M)$ gives us the horizons, $U=0$ gives us the curvature singularity. (In 5d this singularity is not a 'ring' and cannot be traversed.) The locus $W=0$ will give us new θ-horizons in bubble, anti-bubble, and S-brane solutions (see Chapter 5 and [39, 41]).

Letting $\mu = \sin\vartheta$, this simplifies to

$$\begin{aligned} ds^2 &= -\frac{\Theta(\vartheta)(1+\lambda r^2)}{(1-\lambda a^2)(1-\lambda b^2)}dt^2 + \frac{U dr^2}{V-2M} + \frac{2M}{U}(dt - \frac{a\mu^2 d\phi_0}{1-\lambda a^2} - \frac{b\nu^2 d\psi_0}{1-\lambda b^2})^2 \\ &+\frac{r^2+a^2}{1-\lambda a^2}\mu^2(d\phi_0 + \lambda a dt)^2 + \frac{r^2+b^2}{1-\lambda b^2}\nu^2(d\psi_0 + \lambda b dt)^2 + \frac{U d\theta^2}{\Theta(\vartheta)}. \end{aligned}$$

Here, $U = r^2 + a^2\cos^2\vartheta + b^2\sin^2\vartheta$ and $\Theta(\vartheta) = 1 - \lambda a^2\cos^2\vartheta - \lambda b^2\sin^2\vartheta$. The ϑ-horizons would occur at $\Theta(\vartheta) = 0$. For the Kerr-AdS$_5$ black hole, ϑ-horizons are not present if we keep $\lambda a^2, \lambda b^2 < 1$.

If one takes the $r\to\infty$ limit, the conformal boundary geometry is rotating in these coordinates. We thus make the coordinate transformation to $\phi_0 = \phi - \lambda a t$, $\psi_0 = \psi - \lambda b t$ and get

$$\begin{aligned} ds^2 &= -\frac{\Theta(\vartheta)(1+\lambda r^2)}{(1-\lambda a^2)(1-\lambda b^2)}dt^2 + \frac{U dr^2}{V-2M} \\ &+\frac{2M}{U}(\frac{\Theta(\vartheta)dt}{(1-\lambda a^2)(1-\lambda b^2)} - \frac{a\sin^2\vartheta d\phi}{1-\lambda a^2} - \frac{b\cos^2\vartheta d\psi_0}{1-\lambda b^2})^2 \\ &+\frac{r^2+a^2}{1-\lambda a^2}\sin^2\vartheta d\phi^2 + \frac{r^2+b^2}{1-\lambda b^2}\cos^2\vartheta d\psi^2 + \frac{U d\vartheta^2}{\Theta(\vartheta)}. \end{aligned} \tag{6.1}$$

The $r\to\infty$ CBG is

$$ds^2 \propto -\frac{\Theta(\vartheta)dt^2}{(1-\lambda a^2)(1-\lambda b^2)} + \frac{r^2}{1-\lambda a^2}\sin^2\vartheta d\phi^2 + \frac{r^2}{1-\lambda b^2}\cos^2\vartheta d\psi^2 + \frac{d\vartheta^2}{\Theta(\vartheta)},$$

which is clearly not rotating. (The description in [81] is erroneous.) It is quite clear that for the CBG, $\Theta(\vartheta) = 0$ is a Killing horizon. This is also clear from (6.1) that at $\Theta = 0$, the Killing 3×3 submetric has rank 2, with $(\partial/\partial t)_{\phi,\psi}$ null; the horizon has no angular velocity in these coordinates. (The angular velocity of a regular spinning horizon in any case must be constant [88].) The surface gravity (or Euclidean periodicity) of a horizon must also be constant; to see that the r-dependence of (6.1) does not spoil this, note that $U|_{\Theta=0} = \lambda^{-1} + r^2$, so that the relevant submetric is

$$ds^2 \sim (\lambda^{-1} + r^2)\Big(- \frac{\Theta(\vartheta)\lambda dt^2}{(1-\lambda a^2)(1-\lambda b^2)} + \frac{d\vartheta^2}{\Theta(\vartheta)}\Big). \tag{6.2}$$

The expanding bubble must be gotten from double Killing continuation; choosing ψ to become time, the complete continuation is $t \to i\chi$, $\psi \to i\psi$, $a \to ia$. The metric is then

$$\begin{aligned} ds^2 \;=\; & \frac{\Theta(\vartheta)(1+\lambda r^2)d\chi^2}{(1+\lambda a^2)(1-\lambda b^2)} + \frac{U dr^2}{V-2M} - \frac{2M}{U}\Big(\frac{\Theta(\vartheta)d\chi}{(1+\lambda a^2)(1-\lambda b^2)} \\ & -\frac{a\sin^2\vartheta}{1+\lambda a^2}d\phi - \frac{b\cos^2\vartheta}{1-\lambda b^2}d\psi\Big)^2 \\ & +\frac{r^2-a^2}{1+\lambda a^2}\sin^2\vartheta d\phi^2 - \frac{r^2+b^2}{1-\lambda b^2}\cos^2\vartheta d\psi^2 + \frac{U d\vartheta^2}{\Theta(\vartheta)}. \end{aligned} \tag{6.3}$$

Now, $\Theta(\vartheta) = 1 + \lambda a^2\cos^2\vartheta - \lambda b^2\sin^2\vartheta$, $U = r^2 - a^2\cos^2\vartheta + b^2\sin^2\vartheta$, and $V = \frac{1}{r^2}(1+\lambda r^2)(r^2-a^2)(r^2+b^2)$.

The horizon function is $r^2(V-2M) = (1+\lambda r^2)(r^2-a^2)(r^2+b^2) - 2Mr^2$, which we treat as a function of r^2. As $r^2 \to \infty$, it is $\sim \lambda r^6 > 0$, whereas at $r^2 = 0$, it equals $-a^2b^2 < 0$. Thus there must be a root at $r^2 > 0$. In general we can have one, two, or three roots (possibly degenerate) at $r^2 > 0$. Call the largest root $r^2 = r_H^2$, which may be degenerate. (The instanton on the other hand, has $b \to ib$ relative to the bubble, hence has zero, one, or two roots at $r^2 > 0$.)

We want to avoid the $U = 0$ curvature singularity. The function U is smallest at $\vartheta = 0$, where $U|_{\vartheta=0} = r^2 - a^2$. Thus we need $r_H^2 > a^2$. Indeed, the horizon function at $r^2 = a^2$ is $-2Ma^2 < 0$. Below, we will go beyond the acceleration horizon via $\vartheta \to \pi/2 \pm i\mathcal{T}$, and then $U = r^2 + a^2\sinh^2\mathcal{T} + b^2\cosh^2\mathcal{T} > 0$. So the bubble spacetime misses the curvature singularity. We have already shown that the $\Theta(\vartheta) = 0$ horizons are nonsingular for $(\partial/\partial\chi)_{\phi,\psi}$ noncompact (they will be horizon orbifolds for $(\partial/\partial\chi)$ compact; this happens when $b = 0$), so apart from CTCs and CNCs, the bubble spacetime is nonsingular.

From [82], the r^2-horizon velocities for the black hole/bubble are

$$\Omega^\phi_{\rm BH} = \frac{a(1-\lambda a^2)}{r_H^2 + a^2} \to i\Omega^\phi = \frac{ia(1+\lambda a^2)}{r_H^2 - a^2}, \qquad \Omega^\psi = \frac{b(1-\lambda b^2)}{r_H^2 + b^2}.$$

Thus, to close the spacetime at $r^2 = r_H^2$, we twist to (BH→bubble)

$$\begin{aligned} \tilde{\chi} = \chi &\rightarrow \tilde{\chi} = \chi \\ \tilde{\phi} = \phi - \Omega^{\phi}_{\rm BH} t &\rightarrow \tilde{\phi} = \phi + \Omega^{\phi}\chi \\ \tilde{\psi} = \psi - \Omega^{\psi} t &\rightarrow \tilde{\psi} = \psi - \Omega^{\psi}\chi \end{aligned}$$

Then we compactify $\tilde{\chi} \simeq \tilde{\chi} + \beta$ (i.e. at constant $\tilde{\phi}$, $\tilde{\psi}$) where $\kappa = 2\pi/\beta$, and the bubble has (continued from [82])

$$\kappa = r_H(1+\lambda r_H^2)\big(\frac{1}{r_H^2 - a^2} + \frac{1}{r_H^2 + b^2}\big) - \frac{1}{r_H}. \tag{6.4}$$

We replace $d\chi \to d\tilde{\chi}$, $d\phi \to d\tilde{\phi} - \Omega^{\phi} d\tilde{\chi}$, $d\psi \to d\tilde{\psi} + \Omega^{\psi} d\tilde{\chi}$ in the metric (6.3). It seems that the stationary patches have no CTCs if we assume $\lambda b^2 < 1$ and $(\Omega^{\psi})^2 \leq \lambda$.

The region $0 \leq \vartheta \leq \pi/2$ constitutes a stationary patch. $\pi/2 \leq \vartheta \leq \pi$ is another such patch; at the juncture at $\vartheta = \pi/2$ we have a Rindler horizon where $\partial/\partial\psi = \partial/\partial\tilde{\psi}$ goes null. Here, we put $\theta \to \pi/2 \pm i\mathcal{T}$ to go to time-dependent patches. We discuss the $\Theta = 0$ horizons shortly.

As $r \to \infty$ for the bubble, the CBG is similarly patched; for $0 \leq \vartheta \leq \pi/2$ or $\pi/2 \leq \vartheta \leq \pi$, we have

$$ds^2 \propto \frac{\Theta d\tilde{\chi}^2}{(1+\lambda a^2)(1-\lambda b^2)} + \frac{\sin^2\vartheta}{1+\lambda a^2}(d\tilde{\phi} - \Omega^{\phi} d\tilde{\chi})^2 - \frac{\cos^2\vartheta}{1-\lambda b^2}(d\tilde{\psi} + \Omega^{\psi} d\tilde{\chi})^2 + \frac{d\vartheta^2}{\Theta}, \tag{6.5}$$

while sending $\vartheta \to \pi/2 \pm i\mathcal{T}$ gives

$$ds^2 \propto \frac{\Theta d\tilde{\chi}^2}{(1+\lambda a^2)(1-\lambda b^2)} + \frac{\cosh^2\mathcal{T}}{1+\lambda a^2}(d\tilde{\phi} - \Omega^{\phi} d\tilde{\chi})^2 + \frac{\sinh^2\mathcal{T}}{1-\lambda b^2}(d\tilde{\psi} + \Omega^{\psi} d\tilde{\chi})^2 - \frac{d\mathcal{T}^2}{\Theta}, \tag{6.6}$$

where $\Theta = 1 - \lambda a^2 \sinh^2\mathcal{T} - \lambda b^2 \cosh^2\mathcal{T}$.

We now analyze the $\Theta = 0$ horizons. For simplicity, just look at the CBG (6.6). As shown earlier (viz. (6.2)), the entire ϑ-horizon analysis is independent of r and in the bulk it will apply at all $r \geq r_H$.

First, assume $\lambda b^2 < 1$, so that the $\vartheta = \pi/2$ patch-change horizon occurs before the $\Theta = 0$ horizon, i.e. $\Theta = 0$ at some real $\mathcal{T} = \pm\mathcal{T}_0$. At $\mathcal{T} = \pm\mathcal{T}_0$, the vector

$$\frac{\partial}{\partial\tilde{\chi}} + \Omega^{\phi}\frac{\partial}{\partial\tilde{\phi}} - \Omega^{\psi}\frac{\partial}{\partial\tilde{\psi}}$$

is null. For $b \neq 0$, since the $\tilde{\psi}$-direction is noncompact, this vector is noncompact and we have a regular horizon. In this case it is a finite $\mathcal{T}$-distance to the CTC boundary (see the skeleton diagram in Fig. 6.1). For $b = 0$, our vector is compact and we have a twisted Milne orbifold (see Fig. 6.2), and the CTCs begin right at the horizon orbifold.

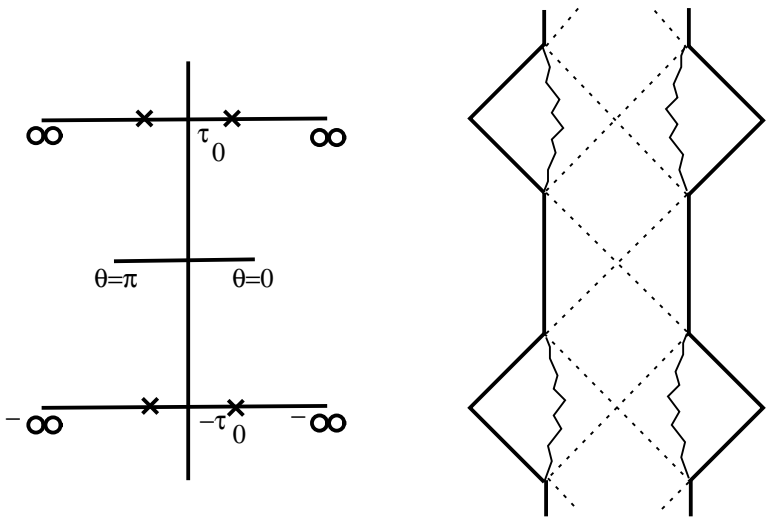

Figure 6.1: The skeleton diagram and Penrose diagram of the CBG for the general a, $b \neq 0$ expanding bubble solution. This runs from $\vartheta = 0, \pi$ to $\vartheta \to \pi/2 + i\mathcal{T}$. The boundary of the CTCs is labelled as a singularity.

The skeleton diagram and Penrose diagram for the CBG are shown in Figs. 6.1, 6.2. The whole spacetime has a structure of the CBG's Penrose diagram times $r \geq r_H$, plus two nondrawn Killing directions. For any fixed r, the $\vartheta = 0$ worldline is complete, just like the right boundary of the dS_3 Penrose diagram.

The CBG is in fact rotating (with one parameter, $\propto b$) for the stationary $0 \leq \vartheta \leq \pi/2$ patch, since we have a mix $(d\tilde{\psi} + \Omega^{\psi} d\tilde{\chi})^2$ in (6.5). The bulk geometry is actually rotating about the axis $r = r_H$ where $\partial/\partial\tilde{\chi}$ vanishes. Unlike the black hole case, the present rotation cannot be removed by a coordinate change $\tilde{\tilde{\psi}} = \tilde{\psi} + \Omega^{\psi}\tilde{\chi}$, because $\tilde{\chi}$ is periodic and we must keep $\tilde{\psi}$ noncompact. The a parameter twists spatial with spatial directions. On the other hand, in the large-$\mathcal{T}$ ($\Theta < 0$) stationary region, we see a 2-parameter rotation in (6.6).

6.1.1 Large b: A different skeleton diagram

As discussed in [41], for large values of b, the zero of Θ can occur before $\vartheta = \pi/2$, resulting in a different skeleton diagram for an $r =$ constant slice (or the $r \to \infty$ CBG) (see Fig. 6.3). This holds for $r \geq r_H$ for the Kerr-AdS_5 bubble, and for sufficiently

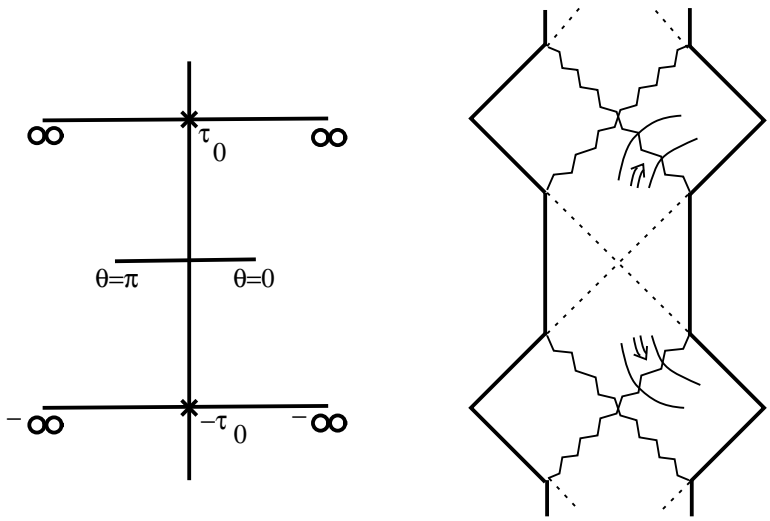

Figure 6.2: The skeleton diagram and Penrose diagram of the CBG for the $b = 0$ expanding bubble solution. The Penrose diagram (which suffers from the same deficiencies as the ordinary 4d Kerr Penrose diagram) tries to represent noncompact Killing orbits at the $\theta = \pi/2$ horizon and compact ones at the $\Theta = 0$ horizon orbifold. The Milne orbifold can connect to just one Rindler orbifold. CTCs begin right at the horizon orbifold.

large r, for the twisted AdS_5 orbifold. For $\lambda b^2 > 1$, we write the metric as

$$\begin{aligned} ds^2 &= -\frac{\Theta(1+\lambda r^2)d\chi^2}{(1+\lambda a^2)(\lambda b^2-1)} + \frac{U dr^2}{V-2M} - \frac{2M}{U}\Big(- \frac{\Theta d\chi}{(1+\lambda a^2)(\lambda b^2-1)} \\ &\quad -\frac{a\sin^2\vartheta}{1+\lambda a^2}d\phi + \frac{b\cos^2\vartheta}{\lambda b^2-1}d\psi\Big)^2 \\ &\quad +\frac{r^2-a^2}{1+\lambda a^2}\sin^2\vartheta d\phi^2 + \frac{r^2+b^2}{\lambda b^2-1}\cos^2\vartheta d\psi^2. \end{aligned} \tag{6.7}$$

We see that $\partial/\partial\chi$ (which is noncompact since $b \neq 0$) gives a horizon at $\vartheta = \vartheta_0$, where $\Theta(\vartheta_0) = 0$. From (6.4), κ is still real, so $\partial/\partial\tilde{\chi}$ still closes the spacetime at $r = r_H$.

At $\vartheta = \pi/2$, we have a Milne horizon where spacelike $\partial/\partial\psi$ goes null. We put $\vartheta \to \pi/2 \pm i\mathcal{T}$, where $\mathcal{T}$ is now spacelike. By considering the smallest square-norm of a closed Killing orbit, continuity, and the fact that there is a unique null Killing direction at the horizon, we can conclude that CTCs must stay a finite $\mathcal{T}$-distance away from this horizon.

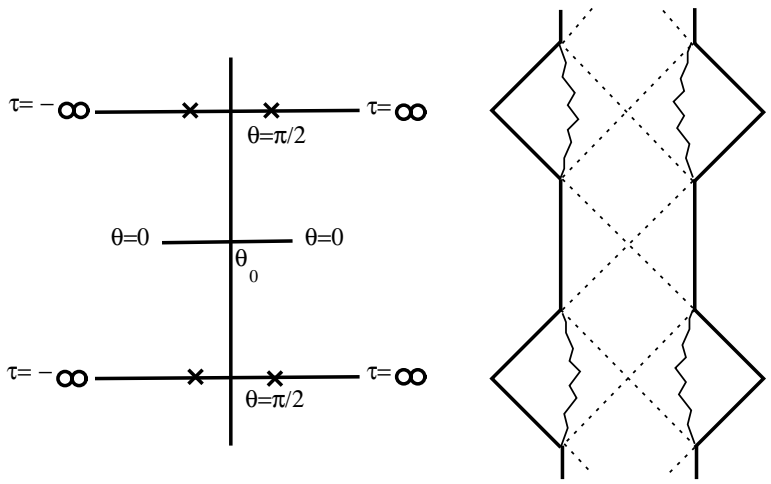

Figure 6.3: For the case $\lambda b^2 > 1$, the skeleton diagram of an $r =$constant slice of the Kerr-AdS$_5$ bubble is different. The $\vartheta = \vartheta_0$ $\partial/\partial\chi$ horizon occurs before the $\vartheta = \pi/2$ $\partial/\partial\psi$ horizon.

6.2 The twisted AdS$_5$ Orbifold

Here we describe the general twisted AdS$_5$ orbifold, which generalizes the constant-curvature black hole of [78]. We first write it in terms of a continuation of a S^3-fibered coordinates (with 'spherically symmetric' radial coordinate R and angle θ), and then in terms of the 'spheroidal' r, ϑ coordinates of [82], which will make contact with the $r \to \infty$ limit of Kerr-AdS$_5$.

AdS$_5$ fibered by S^3 with spherically symmetric radial coordinate R is

$$ds^2 = -(1+R^2)dt^2 + \frac{dR^2}{1+R^2} + R^2(d\theta^2 + \sin^2\theta d\phi^2 + \cos^2\theta d\psi^2),$$

where $0 \le \theta \le \pi/2$, and ϕ and ψ are 2π-periodic. We continue $t \to i\chi$, $\psi \to i\psi$ to achieve another description of AdS$_5$, fibered by dS$_3$:

$$ds^2 = (1+R^2)d\chi^2 + \frac{dR^2}{1+R^2} + R^2(d\theta^2 + \sin^2\theta d\phi^2 - \cos^2\theta d\psi^2).$$

The ordinary orbifold is gotten by compactifying the χ-direction. For the twisted orbifold, we first want to twist to $\tilde{\phi} = \phi - \Omega^\phi\chi$, $\tilde{\psi} = \psi + \Omega^\psi\chi$, $\tilde{\chi} = \chi$, and then compactify $\tilde{\chi} \simeq \tilde{\chi} + \beta$ at constant $\tilde{\phi}$, $\tilde{\psi}$. Equivalently, we compactify along orbits of the Killing vector field $l = \partial_\chi + \Omega^\phi\partial_\phi - \Omega^\psi\partial_\psi$. This has square-norm

$$g_{\mu\nu}l^\mu l^\nu = 1 + R^2 + R^2(\Omega^\phi)^2\sin^2\theta - R^2(\Omega^\psi)^2\cos^2\theta$$

The region $0 \le \theta \le \pi/2$ is stationary (in the language of card diagrams, it is a horizontal card) and could have CTCs. We see that with this twisted compactification,

CTCs are avoided precisely for $(\Omega^\psi)^2 \leq 1$. The angle $\tilde{\phi}$ is still 2π-periodic, and $\tilde{\psi}$ is noncompact stationary time.

We discuss the rest of the global structure of this solution in these coordinates. At $\theta = \pi/2$, the Killing vector $\partial/\partial\psi = \partial/\partial\tilde{\psi}$ goes null. It has noncompact orbits and this is a Rindler horizon. We pass via $\theta \to \pi/2 \pm i\tau$ to the Milne wedges. The metric is then (written for simplicity with untwisted differentials)

$$ds^2 = (1+R^2)d\chi^2 + \frac{dR^2}{1+R^2} + R^2(-d\tau^2 + \cosh^2\tau d\phi^2 + \sinh^2\tau d\psi^2).$$

This time-dependent (vertical card) region has a null boundary at infinity where R, τ go bad: we label it by $R = 0$, $\tau = \infty$. This is the non-Killing horizon for the constant-curvature black hole, described in Kruskal coordinates [79] by the cone $\eta_{\mu\nu}y^\mu y^\nu = 0$. Beyond this, we put $R \to iR'$ and $\tau \to \tau + i\pi/2$, to get

$$ds^2 = (1-R'^2)d\chi^2 - \frac{dR'^2}{1-R'^2} + R'^2(d\tau^2 + \sinh^2\tau d\phi^2 + \cosh^2\tau d\psi^2).$$

At $R' = 1$, there is a Killing horizon: $\partial/\partial\chi$ goes null. Since

$$\frac{\partial}{\partial\chi} = \frac{\partial}{\partial\tilde{\chi}} - \Omega^\phi\frac{\partial}{\partial\tilde{\phi}} + \Omega^\psi\frac{\partial}{\partial\tilde{\psi}},$$

for $\Omega^\psi \neq 0$, this is noncompact and hence a Milne horizon. (For $\Omega^\psi = 0$, this is a Milne orbifold, and we would end the nonsingular spacetime here.)

Into the Rindler wedge for $R' > 1$, we have CTCs from the $\tilde{\chi}$-circle, at a locus

$$R'^2 = \frac{1}{1 - \sinh^2\tau(\Omega^\phi)^2 - \cosh^2\tau(\Omega^\psi)^2}.$$

For $\tau = 0$, this is $R'^2 = 1/(1-(\Omega^\psi)^2)$, and we see now $\Omega^\psi \neq 0$ keeps the CTCs away from the Milne/Rindler $R' = 1$ horizon. The value of R' increases with τ, and at a finite τ the CTC boundary goes to $R' = \infty$.

6.2.1 Card diagram for dS_3-fibered coordinates

AdS_5 fibered by dS_3 has a somewhat complicated card diagram, which we now derive.

We first start with AdS_5 fibered by S^3. Following the technique in [41], the non-Killing metric of

$$\frac{dR^2}{1+R^2} + d\theta^2$$

in can be reduced to spherical prolate form via

$$\frac{1}{R^2} = \frac{\cosh\zeta - 1}{2},$$

giving

$$ds^2 \supset \frac{R^2}{4}(d\zeta^2 + 4d\theta^2).$$

The factor of 4 indicates that in 5d we will run $0 \le \theta \le \pi/2$ over one card, instead of $0 \le \theta \le \pi$. The spherical prolate form then yields a card diagram upon

$$\rho = \frac{1}{2}\sinh\zeta \sin 2\theta, \qquad z = \frac{1}{2}\cosh\zeta\cos 2\theta.$$

The card diagram for AdS_5 fibered by S^3 is thus a spherical prolate (1-rod) half-plane horizontal card. The right ray $\theta = 0$ is the closure of the ϕ-circle, the left ray $\theta = \pi/2$ is the closure of the ψ-circle, and the rod $-1/2 < z < 1/2$ represents $R = \infty$. The point at infinity on the Weyl half-plane represents the worldline $R = 0$.

When we continue $\psi \to i\psi$, $\chi \to i\chi$ to get AdS_5 fibered by dS_3, this half-plane becomes the static patch of dS_3. We call this the 'primary' horizontal card. Continuing $\theta \to \pi/2 \pm i\tau$ gives quarter-plane ('primary') vertical cards each with a special null line from $z = -1/2$. The card coordinates here are

$$\rho' = \frac{1}{2}\sinh\zeta\sinh 2\tau, \qquad z = -\frac{1}{2}\cosh\zeta\cosh 2\tau. \tag{6.8}$$

This card diagram (which is only part of the spacetime) is shown in Fig. 6.4.

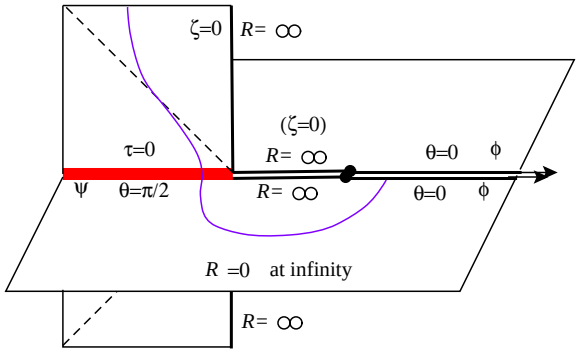

Figure 6.4: The card diagram for AdS_5 fibered by dS_3, showing primary horizontal and vertical cards. This covers real $R > 0$. The locus $\zeta = 0$ is $R = \infty$ and is a rod on each horizontal half-plane and the vertical card boundaries. A typical θ, τ-orbit is drawn.

At $R = 0$, dS_3 degenerates, and we know we must put $R \to iR'$ (or $\zeta \to \zeta + i\pi$), and $2\tau \to 2\tau + i\pi$. We have

$$\frac{1}{R'^2} = \frac{\cosh\zeta + 1}{2}$$

and the card coordinates are still as (6.8). We have a 'secondary' vertical card. However, now ζ is timelike and τ spacelike. We begin to fill out a secondary card diagram which is attached to the primary one along the conformal null infinities of the vertical cards (Fig. 6.5). This attachment takes place at $\zeta = \tau = \infty$ and of course the spacetime is nonsingular. An actual card diagram could be gotten via a $PSL(2, \mathbf{R})$ automorphism of the half-plane moving the point at infinity to a finite point, but we will just treat Fig. 6.5 as schematic.

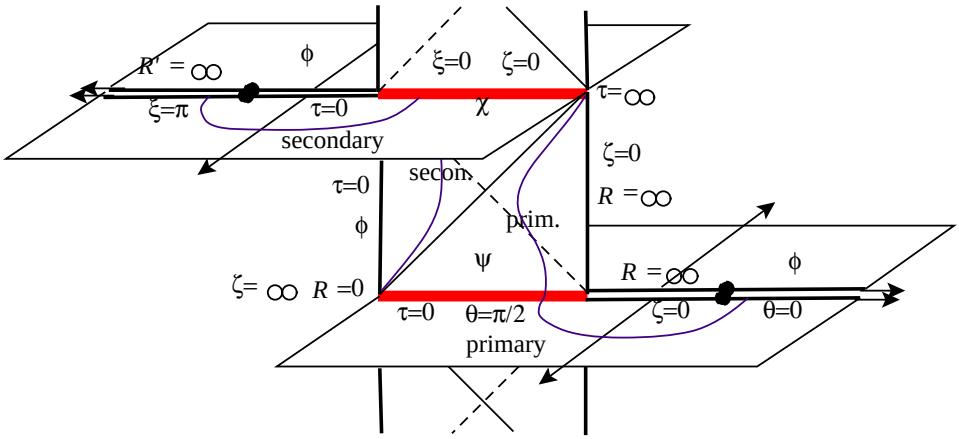

Figure 6.5: A schematic, complete card diagram for AdS_5 covered by dS_3. We refer to horizontal and vertical cards as primary and secondary, as indicated. The primary and secondary vertical cards are joined along their conformal null boundaries, at $\tau = \zeta = \infty$. A typical $R =$constant, θ, τ-orbit is drawn on the primary cards and a $\tau =$constant, R'-orbit on the secondary cards.

At $R' = 1$, we have the χ-horizon, and put $\zeta \to i\xi$. Then

$$\frac{1}{R'^2} = \frac{\cos\xi + 1}{2}$$

and

$$\rho = \frac{1}{2}\sinh\xi\sinh 2\tau, \qquad z = -\frac{1}{2}\cos\xi\cosh 2\tau.$$

We call this the 'secondary' horizontal card. The right ray $\xi = 0$ is the χ-horizon, the rod $-1/2 < z < 1/2$ is $\tau = 0$, the closure of the ϕ-circle, and the left ray $\xi = \pi$ is $R' = \infty$.

There is an infinite stack of card diagrams connected through the conformal null infinities of the vertical cards; this is illustrated in Fig. 6.5. Identifying every other pair of primary horizontal cards gives the canonical time-periodicity of AdS_5.

6.3 AdS_5 in spheroidal coordinates

To make contact with the Kerr-AdS_5 solution and to show they have the same $r \to \infty$ asymptotics, we will write AdS_5 in spheroidal coordinates and then continue to 'de Sitter-oidal' coordinates. We find that in the r coordinate, we know the solutions are asymptotic drawing from our knowledge of the Kerr-Schild form of the metric, whereas for holography, motivated by the AdS_5 twisted orbifold, we will want to dispense with the r coordinate and move to an R coordinate for finding a CBG on which the dual CFT lies.

From [82], and putting $\mu = \sin\vartheta$, $\nu = \cos\vartheta$, AdS_5 in spheroidal coordinates is

$$\begin{aligned} d\mathrm{AdS}_5^2 &= -\frac{\Theta(1+\lambda r^2)dt^2}{(1-\lambda a^2)(1-\lambda b^2)} + \frac{Ur^2dr^2}{(1+\lambda r^2)(r^2+a^2)(r^2+b^2)} + \frac{Ud\vartheta^2}{\Theta} \\ &\quad + \frac{r^2+a^2}{1-\lambda a^2}\sin^2\vartheta d\phi^2 + \frac{r^2+b^2}{1-\lambda b^2}\cos^2\vartheta d\psi^2 \end{aligned}$$

Here, $\Theta(\vartheta) = 1 - \lambda a^2\cos^2\vartheta - \lambda b^2\sin^2\vartheta$, and $U = r^2 + a^2\cos^2\vartheta + b^2\sin^2\vartheta$, and ϑ is a spheroidal angle. The connection to spherically symmetric coordinates (with angle θ, or in the notation of [82] $\hat{\theta}$) is

$$\begin{aligned} (1-\lambda a^2)R^2\sin^2\theta &= (r^2+a^2)\sin^2\vartheta, \\ (1-\lambda b^2)R^2\cos^2\theta &= (r^2+b^2)\cos^2\vartheta. \end{aligned}$$

To mimic Kerr-AdS_5, we continue $t \to i\chi$, $\psi \to i\psi$, and $a \to ia$. Note that since a is a completely redundant parameter for pure AdS_5; its continuation just changes the way we parametrize spheroids. We get

$$\begin{aligned} (1+\lambda a^2)R^2\sin^2\theta &= (r^2-a^2)\sin^2\vartheta, \\ (1-\lambda b^2)R^2\cos^2\theta &= (r^2+b^2)\cos^2\vartheta. \end{aligned} \tag{6.9}$$

Take the case $\lambda b^2 < 1$. The metric is

$$\begin{aligned} d\mathrm{AdS}_5^2 &= \frac{\Theta(1+\lambda r^2)d\chi^2}{(1+\lambda a^2)(1-\lambda b^2)} + \frac{Ur^2dr^2}{(1+\lambda r^2)(r^2-a^2)(r^2+b^2)} + \frac{Ud\vartheta^2}{\Theta} \\ &\quad + \frac{r^2-a^2}{1+\lambda a^2}\sin^2\vartheta d\phi^2 - \frac{r^2+b^2}{1-\lambda b^2}\cos^2\vartheta d\psi^2, \end{aligned}$$

where $\Theta = 1 + \lambda a^2\cos^2\vartheta - \lambda b^2\sin^2\vartheta$, $U = r^2 - a^2\cos^2\vartheta + b^2\sin^2\vartheta$.

Near $r = a$, the metric looks like

$$\frac{Ua^2dr^2}{(r^2-a^2)(1+\lambda a^2)(a^2+b^2)} + \frac{(r^2-a^2)\sin^2\theta d\phi^2}{1+\lambda a^2},$$

and away from $\vartheta = 0$ we have $U \sim (a^2+b^2)\sin^2\vartheta + \epsilon^2$, where $r^2 - a^2 = \epsilon^2$; this gives us the closure of the ϕ-circle, $\phi \simeq \phi + 2\pi$. Of course $\vartheta = 0$ also gives us closure of the ϕ-circle. The loci $\vartheta = 0$ and $r = a$ meet at $U = 0$, which is not a curvature singularity

since $2M = 0$. The r, ϑ coordinates cover the primary Weyl cards as depicted in Fig. 6.6. Note that, including the point at half-plane infinity, these coordinates have four foci and so resemble C-metric coordinates, although they are not precisely C-metric coordinates. In particular we do not have a symmetry between interchange of r and ϑ directions, like we do for spherical prolate or C-metric coordinates. In any event, the requisite Schwarz-Christoffel transformation to the half-plane has been solved implicitly in going to this formulation.

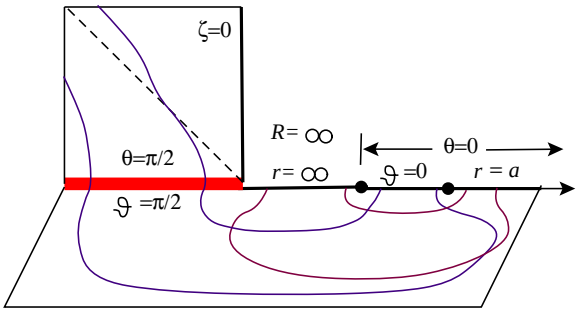

Figure 6.6: The r, ϑ coordinates cover the primary Weyl half-plane as shown. The $\theta = 0$ ray is split into a $\vartheta = 0$ rod and then an $r = a$ ray. They meet at $R = \sqrt{(a^2+b^2)/(1-\lambda b^2)}$. The $\mathcal{T}$-orbits must be asymptotically null on the primary vertical card to pass to the secondary vertical card across their conformal null boundaries.

We can solve (6.9) to get

$$\begin{aligned} R^2 &= \frac{(r^2-a^2)\sin^2\vartheta}{1+\lambda a^2} + \frac{(r^2+b^2)\cos^2\vartheta}{1-\lambda b^2} \\ &\to \frac{(r^2-a^2)\cosh^2\mathcal{T}}{1+\lambda a^2} - \frac{(r^2+b^2)\sinh^2\mathcal{T}}{1-\lambda b^2} \end{aligned} \tag{6.10}$$

This hits $R = 0$ at

$$\tanh^2\mathcal{T} = \frac{r^2-a^2}{r^2+b^2}\frac{1-\lambda b^2}{1+\lambda a^2},$$

which always occurs. Go to $R \to iR'$; as $\mathcal{T} \to \infty$,

$$R'^2 \sim \left(\frac{r^2+b^2}{1-\lambda b^2} - \frac{r^2-a^2}{1+\lambda a^2}\right)\frac{e^{2\mathcal{T}}}{4}.$$

We see that $R'^2 \to \infty$. The $r =$constant slices pass through the non-Killing horizon $\mathcal{NK}$ at $R = 0$, and the χ-horizon at $R' = 1$, and all the way to $R^2 = -\infty$. See Fig. 6.7. They are significantly different than the $R =$constant slices, which always stay 'outside the light cone,' i.e. outside of $\mathcal{NK}$ (see Fig. 6.5).

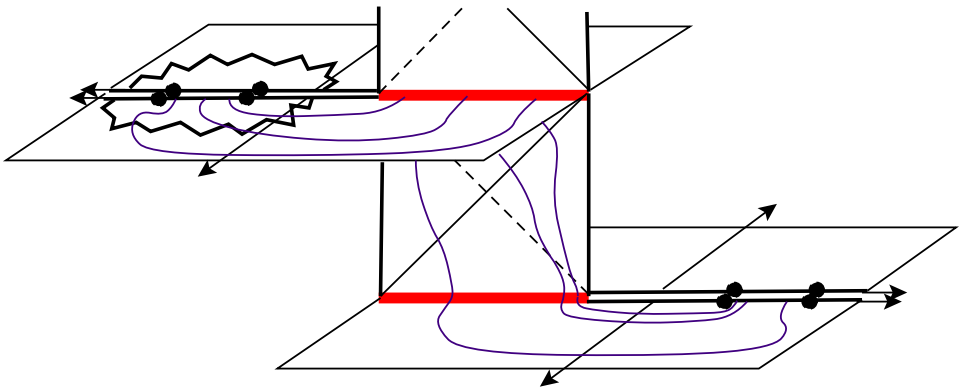

Figure 6.7: Some $\mathcal{T}$ orbits are drawn over the whole card diagram. As $r \to \infty$, they asymptote to $R = \infty$ but also to $R' = \infty$ (the leftmost ray) on the secondary horizontal card. The CTC boundary for $b \neq 0$ is shown as a singularity. The leftmost focus on the secondary horizontal card is at $\tanh^2 \tau = (1 - \lambda b^2)/(1 + \lambda a^2)$. All labels of Fig. 6.5 apply.

Presumably, the Kerr-AdS$_5$ bubble has a card diagram gotten from the Schwarz-Christoffel transformation, but this has not been worked out, and we proceed by analogy to the spheroidal AdS$_5$ geometry.

From the skeleton diagram fibered over $r^2 \geq r_H^2$, we know that the Kerr-AdS$_5$ bubble has a global structure and is covered by r, ϑ coordinates just like this card diagram. Just replace $r^2 = a^2$ with $r^2 = r_H^2$ in the card diagram and take this as a (somewhat loose) representation of the Kerr-AdS$_5$ bubble. Naively, we would have thought that the $r^2 = r_H^2$ closure of the spacetime would have kept us away from the non-Killing horizon $\mathcal{NK}$ (the analog of $R^2 = 0$) and the χ-horizon (analog of $R' = 1$), but as the $r\vartheta$ coordinates show, it does not. So when a or b is nonzero, the structure of the bubble changes significantly. From the card diagram, the $r^2 = r_H^2$ is no *more* 'expanding' than is the left border $\tau = 0$ in the secondary vertical card of Figs. 6.5, 6.7. Of course, this region is expanding; the $\mathbf{H}_3$ has a size proportional to R'. We do not have an expanding hole in the spacetime any more than we would have if the bubble had not formed.

We have not calculated $\mathcal{N}K$'s location for the Kerr-AdS$_5$ bubble, and it is not clear if it has a local geometric characterization. The card diagram for Kerr-AdS$_5$ would clear these matters up.

Despite the complicated nature of the $r =$constant surfaces, on the primary stationary patch $0 \leq \vartheta \leq \pi/2$ they behave quite normally: $r \to \infty$ is the same as $R \to \infty$. Across the whole ϑ skeleton diagram and *a fortiori* in the primary stationary patch, the $r \to \infty$ limit of the AdS$_5$ orbifold precisely matches the $r \to \infty$ limit of the Kerr-AdS$_5$ bubble. This is easy to see from the Kerr-Schild form of Kerr-AdS$_5$:

Kerr is a perturbation of AdS_5, where the perturbation is proportional to a parameter μ, the mass. As $r \to \infty$, all reference to μ disappears, hence the Kerr-AdS_5 bubble is asymptotic to itself with $\mu = 0$, i.e. pure AdS_5.

The twisting to $\tilde{\chi}, \tilde{\phi}, \tilde{\psi}$ occurs in parallel for both pure AdS_5 and the Kerr-AdS_5 bubble.

For purposes of time-dependent holography, we will not want to take an $r \to \infty$ limit of the Kerr-AdS_5 bubble. We have seen that the skeleton diagram of the CBG is complicated and has CTCs (see the orbits in Fig. 6.7). Instead, we will want to take an analog of an $R \to \infty$ limit. To this end, change variables as in (6.9) and take the limit $R \to \infty$. Since $r_H^2 > a^2$, we have no problem at $r^2 = a^2$. Also, from (6.10), $R \to \infty$ implies $r \to \infty$. From (6.9) we have

$$\begin{aligned} r^2 &= \frac{R^2 + \lambda R^2(a^2 \sin^2\theta - b^2 \cos^2\theta) + a^2 - b^2}{2} \\ &\quad \pm\Big[\Big(\frac{R^2 + \lambda R^2(a^2 \sin^2\theta - b^2 \cos^2\theta) + a^2 - b^2}{2}\Big)^2 \\ &\qquad -\lambda a^2 R^2 + R^2(a^2 \cos^2\theta - b^2 \sin^2\theta) + a^2 b^2\Big]^{1/2} \end{aligned}$$

The CBG is the same as for the twisted AdS_5 orbifold: a semidirect product of dS_3 and S^1. Other quantities such as the stress tensor can be computed in these coordinates.

We stress that the $\Theta = 0$ horizons are no longer mysterious; they are just the χ-horizons already present in AdS_5 fibered by dS_3, and do not arise due to the introduction of a physical angular velocity. Instead, $a = b = 0$ is a special case where the rightful χ-horizon is avoided. Further analytic continuation in the spheroidal/de Sitter-oidal coordinates r, ϑ may yield representations of AdS_5 relevant to the anti-bubbles or S-branes of [41].

6.3.1 Case of large b

For $\lambda b^2 > 1$ it is not clear how to interpret

$$\begin{aligned} (1 + \lambda a^2) R^2 \sin^2\theta_{\rm sym} &= (r^2 - a^2)\sin^2\theta, \\ -(\lambda b^2 - 1) R^2 \cos^2\theta_{\rm sym} &= (r^2 + b^2)\cos^2\theta. \end{aligned}$$

The reasoning by analogy of the previous sections fails, and this case requires new insight.

6.4 Flat space KK Reduction and Electromagnetic Dilatonic Melvin

We first discuss the reduction of [61] and add an additional translation-twist component, and then give a boost-twist component.

Take flat 5d space as

$$ds^2 = -dt^2 + dz^2 + d\rho^2 + \rho^2 d\phi^2 + (dx^5)^2.$$

Dowker et al. [61] discuss KK reducing along β-length orbits of the Killing vector

$$l = \partial/\partial x^5 + (B - 2\pi n/\beta)\partial/\partial\phi,$$

where any integer n gives the same 5d spacetime. The proper orbit length is then $\beta\sqrt{1+\rho^2(B-2\pi n/\beta)^2}$. For consistency we must consider regions of $\rho \gg \beta$, and then to keep the l-orbit small we must have $|B - 2\pi n/\beta| \ll 1/\rho$ small. Thus the physical regime is $|B - 2\pi n/\beta| \ll 1/\beta$.

However, this is not quite general. Once one has already compactified the 5d spacetime, one can KK-reduce along

$$l = m\partial/\partial x^5 + (mB - 2\pi n/\beta)\partial/\partial\phi,$$

for some $m \neq 1$. For $B\beta/2\pi$ close to a rational number, the proper circumference of this circle can remain small even for large ρ. For different regimes of ρ, different m will apply to give the minimum circumference. This will give different effective 4d field configurations. The conclusion $|B - 2\pi n/\beta| \ll 1/\beta$ of [61] only applies when ρ is not too large or if we assume $m = 1$.

Now, we also give the formulas for an electromagnetic dilatonic Melvin universe, gotten from two twists, A and B. We twist to $\tilde{t} = t - Ax^5$, $\tilde{\phi} = \phi - Bx^5$, $\tilde{x}^5 = x^5$, so the metric is

$$ds^2 = -(d\tilde{t} + Ad\tilde{x}^5)^2 + dz^2 + d\rho^2 + \rho^2(d\tilde{\phi} + Bd\tilde{x}^5)^2 + (d\tilde{x}^5)^2.$$

The dilaton is $g_{55} = e^{-4\phi/\sqrt{3}} = 1 - A^2 + B^2\rho^2$; and CTCs are avoided by $A^2 < 1$. The 4-geometry is then

$$\begin{aligned} {}^4g_{\mu\nu}dx^\mu dx^\nu &= \sqrt{1-A^2+\rho^2B^2}\Big(-\frac{(1+\rho^2B^2)d\tilde{t}^2}{1-A^2+\rho^2B^2} + \frac{2AB\rho^2 d\tilde{t}d\tilde{\phi}}{1-A^2+\rho^2B^2} \\ &\quad + \frac{\rho^2(1-A^2)d\tilde{\phi}^2}{1-A^2+\rho^2B^2}\Big) + dz^2 + d\rho^2. \end{aligned}$$

and the gauge-field is

$$A_\mu dx^\mu = \frac{1}{1-A^2+B^2\rho^2}(-Ad\tilde{t} + B\rho^2 d\tilde{\phi}).$$

We see that we have a ρ-electric field as well as a z-magnetic field. The case $A = \pm 1$ gives a null orbifold.

6.4.1 Twisted reduction with a rotation and boost

Let us take the near-the-light-cone scaling limit for the general $\Omega^\phi \neq 0$, $\Omega^\psi \neq 0$ twisted AdS_5 orbifold. The metric is, dropping tildes, and for AdS_5 length $l = 1$,

$$\begin{aligned} d\mathrm{AdS}_5^2 &= (1+R^2)d\chi^2 + \frac{dR^2}{1+R^2} + R^2\big(d\theta^2 + \sin^2\theta(d\phi + \Omega^\phi d\chi)^2 \\ &\quad - \cos^2\theta(d\psi + \Omega^\psi d\chi)^2\big). \end{aligned}$$

We wish to perform a scaling limit where $\Lambda \to 0$ and we zoom in on $R = 0$. Since $R = 0$ is where the dS_3 degenerates and passes to $\mathbf{H}_3$, i.e. a light cone, we are performing a near-the-light-cone scaling limit. Specifically, put

$$R \to R/\gamma,\ \chi \to \chi/\gamma,\ \beta \to \beta/\gamma,\ \Omega^{\phi,\psi} \to \gamma\Omega^{\phi,\psi},\ ds^2 \to \gamma^2 ds^2,\ l \to \lambda l,$$

then send $\gamma \to \infty$. Note that $\chi \simeq \chi + \beta$ remains invariant under this scaling; as we enlarge the geometry via $ds^2 \to \gamma^2 ds^2$, we must correspondingly make smaller the χ-circle periodicity β, to keep its proper circumference finite. The $2\pi \times \beta$ coordinate Killing rectangle for (untwisted) ϕ_0 and χ, has fixed width, and becomes less tall; and the twist Ω^ϕ must be enlarged so we have the same ϕ_0-rotation for a single loop around the χ-circle.

The rescaling of β and $\Omega^{\phi,\psi}$ is in some sense extra to the idea of 'zooming in,' as we can clearly see from the following. The primary horizontal card of the twisted AdS_5 orbifold had no CTCs when the condition

$$\big(\Omega^\psi\big)^2 < 1/l^2$$

was satisfied. As $\gamma \to \infty$, this is violated. So this scaling limit is more than a zooming-in (or focusing) on a fixed global Lorentzian geometry. The interpretation of the flat-space orbifold as a local description of physics, or as a connection from the $\Lambda = 0$ to $\Lambda < 0$ physics, as in [79], is made with heavy reservations.

The scaling limit results in

$$ds^2 = d\chi^2 + dR^2 + R^2\Big(d\theta^2 + \sin^2\theta(d\phi + \Omega^\phi d\chi)^2 - \cos^2\theta(d\psi + \Omega^\psi d\chi)^2\Big).$$

We can put this into a Weyl-type form[1] with $\rho = R\sin\theta$, $z = R\cos\theta$:

$$ds^2 = d\chi^2 + \frac{1}{R^2}(d\rho^2 + dz^2) + \rho^2(d\phi + \Omega^\phi d\chi)^2 - z^2(d\psi + \Omega^\psi d\chi)^2.$$

There are CTCs at $1 + (\Omega^\phi)^2\rho^2 - (\Omega^\psi)^2 z^2 < 0$. At $z = 0$ there is a horizon from $\partial/\partial\psi$; we can put $z \to \pm i\tau$ to go to the Milne wedges.

[1] The strict 5d Weyl form would have $\rho = (R/2)\sin 2\theta$, $z = (R/2)\cos 2\theta$, and is gotten from the main text form by $\rho + iz \mapsto (\rho + iz)^2$.

We can perform KK reduction along the χ-direction. This generalizes the result of [61] to a twisted KK reduction of flat space, where the twist is not only a rotation (parameter Ω^ϕ) but also a boost (parameter Ω^ψ).

Following the formulas in [61], we get

$$\begin{aligned} e^{-4\phi/\sqrt{3}} &= 1+(\Omega^\phi)^2\rho^2-(\Omega^\psi)^2z^2, \\ A_1 &= \frac{1}{1+(\Omega^\phi)^2\rho^2-(\Omega^\psi)^2z^2}(\Omega^\phi\rho^2d\phi-\Omega^\psi z^2d\psi), \\ ds_4^2 &= (1+(\Omega^\phi)^2\rho^2-(\Omega^\psi)^2z^2)^{1/2}\Big(d\rho^2+\rho^2d\phi^2+dz^2-z^2d\psi^2 \\ &\qquad -\frac{(\Omega^\phi\rho^2d\phi-\Omega^\psi z^2d\psi)^2}{1+(\Omega^\phi)^2\rho^2-(\Omega^\psi)^2z^2}\Big) \end{aligned}$$

This 4d metric is stationary in this patch; we can also put $z\to\pm i\tau$ to go past the $z=0$ Killing horizon to the Milne wedges.

Near $\rho=0$, $z=0$ (which means near the origin of the rotating 2-plane Π_1, and near the $\times$-structure Killing horizon in the other plane Π_0), the field strength is approximately

$$F_2\sim 2\Omega^\phi d\rho\wedge\rho d\phi-2\Omega^\psi dz\wedge z d\psi.$$

This is a nonvanishing magnetic field pointing in the z-direction (spatial direction of Π_0) as well as an electric field also pointing in the z-direction.

The present solution in general has only 2 Killing vectors; the electromagnetic wave propagates loosely along $1+(\Omega^\phi)^2\rho^2-(\Omega^\psi)^2z^2=$constant. This can be continued to $1+(\Omega^\phi)^2\rho^2+(\Omega^\psi)^2\tau^2=$constant. This scaling limit solution is unphysical, since CTCs occur; only the near-origin (small ρ,z) of the card diagram can be related to the near-origin (small R) of the AdS_5 orbifold.

The solution with $\Omega^\psi=0$ is just Melvin [60]; this has 3 Killing vectors. The solution with $\Omega^\phi=0$ was the cosmological scenario in [64], also called S-Melvin (or Melvin on its side) in [51]; it also has 3 Killing vectors.

6.5 Thermodynamic stability and instanton negative modes

For the 'bounce' instanton to contribute to the semiclassical decay of the orbifold spacetime, it must have a nonconformal negative mode [150]. (Conformal modes are decoupled from the gauge-fixed effective action of Euclidean gravity; see [151]). Explicitly finding such a mode is quite difficult, even for the Schwarzschild-flat space instanton [151], where the mode defies an analytic solution. We instead will explore a link between the existence of a such a mode and the thermodynamic stability of the black hole.

This analysis was done for the nonrotating case (Schwarzschild-AdS) in the canonical ensemble in [149]. When a nonconformal negative mode is present, there is an imaginary factor in $Z(\beta)$ at 1-loop level. Upon inverse Laplace transform to the (microcanonical) density of states $N(E)$, a saddle-point calculation shows that $N(E)$ will be real precisely when the steepest descent is along a real displacement of β, which is precisely when the Helmholtz free energy[2] $F_0 = E - T_0 S$ shows the system is thermodynamically unstable ($C_V < 0$).

We extend this analysis to the rotating case. Take an ensemble of black holes at constant temperature and angular velocity—these intensive quantities are calculated at the instanton horizon and give us the twist and periodicity at infinity. The analog is a gas at constant temperature and pressure. For stable equilibrium, the Gibbs free energy at constant T_0, Ω_0

$$G_0(T,\Omega) = E - T_0 S - \Omega_0 J$$

must be a minimum.

One can analyze equilibrium conditions using any pair of variables, wherever those variables are nonsingular. We demand that the 1st derivative of G_0 vanishes, and that the Hessian 2×2 matrix of 2nd derivatives is positive-definite. Since the 1st derivative vanishes, the Hessian will transform like a symmetric covariant tensor at that point. Its signature is thus invariant under nonsingular changes of variable.

The condition $dG_0 = 0$ tells us that $T = T_0$ and $\Omega = \Omega_0$ (unless we have the exceptional case where the Hessian is singular, i.e. marginal stability).

For the second derivatives, it is easier to use variables (T, J), because $\partial^2 G_0/\partial J \partial T$ vanishes at equilibrium, and the stability condition is easy to read as

$$\left.\frac{\partial^2 G_0}{\partial T^2}\right|_0 = \left.\frac{\partial S}{\partial T}\right|_0 = \frac{1}{T_0} C_J > 0, \qquad \left.\frac{\partial^2 G_0}{\partial J^2}\right|_0 = \left.\frac{\partial \Omega}{\partial J}\right|_0 = \frac{1}{J\kappa} > 0.$$

We have defined $C_J = (\partial E/\partial T)_J$, the specific heat at constant J, and $\kappa = (1/J)(\partial J/\partial \Omega)_T$, the analog of the isothermal compressibility.

For more than one angular momentum parameter, using variables (T, J_1, J_2), the Hessian is no longer diagonal, since $\partial^2 G_0/\partial J_2 \partial J_1 = (\partial \Omega_1/\partial J_2)_{T,J_1} = (\partial \Omega_2/\partial J_1)_{T,J_2} \neq 0$. The condition for 'compressibility' is now more complicated.

Let us instead consider intensive variables (T, Ω). In these variables, the Hessian is then

$$\operatorname{Hess} G_0 = \begin{pmatrix} \frac{\partial S}{\partial T} & \frac{\partial J}{\partial T} \\ \frac{\partial S}{\partial \Omega} & \frac{\partial J}{\partial \Omega} \end{pmatrix},$$

which is symmetric. One positive eigenvalue is guaranteed by $\frac{\partial J}{\partial \Omega} > 0$, which is the same as $J\kappa > 0$ as before. Further defining $\alpha = (1/J)(\partial J/\partial T)_\Omega$, $C_\Omega = T(\partial S/\partial T)_\Omega$,

[2]This standard textbook construction [152], is to be contrasted with $F = E - TS$; it is F_0 that is minimized at stable equilibrium in a $T = T_0$ ensemble.

and using $C_\Omega - C_J = JT\alpha^2/\kappa$, the determinantal condition

$$\frac{1}{T}C_\Omega J\kappa > J^2\alpha^2$$

gives us

$$C_J > 0.$$

This is the same condition as before.[3] The Hessian at equilibrium transforms as a covariant rank 2 tensor, and hence the signature of the Hessian at equilibrium is an invariant.

When comparing to the inverse Laplace transform method, below, we will change to variables

$$\beta' = \beta, \quad \Omega' = \beta\Omega, \qquad \partial_{\beta'} = \partial_\beta - (\Omega/\beta)\partial_\Omega, \quad \partial_{\Omega'} = (1/\beta)\partial_\Omega.$$

The saddle-point function will be $\beta' E - \Omega' J - \beta' G$ where E and J are constants; the linear terms will tell us E and J in terms of their equilibrium values, but do not affect the Hessian in this coordinate system. We have the following remarkable identity at equilibrium:

$$\mathrm{Hess}[\beta', \Omega'](-\beta' G) = \beta' \mathrm{Hess}[\beta', \Omega'](G_0) = \begin{pmatrix} -\frac{\partial E}{\partial \beta'} & \frac{\partial J}{\partial \beta'} \\ -\frac{1}{\beta}\frac{\partial E}{\partial \Omega} & \frac{1}{\beta}\frac{\partial J}{\partial \Omega} \end{pmatrix}. \tag{6.11}$$

At equilibrium, $\mathrm{Hess}(\beta' E - \Omega' J - \beta' G) = \beta' \mathrm{Hess}(G_0)$ holds in any nonsingular coordinate system. To be positive definite, we require $J\kappa > 0$ as usual from the lower-right entry, and the determinant yields $C_J > 0$.

For two angular momenta, we have

$$\mathrm{Hess}[\beta', \Omega'](-\beta' G) = \beta' \mathrm{Hess}[\beta', \Omega'](G_0) = \begin{pmatrix} -\frac{\partial E}{\partial \beta'} & \frac{\partial J_1}{\partial \beta'} & \frac{\partial J_2}{\partial \beta'} \\ -\frac{1}{\beta}\frac{\partial E}{\partial \Omega_1} & \frac{1}{\beta}\frac{\partial J_1}{\partial \Omega_1} & \frac{1}{\beta'}\frac{\partial J_1}{\partial \Omega_2} \\ -\frac{1}{\beta'}\frac{\partial E}{\partial \Omega_2} & \frac{1}{\beta'}\frac{\partial J_2 \Omega_1}{\partial \Omega_1} & \frac{1}{\beta'}\frac{\partial J_2}{\partial \Omega_2} \end{pmatrix}. \tag{6.12}$$

Of course it is easier to evaluate the signature of G_0 using variables T, J_1, J_2. The Hessian is then

$$\begin{pmatrix} \frac{1}{T_0}\frac{\partial E}{\partial T} & 0 & 0 \\ 0 & \frac{\partial \Omega_1}{\partial J_1} & \frac{\partial \Omega_1}{\partial J_2} \\ 0 & \frac{\partial \Omega_2}{\partial J_1} & \frac{\partial \Omega_2}{\partial J_2} \end{pmatrix}, \tag{6.13}$$

[3] It is a common misconception that $C_\Omega > 0$, or constant-pressure specific heat, is an eigenvalue condition for thermodynamic stability in a constant-pressure ensemble. This is incorrect. Constant-pressure ensembles do allow for constant-volume, variable pressure fluctuations, and these must be stable.

and at equilibrium we put $T = T_0$, $\Omega_1 = (\Omega_1)_0$, $\Omega_2 = (\Omega_2)_0$.

We will now invert the Laplace transforms to write the microcanonical density of states in terms of the partition function,

$$Z(\beta, \Omega) = \int_0^\infty dE\, e^{-\beta E} \int_{-\infty}^\infty dJ\, e^{\beta\Omega J} N(E, J).$$

Looking at the outer Laplace transform, in AdS the density of states grows slowly enough that the Laplace transform in E should exist for all $\mathrm{Re}\,\beta > 0$; we will thus invert with a contour $\mathrm{Re}\,\beta = B$ for some $B > 0$. First, set $\beta' = \beta$, $\Omega' = \beta\Omega$; then inversion yields

$$\int_{-\infty}^\infty dJ\, e^{\Omega' J} N(E, J) = \frac{1}{2\pi i} \int_{B-i\infty}^{B+i\infty} d\beta' Z e^{\beta' E}.$$

The inverse Laplace transform proof [83] goes through for a transform defined over $-\infty < J < \infty$, as long as $N(E, J)$ has compact support in J for fixed E. Choosing an arbitrary $\mathrm{Re}\,\Omega' = W$ yields

$$N(E, J) = \frac{1}{2\pi i} \int_{W+i\infty}^{W-i\infty} d\Omega' e^{-\Omega' J} \frac{1}{2\pi i} \int_{B-i\infty}^{B+i\infty} d\beta' e^{\beta' E} Z(\beta', \Omega'/\beta').$$

The integrand is

$$\exp(\beta E - \Omega' J - \beta G(\beta, \Omega'/\beta)),$$

where E and J are just parameters.

Recall that $G(\beta, \Omega)$ has $dG = (S/\beta^2)d\beta - J(\beta, \Omega)d\Omega$. Then the first-order conditions relate the parameters E and J to the expected thermodynamic functions:

$$\frac{\partial}{\partial\beta}(\beta E - \Omega' J - \beta G(\beta, \Omega'/\beta)) = 0$$

gives

$$E = G(\beta, \Omega) + TS(\beta, \Omega) + \Omega J(\beta, \Omega),$$

and

$$\frac{\partial}{\partial\Omega'}(\beta E - \Omega' J - \beta G(\beta, \Omega'/\beta)) = 0$$

gives

$$J = J(\beta, \Omega).$$

Hence we choose (B, W) so our contours reach the saddle point which depends on (E, J). Parametrizing $\beta = B + it$, $\Omega' = W + iu$, we have a 2d real integral $\int dtdu$ expanded to second order about $(t, u) = (0, 0)$. The Hessian can be expanded about principal axes. For simplicity we stick to the (β', Ω') notation; for real convergent saddle-point integration, we want this to be positive definite. By the identity (6.11),

this Hessian is positive proportional to that for G_0.[4] Thus, each negative G_0 eigenvalue will contribute a factor of i to the saddle-point integration, cancelling a factor i in Z to yield a real N. We expect $C_J > 0$ to hold for large black holes in AdS with small rotation parameters, whereas $J\kappa > 0$ for black holes and rings is more subtle. When $C_J < 0$, the saddle-point integration gives a factor of i from which we infer that Z is purely imaginary, hence the instanton has a negative nonconformal mode.

For multiple angular momenta, we can invert each finite-support Laplace transform. The Hessian identity (6.12) has been shown to hold for $n = 2$ angular momenta, and by symmetry it must hold for any $n \geq 2$.

6.6 Thermodynamic stability of Kerr-AdS$_5$

The Kerr-AdS$_5$ black hole has

$$\Omega_a = \frac{a(1 + r_+^2/l^2)}{r_+^2 + a^2}, \qquad \Omega_b = \frac{b(1 + r_+^2/l^2)}{r_+^2 + b^2},$$

where r_+ satisfies

$$(r^2 + a^2)(r^2 + b^2)(1 + r^2/l^2) - 2Mr^2 = 0.$$

We also have

$$2\pi T = \kappa = r_+(1 + r_+^2/l^2)(\frac{1}{r_+^2 + a^2} + \frac{1}{r_+^2 + b^2}) - \frac{1}{r_+},$$

Komar integrals give us unambiguously

$$J_a = \frac{\pi M a}{2\Xi_a^2 \Xi_b}, \quad J_b = \frac{\pi M b}{2\Xi_b^2 \Xi_a}, \qquad \Xi_a = 1 - a^2/l^2, \quad \Xi_b = 1 - b^2/l^2$$

and from [128] we have

$$E = \frac{\pi M(2\Xi_a + 2\Xi_b - \Xi_a \Xi_b)}{4\Xi_a^2 \Xi_b^2}.$$

It remains, and should be forthcoming from the aforementioned contributors, to check the 'isothermal compressibility' conditions and specific heat,

$$\left(\frac{\partial J_1}{\partial \Omega_1}\right)_{T,\, J_2} > 0, \qquad \det\left(\frac{\partial J_i}{\partial \Omega_j}\right) > 0, \qquad \left(\frac{\partial E}{\partial T}\right)_{J_1,\, J_2} > 0.$$

[4] One can more directly relate G's Hessian to thermodynamic stability based on $G(p, T, N)$ and extensivity; see [153].

A technique is to set

$$\begin{aligned} dE &= E_M dM + E_a da + E_b db \\ dT &= T_M dM + T_a da + T_b db \\ dJ_i &= J_{iM} dM + J_{ia} da + J_{ib} db \\ d\Omega_i &= \Omega_{iM} dM + \Omega_{ia} da + \Omega_{ib} db, \end{aligned}$$

then for example we can check the specific heat by setting $\hat{\jmath}_i = \nabla J_i/|\nabla J_i|$, $\vec{E}_\perp = \nabla E - (\nabla E \cdot \hat{\jmath}_i)\hat{\jmath}_i$, $\vec{T}_\perp = \nabla T - (\nabla T \cdot \hat{\jmath}_i)\hat{\jmath}_i$, and check the sign of $\vec{E}_\perp \cdot \vec{T}_\perp$.

Our characterization of thermodynamic stability should be contrasted with that in [154], where specific heat is computed at constant a, b. That quantity is not physically relevant.

6.7 Decay channels

It may be that for a given twisted orbifold, there is more than one Kerr instanton that asymptotes to that orbifold. The reason for this is that if we identify

$$(\chi, \phi, \psi) \simeq (\chi + \beta n_0, \phi + \Omega_1 \beta n_0 + 2\pi n_1, \psi + \Omega_2 \beta n_0 + 2\pi n_2),$$

then putting $\Omega_i \to \Omega_i + 2\pi m_i/\beta$ give the same results for any integers m_i. Equivalently, $\kappa^{-1}\Omega_i \simeq \kappa^{-1}\Omega_i + m_i$, as far as asymptotia are concerned.

Let us restrict to looking at $b = 0$ (or $\Omega_2 = 0$) solutions, where the algebra is greatly simplified. We also assume $M > 0$. For the instantons or bubble-like solutions, we must continue $a \to ia$ from the black hole formulas. Then $(r_+^2 - a^2)(1 + r_+^2/l^2) = 2M$, so r_+ is monotonically increasing in M. Also,

$$\kappa^{-1}\Omega_a = \frac{a}{r_+(1 - \frac{l^2+a^2}{r_+^2+l^2})},$$

so absolute value of $\kappa^{-1}\Omega_a$ is monotonically decreasing with M. But as $M \downarrow 0$, $\kappa^{-1}\Omega_a \to \mathrm{sign}(a)$. Thus $-1 < \kappa^{-1}\Omega_a < 1$, which is the same bound as for $\Lambda = 0$ in [61].

This means that for given $\kappa^{-1}\Omega_a$, which is determined by the orbifold, there will be a Kerr-AdS_5 instanton at that value of κ and rotation parameter Ω_a or also one at κ and a shifted rotation $\Omega_a \pm \kappa$. In the case $\kappa^{-1}\Omega_a \approx 0$, the unshifted instanton dominates actionwise, and its 4d KK description is appropriate showing it as a dilatonic, expanding bubble. There is also the suppressed 'shifted' instanton with a large value of a, which has a 4d KK description (reduced on the same *untwisted* circle, i.e. with small $\Omega = \Omega_a \pm \kappa$) as a pair of dilatonic extremal black holes accelerating in a magnetic field. The dilatonic bubble singularity has been blown-up to a finite-sized 2-sphere with singularities at the north and south poles [61].

For larger $\kappa^{-1}\Omega_a$ (meaning towards $\pm 1/2$ in the $-1/2 < \kappa^{-1}\Omega_a \leq 1/2$ circle), a KK description is not appropriate, because the KK circle is only small at radial distances that are just as small.

The case $b \neq 0$ is harder to analyze. Even with orbifolds where $\Omega_2 = 0$, it could be the case $b \neq 0$ instanton can serve to decay the spacetime. We think this is unlikely and there will be one extra instanton by b-shifting for each nonzero Ω_2.

6.8 Summary and outlook

Via the counterterm method, one can calculate masses and renormalized actions of the Kerr-AdS_5 bubble solutions. Solutions coming from $M > 0$ black holes had negative bubble mass in the Schwarzschild case, and we expect that this will persist here, at least for small rotation parameters. In the case where the bubble mass is smaller than the zero mass of the AdS_5 twisted orbifold, and where there is a thermodynamic instability, semiclassical decay can proceed spontaneously. With a and b off, the bubble locus sealed the black hole singularity from the majority of the spacetime. With a on, the black hole orbifold singularity remains and is accessible from the majority of the spacetime—the expanding bubble does not seal it off. With a and b on, the χ-horizon is still accessible, and the singular CTC region for the bubble is moved away from the χ-horizon into the secondary stationary region. The precise parameter regions for this decay are still forthcoming.

It is quite likely that similar decays could proceed to what were termed S-brane and anti-bubble solutions in [41]. The new Kerr-AdS_D instanton for odd $D = 5, 7, 9, \ldots$ (from the anomalous S-brane with one turned off), is a good place to start. A proper description of the ensuing radiation coming from mass loss, or a holographic description, are not imminent.

There is a long history of literature on black hole thermodynamics, instantons, analytic continuation, and thermodynamic and dynamical instability. Recent interest has been spurred by the AdS/CFT correspondence and the boundary theory. See [155]-[183].

Bibliography

[1] H. Stephani, D. Kramer, M. MacCallum, C. Hoenselaers, E. Herlt, *Exact Solutions of Einstein's Field Equations, 2nd ed.*, Cambridge University Press (2003).

[2] J. Ehlers, "Konstruktionen und Charakterisierungen von Lösungen der Einsteinschen Gravitationsfeldgleichungen," Dissertation, Hamburg (157).

[3] R. Geroch, "Multipole Moments. I. Flat Space," J. Math. Phys. **11** (6), 1955 (1970). "Multipole Moments. II. Curved Space," J. Math. Phys. **11** (8), 2580 (1970).

[4] R. O. Hansen, "Multipole moments of stationary space-times," J. Math. Phys. **15**, 46 (1974).

[5] W. Simon, "The multipole expansion of stationary Einstein-Maxwell fields," J. Math. Phys. **25**, 1035 (1984).

[6] W. Kinnersley "Generation of stationary Einstein-Maxwell fields," J. Math. Phys. **14** 651 (1973).

[7] B. K. Harrison, "New Solutions of the Einstein-Maxwell Equations from Old," J. Math. Phys. **9** No. 11, 1744 (1968).

[8] H. Weyl, "Zur Gravitationstheorie," Ann. Phys. (Leipzig) **54**, 117 (1917).

[9] J. L. Synge, *Relativity: The general theory*, North-Holland, Amsterdam, (1960).

[10] W. Kinnersley, "Symmetries Of The Stationary Einstein-Maxwell Field Equations. I," J. Math. Phys. **18**, 1529 (1977).

[11] W. B. Bonnor, "Exact Solutions of the Einstein-Maxwell Equations," Zeitschrift für Physik **161**, 439 (1961).

[12] W. B. Bonnor, "An Exact Solution of the Einstein-Maxwell Equations Referring to a Magnetic Dipole," Zeitschrift für Physik **190**, 444 (1966).

[13] E. Herlt, "Static and Stationary Axially Symmetric Gravitational Fields of Bounded Sources. I. Solutions Obtainable from the van Stockum Metric," Gen. Rel. Grav. **9**, No. 8, 711 (1978). "II. Solutions Obtainable from Weyl's Class." Gen. Rel. Grav. **11**, No. 5 (1979).

[14] A. Papapetrou, "Eine rotattionssymmetrische Lösung in der allgemeinen Relativitätstheorie," Ann. Physik **12** (1953) 309;

A. Papapetrou, "Champs gravitationels stationaries à symmetrie axiale," Ann. Inst. H. Poincaré A **4** (1966) 83.

[15] R. Emparan and H. S. Reall, "Generalized Weyl solutions," Phys. Rev. D **65**, 084025 (2002) [arXiv:hep-th/0110258].

[16] T. Harmark, "Stationary and axisymmetric solutions of higher-dimensional general relativity," Phys. Rev. D **70**, 124002 (2004) [arXiv:hep-th/0408141].

[17] T. Harmark and P. Olesen, "On the structure of stationary and axisymmetric metrics," arXiv:hep-th/0508208.

[18] P. K. Townsend, "The eleven-dimensional supermembrane revisited," Phys. Lett. B **350**, 184 (1995) [arXiv:hep-th/9501068].

[19] P. K. Townsend, "P-brane democracy," arXiv:hep-th/9507048.

[20] D. Gaiotto, A. Strominger and X. Yin, "New connections between 4D and 5D black holes," arXiv:hep-th/0503217.

[21] D. Gaiotto, A. Strominger and X. Yin, "5D black rings and 4D black holes," arXiv:hep-th/0504126.

[22] W. B. Bonnor, "The Sources of the Vacuum C-Metric," Gen. Rel. Grav. **15** (6) 535 (1983).

[23] A. Maloney, A. Strominger and X. Yin, "S-brane thermodynamics," JHEP **0310**, 048 (2003) [arXiv:hep-th/0302146].

[24] D. Gaiotto, N. Itzhaki and L. Rastelli, "Closed strings as imaginary D-branes," Nucl. Phys. B **688**, 70 (2004) [arXiv:hep-th/0304192].

[25] G. C. Jones, A. Maloney and A. Strominger, "Non-singular solutions for S-branes," Phys. Rev. D **69**, 126008 (2004) [arXiv:hep-th/0403050].

[26] A. Sen, "Non-BPS states and branes in string theory," arXiv:hep-th/9904207.

[27] A. Sen, "Rolling tachyon," JHEP **0204**, 048 (2002) [arXiv: hep-th/0203211];

A. Sen, "Tachyon matter," JHEP **0207**, 065 (2002) [arXiv: hep-th/0203265];

A. Sen, "Field theory of tachyon matter," Mod. Phys. Lett. A **17**, 1797 (2002) [arXiv: hep-th/0204143];

A. Sen, "Time evolution in open string theory," JHEP **0210**, 003 (2002) [arXiv: hep-th/0207105];

A. Sen, "Tachyon dynamics in open string theory," [arXiv: hep-th/0410103].

[28] A. Sen, "Tachyon dynamics in open string theory," arXiv:hep-th/0410103.

[29] M. Gutperle and A. Strominger, "Spacelike branes," JHEP **0204**, 018 (2002) [arXiv:hep-th/0202210].

[30] J. M. Maldacena, "The large N limit of superconformal field theories and supergravity," Adv. Theor. Math. Phys. **2**, 231 (1998) [Int. J. Theor. Phys. **38**, 1113 (1999)] [arXiv:hep-th/9711200].

[31] S. S. Gubser, I. R. Klebanov and A. M. Polyakov, "Gauge theory correlators from non-critical string theory," Phys. Lett. B **428**, 105 (1998) [arXiv: hep-th/9802109].

[32] O. Aharony, S. S. Gubser, J. M. Maldacena, H. Ooguri and Y. Oz, "Large N field theories, string theory and gravity," Phys. Rept. **323**, 183 (2000) [arXiv:hep-th/9905111].

[33] E. Witten, "Anti-de Sitter space and holography," Adv. Theor. Math. Phys. **2**, 253 (1998) [arXiv: hep-th/9802150].

[34] E. Witten, "Anti-de Sitter space, thermal phase transition, and confinement in gauge theories," Adv. Theor. Math. Phys. **2**, 505 (1998) [arXiv:hep-th/9803131].

[35] D. Marolf, "States and boundary terms: Subtleties of Lorentzian AdS/CFT," JHEP **0505**, 042 (2005) [arXiv:hep-th/0412032].

[36] E. Witten, "Instability Of The Kaluza-Klein Vacuum," Nucl. Phys. B **195**, 481 (1982).

[37] O. Aharony, M. Fabinger, G. T. Horowitz and E. Silverstein, "Clean time-dependent string backgrounds from bubble baths," JHEP **0207**, 007 (2002) [arXiv:hep-th/0204158].

[38] D. Birmingham and M. Rinaldi, "Bubbles in anti-de Sitter space," Phys. Lett. B **544**, 316 (2002) [arXiv: hep-th/0205246].

[39] V. Balasubramanian and S. F. Ross, "The dual of nothing," Phys. Rev. D **66**, 086002 (2002) [arXiv: hep-th/0205290].

[40] A. Biswas, T. K. Dey and S. Mukherji, "R-charged AdS bubble," arXiv:hep-th/0412124.

[41] D. Astefanesei and G. C. Jones, "S-branes and (anti-)bubbles in (A)dS space," JHEP **0506**, 037 (2005) [arXiv:hep-th/0502162].

[42] C. M. Chen, D. V. Gal'tsov and M. Gutperle, "S-brane solutions in supergravity theories," Phys. Rev. D **66**, 024043 (2002) [arXiv:hep-th/0204071].

[43] M. Kruczenski, R. C. Myers and A. W. Peet, "Supergravity S-branes," JHEP **0205**, 039 (2002) [arXiv:hep-th/0204144].

[44] J. E. Wang, "Spacelike and time dependent branes from DBI," JHEP **0210**, 037 (2002) [arXiv:hep-th/0207089],

C. P. Burgess, F. Quevedo, S. J. Rey, G. Tasinato and I. Zavala, "Cosmological spacetimes from negative tension brane backgrounds," JHEP **0210**, 028 (2002) [arXiv:hep-th/0207104].

[45] A. Strominger, "Open string creation by S-branes," *Cargèse 2002, Progress in string, field and particle theory*, 335, [arXiv:hep-th/0209090];

B. Chen, M. Li and F. L. Lin, "Gravitational radiation of rolling tachyon," JHEP **0211**, 050 (2002), [arXiv:hep-th/0209222];

C. P. Burgess, P. Martineau, F. Quevedo, G. Tasinato and I. Zavala C., "Instabilities and particle production in S-brane geometries," JHEP **0303**, 050 (2003), [arXiv:hep-th/0301122];

F. Leblond and A. W. Peet, "SD-brane gravity fields and rolling tachyons," JHEP **0304**, 048 (2003), [arXiv:hep-th/0303035];

N. Lambert, H. Liu and J. Maldacena, "Closed strings from decaying D-branes," arXiv:hep-th/0303139.

[46] N. Ohta, "Intersection rules for S-branes," Phys. Lett. B **558**, 213 (2003) [arXiv:hep-th/0301095].

[47] J. E. Wang, "Twisting S-branes," JHEP **0405**, 066 (2004) [arXiv:hep-th/0403094].

[48] G. Tasinato, I. Zavala, C. P. Burgess and F. Quevedo, "Regular S-brane backgrounds," JHEP **0404**, 038 (2004) [arXiv:hep-th/0403156].

[49] H. Lü and J. F. Vázquez-Poritz, "Non-singular twisted S-branes from rotating branes," JHEP **0407**, 050 (2004) [arXiv:hep-th/0403248].

[50] M. Gutperle and W. Sabra, "S-brane solutions in gauged and ungauged supergravities," Phys. Lett. B **601**, 73 (2004) [arXiv:hep-th/0407147].

[51] G. C. Jones and J. E. Wang, "Weyl card diagrams and new S-brane solutions of gravity," arXiv:hep-th/0409070.

[52] A. Biswas, "Constructing more non-singular Sp-branes," Phys. Lett. B **600**, 157 (2004) [arXiv:hep-th/0405225].

[53] R. C. Myers, "Higher Dimensional Black Holes In Compactified Space-Times," Phys. Rev. D **35**, 455 (1987).

[54] R. Emparan and E. Teo, "Macroscopic and microscopic description of black diholes," Nucl. Phys. B **610**, 190 (2001) [arXiv:hep-th/0104206].

[55] K. Hong and E. Teo, "A new form of the C-metric," Class. Quant. Grav. **20**, 3269 (2003) [arXiv:gr-qc/0305089]. "A new form of the rotating C-metric," Class. Quant. Grav. **22**, 109 (2005) [arXiv:gr-qc/0410002].

[56] C. Charmousis and R. Gregory, "Axisymmetric metrics in arbitrary dimensions," Class. Quant. Grav. **21** (2004) 527 [arXiv:hep-th/0306069].

[57] R. Emparan and H. S. Reall, "A rotating black ring in five dimensions," Phys. Rev. Lett. **88**, 101101 (2002) [arXiv:hep-th/0110260].

[58] H. Elvang, "A charged rotating black ring," Phys. Rev. D **68**, 124016 (2003) [arXiv:hep-th/0305247].

H. Elvang and R. Emparan, "Black rings, supertubes, and a stringy resolution of black hole non-uniqueness," JHEP **0311**, 035 (2003) [arXiv:hep-th/0310008].

H. Elvang, R. Emparan, D. Mateos and H. S. Reall, "A supersymmetric black ring," Phys. Rev. Lett. **93**, 211302 (2004) [arXiv:hep-th/0407065].

H. Elvang, R. Emparan, D. Mateos and H. S. Reall, "Supersymmetric black rings and three-charge supertubes," Phys. Rev. D **71**, 024033 (2005) [arXiv:hep-th/0408120].

H. Elvang, R. Emparan and P. Figueras, "Non-supersymmetric black rings as thermally excited supertubes," JHEP **0502**, 031 (2005) [arXiv:hep-th/0412130].

[59] W. Israel, K. A. Khan, "Collinear Particles and Bondi Dipoles in General Relativity," Nuovo Cim. **33**, 3611 (1964).

[60] M. A. Melvin, "Pure Magnetic and Electric Geons," Phys. Lett. **8** (1), 65 (1964).

[61] F. Dowker, J. P. Gauntlett, G. W. Gibbons and G. T. Horowitz, "The Decay of magnetic fields in Kaluza-Klein theory," Phys. Rev. D **52**, 6929 (1995) [arXiv:hep-th/9507143]. "Nucleation of P-Branes and Fundamental Strings," Phys. Rev. D **53**, 7115 (1996) [arXiv:hep-th/9512154].

[62] M. S. Costa and M. Gutperle, "The Kaluza-Klein Melvin solution in M-theory," JHEP **0103**, 027 (2001) [arXiv:hep-th/0012072],

M. Gutperle and A. Strominger, "Fluxbranes in string theory," JHEP **0106**, 035 (2001) [arXiv:hep-th/0104136].

[63] R. Emparan and M. Gutperle, "From p-branes to fluxbranes and back," JHEP **0112**, 023 (2001) [arXiv:hep-th/0111177].

[64] L. Cornalba and M. S. Costa, "A new cosmological scenario in string theory," Phys. Rev. D **66**, 066001 (2002) [arXiv:hep-th/0203031].

[65] Siklos, S. T. C. "Two completely singularity-free NUT space-times," Phys. Lett. A **59**, 173 (1976).

[66] R. Emparan, "Rotating circular strings, and infinite non-uniqueness of black rings," JHEP **0403**, 064 (2004) [arXiv:hep-th/0402149].

[67] G. C. Jones and J. E. Wang, in preparation.

[68] N. R. Sibgatullin, *Oscillations and Waves in Strong Gravitational and Electromagnetic Fields*, Springer-Verlag, Berlin, Heidelberg 1991. (Originally published Nauka, Moscow 1984.)

[69] S. Chandrasekhar and B. C. Xanthopoulos, "Two Black Holes Attached To Strings," Proc. Roy. Soc. Lond. A **423**, 387 (1989).

[70] R. Emparan, "Black diholes," Phys. Rev. D **61**, 104009 (2000) [arXiv:hep-th/9906160].

[71] J. Bičák and V. Pravda, "Spinning C metric: Radiative space-time with accelerating, rotating black holes," Phys. Rev. D **60**, 044004 (1999) [arXiv: gr-qc/9902075];

V. Pravda and A. Pravdová, "Boost rotation symmetric space-times: Review," Czech. J. Phys. **50**, 333 (2000) [arXiv: gr-qc/0003067].

[72] J. F. Plebański and M. Demiański, "Rotating, charged, and uniformly accelerating mass in general relativity," Annals of Phys. **98**, 98 (1976).

[73] R. Debever, "On type D expanding solutions of the Einstein-Maxwell equations," *Bull. Soc. Math. Belgique* **23**, 360 (1971).

[74] A. García D. and A. Macias, "Black holes as exact solutions of the Einstein-Maxwell equations of Petrov type *D*," in *Black holes: Theory and observation*, Lecture notes in physics, vol. **514**, eds. F. W. Hehl, C. Kiefer, and R. J. K. Metzler, Springer, 205 (1998).

[75] K. Matsuzaki and M. Taniguchi, *Hyperbolic Manifolds and Kleinian Groups*, Oxford University Press, New York, 1998.

[76] S. Fairhurst and B. Krishnan, "Distorted black holes with charge," Int. J. Mod. Phys. D **10**, 691 (2001) [arXiv:gr-qc/0010088].

[77] C. Hull, "Timelike T-duality, de Sitter space, large N gauge theories and topological field theory," JHEP **9807**, 021 (1998), [arXiv:hep-th/9806146]; "Duality and the signature of space-time," JHEP **9811**, 017 (1998), [arXiv:hep-th/9807127];

[78] M. Bañados, C. Teitelboim and J. Zanelli, "The Black hole in three-dimensional space-time," Phys. Rev. Lett. **69**, 1849 (1992) [arXiv:hep-th/9204099].

M. Bañados, M. Henneaux, C. Teitelboim and J. Zanelli, "Geometry of the (2+1) black hole," Phys. Rev. D **48**, 1506 (1993) [arXiv:gr-qc/9302012].

S. Åminneborg, I. Bengtsson, S. Holst and P. Peldán, "Making Anti-de Sitter Black Holes," Class. Quant. Grav. **13**, 2707 (1996) [arXiv:gr-qc/9604005].

M. Bañados, "Constant curvature black holes," Phys. Rev. D **57**, 1068 (1998) [arXiv:gr-qc/9703040].

S. Holst and P. Peldán, "Black holes and causal structure in anti-de Sitter isometric spacetimes," Class. Quant. Grav. **14**, 3433 (1997) [arXiv:gr-qc/9705067].

M. Bañados, A. Gomberoff and C. Martínez, "Anti-de Sitter space and black holes," Class. Quant. Grav. **15**, 3575 (1998) [arXiv:hep-th/9805087].

R.-G. Cai, "Constant curvature black hole and dual field theory," Phys. Lett. B **544**, 176 (2002) [arXiv:hep-th/0206223].

[79] V. Balasubramanian, K. Larjo and J. Simón, "Much ado about nothing," arXiv:hep-th/0502111.

[80] J. F. Plebański, "A Class of Solutions of Einstein-Maxwell Equations," Ann. Phys. **90**, 196 (1975).

[81] S. W. Hawking, C. J. Hunter and M. M. Taylor-Robinson, "Rotation and the AdS/CFT correspondence," Phys. Rev. D **59**, 064005 (1999) [arXiv: hep-th/9811056].

[82] G. W. Gibbons, H. Lü, D. N. Page and C. N. Pope, "The general Kerr-de Sitter metrics in all dimensions," arXiv:hep-th/0404008. "Rotating black holes in higher dimensions with a cosmological constant," Phys. Rev. Lett. **93**, 171102 (2004) [arXiv:hep-th/0409155].

[83] N. H. Asmar with G. C. Jones, *Applied Complex Analysis with Partial Differential Equations*, Prentice-Hall (2002).

[84] S. Bhattacharya and S. Roy, "Time dependent supergravity solutions in arbitrary dimensions," JHEP **0312**, 015 (2003) [arXiv:hep-th/0309202].

[85] A. M. Ghezelbash and R. B. Mann, "Nutty bubbles," JHEP **0209**, 045 (2002) [arXiv:hep-th/0207123].

[86] A. M. Ghezelbash and R. B. Mann, "Kerr-AdS bubble spacetimes and time-dependent AdS / CFT correspondence," Mod. Phys. Lett. A **19**, 1585 (2004) [arXiv:hep-th/0210046].

[87] D. Astefanesei, R. B. Mann and C. Stelea, "Nuttier bubbles," arXiv:hep-th/0508162.

[88] B. Carter, "Black hole equilibrium states, Part II" in *Black Holes (Les Houches Lectures)*, eds. B. S. DeWitt and C. DeWitt (Gordon and Breach, N.Y., 1972).

[89] G. C. Jones and J. E. Wang, "Weyl card diagrams," Phys. Rev. D **71**, 124019 (2005) [arXiv:hep-th/0506023].

[90] F. Dowker, J. P. Gauntlett, D. A. Kastor and J. H. Traschen, "Pair creation of dilaton black holes," Phys. Rev. D **49**, 2909 (1994) [arXiv:hep-th/9309075].

[91] A. Davidson and E. Gedalin, "Finite magnetic flux tube as a black and white dihole," Phys. Lett. B **339**, 304 (1994) [arXiv:gr-qc/9408006].

[92] Y. C. Liang and E. Teo, "Black diholes with unbalanced magnetic charges," Phys. Rev. D **64**, 024019 (2001) [arXiv:hep-th/0101221].

[93] K. S. Stelle, "BPS branes in supergravity," arXiv:hep-th/9803116.

[94] A. W. Peet, "TASI lectures on black holes in string theory," arXiv:hep-th/0008241.

[95] A. Vilenkin, "Cosmic Strings and Domain Walls," *Phys. Rep.* **121** (1985) 265.

[96] J. M. Bardeen and G. T. Horowitz, "The extreme Kerr throat geometry: A vacuum analog of AdS(2) x S(2)," Phys. Rev. D **60**, 104030 (1999) [arXiv:hep-th/9905099].

[97] H. Friedrich, "Gravitational fields near space-like and null infinity," J. Geom. Phys. **24** (1998) 83.

[98] R. Geroch, "Structure of the Gravitational Field at Spatial Infinity," J. Math. Phys. **13**, 956 (1972).

[99] D. Klemm, V. Moretti and L. Vanzo, Phys. Rev. D **57**, 6127 (1998) [Erratum-ibid. D **60**, 109902 (1999)] [arXiv: gr-qc/9710123];

D. Klemm, "Rotating black branes wrapped on Einstein spaces," JHEP **9811**, 019 (1998) [arXiv: hep-th/9811126].

[100] R. Penrose, "Zero Rest Mass Fields Including Gravitation: Asymptotic Behavior," Proc. Roy. Soc. Lond. A **284**, 159 (1965).

R. Geroch, in *General Relativity and Cosmology*, International School of Phys. 'Enrico Fermi,' ed. R. K. Sachs, Acad. Press (1971).

R. Penrose, "Some Unsolved Problems in Classical General Relativity," in *Seminar on Differential Geometry,* PUP, ed. S.-T. Yau, 631 (1982).

R. Penrose and W. Rindler, *Spinors and Space-time, Vol. II*, CUP 1986.

[101] L. P. Eisenhart, *Riemannian Geometry*, Princeton University Press (1926).

[102] C. W. Misner, K. S. Thorne, and J. A. Wheeler, *Gravitation*, W. H. Freeman & Co. (1973).

[103] G. W. Gibbons and S. W. Hawking, "Classification Of Gravitational Instanton Symmetries," Commun. Math. Phys. **66**, 291 (1979).

[104] R. C. Myers and M. J. Perry, "Black Holes In Higher Dimensional Space-Times," Annals Phys. **172**, 304 (1986).

[105] J. M. Maldacena and C. Núñez, "Supergravity description of field theories on curved manifolds and a no go theorem," Int. J. Mod. Phys. A **16**, 822 (2001) [arXiv:hep-th/0007018].

[106] M. Cvetič and D. Youm, "Rotating intersecting M-branes," Nucl. Phys. B **499**, 253 (1997) [arXiv:hep-th/9612229].

[107] M. Cvetič, M. J. Duff, P. Hoxha, James T. Liu, H. Lü, J. X. Lu, R. Martinez-Acosta, C. N. Pope, H. Sati, and T. A. Tran, "Embedding AdS black holes in ten and eleven dimensions," Nucl. Phys. B **558**, 96 (1999) [arXiv:hep-th/9903214].

[108] A. H. Taub, "Empty space-times admitting a three parameter group of motions," Ann. Math. **53**, 472 (1951).

[109] E. Newman, L. Tamburino, and T. Unti, "Empty-Space Generalization of the Schwarzschild Metric," J. Math. Phys. **4**, 915 (1963).

[110] C. W. Misner, "The Flatter Regions of Newman, Unti, and Tamburino's Generalized Schwarzschild Space," J. Math. Phys. **4** No. 7 (1963), 924.

[111] D. R. Brill, "Electromagnetic Fields in a Homogeneous, Nonisotropic Universe," Phys. Rev. **133** No. 3B (1964), B845.

[112] S. W. Hawking, "Gravitational Instantons," Phys. Lett. **60A**, No. 2 (1977), 81.

[113] D. N. Page, "Taub-NUT Instanton With an Horizon," Phys. Lett. **78B**, 249 (1978).

[114] H. J. Boonstra, K. Skenderis and P. K. Townsend, "The domain wall/QFT correspondence," JHEP **9901**, 003 (1999) [arXiv:hep-th/9807137].

[115] V. Balasubramanian and P. Kraus, "Spacetime and the holographic renormalization group," Phys. Rev. Lett. **83**, 3605 (1999) [arXiv:hep-th/9903190].

[116] A. Strominger, "The dS/CFT correspondence," JHEP **0110**, 034 (2001) [arXiv: hep-th/0106113].

[117] E. Witten, "Quantum gravity in de Sitter space," [arXiv: hep-th/0106109].

[118] V. Balasubramanian, P. Hořava and D. Minic, "Deconstructing de Sitter," JHEP **0105**, 043 (2001) [arXiv: hep-th/0103171]. "Exploring de Sitter Space and Holography," Class. Quant. Grav. **19**, 5655 (2002), [arXiv:hep-th/0207245];

[119] J. T. Liu and W. A. Sabra, "Charged configurations in (A)dS spaces," Nucl. Phys. B **679**, 329 (2004) [arXiv: hep-th/0307300];

B. McInnes, "Orbifold physics and de Sitter spacetimes," Nucl. Phys. B **692**, 270 (2004) [arXiv: hep-th/0307300];

B. McInnes, "The strong energy condition and the S-brane singularity problem," JHEP **0306**, 043 (2003) [arXiv: hep-th/0305107].

[120] A. Buchel, P. Langfelder and J. Walcher, "On time-dependent backgrounds in supergravity and string theory," Phys. Rev. D **67**, 024011 (2003) [arXiv: hep-th/0207214];

[121] H. Lü, J. F. Vázquez-Poritz and J. E. Wang, "De Sitter bounces," Class. Quant. Grav. **21**, 4963 (2004) [arXiv:hep-th/0406028].

[122] D. Brecher and P. M. Saffin, "Decay modes of intersecting fluxbranes," Phys. Rev. D **67**, 125013 (2003) [arXiv:hep-th/0302206].

[123] B. Durin and B. Pioline, "Aspects of Dirichlet S-branes," arXiv:hep-th/0507059.

[124] A. Chamblin and R. Emparan, "Bubbles in Kaluza-Klein theories with space- or time-like internal dimensions," Phys. Rev. D **55**, 754 (1997) [arXiv:hep-th/9607236].

[125] R.-G. Cai, Y. S. Myung and Y.-Z. Zhang, "Check of the mass bound conjecture in de Sitter space," Phys. Rev. D **65**, 084019 (2002) [arXiv:hep-th/0110234].

[126] H. Lü, C. N. Pope and J. F. Vázquez-Poritz, "From AdS black holes to supersymmetric flux-branes," [arXiv: hep-th/0307001].

[127] B. S. Acharya, J. P. Gauntlett and N. Kim, "Fivebranes wrapped on associative three-cycles," Phys. Rev. D **63**, 106003 (2001) [arXiv: hep-th/0011190];

J. P. Gauntlett, N. Kim and D. Waldram, "M-fivebranes wrapped on supersymmetric cycles," Phys. Rev. D **63**, 126001 (2001) [arXiv: hep-th/0012195];

J. P. Gauntlett and N. Kim, "M-fivebranes wrapped on supersymmetric cycles. II," Phys. Rev. D **65**, 086003 (2002) [arXiv: hep-th/0109039];

C. Núñez, I. Y. Park, M. Schvellinger and T. A. Tran, "Supergravity duals of gauge theories from F(4) gauged supergravity in six dimensions," JHEP **0104**, 025 (2001) [arXiv: hep-th/0103080].

[128] G. W. Gibbons, M. J. Perry and C. N. Pope, "The first law of thermodynamics for Kerr - anti-de Sitter black holes," arXiv:hep-th/0408217.

[129] G. W. Gibbons, M. J. Perry and C. N. Pope, "Bulk / boundary thermodynamic equivalence, and the Bekenstein and cosmic-censorship bounds for rotating charged AdS black holes," arXiv:hep-th/0506233.

[130] G. W. Gibbons, M. J. Perry and C. N. Pope, "AdS/CFT Casimir energy for rotating black holes," arXiv:hep-th/0507034.

[131] G. W. Gibbons, "Euclidean quantum gravity: the view from 2002," in *The Future of Theoretical Physics and Cosmology, Celebrating Stephen Hawking's 60th Birthday*, ed. G. W. Gibbons, E. P. S. Shellard and S. J. Rankin, Cambridge University Press (2003).

[132] I. Papadimitriou and K. Skenderis, "Thermodynamics of asymptotically locally AdS spacetimes," arXiv:hep-th/0505190.

[133] R. McNees, "A new boundary counterterm for asymptotically AdS spacetimes," arXiv:hep-th/0512297.

[134] B. Carter, "Hamilton-Jacobi And Schrödinger Separable Solutions Of Einstein's Equations," Commun. Math. Phys. **10**, 280 (1968).

[135] V. Balasubramanian and P. Kraus, "A stress tensor for anti-de Sitter gravity," Commun. Math. Phys. **208**, 413 (1999) [arXiv: hep-th/9902121].

[136] J. D. Brown and J. W. York, "Quasilocal energy and conserved charges derived from the gravitational action," Phys. Rev. D **47**, 1407 (1993).

[137] A. M. Ghezelbash and R. B. Mann, "Action, mass and entropy of Schwarzschild-de Sitter black holes and the de Sitter/CFT correspondence," JHEP **0201**, 005 (2002) [arXiv: hep-th/0111217].

[138] D. Klemm, "Some aspects of the de Sitter/CFT correspondence," Nucl. Phys. B **625**, 295 (2002) [arXiv: hep-th/0106247].

[139] D. Klemm and L. Vanzo, "Aspects of quantum gravity in de Sitter spaces," JCAP **0411**, 006 (2004) [arXiv:hep-th/0407255].

[140] S. F. Ross and G. Titchener, "Time-dependent spacetimes in AdS/CFT: Bubble and black hole," [aXiv: hep-th/0411128].

[141] D. Astefanesei, R. Mann and E. Radu, "Reissner-Nordström-de Sitter black hole, planar coordinates and dS/CFT," JHEP **0401**, 029 (2004) [arXiv: hep-th/0310273].

[142] V. Balasubramanian, J. de Boer and D. Minic, "Mass, entropy and holography in asymptotically de Sitter spaces," Phys. Rev. D **65**, 123508 (2002) [arXiv: hep-th/0110108].

[143] M. Cvetič, S. Nojiri and S. D. Odintsov, "Cosmological anti-deSitter space-times and time-dependent AdS/CFT correspondence," Phys. Rev. D **69**, 023513 (2004) [arXiv: hep-th/0306031].

[144] A. Hashimoto and S. Sethi, "Holography and string dynamics in time-dependent backgrounds," Phys. Rev. Lett. **89**, 261601 (2002) [arXiv:hep-th/0208126].

[145] J. Simón, "Null orbifolds in AdS, time dependence and holography," JHEP **0210**, 036 (2002) [arXiv:hep-th/0208165].

[146] D. Astefanesei, R. Mann and E. Radu, "Nut charged space-times and closed timelike curves on the boundary" JHEP **0501**, 049 (2005) [arXiv: hep-th/0407110].

[147] S. W. Hawking, G. F. R. Ellis, *The Large Scale Structure of Space-time*, Cambridge University Press (1973).

[148] M. Spradlin, A. Strominger and A. Volovich, "Les Houches lectures on de Sitter space," [arXiv: hep-th/0110007].

[149] S. W. Hawking and D. N. Page, "Thermodynamics Of Black Holes In Anti-De Sitter Space," Commun. Math. Phys. **87**, 577 (1983).

[150] D. Brill and K.-T. Pirk, "A pictorial history of some gravitational instantons," in *College Park 1993, Directions in general relativity, vol. 1* 58-77. arXiv:gr-qc/9302035.

[151] M. Perry, "Instabilities in gravity and supergravity," in *Superspace and Supergravity: Proceedings of the Nuffield Workshop*, Cambridge University Press, 1981.

[152] F. Reif, *Fundamentals of Statistical and Thermal Physics*, McGraw-Hill (1965).

[153] H. B. Callen, *Thermodynamics and an Introduction to Thermostatistics, 2nd ed.*, Wiley (1985).

[154] B. M. N. Carter and I. P. Neupane, "Thermodynamics and stability of higher dimensional rotating (Kerr) AdS black holes," arXiv:gr-qc/0506103.

[155] J. M. Bardeen, B. Carter and S. W. Hawking, "The Four Laws Of Black Hole Mechanics," Commun. Math. Phys. **31**, 161 (1973).

[156] D. J. Gross, M. J. Perry and L. G. Yaffe, "Instability Of Flat Space At Finite Temperature," Phys. Rev. D **25**, 330 (1982).

[157] I. S. N. Booth and R. B. Mann, "Cosmological pair creation of charged and rotating black holes," arXiv:gr-qc/9711038.

[158] C. S. Peça and J. P. S. Lemos, "Thermodynamics of Reissner-Nordström-anti-de Sitter black holes in the grand canonical ensemble," Phys. Rev. D **59**, 124007 (1999) [arXiv:gr-qc/9805004].

[159] C. S. Peça and J. P. S. Lemos, "Thermodynamics of toroidal black holes," J. Math. Phys. **41**, 4783 (2000) [arXiv:gr-qc/9809029].

[160] I. S. Booth and R. B. Mann, "Cosmological pair production of charged and rotating black holes," Nucl. Phys. B **539**, 267 (1999) [arXiv:gr-qc/9806056].

[161] I. S. Booth and R. B. Mann, "Complex instantons and charged rotating black hole pair creation," Phys. Rev. Lett. **81**, 5052 (1998) [arXiv:gr-qc/9806015].

[162] I. S. Booth and R. B. Mann, "Moving observers, non-orthogonal boundaries, and quasilocal energy," Phys. Rev. D **59**, 064021 (1999) [arXiv:gr-qc/9810009].

[163] M. Cvetič and S. S. Gubser, "Phases of R-charged black holes, spinning branes and strongly coupled gauge theories," JHEP **9904**, 024 (1999) [arXiv:hep-th/9902195].

[164] M. Cvetič and S. S. Gubser, "Thermodynamic stability and phases of general spinning branes," JHEP **9907**, 010 (1999) [arXiv:hep-th/9903132].

[165] A. Chamblin, R. Emparan, C. V. Johnson and R. C. Myers, "Charged AdS black holes and catastrophic holography," Phys. Rev. D **60**, 064018 (1999) [arXiv:hep-th/9902170].

[166] A. Chamblin, R. Emparan, C. V. Johnson and R. C. Myers, "Holography, thermodynamics and fluctuations of charged AdS black holes," Phys. Rev. D **60**, 104026 (1999) [arXiv:hep-th/9904197].

[167] T. Prestidge, "Dynamic and thermodynamic stability and negative modes in Schwarzschild-anti-de Sitter," Phys. Rev. D **61**, 084002 (2000) [arXiv:hep-th/9907163].

[168] M. M. Caldarelli, G. Cognola and D. Klemm, "Thermodynamics of Kerr-Newman-AdS black holes and conformal field theories," Class. Quant. Grav. **17**, 399 (2000) [arXiv:hep-th/9908022].

[169] A. Ashtekar and S. Das, "Asymptotically anti-de Sitter space-times: Conserved quantities," Class. Quant. Grav. **17**, L17 (2000) [arXiv:hep-th/9911230].

[170] S. Das and R. B. Mann, "Conserved quantities in Kerr-anti-de Sitter spacetimes in various dimensions," JHEP **0008**, 033 (2000) [arXiv:hep-th/0008028].

[171] S. S. Gubser and I. Mitra, "Instability of charged black holes in anti-de Sitter space," arXiv:hep-th/0009126.

[172] S. S. Gubser and I. Mitra, "The evolution of unstable black holes in anti-de Sitter space," JHEP **0108**, 018 (2001) [arXiv:hep-th/0011127].

[173] R.-G. Cai, "The Cardy-Verlinde formula and AdS black holes," Phys. Rev. D **63**, 124018 (2001) [arXiv:hep-th/0102113].

[174] R.-G. Cai, "Cardy-Verlinde formula and thermodynamics of black holes in de Sitter spaces," Nucl. Phys. B **628**, 375 (2002) [arXiv:hep-th/0112253].

[175] R.-G. Cai, L.-M. Cao and D.-W. Pang, "Thermodynamics of dual CFTs for Kerr-AdS black holes," Phys. Rev. D **72**, 044009 (2005) [arXiv:hep-th/0505133].

[176] M. H. Dehghani, "Quasilocal thermodynamics of Kerr de Sitter spacetimes and the dS/CFT correspondence," Phys. Rev. D **65**, 104030 (2002) [arXiv:hep-th/0201128].

[177] M. H. Dehghani, "Thermodynamics of rotating charged black strings and (A)dS/CFT correspondence," Phys. Rev. D **66**, 044006 (2002) [arXiv:hep-th/0205129].

[178] M. H. Dehghani and H. KhajehAzad, "Thermodynamics of Kerr Newman de Sitter black hole and dS/CFT correspondence," Can. J. Phys. **81**, 1363 (2003) [arXiv:hep-th/0209203].

[179] M. H. Dehghani and A. Khoddam-Mohammadi, "Thermodynamics of d-dimensional charged rotating black brane and AdS/CFT correspondence," Phys. Rev. D **67**, 084006 (2003) [arXiv:hep-th/0212126].

[180] G. Gibbons and S. A. Hartnoll, "A gravitational instability in higher dimensions," Phys. Rev. D **66**, 064024 (2002) [arXiv:hep-th/0206202].

[181] S. A. Hartnoll, "Instability of generalised AdS black holes and thermal field theory," JHEP **0308**, 019 (2003) [arXiv:hep-th/0305001].

[182] T. Ghosh, "Thermodynamics of a class of Kerr-Bolt-Ads spacetime," arXiv:hep-th/0305119.

[183] O. Aharony, J. Marsano, S. Minwalla, K. Papadodimas and M. Van Raamsdonk, "The Hagedorn / deconfinement phase transition in weakly coupled large N gauge theories," arXiv:hep-th/0310285.

[184] V. Cardoso and O. J. C. Dias, "Small Kerr-anti-de Sitter black holes are unstable," Phys. Rev. D **70**, 084011 (2004) [arXiv:hep-th/0405006].

[185] N. Deruelle and J. Katz, "On the mass of a Kerr-anti-de Sitter spacetime in D dimensions," Class. Quant. Grav. **22**, 421 (2005) [arXiv:gr-qc/0410135].

[186] H. Nomura, S. Yoshida, M. Tanabe and K.-i. Maeda, "The fate of a five-dimensional rotating black hole via Hawking radiation," arXiv:hep-th/0502179.

[187] S. Deser, I. Kanik and B. Tekin, "Conserved charges of higher D Kerr-AdS spacetimes," Class. Quant. Grav. **22**, 3383 (2005) [arXiv:gr-qc/0506057].